INTERACTION OF THE HOST IMMUNE SYSTEM WITH TUMOR CELLS IN HUMAN PAPILLOMAVIRUS ASSOCIATED DISEASES

MADELEINE SAUER

- 2014 -

Dissertation

submitted to the

Combined Faculties for the Natural Sciences and for Mathematics
of the Ruperto-Carola University of Heidelberg, Germany

for the degree of

Doctor of Natural Sciences

presented by

Madeleine Sauer

born in Sinsheim

oral examination: 29.01.2015

INTERACTION OF THE HOST IMMUNE SYSTEM WITH TUMOR CELLS IN HUMAN PAPILLOMAVIRUS ASSOCIATED DISEASES

Referees: Prof. Dr. rer. nat. Martin Müller

       Prof. Dr. med. Magnus von Knebel Doeberitz

.

Meiner Familie

ACKNOWLEDGEMENT

ABSTRACT

Human papillomaviruses (HPV) are very common in the sexually active population and contribute to 610,000 cancers per year occurring at different locations. The initial step of HPV-related carcinogenesis is the induction of transforming processes in the host cells mediated by the viral oncoproteins E6 and E7 that interfere with critical host cell pathways. The transforming infection is highlighted by overexpression of the tumor suppressor protein p16^{INK4a}. Only a small number of precancerous lesions progress while the majority can be controlled by the host's immune system and undergo regression. Progressing lesions under the immunoselective pressure seem to acquire characteristics that enable them to circumvent the host's immune attack and promote disease progression. Immune evasion might be mediated by the immune microenvironment of the tumor as well as by tumor cell intrinsic features.

The here presented thesis addressed different questions and strategies with regard to the role of the immune system in HPV-associated diseases and can be subdivided in two main parts: In the first part immunologic characteristics of precancerous lesions and cancers are investigated to gain insight into possible immune evasion mechanisms developed during disease progression. In the second part treatment options to positively influence the balance between immune evasion and anti-tumoral immune responses are evaluated.

In the first part a) the immunohistochemical characterization of cervical precancers and cancers for infiltration with different T cell phenotypes revealed that generally increasing T cell densities occur late in carcinogenesis – and not yet with the onset of early transforming infection - and are accompanied by immunosuppressive regulatory T cells (Tregs). Mean cell densities for Tregs in the stroma significantly increased from 121.6 cells/mm^2 (range: 24-286.8 cells/mm^2) in low-grade lesions to 308.8 cells/mm^2 (24-724.8 cells/mm^2) in high-grade lesions and 673.6 cells/mm^2 (52.8-1564.8 cells/mm^2) in cancer which points to their immunosuppressive role during carcinogenesis. The demonstrated large variances in T cell densities within one diagnostic category, however, point to a remarkable heterogeneity of the immune control with potential interesting prognostic implications. On keratinocytes themselves b) a selective loss for human leukocyte antigen (HLA) class I heavy chain A expression was observed in about 55% high-grade cervical intra-epithelial neoplasia (CIN) and 65% of cervical cancers. HLA class II *de novo* expression was found in 50% of low-grade CIN and in about 85% of high-grade CIN and cervical cancers. These alterations could represent another fundamental mechanism contributing to immune evasion. A c) longitudinal analysis of immune infiltrates in patients treated with imiquimod, an immuno-modulatory Toll-like receptor (TLR) agonist, revealed that the patient's local immune constitution might be decisive for a possible response to immune-enhancing treatment strategies. Importantly, in patients responding to imiquimod immune cell densities increased during the treatment as epithelial CD3+ T cell counts (from 160.8 to 371.1 cells/mm^2) and CD8+ T cell counts (from 113.8 to 174.1 cells/mm^2) demonstrated. The d) development and establishment of an automated cell quantification tool for high-throughput analysis allows the search for immune evasion markers and strategies to be continued in an objective, standardized and faster way.

In consideration of the clinical efficacy of imiquimod and the observed stimulatory effects on the immune infiltrate density in part one of this thesis e) a new second generation TLR-agonist (TMX-202) potentially having less side-effects than imiquimod was tested for the first time in an *in vitro* T

cell stimulation model in part two of this thesis. Its potential to stimulate innate and adaptive immunity was demonstrated by an enhanced killing capacity of T cells that were stimulated with HPV-related antigens loaded on dendritic cells and then co-incubated with HPV16-positive CaSki cells. Based on the dense infiltration with Tregs observed in part one of the presented thesis the f) immune stimulating effects of Treg depletion was tested in an autologous *in vitro* model. In this regard, one major aim of the thesis was the generation of a new HPV-positive tumor cell line derived from an oropharyngeal squamous cell carcinoma that serves as model system for HPV-associated tumors. In combination with peripheral blood lymphocytes obtained from the same patient this autologous system allowed to address Treg depletion as an immunotherapeutic approach. The results demonstrated that this strategy might enhance the cell-mediated immune response against tumor cells and emphasize the role that this particular T cell phenotype is obviously playing in the carcinogenesis of HPV-associated tumors.

Based on the results obtained in the first part of the thesis it is well conceivable that the combination of different immunologic markers contributes to the definition of a prognostic biomarker tool for progression and regression of precancerous lesions. Such a prognostic "immune score" has a high clinical relevance and allows risk-adapted treatment decisions minimizing the costs and long-term sequelae of surgical interventions. In particular the newly developed microscopy based method in this work allowing for the automated histological high-throughput quantification of infiltrating immune cells in cervical intraepithelial neoplasia provides an important methodical tool to realize this long term goal. The immuno-stimulating effects of the novel TLR7-agonist TMX-202 and Treg depletion demonstrated in the second part of this thesis by *in vitro* models indicate that immunomodulatory approaches could play an important role for the treatment of HPV-associated cancers in the future. In this regard, the established novel tumor cell line in combination with autologous immune cells provides a valuable *in vitro* model system for HPV-associated cancers that can be used to investigate further immunotherapeutic intervention and treatment strategies.

KURZFASSUNG

Infektionen mit humanen Papillomviren (HPV) sind in der sexuell aktiven Bevölkerung weit verbreitet und führen zu bis zu 610,000 teilweise unterschiedlich lokalisierter Krebserkrankung pro Jahr. Der Beginn der HPV-assoziierten Karzinogenese stellt dabei die Induktion des Transformationsprozesses durch die viralen Onkoproteine E6 und E7 dar, die mit essentiellen Signaltransduktionswegen der Wirtszelle interagieren. Das transformierende Infektionsstadium korreliert hierbei mit der Überexpression des Tumorsuppressorproteins $p16^{INK4a}$. Nur eine geringe Anzahl der daraus resultierenden präkanzerogenen Läsionen progrediert allerdings weiter zu einem Tumor während die Mehrheit solcher Läsionen unter Kontrolle des Immunsystems wieder regrediert. Progredierende Läsionen, die unter dem Selektionsdruck des Immunsystems stehen, scheinen dabei Charakteristika erworben zu haben um einen Angriff des Immunsystems zu umgehen und ermöglichen dadurch die Progression der Erkrankung. Entsprechende Immunevasionsstrategien könnten sowohl vom Immunmikromilieu um den entstehenden Tumor herum ausgehen als auch auf zellinherenten Tumoreigenschaften beruhen.

Die vorliegende Dissertation beschäftigte sich mit verschiedenen Fragestellungen und verfolgt verschiedene Ansätze, die die Rolle des Immunsystems im Zusammenhang mit HPV-assoziierten Erkrankungen näher beleuchten sollen und ist dabei in zwei Hauptteile untergliedert: Teil eins beschäftigt sich mit der immunologischen Charakterisierung präkanzerogener Läsionen und invasiver Tumore um einen tieferen Einblick in mögliche Immunevasionsmechanismen bei voranschreitender Progredienz der Erkrankung zu gewinnen. In Teil zwei werden dagegen verschiedene Therapiemöglichkeiten evaluiert mit dem Ziel das Gleichgewicht zwischen Immunevasion und anti-tumoraler Immunantwort positiv zu beeinflussen.

Im ersten Teil dieser Arbeit konnte durch a) die immunhistochemische Charakterisierung von Infiltrationsraten verschiedener T-Zellphänotypen in Zervixkarzinomvorstufen und -tumoren gezeigt werden, dass ein Anstieg der T-Zelldichte relativ spät in der Tumorentstehung erfolgt - und nicht mit der Induktion des frühen Transformationsstadium korreliert - und dabei stets von einem Anstieg an immunsupprimierenden regulatorischen T-Zellen (Tregs) begleitet wird. Die Mittelwerte der gemessenen Zelldichten für Tregs im Stroma steigen dabei von 121.6 Zellen/mm^2 (Varianz: 24-286.8 Zellen/mm^2) in niedriggradigen Läsionen über 308.8 Zellen/mm^2 (24-724.8 Zellen/mm^2) in hochgradigen Läsionen auf 673.6 Zellen/mm^2 (52.8-1564.8 Zellen/mm^2) in Tumoren an was auf ihre immunsupprimierende Rolle während der Karzinogenese hinweist. Die beobachteten großen Varianzen in den T-Zelldichten innerhalb einer diagnostischen Kategorie weisen dabei jedoch auf eine bemerkenswerte Heterogenität der Immunsystemkontrolle mit möglicherweise vielversprechenden prognostischen Implikationen hin. Auf Seite der sich verändernden Keratinozyten konnte weiterhin b) ein selektiver Ausfall der Expression der schweren Kette A des humanen Leukozytenantigens (HLA) Klasse I in 55% aller hochgradigen zervikalen intraepithelialen Neoplasien (CIN) und in 65% aller Zervixkarzinome festgestellt werden. HLA Klasse II *de novo* Expression konnte dagegen in 50% aller niedriggradigen CIN und in 85% aller hochgradigen CIN und Zervixkarzinomen beobachtet werden. Die gefundenen Veränderungen könnten dabei einen anderen grundlegenden Mechanismus darstellen, der zur Immunevasion der Tumorzelle beiträgt. Eine c) longitudinal ausgerichtete Analyse von Immuninfiltraten von Patienten die mit Imiquimod behandelt wurden - einem immunmodulatorischen Toll-Like-Rezeptor-(TLR)-Agonisten - ergab, dass die lokale Immunkonstitution des jeweiligen

Patienten entscheidend für das mögliche Ansprechen auf immunstimulatorische Behandlungsstrategien ist. In Biopsien von Patientinnen, die auf eine Imiquimodbehandlung ansprachen konnten bemerkenswerterweise hohe Immunzelldichten im Behandlungszeitraum beobachtet werden, wie die gemittelten epithelialen CD3+ T-Zellzahlen (Anstieg von 160.8 auf 371.1 Zellen/mm^2) und CD8+ T-Zellzahlen (Anstieg von 160.8 auf 371.1 Zellen/mm^2) belegen. Die d) Entwicklung und Etablierung eines automatisierten Zellquantifizierungssystems, das speziell zur Durchführung von Hochdurchsatzanalysen geeignet ist, ermöglicht die Suche nach Immunevasionsmarkern und -strategien in objektiverer, standardisierter und auf schnellere Art und Weise fortzusetzen.

Unter Berücksichtigung der klinischen Wirksamkeit von Imiquimod und den ermittelten immunstimulatorischen Einfluss auf die Immuninfiltrationsraten in Teil eins wurde in Teil zwei dieser Arbeit e) ein TLR-Agonist der zweiten Generation (TMX-202), der potentiell weniger Nebenwirkung als Imiquimod aufweist, zum ersten Mal an einem *in vitro* T-Zellstimulationsmodell getestet. Das Potential von TMX-202 das angeborene und adaptive Immunsystem zu stimulieren wurde in diesem Zusammenhang an Hand gesteigerter zytotoxischer Aktivität von T-Zellen nachgewiesen. Diese wurden mit dendritischen Zellen stimuliert, die mit HPV-assoziierten Antigenen beladen waren und schließlich mit HPV16-positiven CaSki-Zellen koinkubiert. Aufbauend auf die in Teil eins der vorliegenden Arbeit nachgewiesenen hohen Infiltrationsdichten an Tregs wurde zusätzlich f) der immunstimulatorische Effekt einer Verminderung der Treg-Zellzahlen an einem autologen *in vitro* Modell getestet. In diesem Zusammenhang war ein Hauptziel dieser Dissertation die Generierung einer neuen HPV-positiven Tumorzelllinie aus einem Oropharynxkarzinom, die als Modell für HPV-assoziierte Tumore dienen soll. In Kombination mit peripheren Lymphozyten, die aus dem Blut des gleichen Patienten gewonnen werden, sollte das so gewonnene autologe System die Untersuchung einer Treg-Depletion als einen Ansatz zur Immuntherapie ermöglichen. Die Ergebnisse zeigen, dass diese Strategie die zellvermittelte Immunantwort gegenüber Tumorzellen verbessern kann und hebt erneut die Rolle hervor, die dieser spezielle T-Zellphänotyp offensichtlich bei der Entstehung HPV-assoziierter Tumor zukommt. Aufbauend auf den Ergebnissen der vorliegenden Dissertation ist es denkbar, dass eine Kombination verschiedener immunologischer Marker zur Definition eines prognostischen Biomarkersystems führt, das die Vorhersage der Progression und Regression präkanzerogener Läsionen ermöglicht. Ein solcher „Immunindex" ist von hoher klinischer Relevanz und soll risikoangepasste Behandlungsentscheidungen ermöglichen, um somit die Kosten und Spätkomplikationen von chirurgischen Eingriffen zu minimieren. Insbesondere das in dieser Arbeit neu entwickelte Mikroskopie-basierte Verfahren zur automatischen histologischen Hochdurchsatzquantifizierung von Immuninfiltraten in zervikalen intraepithelialen Neoplasien sollte ein entscheidendes methodisches Werkzeug darstellen, um dieses Langzeitziel zu erreichen. Die in dieser Arbeit an *in vitro* Modellen für HPV-assoziierte Krebsarten gezeigten immunstimulierenden Effekte des neuartigen TLR7-Agonisten TMX-202 und der Treg-Depletion zeigen, dass immunmodulatorische Ansätze bei der Behandlung solcher Erkrankungen in Zukunft eine wichtige Rolle einnehmen könnten. Eine Kombination der neu generierten Tumorzelllinie mit autologen Immunzellen sollte in diesem Zusammenhang ein verlässliches *in vitro* Modellsystem für HPV-assoziierte Krebsarten darstellen, das weiterführende Studien zu immuntherapeutischen Interventions- und Behandlungsstrategien ermöglicht.

TABLE OF CONTENTS

ABBREVIATIONS

°C	degree Celsius
μ	micro
AB	antibody
ad inj	ad injectabilia
AP	activator protein
APC	antigen-presenting cell
aqua bidest.	bidistilled water
ARF	alternate reading frame
ATCC	american type culture collection
ATP	adenosine triphosphate
B	bone marrow
B2M	beta-2-microglobulin
BC	B cell, B lymphocyte
bp	base pairs
Ca	carcinoma
CD	cluster of differentiation
CDK	cyclin dependent kinase
cDNA	complementary DNA
CIN	cervical intraepithelial neoplasia
CTL	cytotoxic T lymphocytes
CTLA	cytotoxic T lymphocyte-associated protein
CUL	cullin
DAB	3,3'- Di-amino-benzidine
DAC	decitabine
DC	dendritic cell
dest	destillata
DMEM	Dulbecco's Modified Eagle Medium
DMSO	dimethyl sulfoxide
DNA	deoxyribonucleic acid
Dnmt1	DNA methyltransferase 1
DTT	dithiothreitol
E	early gene/protein
E2F	transcription factor
E6	early HPV protein 6
E7	early HPV protein 7
EDTA	ethylenediaminetetraacetic acid
ELISA	enzyme linked immunosorbent assay
EtOH	ethanol
F	fragment
FACS	fluorescence-activated cell sorting
Fas	apoptosis stimulating fragment
FCS	fetal calf serum
FDA	Food and Drug Administration
FFPE	formalin-fixed paraffin-embedded

FI	fluorescence intensity
FITC	fluorescein isothiocyanate
FOXP3	forkhead box P3
g	gram
G	growth
gDNA	genomic DNA
GM-CSF	granulocyte macrophage colony-stimulating factor
GranB	granzyme B
Gy	Gray
h	hour/s
H	histone
H_2O	water
HCA	human carcinoma antigen
HEPES	4-(2-hydroxyethyl)-1-piperazineethanesulfonic acid
HLA	human leukocyte antigen
HNSCC	head and neck squamous cell carcinoma
HPLC	high pressure liquid chromatography
HPV	human papillomavirus
HR	high risk
HRP	horse raddish peroxidase
HSV	herpes simplex virus
Hz	Hertz
ICD-O	international classification of diseases for oncology
IF	immunofluorescence
IFN	interferon
Ig	immune globulin
IG	immunoglobulin
IHC	immunohistochemistry
IHS	Intensity-Hue-Saturation
IL	interleukin
IMDM	Iscove's modified Dulbecco's medium
iNOS	increased inducible nitric oxide synthase
Jak	Januskinase
JPEG	joint photographic expert group
KDM	histone lysine demethylases
KMT	histone lysine methyltransferases
L	late gene/protein
l	liter
LC	Langerhans cell
LCR	long control region
LPS	lipopolysaccharide
LR	low risk
M	Molar, Mol / liter
m	meter
MACS	magnetic cell sorting
MCP-1	monocyte-chemoattractant-protein-1
MeOH	methanol
MFI	mean fluorescence intensity
MHC	major histocompatibility complex

MICA	MHC class I chain-related molecule
min	minute/s
miRNA	micro ribonucleic acid
MMP	matrix-metalloproteinase
mol	molar
mRNA	messenger ribonucleic acid
MSI	microsatellite instability
MT	methyl transferase
MyD88	myeloid differentiation primary-response protein 88
n	sample size
n	nano
NFkB	nuclear factor-kappa B
NK	natural killer cell
NKT	natural killer T cell
NMSC	non-melanoma skin cancer
NO	nitric oxide
OIS	oncogene induced stress
OPC	oropharynx cancer
ORF	open reading frame
OSCC	oropharyngeal squamous cell carcinoma
p	probability
p	protein, peptide
p.a.	per analysis
p16^{INK4a}	tumor suppressor kinase inhibitor of CDK4
p53	tumor suppressor protein 53
PAGE	polyacrylamide gel electrophoresis
PAMP	pathogen-associated molecular pattern
Pap test	Papanicolau test
PBL	peripheral blood lymphocytes
PBMC	peripheral blood mononuclear cell
PBS	phosphate-buffered saline
PBS-T	PBS containing 0.05% Tween 20
PCR	polymerase chain reaction
PDZ	post synaptic density protein (PSD95), Drosophila disc large tumor suppressor (Dlg1), zonula occludens-1 protein (zo-1)
PE	phycoerythrin
PFA	paraformaldehyde
pRB	phosphorylated retinoblastoma protein
PRR	pattern recognition receptor
PVDF	polyvinylidene difluoride
qPCR	quantitative polymerase chain reaction
Rb	retinoblastoma
RB	retinoblastoma protein
RGB	red green blue
RNA	ribonucleic acid
ROI	region of interest
rpm	rounds per minute
RT	room temperature
RT	reverse transcription

S	synthesis
sec	second/s
SCC	squamous cell carcinoma
SDS	sodiumdodecylsulfate
SSC	squamous cell carcinoma
STAT	signal transducers and activators of transcription
STR	short-tandem-repeat
T	thymus
t	time
TAP	transporter associated with antigen presentation
TAP-1	antigen-processing-protein-1
Taq	thermus aquaticus
TBE	tris-borate EDTA
TBS	tris-buffered saline
TCR	T cell receptor
TEMED	tetramethylethylenediamine
TGF	transforming growth factor
Th	T-helper cell
TIL	tumor infiltrating lymphocyte
TLRs	Toll-like receptor
TMB	Tetramethyl benzidine
TMX	Telormedix
TNF	tumor necrosis factor
TNM	tumor nodes metastasis
Treg cell	regulatory T cell
Tris-HCl	Tris-(hydroxymethyl)aminomethane hydrochloride
V	vacuolar
v/v	volume per volume
VAIN	vaginal intraepithelial lesion
VIN	vulvar intraepithelial neoplasia
VLP	virus like particle
w/v	weight per volume

1. INTRODUCTION

"Do not follow where the path may lead. Go instead where there is no path and leave a trail." (George Bernard Shaw)

1.1 The discovery of human papillomaviruses in the causation of cancer

The knowledge of the relationship between the carcinogenesis of cervical tumors and sexually transmittable agents has already dated back to the 19th century when a link between the sexual behavior and the risk for development of cervical cancers could be established. The Italian physician Domenico Antonio Rigoni-Stern analyzed the causes of death of Veronese women who had died between 1760 and 1839 and observed a significantly higher frequency of cervical cancers occurring in sexually active women, compared to virgins and nuns who were affected by cervical tumors only very rarely (GASPARINI and PANATTO, 2009).

The awareness that cancers can be attributed to infectious agents raised in the beginning 20th century. Peyton Rous, in 1911, demonstrated that cell-free extracts of chicken sarcoma can be transferred from one individual to another (ZUR HAUSEN, 2011).

The history of the discovery of the human papillomavirus (HPV) as causing agent in the development of cervical cancer however started considerably later in the 1970s. At that time, Harald zur Hausen subverted the widespread opinion among scientists and clinicians that the sexually transmittable herpes simples virus type 2 (HSV-2) may be causally linked to carcinomas of the anogenital tract and proposed papillomaviruses to contribute to cervical carcinogenesis (ZUR HAUSEN et al., 1974). He proved that not HSV-2 but HPV DNA is detectable in the tumor tissue and hypothesized that the viral genome is persistently present and transcriptionally active in HPV-infected cancer cells (ZUR HAUSEN et al., 1975).

His findings considerably contributed to a detailed description of the phylogenetic heterogeneity of the human papillomaviruses, to the identification of the major HPV types associated with cancer and the characterization of the oncogenic potential of the HPV proteins E6 and E7. His work awoke the general interest of the scientific community on viruses as cancer causing agents in general and on HPV in particular leading to the opening of a completely new research area which aims at understanding of the molecular mechanisms and, in a second step, combating HPV-related diseases. Having the courage to leave the path chosen by the research community of his time and thus paving the way for the following generations of researchers to participate in the battle against cancer caused by one of the most common sexually transmittable agents he was rewarded the Nobel Prize in 2008.

1.2   Characteristics and life cycle of human papillomaviruses

Human papillomaviruses are non-enveloped DNA viruses containing one single-stranded circular DNA molecule with a size of about 8000 base pairs. They belong to the family of papillomaviridae which can further be subdivided into five genera (Alpha-, Beta-, Gamma-, Mu- and Nupapillomaviruses) (DOORBAR, 2006). The viral genome (Figure 1.1) comprises eight open reading frames (ORF) covering three distinct functional parts, namely the early genes' region (E1-E7), the late genes (L1 and L2) and a non-coding part called long control region (LCR) containing cis-regulatory elements (ZHENG and BAKER, 2006). HPV is characterized by an icosahedral capsid of a diameter of about 55 nm and consisting of 72 pentameric subunits, the capsomers. The capsomers are made of two structural proteins, the late proteins L1 and L2.
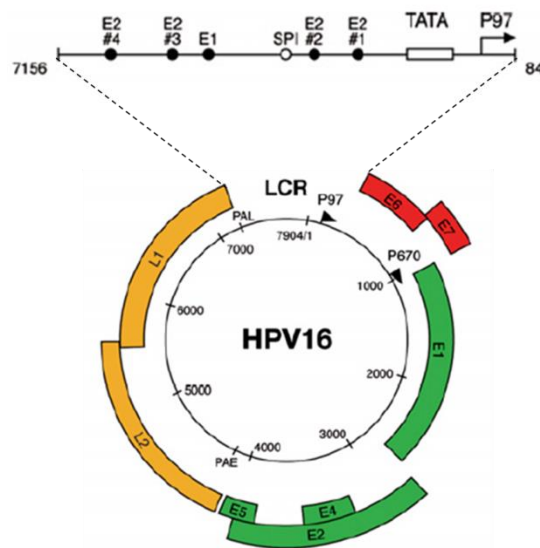
FIGURE 1.1   THE HPV16 GENOME. The genome comprising 7904 bp is represented by a black circle with the early (p97) and the late (p670) promoters marked by arrows. The six early ORFs (E1-E7) are expressed from either p97 or p670. The late ORFs (L1 and L2) are represented as yellow structures and the long control region (enlarged and visualized as black line) contains the E2-binding sites, the binding sites for E1 and the TATA element of the p97 promoter. Adapted from (DOORBAR, 2006).

Human papillomaviruses are characterized by a strong tropism for epithelial cells and the mucosa. The virus' life cycle is initiated with infection of keratinocytes of the basal squamous epithelium which requires either microlesions as they can be found for example in the cervical epithelium or other anatomical structures like the characteristic tonsillar crypt epithelium. HPV infection therefore exclusively affects undifferentiated epithelial stem cells as cell division and keratinocyte differentiation are the prerequisite for the completion of the virus' life cycle and replication (CHOW et al., 2010). The infectivity is predominantly mediated by the viral proteins L1, but also L2 capsid proteins (BUCK et al., 2013) enabling the virus to bind to the host cells which is followed by uptake of the virus via clathrin-based endocytosis. The late proteins also seem to be involved in transferring the viral DNA to the nucleus following disassembling in the late endosomes and lysosomes (DOORBAR, 2006). Initially, following infection the keratinocytes undergo lateral cell divisions and thus build a reservoir of stem cells harboring the virus (NGUYEN et al., 2014). Viral DNA replication

in this phase is tightly synchronized with the amplification of the host cell DNA during S-phase. During this latent phase of the infection the early proteins E1 and E2 are expressed which fulfill different functions during early infection (see also Table 1.1 for HPV protein functions). In addition to the role they play in the replication of the viral genome, they assure that the viral DNA is maintained as an episome at low copy numbers of about 10-200 copies. The viral early proteins E1 and E2 seem to prevent the integration of the viral DNA into the host's genome as well as they assure the correct viral genome segregation during stem cell divisions (MCBRIDE, 2013). E2 initiates the amplification of the viral DNA by binding to the HPV upstream regulatory region and by forming together with E1 that is recruited to this non-coding region the E1/E2 initiation complex. The E1 protein functions as a DNA helicase, and recruits several other, cellular, proteins to the viral origin of replication such as RPA (replication protein A) and DNA polymerase α primase (CONGER et al., 1999; DOORBAR, 2006). Furthermore E2 controls the early promoter of high-risk HPV types, called p97 in HPV16, and thus strictly regulates the early proteins, which is of special importance regarding the expression rates of the viral oncogenes E6 and E7 expressed at low levels only (DOORBAR, 2005).

With the migration of virally infected basal stem cells into the suprabasal cell layer of the epithelium the cells quit the cell cycle in order to undergo terminal differentiation. This initiates the productive phase of the viral infection characterized by activation of the viral genes in parallel to the differentiation program of the keratinocytes.
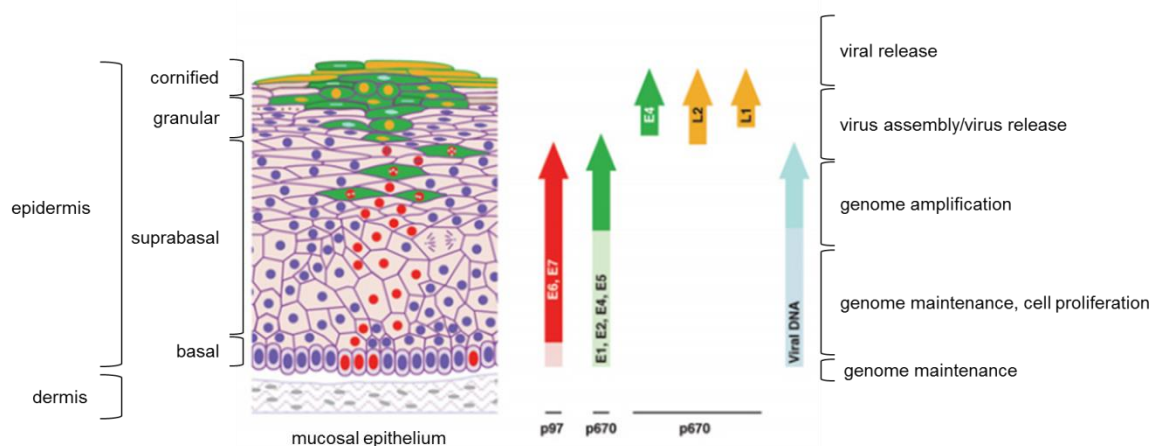
FIGURE 1.2   THE HPV LIFE CYCLE. The cell layers of the mucosal epithelium are indicated on the left. Cells expressing cell cycle markers (red) that occur in the suprabasal cell layer are characterized by viral oncogene expression (E6 and E7) (green cells). The activation of p670 in E6 and E7 expressing cells of the upper epithelium leads to expression of viral proteins required for viral genome replication. The successive viral protein expression stages indicated by arrows represent distinct steps of the viral life cycle directly influencing also the host cell: low-levels of E1, E2, E4 and E5 (light green) accompanied by viral oncogene expression (E6 and E7) leads to induction of cell proliferation. Elevation of the proteins involved in replication (dark green) allows increased viral genome amplification. L1 and L2 (yellow) are expressed in the upper epithelium, where viral genome is packaged into infectious particles. Here, E4 also is expressed and probably contributes to the viral release. Adapted from (DOORBAR, 2006).

As suprabasal keratinocytes that are terminally differentiated undergo cell cycle arrest, the virus has to reactivate S-phase of the host cells to complete its life cycle. The viral oncogenes E6 and E7 are required for the reactivation of the host replication cycle. However, their expression is still under control and locally restricted to a few cells in the lower part of the epithelium. These cells assure the

viral replication to be maintained and infectious virions to be produced once the keratinocytes quit the basal cell layer and migrate towards suprabasal layers (DOORBAR, 2006). The mode of action of the viral oncoproteins acting in the host cells are explained in more detail in section 1.3.2. In the mid and upper layers of the epithelium, the viral DNA is replicated, the amplified genome is packed into viral capsids and infectious virions are finally released. These processes are controlled by the late promoter which is dependent on the differentiation program and activated with the migration of keratinocytes through the epithelium. Its activation leads to increased expression rates of viral early proteins E1, E2, E4 and E5 which are involved in HPV DNA replication (Figure 1.2). However, E6 and E7 expression levels still are tightly controlled by the repressive functions of E2 on the early viral promoter (HAMID et al., 2009).

viral protein	function in the viral life cycle	activities in the host cell
Early proteins:		
E1	viral genome replication	DNA-binding activity, helicase activity, ATPase
E2	viral gene transcription, viral genome replication, viral genome maintenance	transactivation/transrepression, DNA-binding activity, DNA segregation in mitotic cell
E4	viral genome replication (enhanced amplification)	destruction of keratin network, induction of G2M arrest of cell cycle
E5	possibly involved in proliferation and/or inhibition of apoptosis	interference with cellular signaling pathway
E6	reactivation of cellular replication mechanisms, proliferation, immortalization, inhibition of apoptosis, viral genome maintenance	interaction with various cellular proteins, e.g. p53, c-Myc, Bak, Bax, PDZ domain
E7	reactivation of cellular replication mechanisms, proliferation, genomic instability, inhibition of apoptosis, viral genome maintenance	interaction with various cellular proteins, e.g. pRB, HDAC, E2F6, p21, p27, CDK/cyclin
Late proteins:		
L1	major capsid protein	
L2	minor capsid protein	

TABLE 1.1   THE HPV16 PROTEIN FUNCTIONS. Depicted are the early and late proteins, their main functions in the viral life cycle and their activities in the host cell. Adapted from (KAJITANI et al., 2012).

The viral proteins E4 and E5 also seem to be involved in viral DNA replication. E5 is involved in EGF-mediated signaling in order to maintain an environment that is favorable for replicative processes. The viral E4 protein expression levels increase during genome amplification and induce G2 cell cycle arrest of host keratinocytes and thus prevents cell proliferation by counteracting E7 effects; it enhances viral genome amplification and thus is likely to contribute to an increased viral synthesis rate. Its interaction with and destabilizing effects on the keratin network of host cells implies that E4 could also be involved in viral release (reviewed in DOORBAR, 2013).

Finally, the structural L1 and L2 proteins necessary for capsid formation and packaging of the viral DNA are expressed and accumulate during viral replication. Following assembly – in which E2 is also involved by binding viral DNA for loading - of capsids containing one copy of the HPV DNA the

infectious particles are released from the fully differentiated cells that reach the outer surface of the squamous cell epithelium (DOORBAR, 2006).

The viral gene expression pattern is tightly associated with the biological infection stage. The above described life cycle represents the productive or permissive infection stage characterized by viral DNA replication and release of newly assembled virions. In case of persistence of the HPV infection, the productive live cycle may be quit and the proliferation of terminally differentiated epithelial cells in the lower third of the epithelium can be induced (DOORBAR, 2005).

This shift occurs under the influence of deregulated expression of E6 and E7 oncoproteins leading to abolishment of cell cycle arrest while DNA damage responses are inhibited. These processes induce the transforming infection stage which will be described in more detail in chapter 1.3.2.

1.3   HPV-associated cancers

More than 100 different HPV genotypes have been described so far (BERNARD, 2005). Those that are the clinically most relevant ones belong to the genera of alpha-papillomaviruses and cause not only cancerous precursor lesions and cancer but also genital warts (DE VILLIERS et al., 2004). Furthermore, papillomaviruses are classified into two groups depending on their potential to cause cancer: low-risk types leading to ano-genital warts or common skin warts whereas the so called high-risk types - representing only a handful of all genotypes described so far - are involved in cancer development. Among those the high-risk types HPV16 and HPV18 are the most prevalent ones with their DNA being detectable in around 80% of cervical cancers (SCHIFFMAN et al., 2007). The most prevalent low-risk HPV types are HPV11 and HPV6 that cause the vast majority of genital warts (STEBEN and GARLAND, 2014).

This chapter deals with the contribution of HPV to tumor development and the mechanisms involved in the establishment of precancerous lesions and their progression towards invasive disease.

1.3.1   Prevalence, incidence and mortality of HPV-associated diseases

HPV infections are common within the sexual active population and thus considerably contribute to the global health burden: the prevalence in the younger population aged 15 to 25 years is very high and an individual's life time risk to enter in contact with these viruses and get infected is about 80% (DUNNE et al., 2007). Although the majority of HPV infections are cleared within two years – the mean clearance time even is 5 months - remaining without any consequences, more than 5% of cancers appearing worldwide are related to HPV infections that persisted (DE MARTEL et al., 2012). Incidences for different HPV-associated diseases vary between women and men (Figure 1.3).

Cervical cancer is the fourth most common cancer in women following breast cancer, colorectal cancer and lung cancer in the latest GLOBOCAN statistics. Nearly 530,000 new cases of cervical cancer are diagnosed each year (2012), the main burden however occurs in developing countries that show a 10-fold higher incidence compared with industrial nations. Here, cervical cancer represents almost 12% of all female cancers and it still remains the most common cancer in women in Eastern and Middle Africa (FERLAY et al., 2010). This difference is explained by lacking screening programs and early detection of precancerous stages and cervical cancer. The pap-test, developed in the 1930s

by George Papanicolaou, allows the early detection and treatment of precancerous stages and since its introduction has led to a significant decline of the cervical cancer incidence in industry nations (GIBB and MARTENS, 2011). In 2012, an estimated number of around 270 000 women died from cervical cancer worldwide. This makes a percentage of 7.5% of all female cancer deaths. Here again, the majority, more than 85% of all deaths related to cervical cancer, occur in low- or middle-income countries (FERLAY et al., 2010).

Even though cervical cancer is the best characterized among the HPV-associated diseases HPV infection can also occur on other epithelial or mucosal sites and can cause several other cancer types. While virtually all cancers of the cervix uteri are attributable to precedent infection with human papillomaviruses, persistent HPV infection also causes precancerous lesions and cancers at other ano-genital sites and contributes to a proportion of vulvar, vaginal, penile and anal cancers (PARKIN and BRAY, 2006).
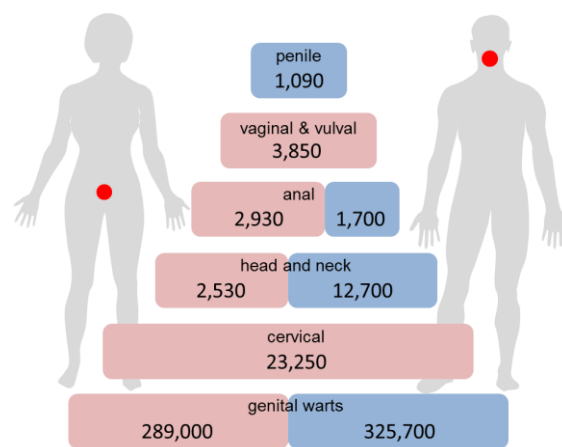
FIGURE 1.3   CONTRIBUTION OF HPV TO THE HEALTH BURDEN. Estimated incidence rates of HPV-associated diseases (related to HPV6, 11, 16, 18) in women and men in Europe. Adapted from (STANLEY, 2012b).

The contribution of HPV in the carcinogenesis of a proportion of head and neck squamous cell carcinoma (HNSCC) today is widely accepted (GILLISON et al., 2000). Especially, the oropharyngeal tract can be concerned by HPV infection and recent studies revealed an increasing incidence of HPV-associated cancers of the oropharynx (OPC), the pharyngeal region located at the back of the throat, and here primarily the tonsils, the base of the tongue and the soft palate are affected (CHATURVEDI et al., 2011). Also here HPV16 is the most prevalent type with about 90% of HPV-positive carcinomas located in the oropharynx being positive for HPV16 DNA. Also in the other ano-genital sites, except the cervix uteri where HPV18 plays a non-negligible role, the vast majority of cancers are associated with HPV16 infections (BOSCOLO-RIZZO et al., 2013). The incidence rate of head and neck squamous cell carcinomas equals that of cervical cancer with about 550 000 new HNSCC cases per year worldwide making it the 7th most common cancer in men. Thereof around 85,000 cases represent oropharyngeal cancers. The mortality rate is higher than in cervical cancer with around 305,000 deaths per year related to HNSCC. However, the etiological heterogeneity – with tobacco and alcohol being the major risk factors for HNSCC – makes it difficult to estimate to which extent HPV contributes to oropharyngeal cancers (GILLISON et al., 2014). Estimates for HPV-association among oropharyngeal cancers are higher for industrial nations (60-70% for the United States) which have experienced an increase in incidence for oropharyngeal cancer in the last two decades, whereas less than 10% of OPCs are believed to be caused by HPV in developing regions (CHATURVEDI et al., 2013). Worldwide,

these data lead to an estimated proportion of about 25% of OPCs attributable to HPV infection following an IARC review published in 2012 (CHATURVEDI et al., 2013).

Distinct HPV types were found to play a role in the autosomal recessive hereditary skin disorder epidermodysplasia verruciformis which is characterized by a higher susceptibility for persistent infections and development of benign lesions and also malignancies of the skin (HARWOOD et al., 2004). HPV also contributes to non-melanoma skin cancer (NMSCC) (reviewed in MOLHO-PESSACH and LOTEM, 2007 and SMOLA, 2014) and might be of higher relevance in immunosuppressed individuals (REUSCHENBACH et al., 2011).

The mechanisms of HPV-induced carcinogenesis in the following chapters will be explained by means of the well-studied cervical cancer and its precursor lesions, the so called cervical intraepithelial neoplasia (CIN). The underlying tumorigenic mechanisms, however, are the same in other HPV-associated cancers.

1.3.2   Viral oncogene overexpression and the transforming infection stage

A small percentage of HPV infections – those that are not cleared and persist over months – finally shift from permissive/productive to transforming infection which is accompanied by a massively deregulated expression of the E6 and E7 oncoproteins. The affected cells that had undergone cell cycle arrest are driven continuously into S-phase and finally shift from the production of viral infectious agents to an intensively supported proliferation (DOORBAR, 2005). The deregulated expression of the E6 and E7 oncoproteins therefore can be considered as the prerequisite for the establishment of precancerous lesions and the development of invasive cancer. The transformation zone of the cervix is preferentially affected by HPV-induced neoplasia. Here, the cells of the stratified squamous epithelium and the columnar endocervical cells converge, for which reason this area is also called the squamocolumnar junction. Under hormonal influence the transition zone during the female life cycle is subject to substantial anatomical changes and rebuilding processes with changing proportions of columnar and stratified epithelium (BURD, 2003).
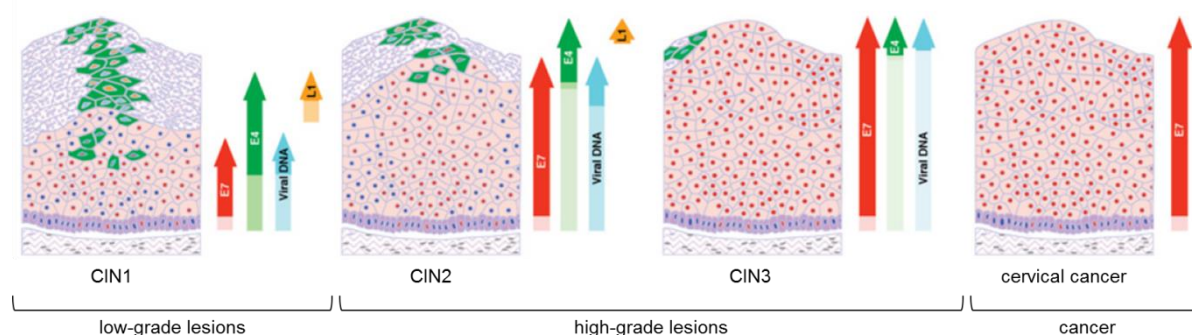
FIGURE 1.4   TRANSFORMING INFECTION IS INDUCED BY FUNDAMENTAL CHANGES IN THE VIRAL GENE EXPRESSION PATTERN. While the majority of low-grade lesions (CIN1) represent permissive infections with the underlying viral gene expression patterns described above, high-grade lesions (CIN 2 and CIN3) are characterized by an increasing proportion of cells with deregulated E7 expression which is accompanied by decreased expression of the early proteins involved in viral replication. This may be accompanied by the integration of the viral DNA into the host cell genome. In CIN3 and cervical cancers are characterized by more and more decreased or absent viral replication and increased E7 expression. Adapted from (DOORBAR, 2006).

Recently, a cell population retaining embryonic characteristics within the junction has been identified that is speculated to be particularly susceptible to HPV-induced carcinogenesis (HERFS et al., 2012). The occurrence of HPV-associated HNSCC at oropharyngeal sites, specifically the tonsils, could also be explained by the histologic characteristics of the lymphoepithelium of the tonsillar crypts. Here, the so called reticulated epithelium seems to be the preferred site for HPV infections (WESTRA, 2012).

The loss of the repressive effects of viral E2 on the early promoter p97 is considered to be the reason for the deregulated oncogene expression and leads to a massive up-regulation of E6 and E7 expression rates in higher lesion grade (Figure 1.4). Different events are discussed as underlying mechanisms for the loss of E2 function. One is the integration of the viral episome into the host's genome which disrupts the gene locus for E2 (VERNON et al., 1997). However, also cells with unintegrated, episomal viral DNA show E6 and E7 overexpression, a finding for which other, epigenetic mechanisms such as methylation of the E2-binding sites changing the binding affinities and thus the transcription rates might be responsible (CHAIWONGKOT et al., 2013).

The oncoproteins E6 and E7, once they are expressed, perfectly act together, complementing the functions of each other, to re-induce proliferation in terminally differentiated cells and to circumvent apoptosis at the same time.
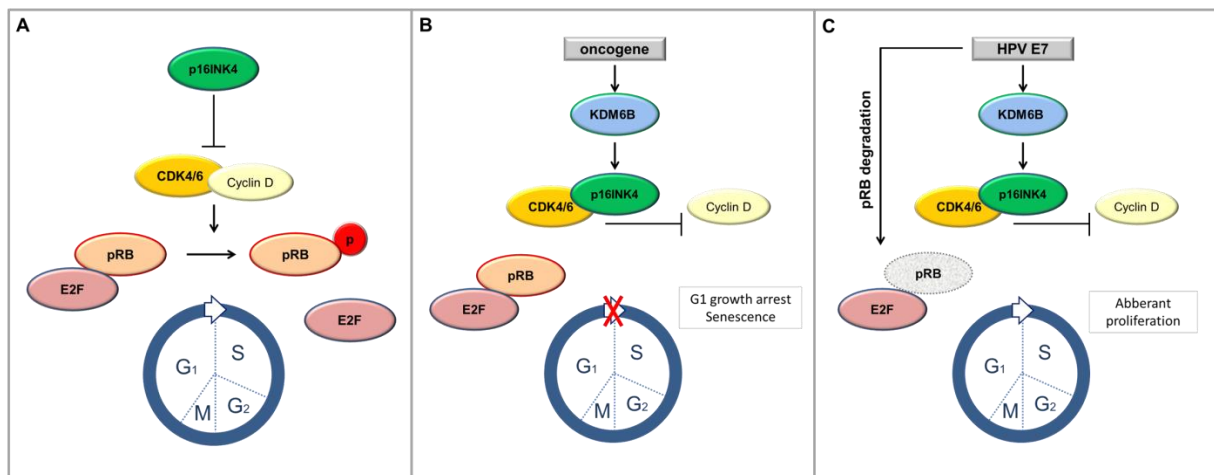
FIGURE 1.5   HPV16 E7 CIRCUMVENTS ONCOGENIC STRESS INDUCED CELL CYLCE ARREST BY TARGETING pRB FOR DEGRADATION. A) In normal cells CDK4/6 is negatively regulated by p16^{INK4a}. If absent CDK4/6 is activated by binding of cyclin D and phosphorylates pRB which is degraded. Loss of the suppressive subunit pRB activates the E2F transcription factor which mediates S-phase entry. B) Oncogenic stress induces KDM6B expression and increased p16^{INK4a} levels which inhibits CDK4/6 activity and phosphorylation of pRB, resulting in G1 cell cycle arrest and senescence. C) HPV E7 targets pRB for degradation and circumvents growth arrest. Adapted from (MCLAUGHLIN-DRUBIN and MUNGER, 2013).

Cell cycle progression, the transition from G1-phase to S-phase in dividing cells, is tightly regulated by the complex built of the cyclin-dependent kinase 4 (CDK4) and cyclin D. Under normal circumstances binding of the regulatory subunit cyclin D to CDK4 activates the complex and allows CDK4 to phosphorylate pRB which then dissociates from the E2F transcription factor. E2F migrates to the nucleus where it induces the transcription of genes necessary for cell cycle progression, such as cyclins A and E. In normal, non-dysplastic cells, the cyclin-dependent kinase inhibitor p16^{INK4a} negatively regulates the kinase activity of CDK4 and CDK6 by binding to them and inhibiting the

formation of active complexes with cyclin D. This prevents hyperphosphorylation and inactivation of pRB and the release of E2F transcription factors. Consequently, cells expressing p16^{INK4a} under normal conditions are retained in the G1 phase and do not enter S-phase (Figure 1.5) (MCLAUGHLIN-DRUBIN and MUNGER, 2013).

Due to the potency to drive host cells into S-phase which is crucial for the induction of the transforming infection stage, E7 directly contributes to carcinogenesis (reviewed in MCLAUGHLIN-DRUBIN and MUNGER, 2009). E7 is assumed to bind to the retinoblastoma (pRB) tumor suppressor thus interfering with the pRB pathway and abrogating the host's capacities to control cell cycle progression in the way similar to how other viruses achieve the same goal (JONES and WELLS, 2006). Binding of the E7 oncoprotein to pRB leads to the disruption of complexes built of pRB and transcription factors belonging to the E2F family (Figure 1.5). Although no external growth stimuli are present, E2F is released from pRB and activates other host cell proteins involved in DNA replication such as the cyclins A and E (DOORBAR, 2006). Furthermore E7 was demonstrated to interact with other proteins of the host's cell cycle regulation machinery, among others the activator protein 1(AP1) transcription complex (ANTINORE et al., 1996), histone deacetylases (LONGWORTH et al., 2005) and also the cyclin-dependent kinase inhibitors p21 and p27 (NOYA et al., 2001) are concerned.

Interestingly, during natural infection E7 does not always induce cell cycle progression in differentiated keratinocytes. In some cells which express high levels of p21 and p27 the CDKs seem to be resistant to oncoprotein effects as here E7 builds inactive complexes with cyclin E. Consequently, mitosis is induced only in cells that are characterized by low p21 and p27 levels or by E7 levels that are high enough to overcome the cycle arrest (DOORBAR, 2006).
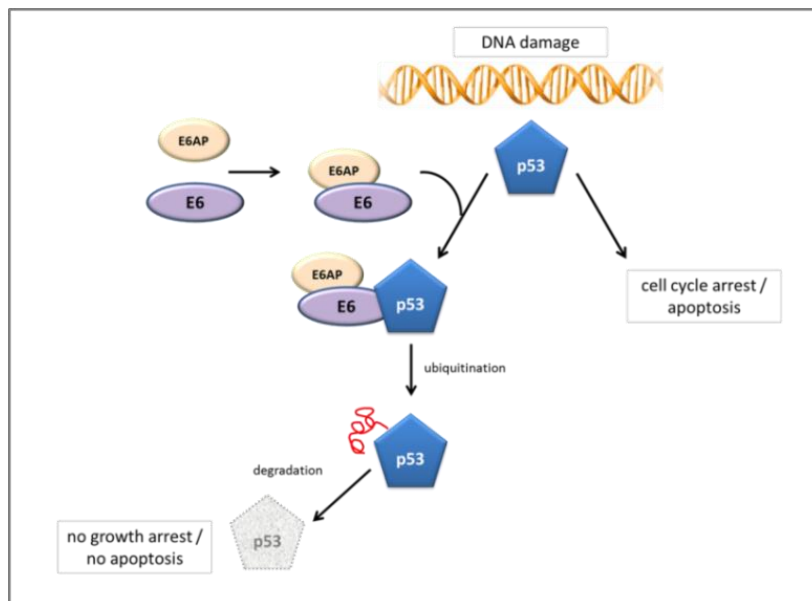
FIGURE 1.6   HPV16 E6 INTERFERES WITH THE P53 PATHWAY. Binding of E6 to p53 promotes its degradation and thus prevents cell cycle arrest and apoptosis. Adapted from (YIM and PARK, 2005).

The interference of E7 with the pRB pathway is complemented by E6 which abolishes the p53-mediated apoptotic signaling. Modulation of apoptotic pathways is a common and effective mechanism known from a number of oncogenic viruses and contributes to malignant progression (reviewed in FUENTES-GONZALEZ et al., 2013)). During transforming HPV infections, the cell-cycle entry of upper epithelial cells normally should lead to apoptosis mediated by ARF (ADP

ribosylation factor). However, under the influence of the viral oncoprotein E6 binding to E6AP (E6-associated protein) p53 is ubiquitinylated and degraded (DOORBAR, 2006). The interplay of E7 together with E6 impairing different host cell pathways leads to deregulated cell proliferation while the central apoptotic pathway is impaired. Apart from the interaction with p53 the viral E6 protein is also reported to target telomerase and different PDZ proteins involved in cell signaling and other cellular processes and thereby further supports transforming processes within the host cells (GANGULY and PARIHAR, 2009; WISE-DRAPER and WELLS, 2008).

The inhibition of central DNA repair mechanisms at the same time when host cells undergo deregulated DNA synthesis has massive further consequences on genome integrity and provokes additional genomic alterations (DUENSING and MUNGER, 2002).

In addition to the well-established mode of action of the viral oncoproteins E6 and E7 also E5 is discussed as another protein being involved in the development of cancers (reviewed in MIGHTY and LAIMINS, 2014)). One possible mechanism might be its ability to also inhibit ubiquitination and subsequent degradation of Bax and thereby preventing hydrogen-peroxide induced apoptosis (OH et al., 2010).

1.3.3   A biomarker for transforming infections: p16^{INK4a} overexpression

The expression of cyclin-dependent kinase inhibitor p16^{INK4a} is induced in aging cells and therefore a sign of senescence accompanied by cell cycle arrest and chromatin condensation. Its ability to prevent cells from further proliferation is of special interest in premalignant and malignant cells that have acquired genomic damages. In these cells p16^{INK4a} acts as a tumor suppressor preventing cell cycle progression and further accumulation of DNA damages. Due to the biological importance of the CDK inhibitor there seems to be an evolutionary pressure for loss of p16^{INK4a} gene function in neoplastic context. Indeed, many cancers of different sites show evidence of a functional loss of p16^{INK4a} by epigenetic modifications, deletions or point mutations. (LIGGETT and SIDRANSKY, 1998; ROCCO and SIDRANSKY, 2001).

In cervical intraepithelial neoplasia and carcinomas however, p16^{INK4a} is overexpressed. This can be directly linked to the deregulated oncogene expression and therefore p16^{INK4a} represents a well-established and recognized marker for transforming HPV infections (VON KNEBEL DOEBERITZ, 2002). In this context its biological function as growth arrest inducing protein is abolished by the viral oncoprotein E7 that inactivates the down-stream inhibitory signals of p16^{INK4a}. The overexpression of the viral protein E7 in dysplastic cells with underlying transforming HPV infection causes oncogenic stress to the host cell. This leads to an epigenetic remodeling particularly of the CDKN2a (p16^{INK4a}/ARF) gene locus and a substantially increased p16^{INK4a} expression.

Histone lysine methylation is one epigenetic mechanism involved in transcriptional activation and repression and for this reason plays a non-negligible role in cell cycle regulations. The enzymes involved in this epigenetic chromatin remodeling are histone lysine methyltransferases (KMTs) and demethylases (KDMs) that influence lysine methylation pattern of histones. The trimethylation mark at lysine 27 of histone H3 (H3K27me3) results in epigenetic silencing of the gene. The histone demethylases KDM6A (UTX) and KDM6B (JMJD3) however are able to remove the repressive methylation pattern and therefore are involved in transcriptional activation. The expression of the viral

E7 leads to oncogene induced stress (OIS) and transcriptional induction of histone demethylases KDM6A and KDM6B which remove the H3K27me3 mark. This results in epigenetic reprogramming by changing the levels of histone methylation of the p16IN4a/ARF gene locus and enhanced p16^{INK4a} expression (MCLAUGHLIN-DRUBIN et al., 2011).

Cells in the transforming infection stage however are not subject to p16^{INK4a} mediated cell cycle arrest and the cells continue to proliferate in presence of the overexpressed cyclin-dependent kinase inhibitor. This is explained by the interference of E7 with p16^{INK4a} downstream targets, namely pRB which is degraded under the influence of E7 activating the CUL2 pathway (HUH et al., 2007).

In this context, p16^{INK4a} therefore cannot be considered as a senescence marker anymore and remains without mechanistic relevance. It is rather a marker for the transforming processes ongoing within the virally infected host cells. The immunohistochemical staining pattern in these cases shifts from patchy in case of real senescence to strong and diffuse in dysplastic lesions (KLAES et al., 2001).
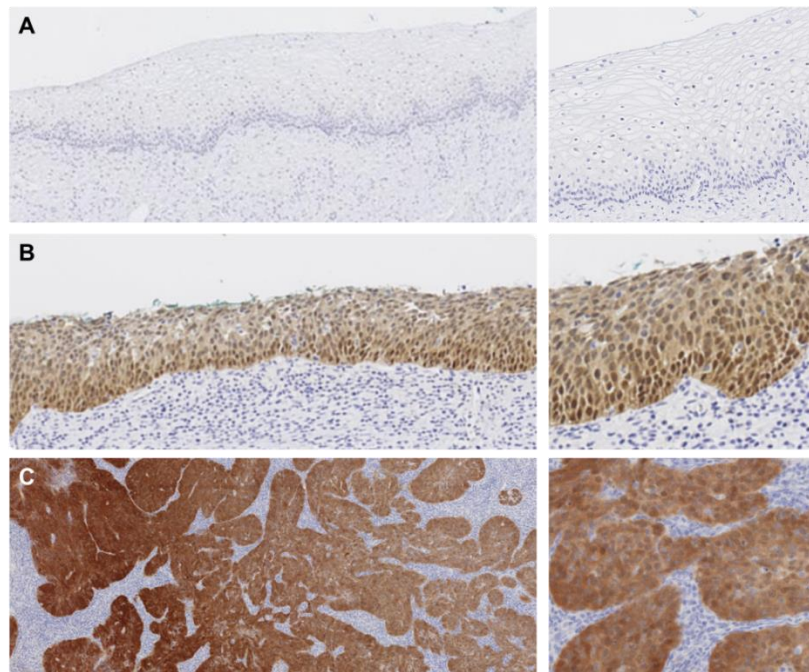
FIGURE 1.7   EXAMPLES OF p16^{INK4a} IMMUNOHISTOCHEMISTRY ON CERVICAL TISSUE SAMPLES: shown are representative examples of A) normal epithelium negative for p16^{INK4a}, B) cervical intraepithelial neoplasia (CIN3) with p16^{INK4a}-positive epithelium and C) cervical carcinoma with strong p16^{INK4a} staining. Details of the epithelium are shown on right side.

Recently published data (MCLAUGHLIN-DRUBIN et al., 2013) on p16^{INK4a} functions demonstrated that p16^{INK4a} overexpression is not only a bystander effect of oncogenic stress induced by HPV E7 protein and not a consequence of pRB inactivation by the viral oncogene, but is elementary to maintain the neoplastic phenotype and the continuous growth of cells with underlying transforming HPV infections. Dysplastic cells under the influence of viral E7 become dependent on KDM6B and p16^{INK4a} expression for survival.

1.3.4   Histomorphological classification of cervical precancers

In histomorphology, HPV-induced lesions are subdivided in three distinct progression steps and described by successive grade of cervical intraepithelial neoplasia (CIN) depending on the extent of morphological aberrations (MARTIN and O'LEARY, 2011). With increasing dysplastic cellular alterations beginning in the basal and suprabasal layers and eventually reaching throughout the complete epithelium the lesions are termed with increasing lesion grades from 1 to 3. CIN1 usually is described by the occurrence of so called koilocytes, indicating that viral replication is ongoing in the suprabasal layers of the epithelium. The altered cellular morphology concerns less than one third of the thickness of the epithelium. Lesions characterized as CIN1 are not yet considered as premalignancy in the narrower sense and therefore usually are not treated. With persistence and progressing disease cells with more severe dysplastic cellular alteration expand and may grow beyond the lower third of the thickness of the affected squamous epithelium and these lesions are named CIN2. The lesions that grow further and even beyond two thirds of the epithelium are referred to as CIN3 lesions (DARRAGH et al., 2013; RICHART, 1973).

The Histomorphological defined CIN grades cannot be translated unequivocally into the biological infection stages. CIN1 and a part of CIN2 lesions retain the capacity to undergo the normal squamous epithelial differentiation and thus for viral replication and represent the permissive (productive) infections. However, the control of the viral oncogene expression in basal and suprabasal cells may have already been lost in a part of CIN1. The vast majority of CIN2 lesions and virtually all CIN3 lesions are in the advanced transforming infection stage. Due to this discrepancy markers are needed to highlight the biological infection stage in biopsies. As it is directly link to oncogene activity $p16^{INK4a}$ overexpression represents a reliable biomarker to identify lesions that have quit productive infection and entered the transforming infection stage independently of their histomorphological appearance (BERGERON et al., 2014; VON KNEBEL DOEBERITZ et al., 2012).

1.3.5   HPV infection stages interpreted as a progression model
of cervical cancer

The cervical carcinogenesis can be subdivided in clearly defined successive steps (Figure 1.8). Latent infections (step 1), during which the viral DNA has been replicated yet, usually remain clinically innocuous and are characterized by basal infected keratinocytes that divide continuously to establish a reservoir of cells harboring the episomal viral DNA. Permissive or productive infections (step 2) are characterized by viral replication cycles which become induced in suprabasal differentiating epithelial cells. This stage is accompanied by the occurrence of visible low-grade lesions. Here, the viral proteins are expressed - with E6 and E7 under transcriptional control -, viral DNA is synthesized and finally viral particles are released. In case of persistent HPV infection the lesions may progress towards the transforming infection stage (step 3) which is accompanied by a fundamental shift in the viral gene expression pattern with E6 and E7 oncogene overexpression as described in chapter 1.3.2.

This shift is the key event for the development of high-grade precancerous lesions and cancers with critical host cell pathways being reprogrammed to overcome the cell cycle arrest of fully differentiated cells and promote the proliferation of these keratinocytes.

With regard to the histomorphological classification precancerous stages are graded from CIN1 lesions to CIN2 and CIN3 depending on the severity and the extent of the affected epithelium as described in chapter 1.3.5. Thereby CIN1 overlaps with both biological categories with the majority of them representing permissive infections and a smaller proportion of them being in the transforming infection stage.

As the shift to E6 and E7 oncogene overexpression is accompanied by the induction of p16^{INK4a} overexpression (chapter 1.3.4) in the affected cells p16^{INK4a} is a surrogate marker for transforming processes ongoing under the influence of the viral oncoproteins that interfere with the host cell replication machinery and tumor suppressors. A strong p16^{INK4a} expression can be detected in around 40 % of low-grade lesions, the vast majority of high-grade lesions and virtually all cervical cancers (DARRAGH et al., 2013; TSOUMPOU et al., 2009). As it is consistently expressed along with viral proteins E6 and E7 it represents an interesting target for immune therapies.

Although virtually all cervical cancers can causally be linked to human papillomaviruses, a woman who is infected does not inevitably develop a precancerous lesion and cancer. Most of the HPV infections are cleared spontaneously within several months. Only a long-lasting persistent HPV infection may lead to the development of precancers which is a rare event. The natural history of HPV infections and the development of premalignancy and eventually cancer can be considered a dynamic process in opposite directions, progression and regression. With more than 90% of HPV infections being cleared within 2 years only a small percentage of women originally infected will develop a precancerous lesion (SCHIFFMAN and WENTZENSEN, 2010). And also established CIN lesions show a clinically heterogeneous behavior: Here again, only a part of them will further progress towards higher lesion grades and the majority of them (60% of CIN 1 and 40% of CIN2) will regress in dependence of the host's immune surveillance capacities (MCCREDIE et al., 2008; OSTOR, 1993). Even CIN3 lesions with extensive morphological abnormalities are reported to regress to a certain extent (MUNK et al., 2007).

There are sporadic reports on a higher progression risk of p16^{INK4a}-positive CIN1 compared to the p16^{INK4a}-negative ones (WANG et al., 2004). Nevertheless high-grade lesions, although they are all in the transforming infection stage and thus all show p16^{INK4a} overexpression, do not all progress. This demonstrates that p16^{INK4a} which is a reliable surrogate for oncoprotein activity and the biological infection stage cannot predict progression of a lesion and other markers are necessary for the development of a prognostically relevant tool.

The prevalence of HPV-infection is highest in young women aged 15-25, and the mean age of women diagnosed with high-grade cervical lesions is approximately 28 years, while invasive cervical cancer is established much later in women aged approximately 50 years at time of diagnosis (DOORBAR, 2006). Only a part of the precancerous lesions persist, progress and grow further out over time to bigger lesions and to higher precancerous stages and finally only the minority of individuals that have acquired a HPV-infection during their life time develop cancer. This demonstrates that cervical carcinogenesis as very slow process. Considering these clinical characteristics one might speculate that

accumulation of genetic changes of the host in combination with predisposing factors might be decisive for whether a tumor develops or not.

The progression towards cancer could biologically be explained by accumulation of specific cellular and chromosomal changes and subsequent outgrowth of distinct cell clones. It has been demonstrated that the viral oncoprotein overexpression affects the integrity of the host genome in different ways:

Both oncoproteins E6 and E7 are able to cause major numeral and structural chromosomal aberrations and also DNA damages (DUENSING and MUNGER, 2002). These changes are caused by disruption of the centrosome duplication control mechanisms and the simultaneous induction of multiple spindle poles (KORZENIEWSKI et al., 2011). The resulting mis-segration of chromosomes and aneuploidy of the host cells contribute to further genomic aberrations. Although deadly for most of the cells raising during such process this might generate some cells with growth advantage and lead to the outgrowth of these cell clones (DUENSING and MUNGER, 2002; KORZENIEWSKI et al., 2011).
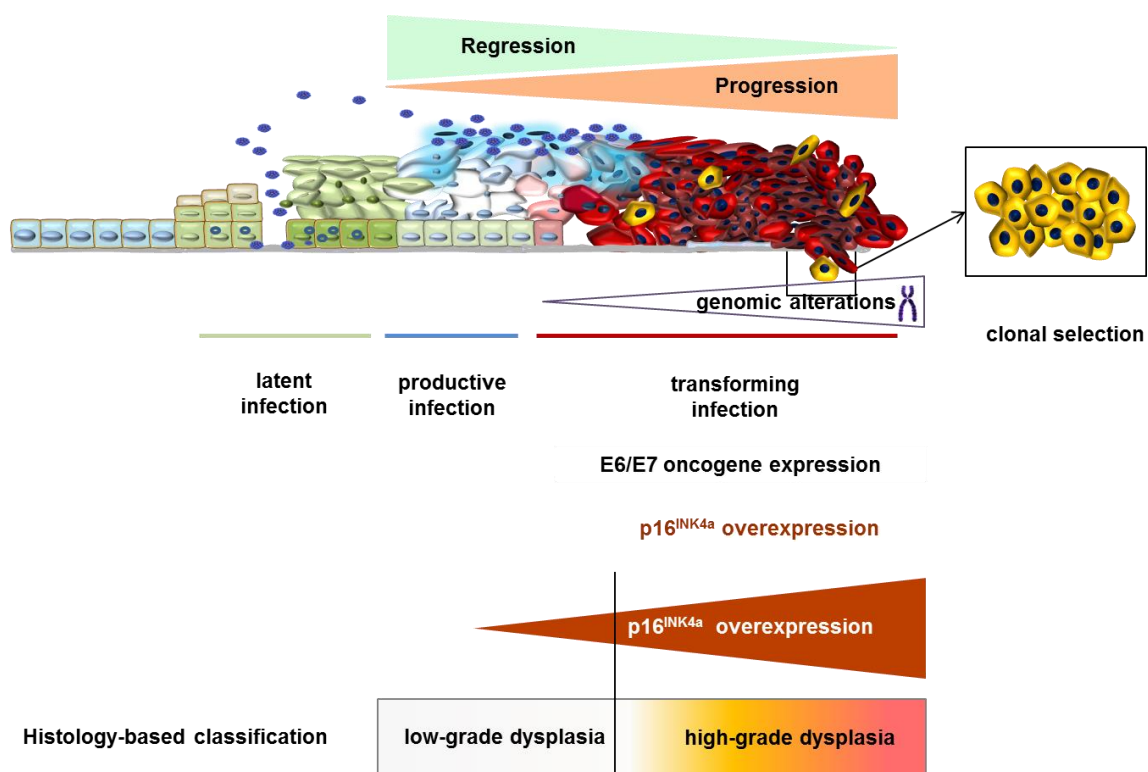
FIGURE 1.8   CERVICAL CANCER PROGRESSION MODEL. Cervical carcinogenesis is a characterized by successive biological infection. It is, however, a dynamic processes as lesions also can undergo regression. Persistent transforming infection is accompanied by accumulation of secondary genomic alterations that might provide distinct cells with growth advantage. Selection for these cell clones and expansion leads to tumor growth and invasive disease. The transforming infection stage is highlighted by p16[INK4a] overexpression. Histomorphological classification represents a two-tiered system that does not match the biological infection stages totally as transforming infections can be observed in a proportion of low-grade lesions already. Adapted from (DOEBERITZ and VINOKUROVA, 2009a).

Studies that are based on comparative genomic hybridization report on different genomic changes in cervical squamous cell carcinoma such as gains at chromosome 3q, losses at 3p and losses at 11q with the aberrations mainly located at the terminal chromosomal regions. In cervical precancerous stages there are also chromosomal aberrations, with increasing frequency from low-grade CIN to high-grade

lesions and finally cancer. The same gains and losses affecting 3p, 3q and 11q of cervical squamous cell carcinoma are already present in high-grade lesions, however at a lower frequency. Genomic copy number alterations have substantial effects on gene dosage that may involve overexpression of oncogenes on the one side and decreased expression of tumor suppressor genes on the other side. As the above described changes of different chromosomal regions are all present in SCC one might speculate that these aberrations provide growth advantage for tumor cells and are selected during cervical carcinogenesis (reviewed in THOMAS et al., 2013).

The chromosomal instability of keratinocytes is likely to induce secondary genomic alterations that may give rise to cells having distinct features providing them with growth advantage (BECKMAN and LOEB, 2005). During continued persistence these cells are further selected by evolutionary mechanisms leading to clonal expansion of cells that are adapted best to the host's immunologic environment.

Still, the causal relationship between integration of the viral genome and induction of chromosomal instability leading to further genomic alterations is discussed controversially. Different hypotheses/concepts regarding the chronology of the events may be discussed: On the one hand integration of the viral DNA is hypothesized to be the first event leading to genomic rearrangement and for this reason is responsible for chromosomal instability and aneuploidisation (HOPMAN et al., 2006; PETER et al., 2010; PETT et al., 2004). On the other hand genomic instability is considered to be an early event and rather prepares the integration of the viral DNA by creating fragile chromosomal sites (DUENSING and MUNGER, 2004; MELSHEIMER et al., 2004, reviewed in WENTZENSEN et al., 2004). Nonetheless, cervical carcinogenesis can be seen as a multi-step process including deregulation of viral protein expression and breakthrough of the host's cell cycle machinery finally leading to chromosomal instability, accumulation of DNA damages and secondary (epi)genetic alterations that altogether favor the outgrowth of cancer cells (SNIJDERS et al., 2006).

Whatever the chronological succession is, chromosomal instability seems to be the decisive event for the onset of malignant processes and the transition from precancerous lesions to invasive disease (BIGNOLD, 2002, 2003). The resulting destabilizing effects of aneuploidy in terms of chromosome synthesis, segregation and repair during mitosis lead to further secondary genomic changes giving rise to a huge number of cells provided with different characteristics (reviewed in DUESBERG et al., 2011). Those that are best adapted to the environment of their host, especially the immunologic environment, will survive and undergo clonal expansion and thus promote carcinogenesis.

An effective immune response is considered to be crucial for the clearance of infections and for regression of established lesions. Considering the complexity of the immunobiology of HPV infections (described in section 1.4.1) and the multitude of mechanisms developed by the virus to circumvent the host's immune attack (see "immune evasion", section 1.4.2) it appears that secondary genomic alterations are likely to affect mechanisms that contribute to immune tolerance or immunosuppression and that enables the virus to remain undetected. Another frequently observed genomic loss (LOH) is that at 6p21.3 locus which harbors the genes for HLA class I antigens (CHATTERJEE et al., 2001; KERSEMAEKERS et al., 1999). This results in MHC-class I down-regulation which substantially contributes to impaired antigen presentation and recognition by immune cells that could eliminate HPV infected or precancerous cells, such as cytotoxic T cells (CTLs). Other secondary genomic changes that alter the immunological features also might contribute to survival and growth advantages of cells which undergo clonal selection to finally grow out to precancerous lesions

and invasive cancers. The HPV-transformed cells within these lesions and tumors are able to circumvent the host's immune attack by different mechanisms and therefore constitute the "immune evasion phenotype".

Considering the fact that all projects of this thesis are centered on questions of immunology, the following chapter will address different immunologic aspects in general and in particular related to HPV-infections.

1.4   The immunobiology of HPV infections

1.4.1   The role of the host's immune system in the defense against HPV

The host's immune system plays a crucial role in whether a HPV infection persists or is cleared and whether a developing lesion regresses spontaneously or persists and finally leads to invasive cancer. It has been demonstrated that immune deficiency and immunosuppression of allograft transplanted patients increase the risk for persistence of the precancerous disease and development of cancer (DENNY et al., 2012; PALEFSKY, 2009). In contrast, cytotoxic T lymphocytes (CTLs) are associated tumor control and a decreased risk for cancer (MATSUI et al., 1999). The presence or absence of distinct immune cell phenotypes in the lesion and the surrounding tissue is considered to be highly important for the prediction of the clinical outcome of the patients and should be considered in the treatment plans as a prognostic parameter.

The following sections will address the different arms – innate and adaptive - of the immune system and their role in HPV-related diseases.

INNATE IMMUNITY AND HPV

The innate responses represent the first line defense against invading pathogens and comprise mechanisms that, in contrast to adaptive immune responses, act independently from antigen specificity. Activation of the innate immune system leads to an immediate reaction without establishing however an immunologic memory of the encountered pathogens (MOGENSEN, 2009). Cells of the innate immune system recognize highly conserved molecular patterns that are shared by many different pathogens leading to a general activation of the immune system. Here, Toll-like receptors (TLRs) play an important role (HEINE and LIEN, 2003) which will be explained in more detail in section 1.4.x. Cells of the innate immune system comprise dendritic cells (DCs) and Langerhans cells (LCs) which are professional antigen-presenting cells (APCs), and also macrophages, natural killer (NK) cells and natural killer T (NKT) cells. They release pro-inflammatory cytokines and thereby substantially change the immune milieu of the infection site by attracting further innate immune cells and, in a second step, by induction of the adaptive immune response (JANEWAY and MEDZHITOV, 2002). Antigen-processing and cross-presentation by DCs and LCs enable T lymphocytes to get activated and to perform their tasks as cells of the adaptive immune system (reviewed in AMADOR-MOLINA et al., 2013).

NK cells are an important cell type mediating innate immunity as they are able to recognize abnormal cells, for example by aberrant Human Leukocyte Antigen (HLA) class I molecule expression. NK cell-

mediated cytotoxicity which is induced upon stimulation of activating NK cell receptors such as NKp30, NKp46 and NKG2D then eliminate these virally infected or precancerous cells (reviewed in AMADOR-MOLINA et al., 2013).

In the setting of established HPV-associated precancers and cancers however, many innate immunity mechanisms are impaired, such as cytokine release, antigen-presentation by LCs and type I interferon (IFN)-responses favoring the persistence and progression of the lesions and carcinogenesis, that will be explained in more detail in section 1.4.2 (reviewed in STANLEY, 2008).

HUMORAL IMMUNE RESPONSE TO HPV

The viral protein that most potently induces antibody responses in patients with underlying HPV-infections is the late protein L1. However, titers of neutralizing antibodies remain relatively low in naturally occurring HPV infections. This might be due to mechanisms developed by the virus to evade recognition and elimination by the host's immune system that will be discussed in chapter 1.4.2. These immune evasion strategies prevent the induction of a strong immune response (STANLEY, 2008). HPV infections studied in animal models revealed that even low antibody titers provided protection against subsequent HPV infections. The observation that the protective characteristics of these sera could be transferred to other individuals gave rise to the development of the currently used prophylactic vaccines that use L1 of different HPV-types as an immunogen in a bivalent (Cervarix®, HPV16 and 18) and a quadrivalent formulation (Gardasil®, HPV 6, 11, 16 and 18) (reviewed in STANLEY, 2006).

T CELL MEDIATED IMMUNE RESPONSE TO HPV

T lymphocytes can - independently of antigen-specificity - be quantified as different T cell subtypes in the epithelium where the lesion or the tumor is located and the adjacent stromal compartment which is generally characterized by higher densities of immune cells (GUL et al., 2004; SHAH et al., 2011). T cell phenotypes that could be relevant in the course of HPV infection and development of precancerous lesions belong to different arms of the immune system and might contribute to either an effectively mounted response against the infected keratinocytes or to immune suppression and T cell anergy and thus to disease progression (GARCIA-CHACON et al., 2009; PATEL and CHIPLUNKAR, 2009). Immune markers that provide information about the quality of the immune cell composition in the locally confined regions around the lesions include different T cell markers: CD3+ T cells generally are quantified in order to obtain information about the total T cell numbers present in the affected tissue. To define the proportions of different specialized T cell subpopulations the total infiltrate consists of, other markers might be interesting: CD4 is generally used to characterize T helper cells whereas CD8 identifies the presence of cytotoxic T lymphocytes (CTLs) that can further be characterized by Granzyme B (GranB) which is typically expressed in activated, granzyme-producing CTLs (BONTKES et al., 1997; NEDERGAARD et al., 2007). Forkhead box transcription factor 3 (Foxp3) however is a marker for regulator T cells (T_{reg} cells) and rather indicates the activation of the opposite, immunosuppressive arm of the immune response (WU et al., 2011). CD3 ζ-chain is a dimeric signal transducing molecule of the T cell receptor (TCR) that is responsible for the activation of T cells following binding to and recognition of HLA-bound antigens. It therefore is

considered to be a parameter for the successful T lymphocyte activation and effectiveness of the T cell-mediated immune response (WHITESIDE, 2004).

With regard to the first approach, previous cross-sectional studies evaluating the densities and phenotypes of tissue infiltrating T cells in general report on elevated numbers of different T lymphocyte subtypes, such as CD3+ T cells, cytotoxic CD8+ CTLs and also T_{reg} infiltration, with increasing histomorphologically defined CIN stages (EDWARDS et al., 1995; NEDERGAARD et al., 2007) (ADURTHI et al., 2008; WU et al., 2011). However, only the minority of CTLs in CIN is reported to be in the activated, GranB-expressing state (BONTKES et al., 1997). Single studies also report the inverse correlation between global T cell infiltration and histomorphologically defined stages (SILVA et al., 2010). Regulatory T cells are considered to exert immunosuppressive functions in the microenvironment and are reported to be increased in high-grade lesions and invasive cancer and might contribute to the progression of the lesions towards cancer (ADURTHI et al., 2008; JAAFAR et al., 2009; NAKAMURA et al., 2007; WU et al., 2011) and (reviewed in PATEL and CHIPLUNKAR, 2009). Down-regulation of CD3 ζ-chain expression has been demonstrated in different tumor entities such as melanoma (DWORACKI et al., 2001), head and neck cancers (KUSS et al., 1999) and also colorectal carcinomas (NAKAGOMI et al., 1993) which emphasizes (NAKAGOMI et al., 1993)its relevance for disease progression. However, the data published for cervical cancer and its precancerous lesions are way scarcer (ZEHBE et al., 2002). Interestingly, CD3 ζ-chain expression was found to be down-regulated in cervical carcinoma patients compared to healthy controls but not in precancerous lesions.

These previous studies on T cell infiltration reported on varying cell densities and phenotypes in correlation with histomorphological disease stages without taking however into consideration the underlying biological infection status defined as non-transforming and transforming infections. Therefore, it has been remained unclear until now whether these changes are induced with beginning transforming infections in low-grade lesions or rather occur later in well-established high-grade lesions that have accumulated secondary genomic alterations and clonal selection.

The density and phenotype of tissue infiltrating T cells has been reported to correlate with outcome in various cancer types (GALON et al., 2006) and it is conceivable that the quantity and the quality of immune cells in CIN is of prognostic importance.

With regard to the characterization of antigen-specific T cells in HPV-related cervical precancers and cancers data are published for peripheral as well as for tumor-infiltrating T cells. T cells specific for HPV-antigens are rare, however several studies demonstrated that at low frequencies they exist.

The immunogenicity of the viral Ll proteins that is able to induce a humoral immune response is also reported to contribute to proliferative T cell responses. Both T cell subtypes, CD4+ and CD8+ T cells were shown to contribute to the cellular immunity (PASSMORE et al., 2002). However, CD4+ T lymphocytes were characterized by a higher IFN-γ release upon stimulation with L1-peptides demonstrating that the antigen is able to induce a T helper cell type 1 (Th1) memory response that enhances the mechanisms of the cell-mediated immunity (SHEPHERD et al., 1996). Interestingly, T cell responses predominated in patients who had cleared the HPV infection or resolved precancerous lesions and one could speculate that CD4+ memory T cell responses are established during the battle against HPV infections and also provide long term protection (CHAN et al., 2011). Conversely, patients with advanced persisting or progressing precancerous lesions lack pro-inflammatory cytokines

(DE VOS VAN STEENWIJK et al., 2008) and although isolated from tumors and lymph nodes of cervical cancer patients CD4+ and CD8+ T cells show only low levels of IFN-γ release upon stimulation with HPV antigens (DE VOS VAN STEENWIJK et al., 2010).

This again is indicative for the inability of these patients to mount an effective T cell-mediated immune response leading to functionally inactive or even immunosuppressive T cell fractions invading the tumors and circulating in the peripheral blood. Factors that might contribute to the impairment of the host's cellular immune response and the inability of these patients to clear the infection and thus prevent malignancies will be highlighted in the following section (1.4.2).

The published data imply that antigen-specific cellular immune responses is associated a successful establishment of immune response against HPV and clearance of the infection and thus occurred in patients whose immune system successfully raised an immune response against HPV. Also the lack of IFN-γ secretion, the cytokine directing cellular cytotoxic responses, suggests that immunosuppressive mechanisms inhibit the raise of an effective cell-mediated immune response and immune attack of the lesions and tumors. This might be an interesting starting-point for therapeutic interventions.

1.4.2   Immune evasion strategies developed by human papillomaviruses

Human papillomaviruses have developed different immune escape mechanisms allowing them not only to modulate the host's immune response that might be raised during infection and establishment of precancerous lesions but also to avoid to be recognized and to remain largely invisible for the host's defense mechanisms. The viral life cycle regarding the site of infection and also the viral replication within the epithelium is perfectly adapted to assure immune ignorance (reviewed in KANODIA et al., 2007 and STANLEY, 2012a).

In general, the infection site is located in the basal cell layer of the stratified squamous epithelium and occurs via microlesions in the tissue giving the virus access to the basal stem cells. During permissive infection the viral genome is maintained in that cell layer at low copy numbers which minimizes the antigen exposure for immunocytes that could potentially invade the epithelium from the stromal tissue beneath. The expression level of the viral proteins, especially the early proteins, remains very low during replication (Figure 1.9). The protein considered to be most immunogenic, the viral capsid protein L1, is not expressed in the basal, undifferentiated layers of the squamous cell epithelium. As only in the upper layers of the squamous epithelium, which circulating immune cells hardly have access to, the viral proteins become expressed at higher levels, and an effective immune response cannot be initiated. The low expression level of HPV proteins in epithelial layers that are closer to immune cells thereby represents an effective immune evasion strategy (FELLER et al., 2010). Furthermore, the assembled virions are released during naturally occurring cell death of differentiated keratinocytes arriving at the upper side of the epithelium and not due to cytolysis or necrosis of the infected host cells. Again, this strategy prevents stromal or epithelial immune cells from having direct contact with the infectious agent and also inhibits inflammation at the infection site. The non-lytic life cycle of HPV does not provoke release of pro-inflammatory cytokines and supports the virus' invisibility to the host's immune defense (STANLEY, 2006). Altogether the viral replication cycle is perfectly adapted to the differentiation of the host's keratinocytes with the aim to reduce antigen exposure and pro-inflammatory mechanisms and thereby to avoid an effective immune response to be

raised. At a later time point, the interaction of the viral proteins E6 and E7 with host cell pathways regulating apoptosis and cell cycle progression contribute to the survival of the virus within keratinocytes by preventing apoptosis and delaying the differentiation program of keratinocytes that consequently remain in the proliferative phase (chapter 1.2).
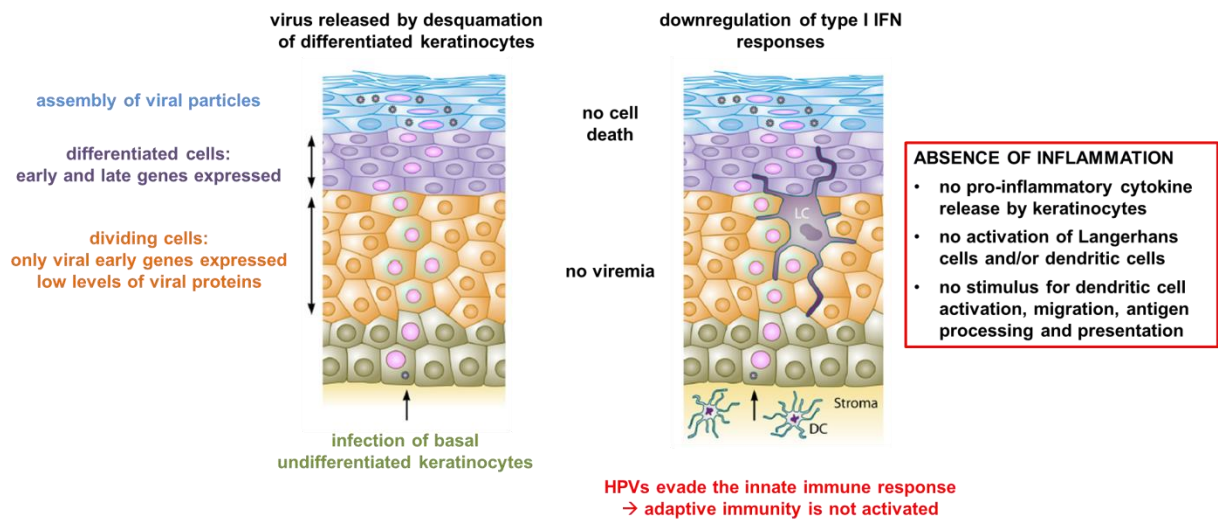
FIGURE 1.9   HPV EVADES THE HOST'S IMMUNE SYSTEM. The virus' life cycle (left) is adapted to the host cells' differentiation program and thus prevents immune recognition: there is no blood-born phase, low viral protein levels in the basal cell layers, no cell death for viral release. Furthermore, HPV actively down-regulates inflammatory processes (right) preventing thus the activation of innate and adaptive immune responses by different mechanisms. Adapted from (STANLEY, 2012a).

Also the fact that the viral genome is not optimized for the mammalian translation machinery and shows a different codon usage that results in decreased translation rates of the viral proteins might explain the low expression profile of viral antigens (reviewed in ZHAO and CHEN, 2011). Furthermore, a mechanism that can be subsumed under the keyword "molecular mimicry" contributes to immune evasion by hindering recognition by and reactivity of immune cells (OLDSTONE, 1998). It has been demonstrated that human papillomavirus proteins display similar epitopes compared with the host cell proteome that leads to less effective immune response due to self-tolerance mechanisms of the host's cells (NATALE et al., 2000).

The immune evasion strategy of HPV does not only include adaptions to remain invisible for the host's immune system but also includes strategies evolved to actively counteract immune responses that are raised by the host.
Immune tolerance and immune suppression per se are important and helpful mechanisms in the regulation of the different arms of the immune system and balance the activation and termination of immune attacks. Mediators of immune suppression such as regulatory T cells are inherent to the immune defense and have evolved to prevent damages by excessive cytotoxic responses especially if they are directed against self-antigens. Adopted by tumors, however, immune tolerance or suppression are mechanisms that enable cancer cells to evade the host's immune attack. They become able to modulate the tumor environment in order to create an immunotolerant micromilieu and thereby to immobilize the host's immune responses.

Chemokines and cytokines are signaling molecules and the key players in the regulation of a complex immunologic network of activating and inhibitory immune responses. They are decisive for the immune cell types attracted to the lesion and the outcome of the immune response. Immune evasion strategies developed by tumors that involve aberrant cytokine or chemokine secretion do not only have singular but rather systemic effects on different immunological pathways. The most immediate effect of HPV infections is the down-regulation of type I IFN responses inhibiting antiviral innate immune defense mechanisms and also the induction of a secondary adaptive response (Figure 1.9). Type I IFN, especially IFN-α, is normally produced by infected cells, has anti-viral effects and also recruits neutrophils, macrophages, NK cells and DCs to the infection site (BASLER and GARCIA-SASTRE, 2002). Its activation is necessary to induce both the innate and the adaptive immune response. The viral oncoproteins have been shown to interact with IFN signaling pathways that normally lead to transcriptional induction of IFN downstream target genes necessary for anti-viral defense, induction of immune response and cell growth regulation. Both E6 and E7 directly interfere with IFN downstream targets (IFN response genes, nuclear factor-kappa B (NFkB)) and signaling pathways to prevent IFN-mediated immune responses. They inhibit among others the transcription of transporter associated with antigen-processing 1 (TAP-1), IFN-β and monocyte-chemoattractant-protein-1 (MCP-1) and interfere with the Jak-STAT-pathway that upon activation regulates DNA transcription and is also involved regulating the activity of immune cells (reviewed in STANLEY, 2008). Further chemokines, such as interleukin (IL)-8, and cytokines (IL-18, IFN-γ) are suppressed in HPV-infected cells. Normally involved in the onset of the inflammatory responses and attracting different sorts of immune cells such as monocytes, memory T cells, NK cell or being involved in the priming of CD8+ T cells the down-regulation of these molecules favors the persistence of the viral infection and the development of precancerous lesions (reviewed in STANLEY, 2012a). Changes of the polarity of the Th1/Th2 cytokine profile to a pronounced Th2 response has also been demonstrated to have immunosuppressive effects and to result in impaired cytotoxic immune responses (BAIS et al., 2005). Such a change is accompanied by reversal of the immune cell composition in precancerous stages and cancers as demonstrated by immunohistochemical analyses and also flow cytometry data (ADURTHI et al., 2012; SHAH et al., 2011).

HPV infection also has effects on antigen presentation via HLA class I molecules. It has been shown several times independently that the viral early proteins E7 and E5 are associated with HLA class I antigen expression on keratinocytes and this impairs recognition of the infected cells by CD8+ T lymphocytes and the induction of a cytotoxic response (BOTTLEY et al., 2008; CAMPO et al., 2010). Theoretically, down-regulation of HLA class I molecules on the cell surface increases the susceptibility to be killed by NK cells. However, as the immunosuppressive cytokine IL-10 is also associated with HLA class I down-regulation (RODRIGUEZ et al., 2012), it is likely that the keratinocytes evade a possible NK cell-mediated immune attack due to the generally immunosuppressive micromilieu probably disturbing the recruitment of immune cells to the lesion. It could be demonstrated that E5 and the oncoprotein E7 both directly regulate HLA class I expression levels (reviewed in KANODIA et al., 2007). The interaction of E7 with the promoter of the HLA class I heavy chain gene has repressive effects on the transcription and leads to down-regulation of HLA class I antigen levels (GEORGOPOULOS et al., 2000). Viral E5 in contrast affects the stability and the transport of HLA class I complexes loaded with peptides that both depend on an acid pH: via interaction with the $H^{(+)}$-ATPases (V-ATPase) it inhibits the acidification of endosomes and the Golgi

complex and thus massively disturbs peptide-HLA-complex trafficking to the cell membrane (ASHRAFI et al., 2005; SCHAPIRO et al., 2000).

Down-regulation of type I IFN production is associated with lacking antiviral innate immune defense mechanisms and consequently inhibition of a secondary adaptive response. It was shown that the initiation of any of these responses by antigen-presenting cells (APCs) is defective because Langerhans cells, the specialized epithelial APCs, are decreased in number and are not activated during HPV-infections and uptake of L1 antigen, leading to inhibition of both innate and adaptive immune response (STANLEY, 2008). Different mechanisms are discussed to contribute to this lacking LC activation: (1) E-cadherin expression in keratinocytes which is required for APCs to migrate through the epithelium is down-regulated under the influence of DNA methyltransferase 1 activity (Dnmt1) (LAURSON et al., 2010). (2) The inhibition of a HPV-specific immune response in the epithelium is caused by activation of phosphoinositide-3-kinase pathway (FAUSCH et al., 2005).

(3) Immunosuppressive cytokines (transforming growth factor (TGF)-β, Fas-ligand) may be released, that among other effects are responsible for the recruitment of regulatory T cells (T_{reg} cells) that again change the cytokine milieu in the lesions by releasing TGF-β and IL-10. This release inhibits thereby the functional activity of CTLs and in the long run favor a deficient recognition of and cytotoxicity against HPV-infected and transformed cells and promote the outgrowth of the lesions and progression towards cancer.

Altogether, these factors inhibit the influx of immune cells into the epithelial compartment, impair the migration and thus lead to a decreased likelihood that immune cells detect HPV and initiate an effective immune response.

Importantly, the rates of HPV clearance and lesion regression proof that in the majority of the patients the immune system is able to combat the disease and that the quality of the immune system, either humoral (mainly against L1) or cell-mediated (against late or early viral proteins), is decisive in the natural course and also treatment of cervical intraepithelial neoplasia and cancers. Immunotherapeutic inventions therefore should aim at the activation of a strong, T cell-based immune response that may induce destruction of HPV infected keratinocytes by CTLs either by recognition of tumor antigens or tumor-associated antigens.

Also, the composition of the T cell infiltrates and the cytokine profile in the microenvironment may be indicative for the clinical course of the disease and the patient's outcome and therefore represent potential markers for progression or regression. They also contain information that could potentially be considered for treatment decisions in precancers in order to minimize unnecessary surgical interventions in patients that - from their immune status - are likely to overcome the disease.

1.5 Immunologic intervention strategies in HPV-associated diseases

1.5.1 The urgent need for therapeutic interventions in HPV-associated precancers and cancers

The prophylactic L1 VLP based vaccines Cervarix and Gardasil aim at the induction of a systemic immune response and are based on the production of neutralizing antibodies floating the whole body. The represent, however, HPV type-specific approaches and are considered - aside from sporadic reports on cross-protection - to offer protection against only two high-risk HPV types, HPV16 and 18, (reviewed in KAWANA et al., 2009). Also, they do not have any known advantageous effects on preexisting HPV infections or established lesions.

A recently developed mathematical model can be used to estimate the impact of the prophylactic vaccines on the development of the incidence of HPV-associated cervical precancers and cancers and also anogenital warts. This model is based on epidemiological information of the natural history of HPV infections, the frequency and natural history of HPV-infections and resulting precancerous lesions and considers also cervical cancer screening program implemented in Germany. This model predicts that with a vaccination coverage of about 50% only, which reflects the actual situation in Germany, over the next 100 years about 22% of cervical intraepithelial neoplasia and 37% of cervical cancers will be prevented by the available prophylactic vaccines (HORN et al., 2013).

These data demonstrate that the situation within the next 20-30 years will not substantially change and that cervical precancerous lesions and cancers as well as anogenital warts still are a major health problem to resolve. Therefore, there is a non-negligible need for secondary vaccination strategies or other approaches enabling the immune system to recognize and eliminate HPV-infected and transformed cells. In contrast to primary vaccines, secondary therapeutic intervention strategies aim at establishing an effective cellular immunity and especially enhancing the T cell responses to antigens expressed by HPV-infected cells that additionally might undergo transforming processes (BRINKMAN et al., 2007). A multitude of secondary vaccination approaches is under investigation in preclinical trials and some are investigated in clinical trials (reviewed in ALBERS and KAUFMANN, 2009 and KANODIA et al., 2008).

It has been reported that the majority of the therapeutic vaccination trials only sporadically induce an efficacious clinical response accompanied by cytotoxic cellular responses that might be able to overcome the viral evasion mechanisms and subvert immune suppression. Some other approaches led to promising results in patients with vulvar precancerous lesions but rarely in cervical intraepithelial neoplasia. This might be due to special features of the mucosal immunity in comparison to the epithelial immune reactions in VIN that hinders the induction of cellular response upon systemic vaccine administration (reviewed in KAWANA et al., 2012).

For these reasons other approaches, alone or in combination with the above described therapeutic vaccines represent an interesting option to enhance the host immune reaction, also at mucosal sites in order to elicit a strong T cell mediated immune response. One of these treatment strategies involves immuno-modulatory agents that modify the quality of the immune response and reverse the immunosuppressive environment. The following chapter is dedicated to Toll-like receptors that can be targeted by specific immuno-stimulatory compounds. Once they are activated by these compounds

they are able to link innate and adaptive immune responses to finally induce a strong anti-viral and anti-tumoral cellular response.

1.5.2 Toll-like receptors are key players in linking the innate and adaptive immune responses

Discovered in the 1990s and since then subject to many functional studies Toll-like receptors were identified as main molecules of the innate immune system and major players of the first wall encountered by pathogens that enter the body. TLRs can mainly be found in immune cells of the innate immune system including DCs, monocytes and mast cells. They can, however, occasionally also be found in T and B lymphocytes as well as in NK cells (CRAIN et al., 2013). Their expression also was demonstrated in cells of the endothelium and epithelium and in a subset of tumor cells (HOLLDACK, 2014).
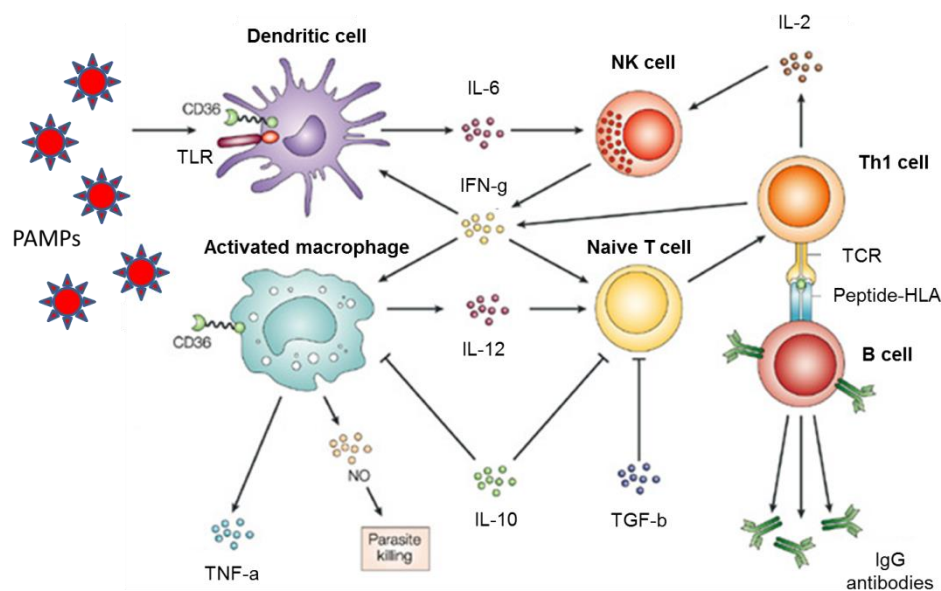
FIGURE 1.10   TLRs LINK INNATE WITH ADAPTIVE IMMUNE RESPONSES. Upon recognition of pathogen-associated molecule patterns (PAMPs) by TLRs dendritic cells release cytokines (IL-6, IL-12) that via complex regulatory mechanisms stimulate further innate immune cells but also adaptive immune responses. Adapted from (STEVENSON and RILEY, 2004)

TLRs fall into the category of the so called pattern recognition receptors (PRRs) that are able to detect microbial infections. They bind to and recognize highly conserved microbial structures, so called pathogen-associated molecular patterns (PAMPs) that are common to a broad variety of infectious agents and comprise molecules such as lipopolysaccharides (LPS), bacterial DNA or double-stranded RNA (CHAN et al., 2009). Binding of PAMPs results to interaction of the TLRs with adaptor molecules, for example with myeloid differentiation primary-response protein 88 (MyD88) (AKIRA and TAKEDA, 2004). This initiates complex intracellular signaling pathways mediating the signal to the nucleus where NFκB becomes activated regulating the expression of downstream target genes including primarily pro-inflammatory cytokines such as IL-1, IL-6, IL-8, IL-12, tumor necrosis factor (TNF)-α, IFN-α and IFN-β. Their expression further enhances the innate immunity. Immediate

protection against pathogens is provided, in an antigen non-specific manner, by activation of NK cells, recruitment of macrophages and activation of the complement cascade (reviewed in MEDZHITOV, 2007). The induction of the expression of co-stimulatory molecules of antigen-presenting cells such as CD40, CD80 and CD86 that contribute to T cell activation (ZHOU et al., 2013) as well as the created pro-inflammatory milieu that recruits further immune cells to the infection site enables an antigen-specific, adaptive immune response to be raised against the tumor (Figure 1.10) (DE GIORGI et al., 2009). Obviously, TLRs activated in locally confined regions can also induce NK cell mediated killing, enhance MHC class I expression on tumor cells and interfere with apoptotic pathways of the tumor cells leading to tissue destruction and a further release of pro-inflammatory cytokines enhancing the immune response (HOLLDACK, 2014).

1.5.3   Toll-like receptor ligands have immuno-stimulatory properties

TLR agonists represent a promising approach for the activation of the innate and adaptive immune response by binding to and stimulation of TLRs. In the context of this thesis TLR7 is of special interest which is an intracellular non-catalytic receptor that is located within the endosomal compartment of immune cells (CRAIN et al., 2013). The natural ligands for TLR7 are single-stranded RNA molecules which preferentially are rich in guanine and uridine (DIEBOLD et al., 2004). However, they also respond to synthetic small molecules such as imidazoquinolines and molecules that structurally resemble purine bases (Figure 1.11) (HEMMI et al., 2002) making them an interesting target for immuno-modulatory treatment strategies.

One of these synthetic TLR ligands is the imidazoquinoline compound imiquimod that acts as an immune modifier by changing the immune milieu by binding to TLR7 and, to a lesser extent, to TLR8 (TERLOU et al., 2010). Imiquimod is approved by the Food and Drug Administration (FDA) as a 5% cream – and as such called Aldara® - and clinically applied for the treatment of genital warts, superficial basal cell carcinoma and actinic keratosis (GASPARI et al., 2009). Imiquimod appears as important non-invasive treatment option also in patients with vulvar intraepithelial neoplasia allowing the conservation of the vulvar anatomy and is of special interest in multifocal VINs that show high rate of recurrence. Two imiquimod-treatment studies, a pilot study and the following placebo-controlled, randomized trial, were conducted that included patients with diagnosed vulvar precancerous lesions (grade 2 or 3). The trials demonstrated the efficiency of locally applied (topical) imiquimod treatment that induces (at least partial) clinical response in the majority of the patients defined as reduction of the lesion size, histologic regression and HPV clearance (VAN SETERS et al., 2002; VAN SETERS et al., 2008).

In general, Aldara® is well-tolerated by patients if locally applied. Nevertheless, clinical studies demonstrated that systemic and local adverse effects cannot be avoided. They appear as fever, arthralgia, headache, myalgia or lymphadenopathy and all these symptoms are caused by pro-inflammatory cytokine release in the blood stream having systemic effects (CRAIN et al., 2013).

These observations induced chemists and biologist to search for new derivatives with an at least as high immune stimulatory potential as imiquimod but reduced side effects. In this context, a TLR7-specific ligand called SM360320 (Figure 1.11) was synthesized on the basis of an adenine skeleton and pharmacologically evaluated. In a mouse model, this substance demonstrated to have an adjuvant effect in combination with DNA vaccination (DHARMAPURI et al., 2009). It could also be shown

that SM360320 is up to 100-fold more potent in inducing interferons compared with imiquimod (KURIMOTO et al., 2004).

In order to further improve the effects mediated by SM360320 further derivative molecules based on this core molecules were synthesized by conjugating it to different macromolecules such as proteins, lipids or polyethylene glycol. These attempts gave rise to TMX-202 which is the core TLR7 agonist conjugated to a C-12 phospholipid (Figure 1.11).
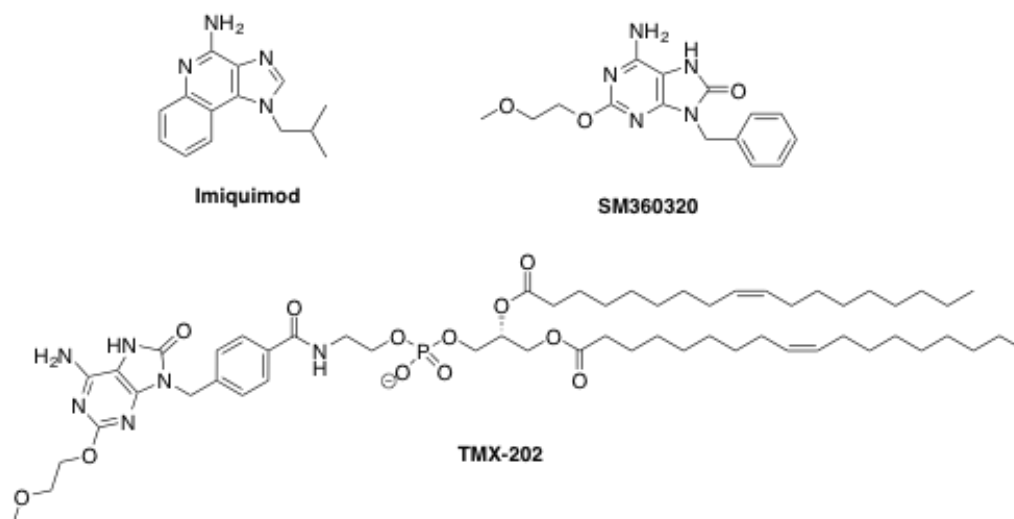
FIGURE 1.11   CHEMICAL STRUCTURES OF TLR AGONISTS. Shown are the chemical structures of the imidazoquinoline imiquimod and the purine-like TLR7 ligand SM360320 which represents the core molecule of TMX-202 obtained by conjugation of a C-12 phospholipid.

In a cooperation project with a company specialized in TLR agonist, Telormedix S.A., Bioggio, Switzerland, we could gain access to the new TLR agonist TMX-202 and characterize its immuno-stimulatory potential on different levels and *in vitro* experiments.

2. MOTIVATION AND RATIONALE

Infections with human papillomaviruses are very common in the sexually active population and under certain circumstances might give rise to dysplastic abnormalities of the squamous cell epithelium – for example in the cervix uteri where the lesions then are called cervical intraepithelial neoplasia (CIN). The initial step of cervical carcinogenesis is the transition from permissive infection to transformation of the HPV-infected cells, induced by expression of the oncogenes E6 and E7 that interfere with critical host cell pathways and which can be highlighted by $p16^{INK4a}$ overexpression. However, the induction of transformation is not sufficient to drive a lesion into further progression and development of invasive cancer, as proven by the proportion of transformed high-grade lesions that are reported to undergo regression. The deregulated host cell pathways lead to chromosomal instability and subsequent secondary genomic aberrations. These might give rise to cell clones having distinct features providing them with growth advantage over normal cells promoting disease progression. The higher progression rates in immunosuppressed or immunocompromised individuals clearly demonstrate the importance of the host's immune system in HPV clearance and prevention from HPV-related cancer. Clonally selected and expanding cells might have developed mechanisms that promote immune evasion and thus disease progression (see Figure 2.1 for conceptual background). These mechanisms might affect the immune microenvironment by creating an immunosuppressive milieu as well as tumor cell intrinsic features enabling tumor cells to directly evade the immune attack.
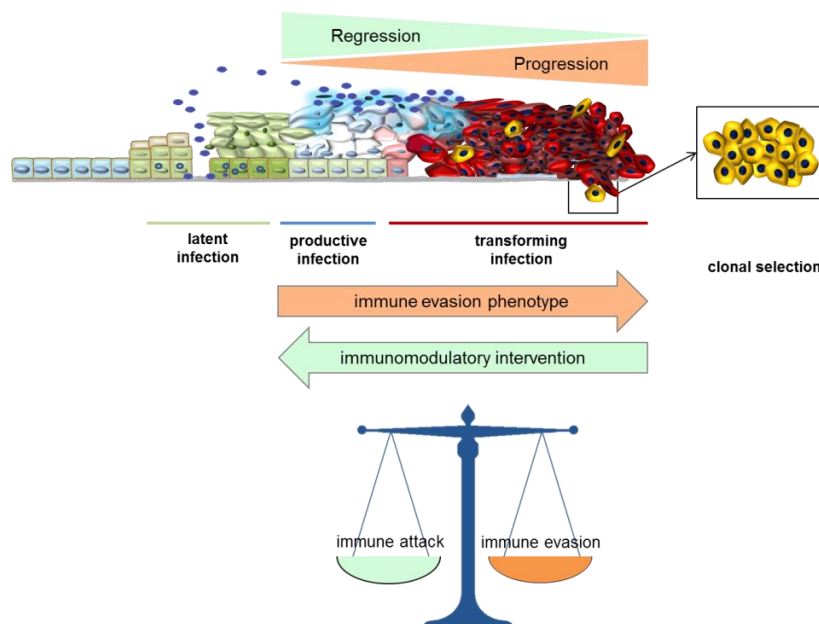
FIGURE 2.1   CONCEPTUAL MODEL ILLUSTRATING CENTRAL QUESTIONS ADDRESSED IN THIS THESIS. Immune evasion mechanisms in cervical intraepithelial neoplasia might contribute to the induction of transforming infection and progression of cervical intraepithelial neoplasia towards invasive cancer. Clonal selection for tumor cells favoring immune evasion leads to the outgrowth of a so called immune evasion phenotype which might be reversed by proper immuno-modulatory drug intervention. Adapted from (DOEBERITZ and VINOKUROVA, 2009b).

The objective of this thesis was to gain a better understanding of the battle of the host's immune system against HPV-associated precancerous lesions of different grades and also cancer. This is crucial to improve prognostic markers for guiding treatment decisions and also therapeutic interventions. Therefore, in this thesis the following two central goals were pursued:

In the first part of this thesis, the immune evasion phenotype of cervical precancerous lesions was characterized to improve the understanding of the quality of possibly initiated immune responses against HPV-induced neoplasia and evaluate how successful the immune system battles against dysplastic cells. Possible immune evasion or suppression mechanisms were investigated and their occurrence was correlated with different time points of the disease progression. Thereby features observed on the immune cells' side as well as mechanisms inherent to HPV-infected keratinocytes were investigated.
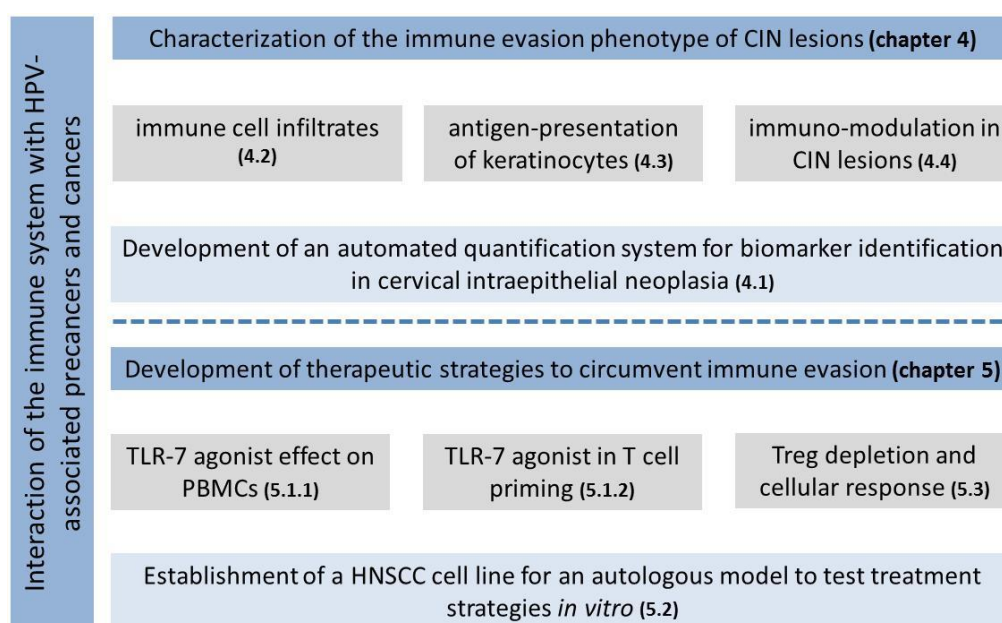
FIGURE 2.2   GRAPHICAL OVERVIEW OF THE AIMS AND THE WORKFLOW OF THE PRESENTED THESIS. Shown are the main questions of each part (dark blue), the different aspects investigated in this context (grey) and the central methodological approaches (light blue).

The second part of this work aimed at the development of non-invasive therapeutic strategies to circumvent possible immune evasion mechanisms in HPV-associated diseases. Different approaches aiming at immune-modulation of potentially suppressed immune responses were evaluated that possibly influence the balance between immune evasion and anti-tumoral immune response and thus might lead to an effect tumor attack.

All these aspects of the interaction of the host's immune system with lesion or tumor cells in HPV-associated diseases were investigated by a broad spectrum of different approaches to address specific problems (outlined in Figure 2.2).

❖ Objective and standardized quantification methods for immune cell infiltrate in HPV-associated precancerous lesions of the cervix are lacking.

➢ Development of a computational tissue analysis platform combining histological analysis and automated whole slide imaging allowing the objective quantification of tissue infiltrating immunocytes. This method is required to establish an immune-based prognostic biomarker tool for cervical intraepithelial neoplasia that would also allow the monitoring of the efficacy of tumor therapies (chapter 4.1).

❖ It is still unclear which mechanisms trigger the infiltration of immune cells into lesions and a shift in immune cell densities and composition still cannot be related to any time point of the natural history of CIN. It is of particular interest whether this correlates with the biological infection status, e.g. with the shift from permissive to transforming infection.

➢ Characterization of the immune cell infiltrates as CD3, CD8, GranB, Foxp3 and CD3 ζ-chain expressing cells in an antigen-independent way in cervical precancerous lesions of different grades and infection stages by immunohistochemistry. The main focus was lying on possible differences between permissive and transforming infections as represented by p16^{INK4a} overexpression (chapter 4.2).

❖ HPV might interfere with antigen-presentation mechanisms and thus contribute to immune evasion. Altered HLA expression is reported in cervical cancer, the time point when this occurs during progression of precancerous lesions however remains to be elucidated.

➢ Analysis of the expression of molecules involved in antigen-processing and -presentation (HLA class I heavy chains and light chains, and HLA class II antigens) on keratinocytes by immunohistochemistry in different progression grades of cervical precancerous lesions and cancers (chapter 4.3).

❖ Topical treatment with an immune-modulatory drug, imiquimod, might have effects on immune cell densities and composition in cervical intraepithelial neoplasia. These changes might be associated with the clinical outcome of patients.

➢ Longitudinal characterization of the immune cell infiltrates as CD3 and CD8 expressing cells by immunohistochemistry in cervical precancerous lesions that were topically treated with a Toll-like receptor agonist-based immune modulator (chapter 4.4).

❖ Second generation Toll-like receptor agonists might have less side effects compared with imiquimod, however their effects on immune cells and the potential to raise an anti-tumoral immune response in the context of HPV-associated diseases have to be demonstrated.

➢ Evaluation of the effects of a new immuno-modulatory drug (TMX-202) on TLR7 expression in immune cells on the transcript and protein level by quantitative real-time PCR and western blot. Evaluation of its efficiency to induce a pro-inflammatory cytokine milieu (as measured by IL-6 ELISA). Investigation of its potency to enhance the immune attack against HPV-associated cancers by an *in vitro* priming experiment of naïve T cells and measurement of cytotoxic responses against CaSki cells monitored by CD107a degranulation assay (chapter 5.1).

❖   Models based on HPV-positive tumor cell lines and autologous immune cells for the investigation of immune responses against HPV-associated tumors are lacking. These, however, are of special importance to test immune-modulatory treatment options.

➢   Generation of a HPV-associated cell line from HNSCC patients in order to establish an autologous model for *in vitro* functional analyses of tumor cell and immune cell interaction. Tumor samples could be obtained from HPV-positive head and neck squamous cell carcinomas that develop through the same tumorigenic mechanisms as cervical cancers and therefore represent a valuable model for HPV-related cancers (chapter 5.2)

❖   The immunophenotypic characterization of CIN and cervical cancer revealed regulatory T lymphocytes as one possible contributor to HPV-related carcinogenesis and possible target for immuno-modulatory intervention strategies.

➢   Analysis of the immunosuppressive effects mediated by regulatory T lymphocytes in HPV-associated diseases using the established autologous tumor model and evaluating Treg depletion as one possible therapeutic intervention strategy to reverse immune evasion phenotype. The antitumoral effects of Treg depleted T cells and the total T cell fraction was compared in CD107a degranulation assay and impedance measurement (chapter 5.3).

3. MATERIALS AND METHODS

3.1   Materials

3.1.1   Technical equipment, instruments

Agarose gel carriage	Tecnomara (Fernwald)
Agarose gel running chamber *SubCell GT*	Biorad (Munich)
Analytical balance *BP 210D*	Sartorius (Goettingen)
Balance *BP 310S*	Sartorius (Goettingen)
Bond Autostainer	Leica Microsystems (Wetzlar)
Camera *Electrophoresis Docu System 120*	Kodak (Stuttgart)
Centrifuge *5810R*	Eppendorf (Hamburg)
Digital camera *Leica DFC480*	Leica Microsystems (Wetzlar)
Electrophoresis chamber (Sub Cell GT)	Biorad (München)
Flow cytometer (FACSCalibur)	Becton Dickinson (Franklin Lakes, USA)
Fluorometer for microtiter plates *Luminex 100*	Luminex (Austin, USA)
Gel Documentation GelDoc 2000	Biorad (München)
Incubator	Memmert (Schwabach)
Leica Bond Autostainer II	Leica Microsystems (Wetzlar)
Magnetic stirrer *MR 2002*	Heidolph (Schwabach)
Microscope for cell culture *Olympus CK40*	Olympus optical CO (Center Valley, USA)
Microscope *Leica DMRBE*	Leica Microsystems (Wetzlar)
Microtiter plate reader *Multiscan EX*	Thermo Electron Corporation (Karlsruhe)
Microtome *Leica RM 2035*	Leica Microsystems (Wetzlar)
Microwave	Panasonic (Hamburg)
Minishaker *Vortex MS1*	IKA-Works (Wilmington, NC)
NanoZoomer 2.0-HT Scan System	Hamamatsu (Herrsching)
PCR system (Mastercycler Gradient)	Eppendorf (Hamburg)
PH meter (PB-11)	Sartorius (Göttingen)
Photometer for microtiter plates *GENios*	Tecan (Crailsheim)
Photometer *Ultrospec 7000*	GE Healthcare (Uppsala, Sweden)
Pipettes 2-1000µl *Pipetman*	Gilson (Bad Camberg)
Pipettor 8-5010	Neolab (Heidelberg)
Power supply Power Pac 300	Biorad (Munich)
Real-Time PCR system (StepOnePlus)	Applied Biosystems (Foster City, USA)
Robocycler *Gradient 96*	Stratagene (Santa Clara, USA)
Rolling mixer *CAT RM 5*	Neolab (Heidelberg)
RTCA Analyzer *W380*	ACEA Biosciences (San Diego, USA)

RTCA SP Station *1x96*   ACEA Biosciences (San Diego, USA)
Safety cabinet *Class II, SL-130 Blue Series*   Kojair (Vilppula, Finland)
Shaker for microtiter plates *Titramax 100*   Heidolph (Schwalbach)
Speed Vac *DNA Speed Vac 110*   Savant (Holbrook, USA)
Table top centrifuge *5424*   Eppendorf (Hamburg)
Thermomixer *5436*   Eppendorf (Hamburg)
Vacuum manifold *Vacusafe Comfort*   Millipore (Billerica, USA)
Vortex (MS1 Minishaker)   IKA (Staufen)
Water bath Grant *SUB14*   *Grant* Instruments (Cambridge, UK)

3.1.2   Chemicals and Reagents

Acetic acid 100%   Merck (Darmstadt)
Acryl amide *RotiphoreseGel 30*   Roth (Karlsruhe)
Agarose *Ultra Pure*   Invitrogen (Carlsbad, CA, USA)
Albumine Bovine Fraction V pH 7.0   Serva (Heidelberg)
Amphotericin B   Invitrogen (Karlsruhe)
Aquatex   Merck (Darmstadt)
B2-microglobuline (human)   Sigma Aldrich (Steinheim)
Boric acid   Merck (Darmstadt)
Brefeldin A   Sigma-Aldrich (Steinheim)
Bromphenol blue   Serva (Heidelberg)
Caseine from bovine milk   Sigma Aldrich (Steinheim)
CellGro® DC   CellGenix Technologie Transfer (Freiburg)
Citric acid   Merck (Darmstadt)
DAB+ Substrate Chromogen System   Dako (Carpinteria, USA)
Decitabine (5-Aza-2'-deoxycytidine, DAC)   Sigma-Aldrich (Steinheim)
Developer for photographic processing   Adefo-Chemie (Dietzenbach)
Dimethyl sulfoxide (DMSO) 99.5%   Sigma Aldrich (Steinheim)
Dipotassium phosphate   Gerbu (Gaiberg)
Disodium hydrogenphosphate   VWR (Darmstadt)
Disodium phosphate   VWR International (Leuven, Belgium)
DMEM / Ham's-F12   Gibco (Paisley, UK)
DNA ladder 100 bp   Invitrogen (Karlsruhe)
Dulbeco's PBS (1x)   Gibco (Paisley, UK)
Ethanol 96%   Sigma Aldrich (Steinheim)
Ethanol 99%   Sigma Aldrich (Steinheim)
Ethanol absolute   Sigma Aldrich (Steinheim)
Ethanol absolute   Sigma-Aldrich (Steinheim)
Ethylenediaminetetraacetic acid (EDTA)   Merck (Darmstadt)
Fetal bovine   Gibco (Paisley, UK)
Fixer for photographic processing   Adefo-Chemie (Dietzenbach)
GelRed Nucleic Acid Stain   Biotium (Hayward, CA)

Gentamycin	Invitrogen (Karlsruhe)
Glutamine	PAA Laboratories (Pasching, Austria)
Glycerol (86%)	Carl Roth (Karlsruhe)
Glycerol	Roth (Karlsruhe)
Glycine	AppliChem (Darmstadt)
GM-CSF	PromoCell (Heidelberg)
H_2O HPLC-grade	VWR (Darmstadt)
Haematoxylin	Sigma Aldrich (St. Louis, USA)
Hemalaun	AppliChem (Darmstadt)
Heparin-Natrium 25000	Ratiopharm (Ulm)
Horse serum	Vector Laboratories (Burlingame, CA)
Human epithelial growth factor (EGF)	Sigma Aldrich (Steinheim)
Human serum	PAA Laboratories (Pasching, Austria)
Hydrochloric acid (HCl 37%)	Carl Roth (Karlsruhe)
Hydrocortisone	Sigma Aldrich (Steinheim)
Hydrogen peroxide 30%	Merck (Darmstadt)
IMDM	Gibco (Paisley, UK)
Imiquimod	Calbiochem (San Diego, USA)
Insuline	Sigma Aldrich (Steinheim)
Isopropyl alcohol	Sigma Aldrich (Steinheim)
Luminol Reagent for Western Blot *sc-2048*	SC Biotechnology (Santa Cruz, USA)
Lymphocyte Separation Medium *LSM 1077*	PAA Laboratories (Pasching, Austria)
Magnesium chloride (MgCl2)	Solis Biodyne (Tartu, Estonia)
Mercaptoethanol	Merck (Darmstadt)
Methanol	Sigma Aldrich (Steinheim)
Paraformaldehyde (PFA)	Carl Roth (Karlsruhe)
PBS	Gibco (Paisley, UK)
Penicillin/Streptomycin (100x)	Gibco (Paisley, UK)
Ponceau S Solution 0.1%	Sigma Aldrich (Steinheim)
Potassium chloride	Merck (Darmstadt)
Potassium dihydrogen phosphate	Gerbu (Gaiberg)
Precision Plus Protein Standard	Bio-Rad (Munich)
Protease Inhibitor Cocktail	Sigma (Steinheim)
Protein Assay Dye Reagent Concentrate	BioRad (München)
Quantum 263 Medium for Tumor Cells	PAA Laboratories (Pasching, Austria)
Reaction buffer BD (10 x)	Solis Biodyne (Tartu, Estonia)
Recombinant Human Interleukin-2	PromoCell (Heidelberg)
Recombinant Human Interleukin-4	PromoCell (Heidelberg)
Recombinant Human Interleukin-7	PromoCell (Heidelberg)
RIPA Buffer	Sigma Aldrich (Steinheim)
RNase Out	Invitrogen (Karlsruhe)
ROX size standard	Applied Biosystems (Darmstadt)
RPMI 1640	Gibco (Paisley, UK)

Sodium acetate	Roth (Karlsruhe)
Sodium carbonate	J.T. Baker (Deventer, Netherlands)
Sodium chloride (NaCl)	Sigma Aldrich (Steinheim)
Sodium dihydrogen phosphate dihydrate	J.T. Baker (Deventer, Netherlands)
Sodium dihydrogenphosphate monohydrate	J.T. Baker (Deventer, Netherlands)
Sodium heparin	Ratiopharm (Ulm)
Sodium hydrogene carbonate	Merck (Darmstadt)
Sodium hydroxide (NaOH)	Sigma Aldrich (Steinheim)
Sodium thiosulfate	Gerbu (Gaiberg)
Sodiumdodecylsulfate (SDS)	Serva (Heidelberg)
Supplement Insulin-Transferrin-Selenium	Gibco (Paisley, UK)
Tetramethylbenzidine (TMB)	Sigma Aldrich (Steinheim)
Tetramethylethylenediamine (TEMED)	Sigma Aldrich (Steinheim)
TMX-202	Telormedix (Bioggio, Switzerland)
Tris-(hydroxymethyl)aminomethane	Roth (Karlsruhe)
Tris-HCl	Roth (Karlsruhe)
Trypan blue solution	Sigma-Aldrich (Steinheim)
Trypsin-EDTA	Gibco (Paisley, UK)
Tween 20	BioRad (München)
Ultima Gold	PerkinElmer (Waltham, USA)
Xylene	Merck (Darmstadt)

3.1.3   Consumables

96-well plates, U-bottom	BD Falcon (Durham, NC, USA)
96-well plates, V-bottom	BD Falcon (Durham, NC, USA)
Cannulas *Microlance 3*	Becton Dickinson (Fraga, Spain)
Cell culture plate *Cellstar* (6/12/96 wells)	Greiner Bio-One (Frickenhausen)
Cell culture plate *Nunclon Surface*	Nunc (Roskilde, Danmark)
Cell strainer (100 µm)	BD Biosciences (Erembodegen, Belgium)
Columns (LS)	Miltenyi Biotec (Bergisch Gladbach)
Columns (MS)	Miltenyi Biotec (Bergisch Gladbach)
E-Plate *VIEW 96*	ACEA Biosciences (San Diego, USA)
Examination gloves, *Sempercare® nitrile*	Semperit (Vienna, Austria)
Filter paper	Whatman (Dassel)
Filter systems (0.22 µm)	Corning incorporated (New York, USA)
Filter tips (10 µl, 20 µl, 200 µl, 1000 µl)	Corning Incorporated (New York, USA)
Filter tips *Tip One*	StarLab (Ahrensburg)
Freezing tubes *Cryo.s with screw cap (2ml)*	Greiner Bio-One (Frickenhausen)
Laboratory film *Parafilm „M"*	American National Can (Greenwich)
Microscope cover glasses	Marienfeld (Lauda-Königshofen)
Microscope slides *Superfrost Plus*	Menzel (Braunschweig)
Microscopy Aquatex	Merck (Darmstadt)

Microtome blades *R35*	PFM Medica (Köln)
Microwell plate *NUNC 96 flat bottom*	NUNC (Langenselbold)
PCR tubes	Steinbrenner (Wiesenbach)
Petri dishes	Greiner Bio-One (Frickenhausen)
Petri dishes (sterile)	Nunc (Roskilde, Denmark)
Photographic film *Kodak*	Sigma-Aldrich (St. Louis, USA)
Pipet tips	Greiner Bio-One (Frickenhausen)
Polystyrene tubes	BD Biosciences (Erembodegen, Belgium)
PVDF membrane *Hybond N+*	Amersham (Buckinghamshire, UK)
Reaction tubes (1.5 and 2 ml)	Eppendorf (Hamburg)
Reaction tubes (15 ml and 50 ml)	Greiner Bio-One (Frickenhausen)
Scalpel *No. 11*	PFM Medical (Köln)
Serological pipette (2-25 ml)	Sarstedt (Nümbrecht)
Serological pipette *Costar Stripette*	Corning (New York, USA)
Sterile filter (0.2 µm)	Corning Incorporated (New York, USA)
Tissue culture flasks (sterile, pyrogen-free) *Cellstar*	Greiner Bio-One (Frickenhausen)
Western Blotting Luminol Reagent	Santa Cruz (Heidelberg)

3.1.4   Commercially available kits

$CD4^+CD25^+$ Regulatory T Cell Isolation Kit human	Miltenyi Biotec (Bergisch Gladbach)
CINtec Plus (Cytology, Histology)	Roche (Mannheim)
DNeasy Blood & Tissue Kit	Qiagen (Hilden)
dNTP Set 100 mM	Invitrogen (Karlsruhe)
Hexanucleotide mix (10 x)	Roche Diagnostics (Mannheim)
Multiplex HPV Genotyping Kit	Diamex (Heidelberg)
Mycoplasma detection kit *MycoAlert™*	Lonza (Köln)
Pan T Cell isolation Kit II	Miltenyi Biotec (Bergisch Gladbach)
Power SYBR Green PCR Master mix	Applied Biosystems (Foster City, USA)
QIAamp DNA FFPE Tissue Kit	Qiagen (Hilden)
Quantikine®ELISA Human IL-6	R&D Systems (Abingdon, UK)
RNeasy Mini Kit	Qiagen (Hilden)
SuperScript II Reverse Transcriptase	Invitrogen (Karlsruhe)
Vectastain Elite ABC Kit	Vector (Burlingame, USA)

3.1.5   Antibodies

Reactivity	Clone	Modi-fication	Application (dil./conc.)	Supplier
p16^{INK4a}	E6H4	none	ready to use in CINtec® Plus Kit	(Roche, Mannheim)
CD3	PS1	none	IHC (1:50)	Acris antibodies (Herford)
Foxp3	236A/E7	none	IHC (1:50)	eBioscience (Frankfurt a. M.)
GranzymeB	11F1	none	IHC (1:50)	Novocastra (Newcastle upon Tyne, UK)
CD8	4B11	none	IHC (1:50)	Novocastra (Newcastle upon Tyne, UK)
CD3-ζ	6.B10.2	none	IHC (1:200)	Santa Cruz (Heidelberg)
HC-10	n.a.	none	IHC (1:50)	kind gift of Soldano Ferrone
HCA-2	n.a.	none	IHC (1:50)	kind gift of Soldano Ferrone
L368	n.a.	none	IHC (1:50)	kind gift of Soldano Ferrone
LG-612.14	n.a.	none	IHC 1:300	kind gift of Soldano Ferrone
mouse IgG / rabbit IgG	polyclonal	biotin	IHC (1:50)	Vector Laboratories (Burlingame, USA)
CD4	RPA-T4	FITC	FACS (1:50)	BD Pharmingen (Heidelberg)
CD8	RPA-T8	FITC	FACS (1:50)	BD Pharmingen (Heidelberg)
CD25	4E3	PE	FACS (1:50)	Miltenyi Biotec (Bergisch Gladbach)
CD107a	n.a.	PE	FACS (1:50)	BD Pharmingen (Heidelberg)
HLA-A2	n.a.	FITC	FACS (1:50)	AbD Serotec (Puchheim)
HLA-A/B/C	W6/32	FITC	FACS (1:50)	eBioscience (Frankfurt a. M.)
epithelial antigen	BerEP4	FITC	FACS (1:50)	Dako (Eching)
isotype control IgG1	n.a.	FITC	FACS (1:50)	BD Pharmingen (Heidelberg)

isotype control IgG1	n.a.	PE	FACS (1:50)	BD Pharmingen (Heidelberg)
isotype control IgG2a	n.a.	FITC	FACS (1:50)	BD Pharmingen (Heidelberg)
isotype control IgG2b	n.a.	PE	FACS (1:50)	BD Pharmingen (Heidelberg)
isotype control IgG2b	n.a.	PE	FACS (1:50)	BD Pharmingen (Heidelberg)
TLR7	monoclonal	none	WB (1:1000)	Abcam (Cambridge, UK)
HPV16 E7	NM2	none	WB (1:500)	Santa Cruz (Heidelberg)
actin	n.a.	none	WB (1:20000)	MP Biomedicals, Heidelberg.
rabbit IgG	n.a.	HRP	WB (1:2000)	Promega (Mannheim)
mouse IgG	n.a.	HRP	WB (1:4000)	GE Healthcare (Freiburg)

n.a = not available; IHC = immunohistochemistry; WB = Western Blot

3.1.6   Enzymes

Collagenase Type IV	Sigma-Aldrich (Steinheim)
DNase I	Sigma-Aldrich (Steinheim)
Hyaluronidase	Sigma-Aldrich (Steinheim)
Super Script Reverse Transcriptase (200U/µl)	Invitrogen (Karlsruhe)
Tag DNA Polymerase (5U/µl)	Invitrogen (Karlsruhe)

3.1.7   Peptides

p16^{INK4a}

peptide name	Amino acid positions	amino acid sequence
p16^{INK4a} peptide R1	51-59	VMMMGSARV

The p16^{INK4a} 9mer peptide was synthesized by the core facility for peptide synthesis, German Cancer Research Center, Heidelberg.

HPV16 L1

peptide name	Amino acid positions	amino acid sequence
HPV16 L1_2	2-11	SLWLPSEATV
HPV16 L1_12	12-21	YLPPVPVSKV
HPV16 L1_60	60-68	ILVPKVSGL
HPV16 L1_67	67-75	GLQYRVFRI
HPV16 L1_97	97-105	RLVWACVGV
HPV16 L1_249	249-257	YLRREQMFV
HPV16 L1_323	323-331	ICWGNQLFV

The HPV16 L1 9mer and 10mer peptides were synthesized by Genaxxon Bioscience, Ulm.

Influenza virus matrix protein

peptide name	Amino acid positions	amino acid sequence
viral MP	57-68	GILGFVFTL

The virus matrix protein was synthesized by the core facility for peptide synthesis, German Cancer Research Center, Heidelberg.

3.1.8   Primers

primer name	sequence (5'-3')
TLR7 forward	AAGCCCTTTCAGAAGTCCAAGTT
TLR7 reverse	GGTGAGCTTGCGGGTTTGT
β-actin forward	ATGTGGCCGAGGACTTTGATT
β-actin reverse	AGTGGGGTGGCTTTTAGGATG

The primers were obtained from Thermo Scientific, Ulm.

3.1.9   Buffers and Solutions

Agarose Gel (1.5%):   1.5 g Agarose

                                    100 ml TBE buffer

                                    1 µl Gel Red

10% APS: 10 % (w/v) Ammonium persulfate in aqua bidest

Blotting Buffer (10x):   30.37 g Tris
              144.13 g Glycine
              ad 1l Aqua bidest.

Blotting Buffer (1x) working solution: 100 ml 10x Blotting Buffer
              200 ml methanol
              700 ml Aqua bidest.

10x Citrate buffer: 100 mM Citric acid monohydrate (21 g)
              ad 1l Aqua bidest.
              adjust pH to 6.0 with NaOH

DNA loading buffer (6x):   25 ml Glycerol
              125 mg Xylenecyanol
              25 ml H_2O dest.

Laemmli sample buffer (4x) : 2.5 ml 1M Tris pH 8.0 (125mM)
              8 ml 10% SDS (4%)
              2 ml glycerin (10%)
              2 ml β-mercaptoethanol (10%)
              4 mg bromphenol blue (0.02%)
              ad 20 ml H_2O

5 M NaOH: 100 g NaOH
              ad 500 ml Aqua bidest

10x PBS: 84 g NaCl (= 0.8 % w/v)
              2 g KCl (= 0.02 % w/v)
              11.5 g Na_2HPO_4 (= 0.1 % w/v)
              2 g KH_2PO_4 (= 0.02 % w/v)
              ad 800 ml Aqua bidest, pH 7.4

4% PFA Stock Solution: 4g paraformaldehyde
              100 ml PBS

10x SDS-PAGE running buffer: 30.3 g Tris-Base
              144 g Glycine
              100 ml 10% SDS
              ad 1 l Aqua bidest.

10x TBE:	108 g Tris
	55 g boric acid
	40 ml 0.5 M EDTA, pH 8.0
	ad 1 l Aqua bidest.
10x TBS:	60.55 g Tris
	87.66 g NaCl
	ad 1 l Aqua bidest.
	adjust pH to 7.6 with 37% HCl
1x TBS:	dilute 10x TBS 1:10 in Aqua bidest
1x TBS-T for Western Blot:	dilute 10x TBS 1:10 in Aqua bidest
	add 0.1% Tween
Tris 0.5 M, pH 6.8:	20.29 g Tris
	20 ml 10% SDS
	ad 500 ml Aqua bidest.
	adjust pH to 6.8, autoclave
Tris 1.5 M, pH 8.8 :	90.9 g Tris
	20 ml 10% SDS
	ad 500 ml Aqua bidest
	adjust pH to 8.8 with HCl, autoclave

3.1.10   Cell culture media

B cell/T cell basis medium	500 ml IMDM
	50 ml human serum
	6 ml L-glutamine
	25 µg/ml gentamicin
Dendritic cell medium	CellGro medium
	1% penicillin / streptomycin
	3% human serum
Freezing medium for PBMCs	human serum
	+ 10 % DMSO

MACS Buffer	PBS
	5% human AB serum
	1 mM EDTA
	sterile filtrate
Peptide-Load medium	500 ml IMDM (serum free)
	25 µg/ml gentamicin
Quantum Tumor Medium	Quantum 263 for Tumor cells
(used for cell line generation)	5 µg/ml insulin
	0.5 µg/ml hydrocortisone
	10 ng/ml hEGF
	25 µg/ml gentamicin
T cell medium:	Bc/Tc basis medium
	1 x Insulin Transferrin Selenium
	10 U/ml IL-2
	10 U/ml IL-7
Tumor digestion solution:	10 ml Tumor preparation solution
	1 mg/ml Collagenase Type IV
	0.1 mg/ml Hyaluronidase
	20 µg/ml DNase I
Tumor preparation solution	200 ml RPMI 1640
	25 mM HEPES
	3.6 ml Penicillin/Streptomycin (100x)
	5 µg/ml amphotericin B
	2 mM Glutamin
Tumor transport solution	DMEM medium
	10% FCS
	100 µg/ml gentamycin
	10 µg/ml amphotericin B
Tumor cell line Medium	RPMI 1640
(used for standard cell lines)	10% FCS
	25 µg/ml gentamicin

3.1.11   Cell lines

cell line	origin, characteristics	experiment
CaSki	HPV16 positive cervical cancer cell line	killing assay (chapters 3.2.4, 5.2.4)
Raji	B cell lymphoma cell line, high TLR7 expression	Positive control for TLR7 expression (chapters 3.2.4, 5.1.2)
T2	TAP-deficient T-B lymphoblastoid hybridoma	Peptide binding assay (3.2.4, 5.2.1)

3.1.12   Patients' material

1) Cervical intraepithelial neoplasia and cervical cancer patients		
study "immune cell infiltration in relation to p16^{INK4a} expression" (chapter 4.2)		
University Hospital, Heidelberg and Institute of Pathology, Mannheim, Germany		
period of recruitment	2003-2004 (Mannheim) and 2007-2010 (Heidelberg)	
number of patients	69	
resected tissue	cervical cone biopsies	
stages		p16^{INK4a}-positive [n, (%)]
CIN1	n = 22	13 (59.1%)
CIN2	n = 11	11 (100.0%)
CIN3	n = 19	19 (100.0%)
invasive cervical carcinoma	n = 17	17 (100.0%)

2) Cervical intraepithelial neoplasia and cervical cancer patients		
antigen-presentation HLA class I and HLA class II study (chapter 4.3)		
Institute of Pathology, Mannheim, Germany		
period of recruitment	2003-2004	
number of patients	n = 41 (* n = 69)	
resected tissue	cervical cone biopsies	
<u>**disease stages**</u>		p16^{INK4a}-positive [n, (%)]
* CIN1	n = 19	10 (52.6 %)
CIN2	n = 9 (* n = 9)	9 (*9) 100.0%
CIN3	n = 13	13 (100.0%)
invasive cervical carcinoma	n = 19	19 (100.0%)

* cohort enlarged by CIN1 (n=19) and an additional subset of CIN2 (n=9) for HLA class II analysis (deriving from cohort 1)

3) Cervical intraepithelial neoplasia patients:	
imiquimod study (chapter 4.4)	
University Hospital, Vienna, Austria	
period of recruitment	2009-2010
number of patients	10
resected tissue	punch biopsies
disease stages	all patients had CIN2/3 at study entry (inclusion criterion)

4) Oropharyngeal carcinoma patients	
Generation of HPV-positive tumor cell line (chapter 5.2)	
University Hospital, Giessen, Germany	
period of recruitment	2011-2014
number of patients	58
resected tissue	primary tumors located in the oropharynx and metastatic lymph nodes in the head and neck region
HPV-status **HPV-positive** **HPV-negative**	n = 31 n = 27

5) healthy blood donors	
TMX-202 treatment on PBMCs	
Institute of Pathology, Heidelberg, Germany	
period of recruitment	2013/2014
number of patients	4
Sex **male** **female**	50% 50%

3.1.13   Software

Adobe Acrobat Reader 6	Adobe (San Jose, CA, USA)
BIMAS	(PARKER et al., 1994)
CellQuest pro (5.2)	Becton Dickinson (San Jose, USA)
Diskus Bilddarstellung (4.30)	Techn. Büro Hilgers (Königswinter)
Endnote X6	Thomson Reuters (New York, NY, USA)
Magellan Standard	Tecan Group Ltd. (Männedorf, Switzerland)
MedCalc, version 11.5.1.0	MedCalc Software (Ostend, Belgium)
NDP.view Software	Hamamatsu (Herrsching)

RTCA software 2.0.0	ACEA Biosiences (San Diego, USA)
SPSS Statistics 22	IBM (Ehningen)
STATISTICA (7)	StatSoft (Europe) GmbH (Hamburg)
Statistica, version 8.0.3.6	Statsoft (Hamburg)
StepOne (2.1)	Applied Biosystems (Foster City, USA)
SYFPEITHI	(RAMMENSEE et al., 1999)
TissuemorphDP™M	Visiopharm, Hørsholm, Denmark

3.2   Methods

3.2.1   Immunohistochemistry for archived tissue samples

p16^{INK4a} Immunohistochemistry

The identification and diagnosis of precancerous lesions of the cervix uteri is based on the biomarker p16^{INK4a}, a cyclin-dependent kinase inhibitor which is normally involved in tumor suppression. It is a well-established biomarker for early oncogenic processes in HPV-related cancers, especially cervical cancer as p16^{INK4a} becomes markedly overexpressed in persistent HPV-infections in which the oncogenic transformation is induced by HPV proteins which is the first step necessary for the development of cervical cancer.

The CINtec® PLUS Kit was used for the qualitative detection of p16^{INK4a} and the immunohistochemical staining procedure was carried out as proposed in the manufacturer's protocol. The provided reagents were used as described in the protocol with the following exceptions: the substrate incubation with DAB was carried out in two consecutive steps comprising 8 minutes each.

Immunohistochemical staining for CD3-, Foxp3-, Granzyme B- and CD8-positive cells and the antigen-presentation molecules HLA class I and HLA class II

Different T cell markers were qualitatively and quantitatively investigated by immunohistochemical analyses. The global T cell infiltration in tissue specimens was analyzed by staining for CD3. T cell markers representing different T cell subtypes were used to characterize T cell activation (CD8, Granzyme B and CD3 ζ-chain) and T cell inhibition (Foxp3). Precancerous lesions and cancers were characterized for HLA class I heavy chain (HLA-A/B/C) and light chain (beta2-microglobuline, β2m) and HLA class II antigen expression.

Formalin-fixed paraffin-embedded tissue sections were mounted on aminopropylsilane-coated slides and following deparaffinisation in xylene and rehydration in decreasing ethanol concentrations (100%-70%) the slides were heated for 15 minutes in 10mM citrate buffer (pH=6) in order to retrieve antigen epitopes to be analyzed. Blocking of endogenous peroxidase was performed by using 0.6% H_2O_2 in methanol. In order to reduce non-specific antibody binding and background staining the tissue sections were then blocked with 10% horse serum in PBS before the various first antibodies were applied (for dilutions see section "Antibodies") and incubated at 4°C overnight. Slides were then incubated with biotinylated anti-mouse/anti-rabbit IgG secondary antibodies for 30 minutes at room temperature.

Following the application of avidin-biotin reagent according to the manufacturer's instructions, the color reaction with 3,3-diaminobenzidine (DAB+ chromogen) allowed the detection of the antigens to be characterized. Finally, the slides were counterstained with hematoxylin and mounted with Aquatex.

Automated immunohistochemical staining protocol (CD3 and CD8)

Tissue sections (2µm) were mounted on aminopropylsilane-coated slides and subject to automated immunohistochemical staining with the Leica-Bond II Max autostainer by applying the following staining protocol with reagents provided by Leica Biosystems:

Step (solution applied)	duration	temperature
BOND Dewax Solution	30 sec	72°C
BOND Dewax Solution	30 sec	72°C
BOND Dewax Solution	30 sec	RT
ethanol (99%) (3 repetitions)		RT
BOND wash solution (3 repetitions)		RT
BOND ER Solution 1 (citrate buffer, pH 6.0) (2x)		RT
BOND ER Solution 1 (citrate buffer, pH 6.0)	20 min	100°C
BOND ER Solution 1 (citrate buffer, pH 6.0)	12 min	RT
BOND wash solution (3 repetitions)		37°C
peroxide block	20 min	RT
BOND wash solution (3 repetitions)		RT
serum block (10% goat serum in PBS)	30 min	RT
BOND wash solution (3 repetitions)		RT
primary antibody in TBS/10% FBS)	30 min	RT
BOND wash solution (3 repetitions)		RT
post primary (polymer penetration enhancer in TBS/10% FBS)	8 min	RT
BOND wash solution (3 repetitions)	2min	RT
polymer (secondary antibody, poly-HRP-anti-mouse/anti-rabbit IgG)	8 min	RT
BOND wash solution (2 repetitions)	2min	RT
deionized water		RT
mixed DAB Refine	???	RT
mixed DAB Refine	10 min	RT
deionized Water (3x)		RT

hematoxylin counterstaining	**5 min**	**RT**
deionized Water (3x)		RT
BOND wash solution	5 min	RT
deionized water		RT
embed slides in Aquatex		RT

Microscopic evaluation

p16^{INK4a} staining

Sections were defined to be negative in cases where no p16^{INK4a} expression was detectable or where p16^{INK4a}-positive cells showed a focal staining pattern (patchy, restricted to single cells). Lesions with a strong and diffuse p16^{INK4a} staining were considered to p16^{INK4a}-positive.

T cell markers

Immunohistochemically stained slides were analyzed independently in a blinded fashion during two sessions and blinded to histopathological grade. For counting and evaluation of the tumor-infiltrating lymphocytes, a Leica DMRBE microscope with a 10x10 ocular grid covering an area of 0.0625 mm^2 at a 400-fold magnification was used. In total, seven grid areas were counted in the in lesion/tumor and the adjacent stromal tissue, three located in the epithelium and four located in the stroma. In total, an area of 0.4375 mm^2 was considered for counting.

HLA class I and II

Lesions and tumors that showed a strong cytoplasmic or membranous staining in more than 75% of cells were classified as positive for HLA class I or class II expression. Heterogeneous expression was defined as faint and patchy staining (cytoplasmic or membranous) observable in 75% to 25% of the cells of a lesion or tumor. Lesions were defined to be negative for HLA expression when the staining was absent or restricted to single cells (representing invading APCs) or could be identified as locally induced expression due to the presence of immune cells (faint staining, locally restricted in areas with infiltrating immune cells) and concerned less than 25% of the lesion cells.

Automated evaluation of immunohistochemically stained slides

The establishment of an automated immune cell quantification platform and the adaption of the underlying imagine analysis algorithms were a major goal of this thesis and are described in detail in chapter 4.1. The major steps of the workflow are automated staining, whole-slide-imaging and computational image analysis and were carried out under the supervision of PD Dr. Niels Grabe and Dr. Bernd Lahrmann, TIGA Center, Heidelberg.

3.2.2   Molecular Biology Methods

Isolation of genomic DNA from cells or tissue

DNA was isolated from either FFPE tissue sections or from cultured cells deriving from fresh tumor tissue following the manufacturer's instructions.

Briefly, for the purification of genomic DNA (gDNA) from fresh or frozen cells, the pellet was resuspended in 200µl PBS and 20µl proteinase K were added. Then 200µl Buffer AL were added and the sample was incubated at 56°C for 10 min before it was resuspended in 200µl ethanol and loaded on a spin column by centrifuging at 8000 rpm for 1 min. After having washed the column with bound DNA two times with the provided wash buffers AW1 and AW2, DNA was eluted with Buffer AE in two subsequent steps and by using 30µl buffer only for each step to increase the final DNA concentration without losing to much of the maximum DNA yield.

For the isolation of gDNA from formalin fixed paraffin-embedded tissue sections, samples had to be pretreated by xylene to remove paraffin. Following centrifugation and removal of the supernatant by pipetting, ethanol was added to the pellet to remove residual xylene. Ethanol was removed by pipetting following centrifugation. This step was repeated once before the pellet was dried in the SpeedVac at 37°C for 15 min, resuspended in 180µl buffer ATL and completely lysed by adding 20µl Proteinase K at 56°C (minimum 1 hour until overnight incubation). Then the samples were incubated at 90°C for 1 hour before 200 µl Buffer AL and 200µl ethanol were added to the sample. The lysate was transferred and the provided QIAamp MinElute column which – following binding of DNA to the column – was washed twice with Buffers AW1 and AW2. Finally, following complete drying of the membrane by centrifugation at full speed, DNA was eluted in two steps with 30µl buffer in each step.

The concentration of eluted gDNA was determined by measuring the absorbance at 260 nm with the elution buffer used as blank for the zero adjustment.

GP5+/6+ PCR for Luminex® -based HPV-Genotyping

amount	reagent
26.75 µl	H_2O
5.0 µl	10x PCR Buffer
7.0 µl	50 mM $MgCl_2$
1.5 µl	10 mM dNTPs
2.0 µl	primer set 1
0.5 µl	primer set 2
0.25 µl	Taq polymerase
7.0 µl	template

Temperature profile:

94°C	10 min initial denaturation	
94°C	30 sec denaturation	
38 °C	30 sec primer annealing	40 x
72°C	80 sec primer extension	
72°C	6 min final extension	
4°C	forever	

HPV genotyping based on Luminex® technology

Luminex Technology based on polystyrene beads with various but specifically identifiable absorption spectra allow the multiplexed detection of different factors. Specifically amplified DNA from tumor samples is bound to the beads that are coupled to HPV specific oligonucleotide probes. By this approach 24 of the most common HPV types (15 high-risk and 6 low-risk and 3 putative high-risk types) can be detected simultaneously in one sample by reporter fluorescence. For the assay procedure the manufacturer's protocol was followed:

First, 40µl/well of the Bead Mix were pipetted to each required sample well of a 96 well Hybridization Plate. As a negative control 10 µl H$_2$O, 10µl Hybridization Control (1:10 diluted in H$_2$O) ad 10µl PCR product per sample well were pipetted. The PCR plate was covered tightly with a seal foil and incubated at 95°C for 10 min in a preheated PCR machine. The plate was then incubated on ice for 1 min and then for hybridization subsequently transferred to the PCR machine and incubated at 41°C for 30 min. In the meantime a filter plate was equilibrated by pipetting 100 µl Assay Buffer in each well and incubating the plate for 30min at room temperature. Wash Buffer was removed by vacuum filtration and the Bead Mix PCR samples were transferred to the filter plate after having the samples mixed vigorously by pipetting up and down and with the hybridization plate still being located in the PCR machine. Liquid is removed from the filter plate by vacuum filtration and the plate was washed twice with 100µl/well Assay Buffer. 70µl Staining solution were added to each well and incubated protected from light for 30min at room temperature under slight agitation. Then the liquid was again removed by vacuum filtration and the plate was washed trice with 100µl/well Assay Buffer respectively. The beads were then resuspended in 100µl Assay Buffer and transferred to a 96 lock-microtiter plate to measure samples then in the Luminex analyzer.

RNA extraction from cultured cells

RNA purification from human cells was performed with RNeasy Mini Kit from QIAgen with slight modifications to the manufacturer's protocol. All centrifugation steps were carried out at 10000 rpm if not indicated otherwise. Cells were disrupted by adding Buffer RLT and β-mercaptoethanol (1:100) to the cells and vortexed. The lysate was homogenized by adding 70% ethanol and vigorous vortexing or pipetting. Then 700µl of the sample were transferred onto the membrane of an RNeasy spin column and centrifuged for 90 s. The flow-through was discarded. For DNA elimination 350 µl Buffer RW1

were added to the spin column, centrifuged for 90 sec to wash the membrane and the flow-through was discarded. DNase 1 incubation mix (consisting of 62µl H_2O, 7µl 10xDNase Buffer + 1µl DNase 1 (Invitrogen) per sample) was added onto spin column membrane and incubated for 15 min at RT. 350µl Buffer RW1 were added to the membrane, centrifuged for 90 sec at 10000 rpm and the flow-through was discarded. To wash the spin column membrane, 500µl Buffer RPE were then added to the membrane, centrifuged for 90 sec and the flow-through was discarded. This washing step was repeated once by centrifuging the spin column for 3 min. The spin column was then dried by centrifuging it at 14000 rpm for 2 min and was then placed in a new 1.5 ml reaction tube. Then, 50µl RNase-free water were pipetted on the spin column membrane, incubated for 7 min on ice and then centrifuged at 10000 rpm for 2 min to elute the RNA. This step was repeated to increase the overall RNA yield accompanied however by decreased RNA concentration.

DNA concentration was measured at 260nm wavelength via photometer and RNA purity was assessed as the ratio of absorbance measured at 260nm to the absorbance measured at 280nm wavelength.

Reverse Transcription

Isolated RNA underwent reverse transcription for the generation of complementary DNA (cDNA). Complete RNA samples or a negative control (H_2O HPLC-grade) were used for reverse transcription in addition with the following components:

amount	reagent
11.0 µl	RNA (1 µg, prediluted with H_2O)
4.0 µl	5 x First-Strand Buffer
2.0 µl	0.1M DTT
0.5 µl	Oligo-dT-nucleotide
0.5 µl	Hexanucleotide Mix (1:10 pre-diluted)
1.0 µl	10 mM dNTPs
1.0 µl	Reverse Transcriptase (200U/µl)

The First-Strand Buffer, DTT and the Reverse Transcriptase (all contained in the SuperScript II Reverse Transcription Kit) were mixed with remaining reagent and RNA as listed above. The mixture was incubated at 70°C for 10 min, the briefly put on ice, incubated at 37°C for 15 min and finally at 42°C for 60 min. The reverse transcription was completed with a denaturation step carried out at 90°C for 5 min. As the resulting cDNA concentration was assumed to equal the initial RNA concentration, cDNA was diluted based on RNA concentrations to 20ng/µl in H_2O (HPLC-grade). The samples were either stored at -20°C until further usage or immediately used in quantitative real-time PCR.

Real-time quantitative PCR

Quantitative Real-time RT-PCR was performed with primers to detect human toll-like receptor 7 (TLR7) gene expression. The human β-actin gene expression was used as a normalization control (primer sequences listed in section 3.1.8). Quantitative real-time PCR was performed in triplicates in a 96-well plate format. Power SYBR Green Master Mix (5µl), the corresponding forward and reverse primers (final concentration 150 nM) and cDNA template (5µl) or water for the non-template controls were mixed. The cycling conditions are shown in the table below.

	Temperature	Duration	Number of cycles
Enzyme activation	95°C	15 min	1 cycle
Denaturation	95°C	15 sec	
Annealing	60°C	30 sec	40 cycles
Extension	72°C	30 sec	

Calculation of TLR7 mRNA levels

The threshold cycle PCR values (Ct) were obtained during exponential amplification. The calculation of relative changes in TLR7 mRNA levels was based on the ΔΔCt method, which means that TLR7 gene expression – in relative units – was calculated by comparing the Ct values of the target gene with the normalization control gene. The Ct values for β-actin and TLR7 of technical triplicates of each sample were averaged. Standard deviations (threshold cycle differences) between triplicate reactions less than 0.5 cycles were considered to be acceptable and the Ct values were used for further calculation. The relative expression level of TLR7 mRNA was calculated in comparison to β-actin mRNA expression. In a first step, ΔCt-values were calculated for TLR7:

$$\Delta Ct_{gene} = Ct_{target} - Ct_{control\ cDNA}$$

Then, the ΔΔCt value for each treated samples was calculated by subtracting the ΔCt of the control (untreated or DMSO-treated) from the ΔCt of the sample.

$$\Delta\Delta Ct = \Delta Ct_{gene}(treated) - \Delta Ct_{gene}(untreated/control)$$

The fold exchange in TLR7 expression was then obtained by calculation $2^{-\Delta\Delta Ct}$ and visualized as bar graphs in a log2 scale.

3.2.3 Biochemical Methods

Whole cell lysates

Whole cell lysates were prepared by resuspending cell pellets containing a defined numbers of cells in 4x Laemmli buffer and heated for 10 min at 95°C before subjected to gel electrophoresis.

Protein lysates and Bradford assay

Cell pellets were resuspended in 50µl RIPA Buffer containing Protease Inhibitor Cocktail and incubated for 20 min on ice. Samples were centrifuged at 13000rpm for 15 min at 4°C and supernatants were transferred in new 1.5 ml reaction tubes for further processing. Protein concentrations were determined using Bradford protein assay, a photometric method based on the dye Coomassie Brillant Blue changing its color from red to blue if complexes with proteins are formed. For the quantification of protein concentrations a 10 mg/ml aqueous BSA solution was serially diluted to produce a standard curve ranging from 0.0 mg/ml to 2.0 mg/ml BSA. The samples to be tested were diluted 1:20 in water and Bradford Reagent which was filtered with a 0.22µm sterile filter was diluted 1:5 in water. 5 µl of the standards and the diluted samples were pipetted into a 96 well flat bottom plate and 250 µl of the Bradford solution were added to each well and incubated for 5 min at room temperature while shaking until measurement. The absorbance was measured at 595 nm without wavelength correction and the protein concentrations of the samples were determined by using the formula of the best-fit curve for the standard values. Samples were either directly used for SDS-PAGE or stored at -20°C for further analysis.

Sodium-dodecyl-sulfate polyacrylamide gel electrophoresis (SDS-PAGE)

Protein separation was performed with polyacrylamide gel electrophoresis based on the method by Laemmli. Proteins are denatured and negatively charged after binding of the detergent SDS. In an electric field the negatively charged proteins migrate towards the anode and are thus separated according to their molecular weight.

For TLR7 SDS-PAGE whole cell lysate were used, while for HPV16 E7 electrophoresis protein lysates as described above were used

Dependent on the size of the protein of interest, the resolving gels were produced with different percentages of acrylamide contained in the formulation to vary the pore size for protein separation. For the early protein of HPV16, E7, a 20% resolving gel was used, whereas for the separation of TLR7 protein a 7% gel was required.

	stacking gel	resolving gels	
	5% gel	**7% gel**	**20% gel**
Aqua dest.	2.9 ml	5.1 ml	0.73 ml
Tris Buffer	1.25 ml (0.5 M Tris, pH 6.8)	2.5 ml (1.5 M Tris, pH 8.8)	2.5 ml (1.5 M Tris, pH 8.8)
Bis-Acrylamide (30%)	0.85 ml	2.3 ml	6.67 ml
10% APS	50 µl	100 µl	100 µl
Temed	5 µl	10 µl	10 µl

Dependent on the required total protein amount, protein lysates were mixed with 4x Laemmli sample buffer and water and adjusted to a total volume of 50 µl. The samples are cooked for 10 minutes at 95°C for protein denaturation and then loaded on the gel. Gels were run at 200V, 250 mA and 50W for about 50 minutes.

Western Blot

Filters and sponges for the Western Blot chamber were treated with blotting buffer before use. The PVDF membrane was prewetted with 100% methanol for 30 seconds before use and was then washed in Blotting Buffer. The membrane and the acryl amide gel were stuck between three filter papers and one sponge from both sides. The blot was performed in Blotting Buffer at 400mA, 50W for 60-90 minutes. After the blotting step the membrane was stained with Ponceau Red solution indicating the success of the protein transfer. After removing of the color by applying distilled water, the membrane was blocked with 5% casein solution (in TBS buffer) for one hour at room temperature on the rolling mixer and was then incubated over night at 4°C with first antibody diluted in 5% casein solution (for antibody concentrations see Table). The next day, the membrane was washed 3 times for 10 minutes with TBS containing 0.1% Tween before incubated with the corresponding secondary antibody diluted in 5% casein solution. After another washing step (3x10 minutes in TBS-T) the membrane was incubated with the premixed ECL substrate (solution A and B) for 1 min before the antigens could be detected by developing the photographic films exposed to luminescent light in the darkroom. Exposure time was variable ranging from 10 seconds to 1 hour depending on the strength of the signal.

3.2.4   Cell culture methods

Flow cytometry analysis

In order to characterize the phenotypes of different primary cells as well as to monitor the generation of tumor cell lines and purification of different cell types from the whole PBMC fraction, flow cytometry analysis was performed. Therefore living cells were stained with directly fluorochrome-

labeled antibodies specific for extracellular antigens expressed by different cell types. The light emitted by the fluorochromes following absorption is three-dimensionally scattered and registered as forward scatter representing the cell size and as sideward scatter representing the cell granularity. Not only the percentage of positive cells can be determined, but also the mean fluorescence intensity providing information about the levels of antigen expression can be measured.

Depending on their availability an average of 2.5 $\times 10^5$ cells were used per staining. Cells were harvested, washed twice in PBS by centrifugation for 10 min at 4°C and 1200 rpm. Incubation with directly labeled primary antibodies (each diluted 1:50 in PBS) was carried out on ice for 30 min and protected from light. If double staining was performed, the second antibody was applied in a second incubation step following an additional washing step to remove the first antibody. Additionally, for every staining an isotype control based on an antibody directed against the corresponding IgG subtype (diluted 1:50 in PBS) was included. Following the incubation with the antibodies, cells were washed twice again in PBS by centrifuging at 4°C and 1200 rpm for 8 min and finally fixed in 1% PFA solution and stored in the dark until measurement. The samples were analyzed in a FACSCalibur and fluoresce data obtained were evaluated using CellQuest Pro Software.

Density gradient centrifugation for the isolation of mononuclear cells from peripheral blood

For immunological studies peripheral blood mononuclear cells (PBMCs) were isolated by density gradient centrifugation. PBMCs are comprise different cell types such as lymphocytes, monocytes and macrophages that can be used directly or following further separation in different immunological approaches. Density gradient centrifugation allows isolating PBMCs from whole blood and is carried out with a ficoll-based separation medium that contains a hydrophilic polysaccharide of a distinct density. Centrifugation of overlaid blood leads to the separation of the whole blood sample into plasma on the top of tube, PBMCs (middle fraction), and a fraction mainly consisting of erythrocytes on the bottom of the tube.

For extraction of PBMCs heparinized blood samples were diluted with equal amounts of RPMI 1640 medium and the mixture was carefully layered on 15ml lymphocyte separation medium. Density gradient centrifugation was carried out at 2500 rpm for 15 minutes with inactivated brake. The supernatant containing plasma was taken off and stored at −20°C. Then the interphase containing peripheral blood mononuclear cells (PBMCs) was collected and cells were washed twice in RPMI 1640 medium by centrifugation at 1800 rpm and 1500 rpm (15 min each) to purify PBMCs from eventually contaminating separation medium and also from thrombocytes. Following the washing steps the pellet was resuspended in 20 ml RPMI 1640 medium and cells were counted with trypan blue solution. PBMCs then were either directly used in experiments or stored at -80°C in human serum containing 10% DMSO.

Tumor preparation and tumor tissue culture

Tumor samples of HNSCC patients were sent overnight within 16-24 hours after surgical resection while lying in transport medium and on ice packs. All washing steps were performed with cooled

solutions and at 4°C. The tumor sample deriving from primary tumor of different localizations (base of the tongue, edge of the tongue, tonsils) or lymph node metastasis were transferred into a sterile 50 ml tube and washed twice in 10 ml tumor preparation solution by centrifuging for 10 min at 1200 rpm. Then the tissue was transferred to a sterile petri dish and eventually necrotic tissue, fatty tissue surrounding lymph nodes and larger blood vessels were removed mechanically. Following two additional washing steps in a new 50 ml tube the samples were again transferred to a new petri dish and cut into very small pieces ($\geq$ 1 mm^2) with a scalpel. The tissue pieces were again transferred into a new 50 ml tube with the help of forceps and 10 ml pipettes washed twice in a new 50 ml tube with tumor preparation solution and then digested overnight (16-20 hours depending on the size of tissue pieces) by applying 5 ml tumor digestion solution. Due to the limited size of tumor tissue, isolation of tumor infiltrating lymphocytes was not carried out and the complete amount of digested tumor tissue was used for generation of HNSCC tumor cell lines. The next day the tissue was washed twice in RPMI 1640 medium by centrifuging for 10 min at 1200 rpm and finally resuspended either in Quantum medium or FAD medium and cultured in cell culture flasks or plates. Cultures with adherent and outgrowing tumor cells were checked regularly via flow cytometry for the proportion of tumor cells. Cultures with at least 10% tumor cells were further cultured, whereas cultures with less tumor cells and those containing only fibroblasts were discarded. Sequential trypsinization of fibroblasts from young tumor cell cultures was performed to remove fibroblasts and if necessary a second trypsinization step of the remaining adherent tumor cells was carried out to detach single cells from tumor cell clusters and allow these areas to expand.

T2- peptide binding assay

The human T2 cell line deriving from T-B lymphoblast hybrids was used to test the binding affinities of different L1 peptides that were synthesized based on epitope prediction algorithms. T2 cells are transporter associated with antigen processing (TAP1/TAP2) deficient and therefore defective in loading human leukocyte antigen (HLA) class I molecules with endogenous peptides. However, HLA class I molecules of T2 cells can be loaded exogenously with peptides present in the medium, whereby different epitopes bind to HLA class I molecules with higher or lower affinities. Only peptide-HLA-complexes are stable and can be detected by flow cytometry analysis following staining with a HLA class I specific antibody whereas free HLA class I molecules not bound to any peptide are instable and degraded and therefore cannot be detected. The higher the affinity of predicted epitopes to HLA class molecules, the more stable is the complex formed and the higher is the fluorescence intensity measured.

T2 cells were harvested and resuspended in T2 medium at a density of 0.5×10^6 cells/100 µl. 100 µl/well was pipetted into a 96-well round bottom plate. Then β-2-microglobulin at concentration of 5 µg/ml as well as the newly synthesized peptides to be analyzed for their binding affinity (at 50 µg/ml) were added to each well. Peptides already known to have a high affinity to HLA class I were included as positive controls and determined the cut-off (viral MP, p16_R1, L1_323). All antigens were tested in quadruplicates. The plate was incubated over night at 27°C for 17 hours. Following the 17 hours incubation period the plate had to be incubated another 2.5 hours at 37°C, 5% CO_2. Then cells were harvested and transferred into a 1.5 ml reaction tube. They were washed one with PBS and then

stained with directly labeled HLA-A2 antibody. Finally, samples were washed twice with PBS, fixed with 1% PFA and stored at 4°C in the dark until measurement.

For analysis the MFI values for all antigens were recorded and compared with the positive controls after background subtraction (obtained by measuring T2 cells incubated in absence of any antigen). Peptides were considered to have sufficient binding capacity to HLA-A2 if the MFI was significantly higher as negative controls and at the same time exceed the lowest MFI measured for the positive controls. Peptides that fulfilled both criteria were considered to form stable peptide-HLA-complexes and to be suitable for simulation experiments.

IL-6 ELISA

Enzyme-linked immunosorbent assay (ELISA) allows the detection and quantification of antigen by specific antibodies. The ELISA used for measuring IL-6 levels is a classical "sandwich" ELISA with the antigen contained in a sample being attached to the surface of wells coated with a first antigen-specific antibody. Bound antigens are detected by a second specific antibody linked to an enzyme allowing the detection of antigen-antibody complexes via a color reaction after adding the corresponding substrate for the enzyme. Antigen concentrations can be calculated by comparing the measured optical density values with those of defined standard concentrations. For measuring the interleukin-6 release following PBMC stimulation, a commercially available IL-6 ELISA was used providing pre-coated and blocked plates. The assay was performed following the manufacturer's protocol and all standards, samples and controls were tested in duplicate. Briefly, after having prepared an IL-6 standard dilution series, the assay diluent provided was added to the wells, followed by 100µl/well of standard, sample or control. After 2 hours incubation, wells were washed, 200µl/well of IL-6 conjugate was added, incubated for another 2 hours and washed again. Substrate solution (200µl/well) was added, incubated for 20 minutes protected from light and then the color reaction was stopped by adding 50µl/well of stop solution. The optical density was determined at a wavelength of 450nm and the reference wavelength for wavelength corrections was 540nm. A standard curve was created by plotting the mean absorbance for each standard against the concentrations and drawing a best fit curve through the data points which allowed the concentration of the samples to be calculated.

Generation of dendritic cells from monocytes

Dendritic cells are the most potent antigen-presenting cells and play an important role in the raise of an antigen-specific immune response as the process and present antigens to T cells. Except from culturing dendritic cells from hematopoietic progenitor cells they also can easily be generated using CD34-positive monocytes circulating in the peripheral blood. Generation of dendritic cells requires external granulocyte-macrophage colony stimulating factor (GM-CSF) and IL-4 contained in the media.
The standard protocol requires PBMCs freshly isolated from peripheral blood. They were washed in serum free CellGro medium and resuspended in CellGro medium supplemented with 3% human serum. After one hour of adherence in a 10cm cell culture plate at 37°C the non-adherent cells were

detached by tapping to avoid clumping and the cell culture flask was then incubated overnight at 37°C, 5 % CO2. The next day, the non-adherent cells were removed and the remaining adherent monocytes were cultured to generate mature dendritic cells. To stimulate the differentiation of monocytes into dendritic cells, the monocytes were cultured in CellGro medium containing GM-CSF (1000U/ml) and IL-4 (667 U/ml) for 6 days at 37°C and 5% CO2 in a humified atmosphere. The standard maturation cocktail was supplemented by addition of TMX-202 to the medium (treatment schedule see below) on days 0, 2, 4 and 5 of the culture. Cells were harvested on day 6 by using 0.05% EDTA solution and a cell scraper. Cells were immediately used for immunoassays. For the T cell *in vitro* priming DCs generation with cells from the same donor was repeated weekly (every 6 days) and used as fresh cells for T cell re-stimulation.

Isolation of T lymphocytes from PBMCs

In order to obtain total T cells from the whole PBMC fraction, isolated mononuclear cells were subject to plastic adherence for 4 hours in RPMI containing 5% human serum as described for the generation of dendritic cells. T cells then were isolated from the non-adherent cell fraction by Pan T cell isolation based on magnetic depletion of non-T cells. Therefore floating cells were harvested, passed through a 40μm cell strainer to avoid clumping, counted and washed once in MACS Buffer. T cells were purified from that fraction by using MACS Pan T cell Isolation Kit II from Miltenyi Biotec following the manufacturer's protocol. Briefly, cells were resuspended in 40 µl MACS buffer per 10^7 cells and then incubated for 5 minutes with 10 µl per 10^7 cells of the biotin-antibody cocktail (containing monoclonal antibodies against CD14, CD15, CD16, CD19, CD34, CD36, CD56, CD123, and CD235a) targeting non-T cells. Following addition of 30 µl MACS buffer and 20 µl anti-biotin microbeads per 10^7 cells to the sample and incubation for 10 minutes, T cells could be isolated by magnetic separation. The specific binding of magnetic microbeads to labeled cells allows the depletion of the non-target cells by retaining them in the magnetic field of the MACS column while unlabeled T cells pass through. Eluted T cells were counted and immediately used in immunoassays. T cells were cultured in T cell medium containing IL-2 and IL-7.

Isolation of regulatory T cells from PBMCs (Regulatory T cell depletion)

Treg depletion was performed in order to compare the effects of T cell mediated killing of tumor cells between the total T cell fraction (including regulatory T cells) and T cells that are depleted from regulatory T cells. Tregs were depleted from the total CD3+ T cell fraction by using MACS technology based on magnetic labelling of CD25$^+$ T cells with CD25 MicroBeads and isolation of the labelled cells by positive selection over a MACS column in a magnetic field. Tregs were depleted in two successive steps following the manufacturer's protocol and comparable to the procedure describe for T cell isolation. In the first step non-CD4 positive cells were magnetically labelled and separated from CD4+ T cells to enrich the CD4+ T cell fraction. These cells were eluted from the column and stored for the experiments. In the second step, CD4+CD25+ regulatory T cells were labelled and separated from the remaining CD4+ T cell population over a column. Briefly, the cell pellet of CD4+

T cells was resuspended in 90 µl MACS buffer per 10^7 cells and 10 µl of anti-CD25 microbeads per 10^7 cells were added and incubated for 15 minutes on ice. Cells were then washed twice in 2 ml of MACS buffer by centrifuging at 1200 rpm for 10 minutes and finally resuspended in 500 µl of MACS buffer. Cells were then subject to magnetic separation for positive selection of labeled CD25+ cells while unlabeled cells pass through the column. Non-CD4+ T cells separated in first step were combined with the CD4+ enriched and Treg depleted fraction and used for further experiments.

In vitro priming of T cells with HPV16 L1 and p16^{INK4a} peptides

The induction of a specific T cell response depends on the recognition of the antigen via MHC complex and the activation by co-stimulatory molecules. The activation of naïve T cells after the recognition of antigens presented by antigen presenting cells and their development into effector T cells is called "priming" and can be simulated *in vitro* to monitor the ability of peptides to induce a cell-mediated immune response in naïve individuals giving rise to T cells that are able to recognize and target tumor cells that express the protein.

In order to induce a primary cell-mediated immune response against HPV16 L1-peptides and a p16^{INK4a}-peptide naïve T cells of a HLA-A*0201 positive healthy donor were stimulated with 9mer and 10mer L1 and p16^{INK4a} peptides predicted for HLA-A2 and validated in peptide binding assay.

Dendritic cells as potent antigen-presenting cells were used to prime naïve T cells to the peptides and were generated in 4 cycles as described above. T cells were obtained by T cell isolation from PBMCs as described above. The ratio between DC and T cell during stimulation was 1:10.
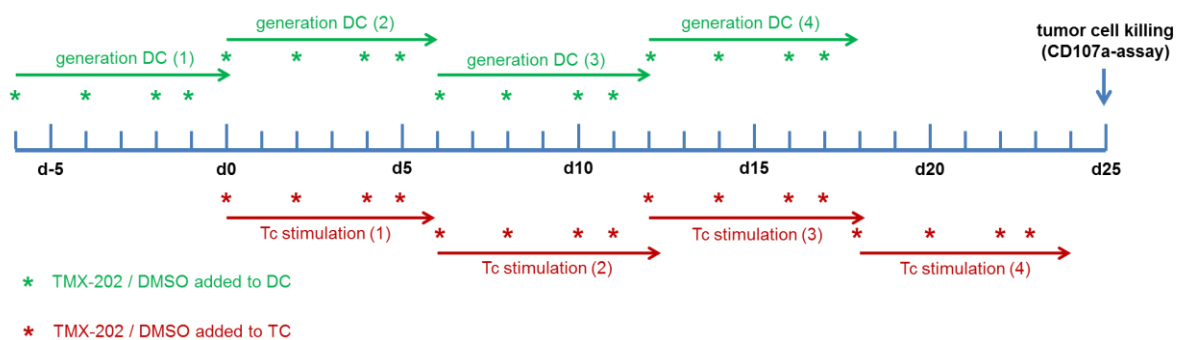
FIGURE 3.1 TMX-202 AND DMSO TREATMENT SCHEDULE FOR DENDRITIC CELLS AND T CELLS DURING THE *IN VITRO* PRIMING APPROACH.

Dendritic cells were harvested and loaded with peptides by incubating them in peptide-load medium with 20µg/ml of each peptide and in presence of Lipofectamine 2000 for 2.5 hours at 37°C, 5% CO_2. Cells were irradiated with 30 Gray after loading and washed twice. They were then added to T cells in a 12-well plate in T cell medium and were co-cultured until the next restimulation 6 days later. For restimulation T cells were harvested, washed and counted and the required amounts of DC were loaded again with peptides by repeating the procedure described above. In total, T cells had four stimulation cycles over 24 days (Figure 3.1). The experiment was based on two distinct T cell fractions that were treated with either TMX-202 or DMSO during the complete duration of the

experiment (4 treatments per cycle) and also were stimulated with either TMX- or DMSO-treated dendritic cells. The treatment schedule is shown in Figure 3.1.

PBMC treatment with TMX-202

PBMCs were obtained by density gradient centrifugation as described above and cultured in 24-well plates in medium for T cells. PBMCs were cultured for 3 days and were treated daily with either 1 μM TMX-202, 10μM TMX-202, 30μM imiquimod or the same amount of DMSO as added with the substances as control. Cells were harvested after 72 hours. Due to the adherence capacities of monocytes two distinct cell fractions had to be harvested: non-adherent peripheral blood lymphocytes (PBLs) and adherent monocytes that were harvested by using a cell scraper. Cells were washed and pellets were stored at -20°C until used for further analyses. Supernatants were also harvested, centrifuged to remove cells and stored at -80°C for cytokine analysis.

Tumor cell line maintenance

Tumor cell lines were cultured in the corresponding tumor cell media listed above. Adherent tumor cell lines were split when confluent. Prior to use in killing assays tumor cells were treated with 1 μM DAC following a standard treatment protocol to increase antigenicity of the tumor cells which was developed in the department: tumor cells were treated for 96 hours, with daily change of half of the media and addition of 1 μM final concentration with the supplemented media. Cells were then harvested and used in the corresponding experiments.

xCELLigence Impedance Measurement

The xCELLigence system is based on a microelectronic readout using electronic cell sensor array technology and allows for real-time monitoring of cellular processes without requiring labeling of cells with additional compounds and therefore being less invasive and allowing more physiological conditions. The assay principle is based on changes of the electrode impedance by adherent cells (Figure 3.3) As the measurement reflects the entire duration of the assay, the conditions can be monitored in real-time allowing the characterization of the kinetic response of cells within an assay, prior and following certain treatments. Thereby information regarding the biological status of the cell (growth rate, growth arrest, morphology, apoptosis) can be obtained rendering the assay also suitable for the quantification of compound-mediated or cell-mediated cytotoxicity. The assay principle is based on the measurement of changes of the electrode impedance due to cell-electrode interactions, as adherence of cells onto the electrodes affects the local ionic environment at the electrode/solution interface. Impedance increase is dependent on the numbers of cells attached to the electrodes but also on the quality of the interaction between cells and electrodes. The electrode impedance is represented by a dimensionless value, termed cell index, which indicates the relative change in measured electrical impedance and thus the cell status. It contains information about cell viability, cell growth or growth arrest, apoptosis, morphology and adhesion degree (Figure 3.3).
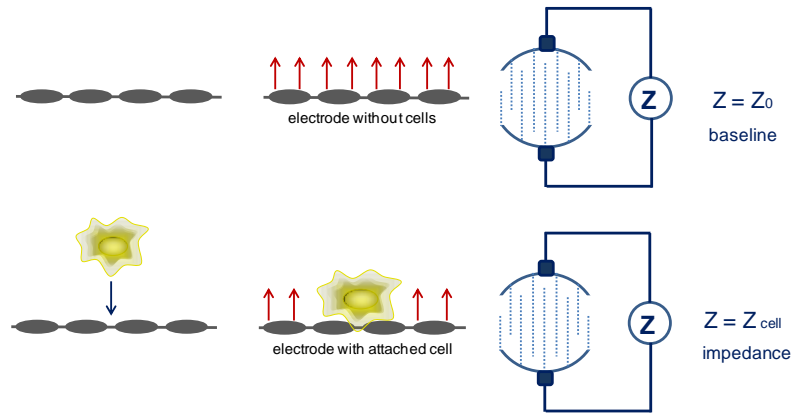
FIGURE 3.2 PRINCIPLE OF THE xCELLigence TECHNOLOGY. Adherence of cells to the electrodes affects the electrode impedance (Z_{cell}) compared with the baseline impedance (no cells, non-adhered cells) by changing the local ionic environment at the electrode/solution interface). Adapted from www.aceabio.com.

Without cells or cells not adhered to the electrodes the cell index is zero. Under the same conditions, cell index values increases with adherence of cells to the electrodes, and even more increases if cells spread over the electrodes or become more strongly attached to them. The values decrease with cells detaching from the electrodes due to apoptosis or cytotoxicity.
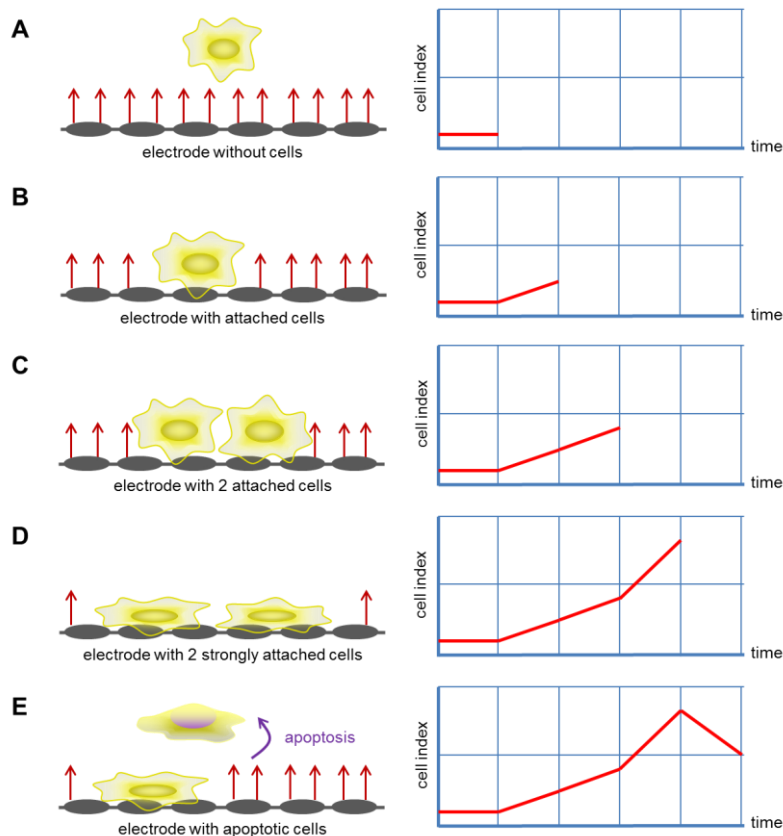
FIGURE 3.3 CHANGES OF THE CELL INDEX REPRESENTATIVE OF THE ELECTRODE IMPEDANCE OVER TIME UNDER DIFFERENT CONDITIONS. A) Electrode and cell index (CI) is zero if no cells or only non-adherent cells are contained in the wells and B) increases with adherence of cells to the electrodes. The CI positively correlates with C) the cell number and D) the strength of adherence. E) Detaching cells due to apoptosis or cytotoxicity lead to decreasing CI values. Adapted from www.aceabio.com.

The xCELLigence system was used to compare and quantify the effects of depletion of regulatory T lymphocytes from the total T cell fraction on the killing rate of tumor cells. It served as platform to characterize the cell-mediated cytotoxicity in an autologous tumor model.

The 96 well E-plate was prepared by adding 100 µl PBS in all interspaces between the wells to reduce evaporation of the medium and drying-out of the plate. Then, 75 µl/well Quantum tumor cell medium were added in well (150 µl/well in the wells designated for medium control). The plate then was incubated for 30 min at RT, put onto the SP station for measurement and impedance was measured for determination of the background (sequence 1). Per well, 25000 tumor cells were seeded in a volume of 150 µl Quantum tumor cell medium and were grown for 96 hours while pre-treated with 1 µM DAC following the standard treatment protocol developed in our laboratory (see above). Therefore the measurement was interrupted every 24 hours until day 4 (96 hours) when effector cells were added. This was done by changing half of the media and adding 25000 T cells per well in 75 µl T cell medium. The plate was then measured for an additional period of 96 hours without interruption while T cells and tumors were co-incubated. Throughout whole experiment the electrode impedance was measured every 30 minutes leading to approx. 48 time points measured for each 24 hours-interval and approx. 190 time points recorded during the tumor cell growing and the co-incubation phase.

CD107 degranulation assay

Cytotoxic T lymphocytes (CTLs) can get activated upon contact with and recognition of target cells. In the activated state during the CTL-target interaction they start to release cytotoxic granules which is accompanied by the mobilization of CD107a (lysosomal-associated membrane protein-1, LAMP-1) to the cell surface which is normally present in vesicle membranes. The CD107a surface expression thus correlates with the cytotoxic activity of T cells and the killing rate of target cells and can be quantitated by flow cytometry analysis. This method allows also for the simultaneous staining with other markers to gain further information about T cell phenotypes. The assay principle is displayed in Figure 3.4.

CD107a mobilization assay was used in two different settings: for the analysis of the killing potential of T cells after *in vitro* priming under treatment with immune modulators and of the killing effect of T cells after Treg depletion in an autologous setting.

The specific conditions and setups for each of these assays are demonstrated in Tables x and x. In general, 2.5×10^5 T cells (effectors) were co-incubated with tumor cells (targets) in a 1:1 ratio. Following isolation of fresh cells or harvesting of cultured cells, T cells were washed once in RPMI medium and adjusted to 2.5×10^6 cells per 100 µl in T cell medium. Effector cells and target cells were co-incubated in a total volume of 200µl in a 96-well round bottom under sterile conditions. As the experiment was demonstrated in previous approaches to provide reliable results with small standard deviations between quadruplicates it was performed in duplicates as T cell numbers were restricted. As controls for spontaneous CD107a release and background reactivity T cells were incubated without tumor cells. To the corresponding wells (except those where only T cell markers were investigated or served as isotype controls), 10 µl of fluorescent-labeled anti-CD107a antibody were added (see Table "Antibodies" section 1.3.5).
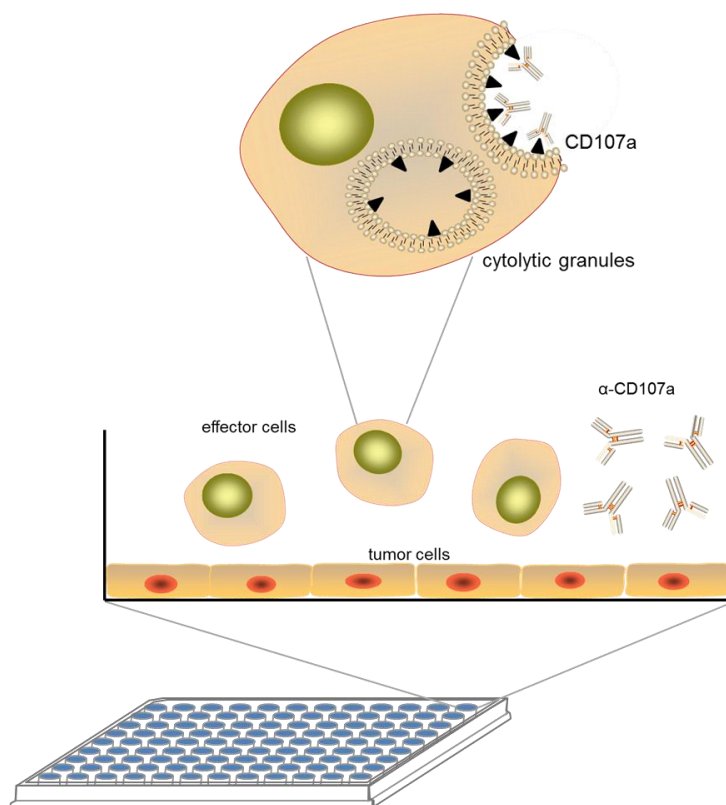
FIGURE 3.4   PRINCIPLE OF THE CD107A DEGRANULATION ASSAY. Effector cells (T cells) are co-incubated with target cells (tumor cells) and an antibody against CD107a is added to the culture (A). Upon T cell activation CD107a is mobilized to the cell surface with the release of cytotoxic granules and can be bound by the antibody. CD107a surface expression can then be analyzed by flow cytometry analysis (B).

The plate was then incubated at 37°C in a humidified atmosphere with 5% CO_2. After 1 hour of co-incubation, brefeldin A at a final concentration of 5µg/ml was added to each well and the plate was incubated for further 4 hours. The plate was then centrifuged (1200 rpm, 10 minutes, room temperature) and the supernatant was removed. T cell/tumor cell conjugates were dissolved by resuspending the pellets in 200 µl PBS/0.5mM EDTA buffer and cells were then transferred into a 1.5 ml reaction tube. The wells were washed a second time with 200 µl PBS/0.5mM EDTA buffer and remaining cells were also transferred into the tubes. After centrifugation (1200 rpm/10 minutes/ 4°C), cells were washed once with FACS-PBS and samples were either directly fixed with 1% PFA solution (CD107a single staining) or subjected to FACS staining (isotype control and T cell markers as single staining or in double staining with CD107a) by applying the FACS staining protocol described above., Finally, cells were fixed with 1% PFA solution and transferred into FACS tubes for measurement.

During FACS analysis, T cells could be distinguished from tumor cells in the FSC/SSC based on their size and granularity. The corresponding FITC and PE isotype controls allowed the definition of quadrant borders and single stains for CD107a and T cell markers were used to adjust the fluorescence compensation for the measurement of double stains. Samples containing only tumor cells were used to verify that with the instruments settings and gates chosen for analysis only T cells are included in the analysis and tumor cells are excluded from the quantitation. Then the samples of co-incubated T cells and tumor cells for the analysis of the killing rate were measured in duplicates by applying the same settings and conditions.

In vitro priming of T cells with subsequent CaSki killing

sample no	Tc untreated	Tc treated	tumor cells	anti-CD107a	FACS-stain
1	yes	no	no	none	IgG$_1$-FITC
2	yes	no	no	none	IgG$_1$-PE
3	yes	no	no	yes	none
4	yes	no	no	none	CD8
5	yes	no	no	yes	CD8
6	no	yes	no	none	IgG$_1$-FITC
7	no	yes	no	none	IgG$_1$-PE
8	no	yes	no	yes	none
9	no	yes	no	none	CD8
10	no	yes	no	yes	CD8
11	no	no	yes	none	IgG$_1$-FITC
12	no	no	yes	none	IgG$_1$-PE
13	no	no	yes	yes	none
14	no	no	yes	none	CD8
15	no	no	yes	yes	CD8
16-17	yes	no	yes	no	CD8
18-19	yes	no	yes	yes	none
20-21	yes	no	yes	yes	CD8
22-23	no	yes	yes	no	CD8
24-25	no	yes	yes	yes	none
26-27	no	yes	yes	yes	CD8

Samples 1-5 represent controls for untreated T cells, samples 6-10 controls for treated cells. Controls for tumor cells are represented by samples 11-15. The killing experiment (co-incubation of T cells with tumor cells) is represented by samples 16-23.

Treg depletion with subsequent killing of the autologous cell line HN038M

sample no	Tc total	Tc depleted	tumor cells	anti-CD107a	FACS-stain
1	yes	no	no	none	IgG$_1$-FITC
2	yes	no	no	none	IgG$_1$-PE
3	yes	no	no	yes	none
4	yes	no	no	none	CD4
5	no	yes	no	none	IgG$_1$-FITC
6	no	yes	no	none	IgG$_1$-PE
7	no	yes	no	yes	none
8	no	yes	no	none	CD4
9	no	no	yes	yes	none
10	no	no	yes	none	CD4
11	no	no	yes	yes	yes
12-13	yes	no	yes	yes	yes
14-15	no	yes	yes	yes	yes

Samples 1-4 represent controls for total T cells, samples 5-8 controls for Treg depleted T cells. Controls for tumor cells are represented by samples 9-11. The killing experiment (co-incubation of T cells with tumor cells) is represented by samples 12-15.

Mycoplasma detection assay

Mycoplasma are the simplest prokaryotes and a major problem in cell culture as contamination is very common and may influence the cell proliferation of cell lines but also their gene expression patterns which might be a problem for different assays. To exclude infections with mycoplasma, cell lines, especially those of primary cell culture, were regularly tested with the MycoAlert™ assay. This assay is a rapid and easy method to detect mycoplasma contamination in cell cultures and is based on the selective biochemical analysis of the activity of special mycoplasma enzymes. Mycoplasma contained in the culture are lysed and set free enzymes that react with the MycoAlert substrate catalyzing the conversion of ADP to ATP. The ATP levels measured in a sample before and after the substrate is added allow the calculation of a ratio that indicates presence or absence of mycoplasma. The underlying biochemical reaction is based on the oxidation of Luciferin in presence of ATP by Luciferase and allows the quantification of emitted light.

$$ATP + Luciferin + O_2 \xrightarrow{\text{Luciferase} + Mg_2} Oxyluciferin + AMP + Pp_i + CO_2 + h \cdot \nu$$
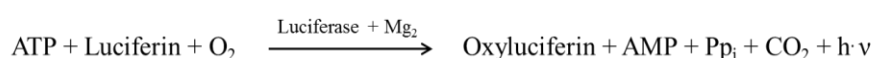
The intensity of the emitted light is linearly related to the ATP concentration and can be measured by a luminometer. The assay was performed following the manufacturer's protocol. Briefly, 2 ml of cell culture supernatant or cell culture were transferred into a reaction tube and any cells contained in the sample were pelleted at 1500 rpm for 5 minutes. 100 µl of the cleared supernatant were transferred into a luminometer cuvette and 100 µl of MycoAlert reagent were added to each sample and incubated for 5 minutes. The cuvette was placed in the luminometer and read (with a program set to 1 minute integrated reading) to obtain a value for Reading A. Then 100 µl of the MycoAlert substrate were added to each sample and incubated for 10 minutes before the cuvette was measured again (Reading B). The ratio "Reading B/Reading A" was calculated and interpreted as follows:

Ratio	Interpretation
< 0.9	negative for mycoplasma
0.9 - 1.2	borderline: quarantine cells and retest in 24 hours
> 1.2	mycoplasma contamination

3.2.5   Statistical Methods

For the comparison of continuous data between two groups either Student's t-test or Mann-Whitney U test for non-parametrical data were used.

For the estimation of differences in categorical in terms of between two groups chi-square test was used.

For all tests, differences were considered to be significant if the calculated p-value was 0.05 or less.

4. IMMUNE CELL INFILTRATES AND POSSIBLE IMMUNE EVASION MECHANISMS IN CERVICAL LESIONS

The present chapter deals with the immunological characterization of cervical intraepithelial neoplasia and cancers. Final goal of this part is to gain a better understanding of the clinically heterogeneous behavior of the precancerous lesions in terms of regression and progression rates.

In the first part a central methodological approach of histological analyses of immune cell infiltrates in CIN was established using a computer-based tool for the standardized quantification of immune cell infiltrates in cooperation with the TIGA Centre Heidelberg (chapter 4.1).

In the following part immune cell infiltrates were investigated in CIN to find out if samples of different infection stages are different in terms of immune cell phenotypes. Changes in immune cell densities and composition might be a hint for either underlying immune-regulatory mechanisms or effective anti-tumoral immune responses. In this context, the time point of when changes in the immune cell infiltration become apparent during the natural history of CIN lesions and a possible association with the initiation of the transforming infection stage as represented by $p16^{INK4a}$ overexpression are of special interest. Therefore different T cell markers of which most are well-characterized, and which are representative of T cell activation and also of immuno-regulatory mechanisms were investigated (chapter 4.2).

To better understand to which extent intrinsic features of the epithelial cells play a role in the pathogenesis of cervical cancer the antigen-presentation capacity of the lesion cells was investigated. Antigen presentation might be influenced by HPV infection and alterations regarding the expression of the involved molecules probably promote disease progression by causing immune escape despite the presence of infiltrating lymphocytes (chapter 4.3).

Finally, the immune infiltrates of patients with CIN who were topically treated with the clinically approved immuno-modulatory substance imiquimod, were characterized in a longitudinal approach (chapter 4.4). These analyses aim at a better understanding of how the immune cell composition could be positively influenced and how these changes might correlate with the clinical course of the disease.

4.1 Development of an automated quantification system for the computational profiling of cervical intraepithelial neoplasia and its microenvironment

4.1.1 Scanning and digitalization of stained tissue sections

As the analysis of immune cell infiltrates in the lesions and the adjacent stroma was based on digitalized images of the tissue sections, the slides were scanned after having been fully automated stained with monoclonal antibodies against CD3 and CD8. The tissue sections were automatically imaged with the Hamamatsu NanoZoomer 2.0-HT Scan System (Figure 4.1) at 20-fold magnification resulting in a resolution of 0.46µm/pixel. The scan system is equipped with three 4096x64 pixel Time Delay and Integration (TDI) CCD (charge-coupled device) sensors enabling imaging based on a three-dimensional XYZ-zoom technology (ROJO et al., 2006). This type of sensor allows multilayer scanning and is not restricted to one single, two-dimensional layer. The resulting virtual slides can then be analyzed in a similar manner as using classical microscopy allowing focusing through different layers of the tissue, dependent on the number of layers that were scanned and the distance between them. With a total capacity of 210 slides per batch and a scanning speed of 60 seconds for a tissue sample sized 15x15mm² the system allows for high-throughput scanning, digitalization and archiving of tissue samples. While scanning a glass slide, the system automatically detects the region of interest defined by presence of any tissue and also automatically chooses the correct and valid focal plane for the scanning processing. The file size of the virtual slides resulting from the digitalization process originally is up to 20 GB as uncompressed files and depends on the total size of the scanned area, the number of scanned layers and the magnification used during scanning. The file size retroactively can be reduced (approximately by the factor 25) by applying lossless JPEG compressing algorithms reducing for example a 16.3 GB slide to a 636 MB JPEG file.
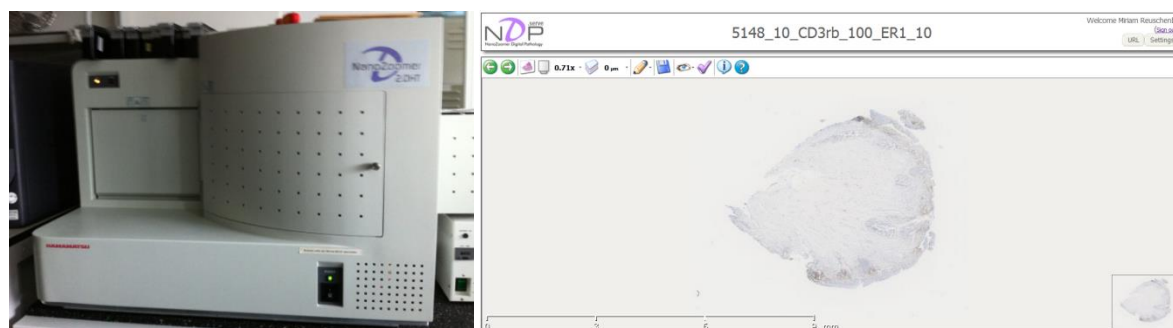
FIGURE 4.1 THE NANOZOOMER 2.0-HT SCAN SYSTEM USED FOR DIGITALIZATION OF STAINED SLIDES AND THE USER INTERFACE OF THE NDP SLIDE SERVER. With the NDPView software digitalized slides can be analyzed on a computer and allows the user to navigate through the slide in all three dimensions. Slides can be annotated, screenshots can be made and parameters such as intensity of the color channel, contrast and brightness can be adapted.

The scanned slides were made accessible on the TIGA's Slide Server (http://tigacenter.bioquant.uni-heidelberg.de/ndp-slide-server.html) for all cooperation partners and thus facilitated the exchange of data and information. This tool was also used for the definition of the lesion based on the p16^{INK4a} staining and in cases of unclear morphology in low-grade lesions served as a platform for the pathologist's review of the tissue (Figure 4.1).

4.1.2 Development of an image processing tool adapted to cervical intraepithelial neoplasia

The algorithms used for image processing have been developed using TissuemorphDP™M from Visiopharm, a company specialized in tissue analysis. The image processing software applied in this project was based on different algorithms and developed in cooperation with the TIGA Center, Heidelberg. An overview of the user interface of the Visiopharm image processing software with exemplary tools developed in the frame of this project that are applicable to the analysis of immune cells infiltrates in cervical intraepithelial neoplasia is given in Figure 4.2.
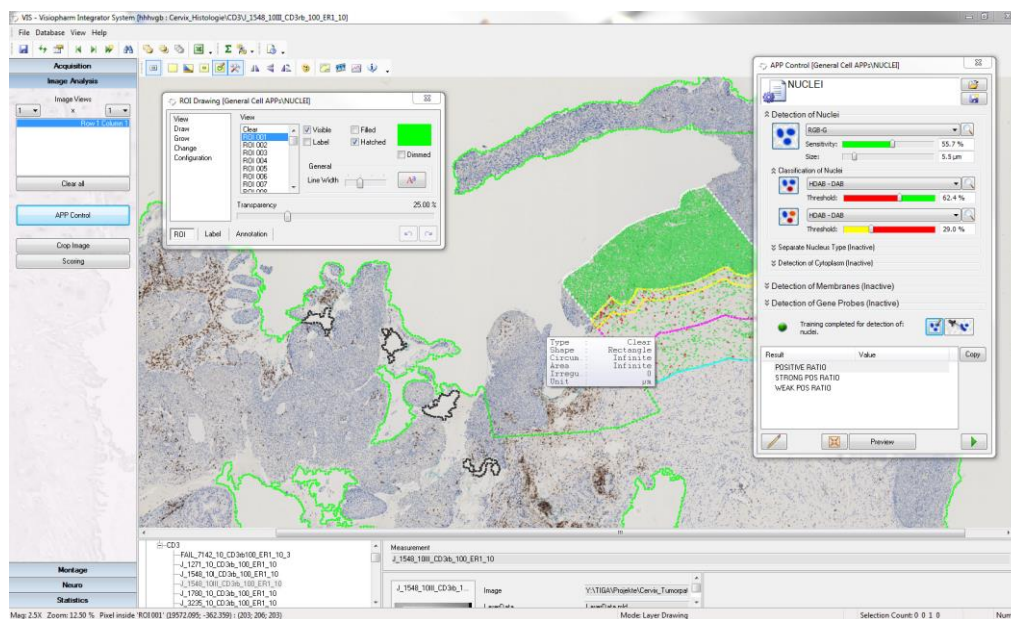
FIGURE 4.2   OVERVIEW OF THE USER INTERFACE OF THE VISIOPHARM IMAGE PROCESSING SOFTWARE. Tools were developed for the annotation of the lesion and basal membrane, generation of ROIs, clearance of non-ROIs before starting the processing for cell segmentation.

Image processing was developed and adapted to CIN lesions using the Visiopharm image processing software before algorithms could finally be applied to the digitalized slides. Image processing is performed in four distinct steps.

(i)   Automated tissue detection

The fully automated detection of all analyzable tissue contained on the glass is the first step towards the cell quantification in the lesion and its microenvironment. The region of interest (ROI) is defined as the tissue area that shall be subjected to further analysis. ROI detection was performed on the whole slide after converting a color overview image (RGB) into a greyscale image. By applying simple thresholding methods on the grey scale image as described previously (OTSU, 1979), ROIs could be separated from the background regions of the slides. Thereby the background representing any non-tissue regions is separated from the relevant tissue regions which can then be subject to further image processing steps and analysis (Figure 4.3 A). As a post-processing step for the ROI detection, areas that cannot be analyzed because they are too small or inappropriate such as small tissue fragments, folded tissue, staining artifacts or dust particles were removed (Figure 4.3 B) by applying morphological operations like opening or closing (GONZALES, 2009). These are standard imaging operations to remove small disturbing objects from the image or to remove small holes contained in the tissue.
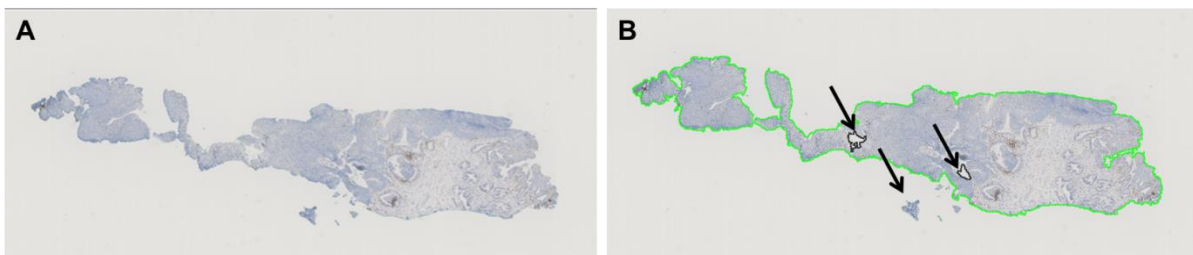
FIGURE 4.3   EXAMPLE OF THE ROI DETECTION PROCESS. A) Regions of interest are detected automatically using thresholding methods to separate the tissue from the background (green line). B) Post-processing steps remove artifacts and areas (indicated by arrows) that are too small for further analysis.

(ii)   Manual annotation of the lesion and the basal membrane and automated generation of different invasive margins in the stroma

In a second step the regions to be analyzed had to be defined which was done partially by manual annotation and partially by automated generation of regions that were then subjected to further analysis. Due to the high tissue heterogeneity in CIN and the resulting difficulties to separate normal tissue from the lesion and also the presence of p16^{INK4a}-positive and p16^{INK4a}-negative lesion areas among the low-grade lesions renders fully automated computational image processing challenging. One major concern is that p16^{INK4a}-negative low-grade lesions would not have been identified as such by the established automated annotation algorithm and would have falsely been annotated as "normal" tissue. Therefore in this first approach for the establishment of the basic method, automated

tumor/lesion-identification was replaced by manual annotation based on a comparison with the p16^{INK4a}-stained reference slide. Lesions positive for p16^{INK4a}-overexpression were visually identified and the corresponding region was annotated manually in the slides stained for the defined T cell markers (white line, Figure 4.4). In unclear cases due to aberrations between the histological stage given by the pathologist and the morphology of the lesion, tissue sections were reviewed by the pathologist again. The manual approach described here also allowed for the separate investigation of p16^{INK4a}-positive and -negative lesion areas within the same sample. In the second step the basal membrane underneath the annotated lesion was also manually marked. These annotation steps are the prerequisite to proceed to the next step that divided the adjacent stromal tissue into several distinct areas (invasive margins). The algorithms applied for region growing are used from the baseline (basal membrane/lamina) and separate the tissue into specific regions by growing in fixed and determined directions. Starting at the basal lamina, the first region grows with a distance of 100µm into the surrounding tissue of the epithelial region (yellow line, Figure 4.4). Then the second defined region grows with further 400µm into the tissue (border at 500µm, pink line) and is followed by the last growing with 500µm (border at 1000µm) leading finally to the last margin with a maximal distance of 1000µm located from the basal membrane (green line, Figure 4.4). After processing the slides were manually inspected and regions that did not represent typical stromal tissue (artifacts such as disruptions, or glandular tissue, endothelial cells and cavities of large blood vessels) and that therefore had to be excluded from further processing were removed manually from the regions by annotating them as regions to be cleared (Figure 4.4).
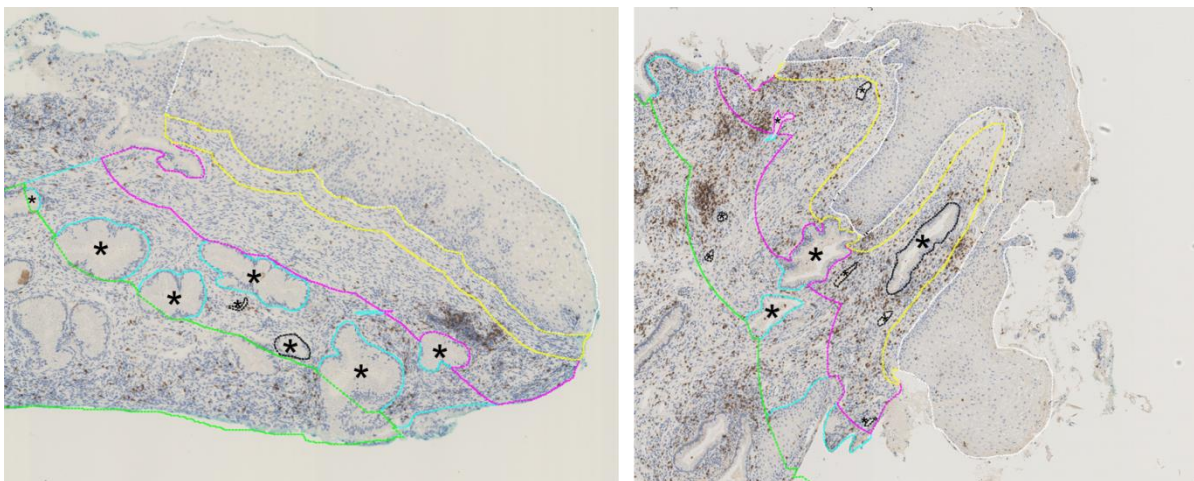
FIGURE 4.4   EXAMPLES OF PROCESSED SLIDES WITH AND THE CLEANING POST-PROCESSING STEP. The regions of interest (ROIs) are visualized by color-coded lines and represent the epithelium (white), margin 100 (yellow), margin 500 (pink) and margin 1000 (green). Cleared regions are marked by an asterisk.

(iii)   Cell segmentation

During the last image processing step positively stained and unstained cells were detected by cell segmentation and subsequently the expression level (determined as brown (positive) or non-brown (negative)) is determined. The segmentation of the cell nuclei was performed separately in all determined stromal ROI generated in the previous step and also of all nuclei in the epithelial region. The segmentation of all nuclei (brown and blue) is based on a watershed segmentation described elsewhere (BEUCHER, 1992; JUNG and KIM, 2010) on the IHS (Intensity, Hue, Saturation)-S color band. The basic principle of watershed segmentation is the transformation of an intensity image into a three-dimensional topographic image. The intensity of each pixel of an image thereby is represented by the altitude of the relief. Watershed algorithms then are applied, the relief is "floated" and the watersheds around peaks can be interpreted as borders defining different components which can thus be segmented from each other.
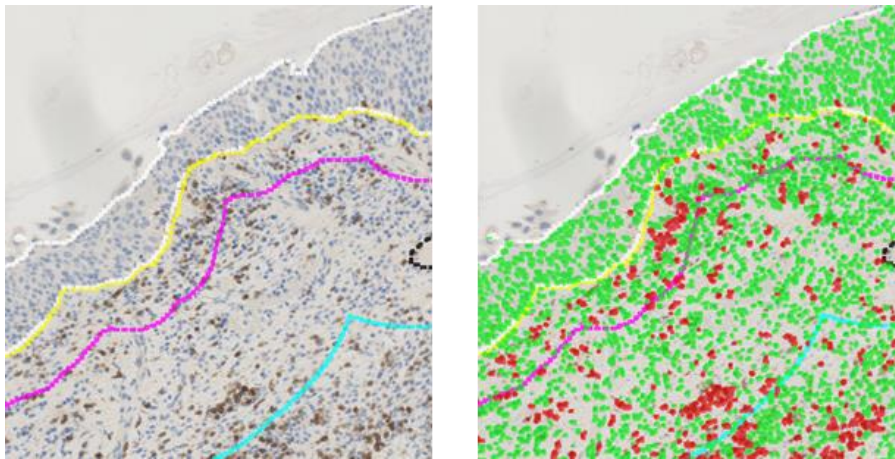
FIGURE 4.5   EXAMPLE OF THE CELL DETECTION STEP. Shown is the annotated tissue (A) before cell segmentation and (B) after cell segmentation. DAB-negative cells are displayed in green, DAB-positive cells in red.

Finally, the DAB-positive (brown stained) cells were detected within a HDAB-DAB color band, provided by a color deconvolution algorithm (RUIFROK and JOHNSTON, 2001). In dependence on the DAB staining signal of the surrounding membranes nuclei were categorized into two groups by simple thresholding, namely blue nuclei with brown (DAB-positive) membranes and blue nuclei without brown staining signal (Figure 4.5). In a post-processing step nuclei detected that were defined as being too small where removed by an area-filter. An overview of all image processing steps is given in Figure 4.6.
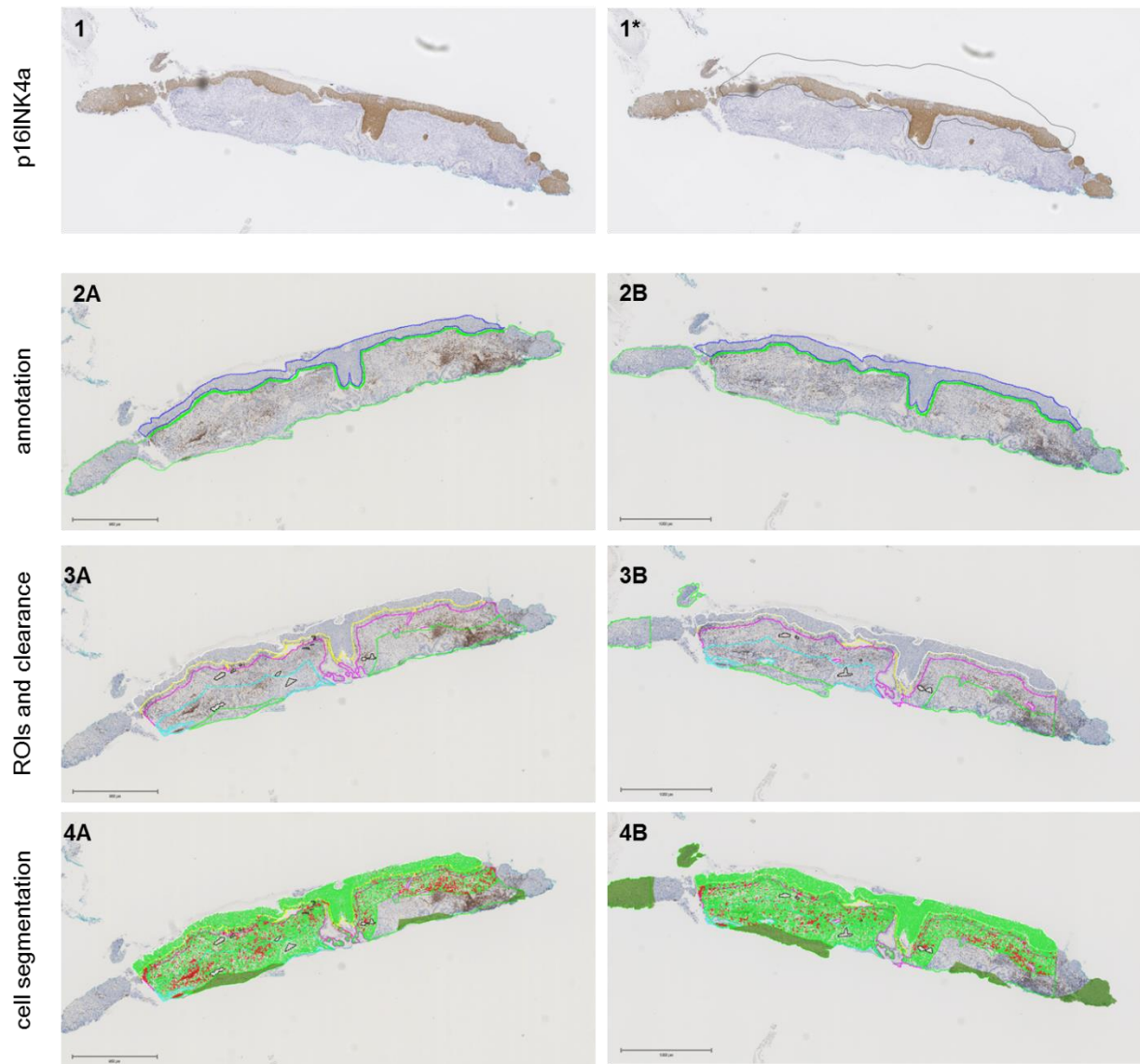
FIGURE 4.6   EXAMPLE OF THE SUCCESSIVE STEPS OF THE AUTOMATED QUANTIFICATION PROCESS. Based on the p16INK4 reference slide (1) on which the lesion was marked after reviewed by a pathologist (1*) the slides stained for CD3 (left side, (A)) and CD8 (right side, (B)) were annotated by demarking the epithelium and the basal membrane (2). Then the different invasive margins with 100 µm, 500 µm and 1000 µm reaching into the stromal compartment were generated (3). Finally, cells stained for the corresponding immune cell markers (red) and those that are negative (green) are detected and quantified.

4.1.3   Calculation of cell densities from the output data

The successive application of image processing steps described above resulted in different output variables comprising number and area of the nuclei for every staining category (negative = blue, positive = brown) and, in addition, the white areas surrounding the nuclei and representing cytoplasm. All output variables are listed below in table 4.1.

ROI 001	RO002	ROI 003	ROI 004
epithelium	margin 100	margin 500	margin 1000
counts of negative nuclei inside the corresponding ROI (blue signal)			
counts of positive nuclei inside the corresponding ROI (brown signal)			
area covered by negative nuclei inside the corresponding ROI			
area covered by positive nuclei inside the corresponding ROI			
remaining (non-nuclei) area inside the corresponding ROI (white area)			

TABLE 4.1   OVERVIEW OF THE OUTPUT VARIABLES OBTAINED FOR ALL DEFINED REGIONS OF INTEREST (ROI) FOLLOWING APPLICATION OF IMAGE PROCESSING STEPS.

The output data comprise cell counts of positive and negative cells and the areas that are covered by cell in a distinct ROI. Single values are given for the negative nuclei, positive nuclei and the white surroundings representing cytoplasm. The total areas of all compartments, ROIs, could then be calculated from these values. This was done for each compartment separately (margin 100, margin 500 and margin 1000), but also for the continuous regions that reach from the basal membrane up to the 500µm and the 1000µm borders. The ratios between cell counts in a distinct ROI and the corresponding area of this compartment were calculated in order to obtain the cell densities as "positive cells/mm^2") from the output data.

4.2   The local immune cell infiltration in cervical intraepithelial neoplasia in relation to p16^{INK4a} expression

The study presented in this chapter adresses the question whether changes in the composition and densities of immune cell markers are correlated to p16^{INK4a} overexpression in cervical dysplasia, as a marker stratifying CIN into two infection states (permissive infections, p16^{INK4a}-negative, and tansforming infections, p16^{INK4a}-positive). The correlation of possible changes in immune cell density and composition with p16^{INK4a}-defined biologic stages may reveal import insights into the immune control and changes of these mechanisms during cervical carcinogenesis.

For the investigation of a possible link between the infection stage and infiltrating immune cells in CIN mainly well-characterized standard T cell markers were chosen (for details see Introduction chapter 1.4.1).

A mixture of activation and inhibition markers should allow to investigate to which extent T cells present in the lesion microenvironment are in an activated state and possibly able to combat the HPV infection and transformed cells or are inhibited. The global T cell infiltration was characterized by CD3-expressing cells while CD8 and Granzyme B were used as markers for cytotoxic T lymphocytes (CTLs) and activated CTLs displaying lytic activity. Forkhead box transcription factor 3 (Foxp3), a marker for regulatory T cells and thus representing the suppressive state of immune cells was also included. CD3-ζ was included as a marker for the susceptibility of T cells for activation upon antigen recognition.

4.2.1   p16^{INK4a}-expression status of the lesions

As a marker highlighting transforming HPV infections (BERGERON et al., 2014; VON KNEBEL DOEBERITZ et al., 2012) p16^{INK4a} was used to biologically define the different lesion grades that were available for this study. Immunohistochemical staining for 16^{INK4a} (chapter 3.21) revealed that all cervical carcinoma samples and all high-grade CIN (CIN2/3) were p16^{INK4a}-positive. However, low-grade CIN (CIN1) could be classified into two groups with 9 of 22 lesions being p16^{INK4a}-negative (permissive infection) and 13 of 22 lesions being p16^{INK4a}-positive representing the early transforming infection stage in CIN (Table 4.2).

	CIN1	CIN2	CIN3	CxCa	Overall population
number of patients	22	11	19	17	69
p16^{INK4a}-positive samples: n (%)	13 (59.1%)	11 (100.0%)	19 (100.0%)	17 (100.0%)	60 (86.96%)

TABLE 4.2   SAMPLE CHARACTERISITCS REGARDING THE HISTOLOGICAL CLASSIFCIATON AND THE TRANSFORMING INFECTION STAGE AS REPRESENTED BY THE p16^{INKa} STATUS.

4.2.2   Comparison of T cell infiltrates in p16^{INK4a}-positive and p16^{INK4a}-negative low-grade CIN

In terms of histomorphological classification CIN1 lesion are regarded as a uniform group. Biologically they are, however, more diverse with a proportion of these lesions being already in the early transforming infection stage which is highlighted by beginning p16^{INK4a}-overexpression.

T cell infiltrates of all phenotypes were compared between p16^{INK4a}-negative and p16^{INK4a}-positive low-grade lesions (representative examples for the immunohistochemical characterization of infiltrating immune cells are given in Figure 4.7).
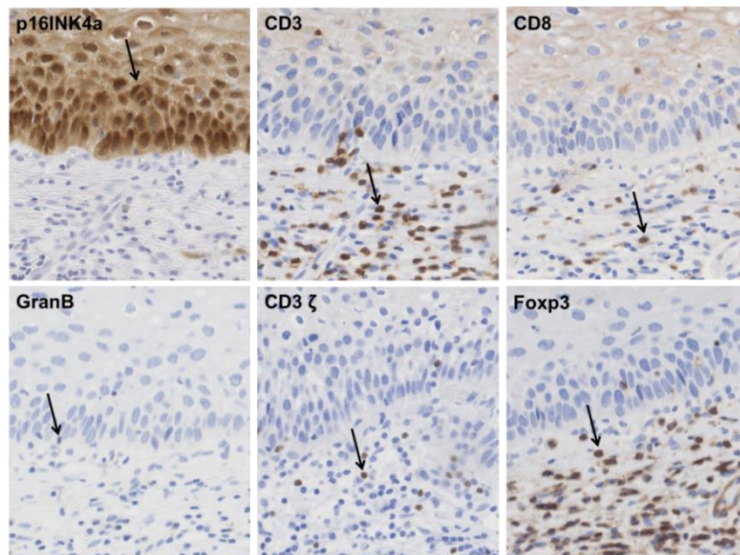
FIGURE 4.7 REPRESENTATIVE DETAILS OF IMMUNOHISTOCHEMICAL STAININGS (AT 200x MAGNIFICATION) FOR p16^{INK4a}, CD3, CD8, GRANB, CD3ζ AND FOXP3. Representative areas of the epithelium (upper part of the tissue) and the adjacent stroma (lower part) are shown and examples of positive cells are indicated by arrows.

Low-grade lesions (all CIN1 irrespective of the p16^{INK4a} expression state) and the adjacent stromal compartment had generally lower total numbers of infiltrating immune cells compared with the higher grade CIN (mean cell numbers, ranges and standard deviations are summarized in Table S9.1). Nevertheless, the comparison of p16^{INK4a}-negative and p16^{INK4a}-positive samples within the group of low-grade CIN did not reveal significant differences regarding the infiltration densities of the five investigated T lymphocyte phenotypes (4.8 and Table S9.1). The ratio between epithelial and stromal cell numbers representing the percentage of T cells invading from the lesion-adjacent stroma into the lesion neither did reveal significant differences between p16^{INK4a}-negative and p16^{INK4a}-positive CIN1 lesions (Figure 4.8 and Table S9.1). Furthermore, the ratios of all T cell subtypes to CD3+ cell counts were calculated for both compartments as a measure for the proportion of distinct T lymphocyte phenotypes among all present T cells. Here again, no significant differences between p16^{INK4a}-negative and p16^{INK4a}-positive low-grade lesions were observed (Figure 4.9 and Table S9.2).
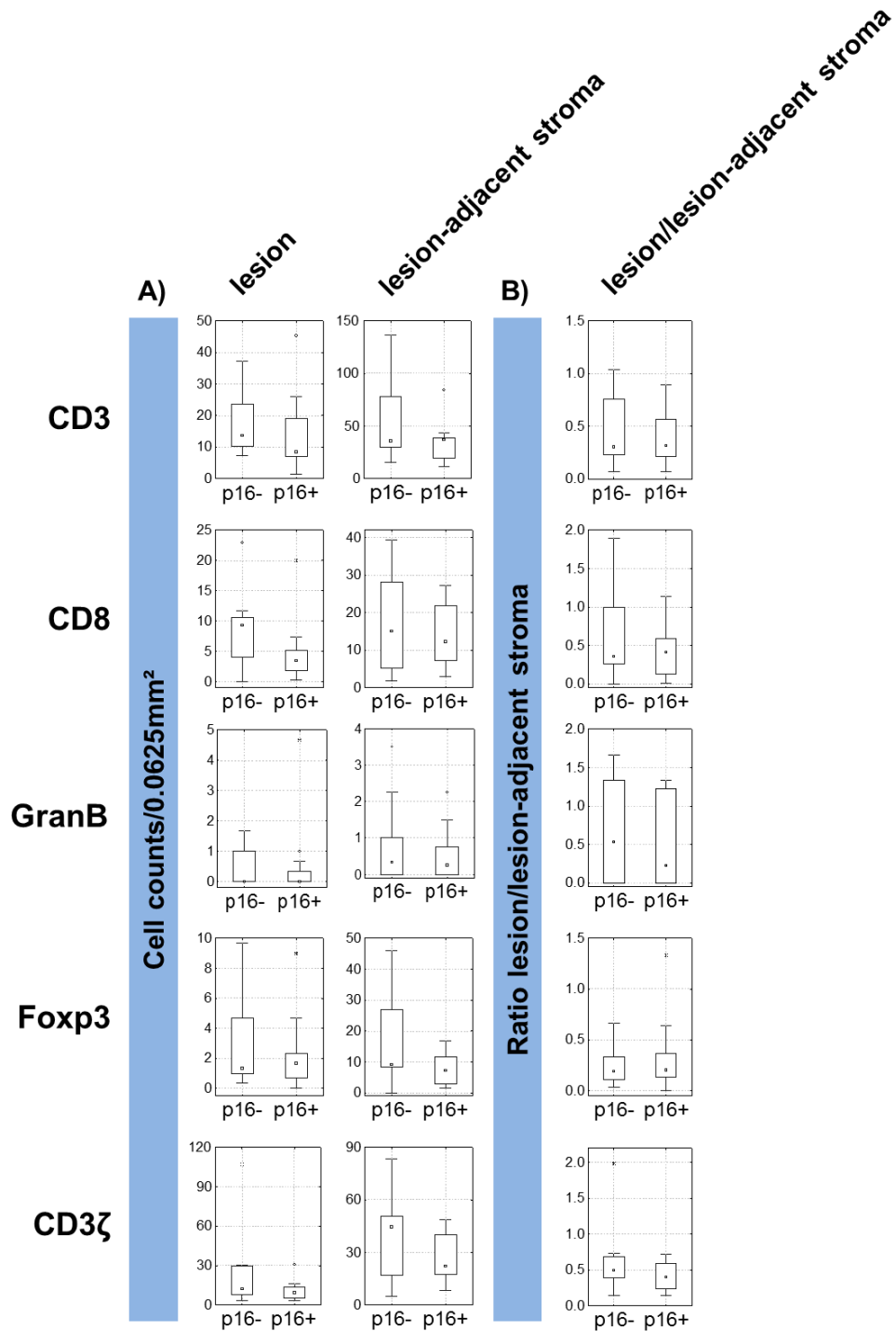
FIGURE 4.8   DISTRIBUTION OF T CELL SUBTYPES IN DIFFERENT COMPARTMENTS IN p16^{INK4a}-NEGATIVE LOW-GRADE LESIONS COMPARED WITH p16^{INK4a}-POSITIVE LOW-GRADE LESIONS. A) Absolute T cell counts per 0.0625mm² in the lesion and lesion-adjacent stroma. B) Ratio between the lesion and lesion-adjacent stroma for all T cell phenotypes. The dot in the center of each box represents the median value of the distribution; the borders of the box represent the upper and lower quartiles (25%-75%). Significant levels are indicated by asterisks:

* $p < 0.05$ (significant)
** $p < 0.01$ (very significant)
*** $p < 0.001$ (extremely significant)
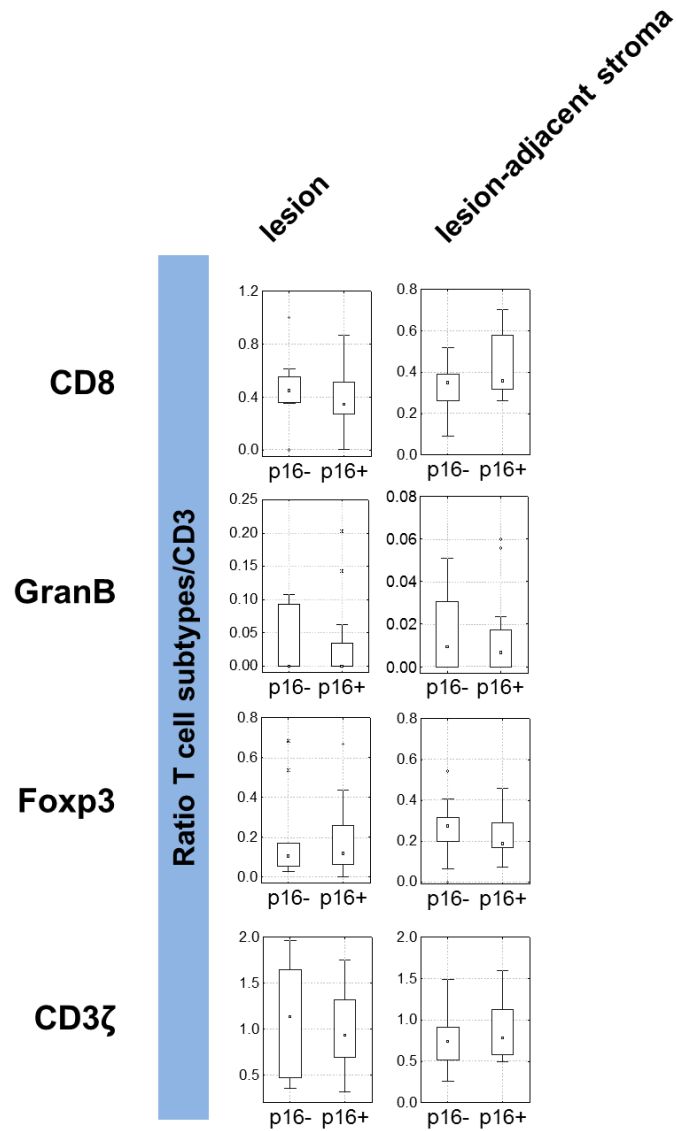
FIGURE 4.9 RATIOS OF T CELL SUBTYPES TO CD3+ T CELLS PRESENT IN THE LESION AND LESION-ADJACENT STROMA IN $p16^{INK4a}$-NEGATIVE LOW-GRADE LESIONS COMPARED WITH $p16^{INK4a}$-POSITIVE LOW-GRADE LESIONS. The dot in the center of each box represents the median value of the distribution; the borders of the box represent the upper and lower quartiles (25%-75%). Significant levels are indicated by asterisks:

*	$p < 0.05$ (significant)
**	$p < 0.01$ (very significant)
***	$p < 0.001$ (extremely significant)

4.2.3   T cell infiltrates in p16^{INK4a}-positive high-grade CIN

The high-grade CIN (CIN2/3) were all p16^{INK4a}-positive indicating true transforming HPV infection in these lesions that furthermore probably have acquired secondary genomic alterations.

The comparison of T cell counts between high-grade CIN (CIN2/3, all p16^{INK4a}-positive) and all low-grade CIN (of which n=13 were p16^{INK4a}-positive and n=9 were p16^{INK4a}-negative) revealed that the number of total T cells represented by CD3+ cells significantly was increased in high-grade lesions compared with low-grade CIN in both the epithelium (p=0.0273) and the stromal compartment (p<0.0001). This general increase is also reflected by the higher stromal infiltration of Foxp3+ T cells (p=0.0076), the higher infiltration with GranB+ T cells in the epithelium (p=0.0028 for the epithelium and p=0.0014 for the stromal), of CD8+ T cells (p=0.0012 for the epithelium and p<0.0001 for the stroma) and also of CD3ζ+ T cells (p=0.0286 for the epithelium p=0.0022 for the stroma) (Figure 4.10, Table S9.1). With regard to the epithelial to stromal cell number ratios a trend for decreased ratios was found for CD3+ cells (p=0.0799) and also CD3ζ+ cells (p=0.0672) in high-grade CIN compared to low-grade lesions (Figure 4.10 and Table S9.1). Again, the ratios for all T cell phenotypes to CD3+ T cell counts were calculated and were found to be significantly increased in high-grade CIN for GranB+ T cells (p=0.0041) and for CD8+ T cells (p=0.0258) in the epithelium. The ratio calculated for CD3ζ+ T lymphocytes showed the inverse correlation and tended to be decreased in the stromal compartment of high-grade CIN (p=0.0700) (Figure 4.11 and Table S9.2).

Interestingly, the absolute T cell numbers but also the ratios calculated for different T cell subtypes to CD3+ T cells are very heterogeneous in high-grade lesions (Figures 4.10 and 4.11) and within a distinct histomorphological category (Table S9.1) and span wide ranges. Epithelial numbers for CD8+ T cell for example range from 3.7 to 32.3 cells per 0.0625mm² in CIN2 lesions. These enormous variances can also be observed for epithelial Foxp3+ T cell numbers in CIN2 lesions ranging from 2.0 to 17.0 cells per 0.0625mm^2 (Table S9.1).

FIGURE 4.10   DISTRIBUTION OF T CELL SUBTYPES IN DIFFERENT COMPARTMENTS IN LOW-GRADE (LG) LESIONS COMPARED WITH HIGH-GRADE (HG) LESIONS. A) Absolute T cell counts per 0.0625mm² in the lesion and lesion-adjacent stroma. B) Ratio between the lesion and lesion-adjacent stroma for all T cell phenotypes. The dot in the center of each box represents the median value of the distribution; the borders of the box represent the upper and lower quartiles (25%-75%). Significant levels are indicated by asterisks:

* $p < 0.05$ (significant)
** $p < 0.01$ (very significant)
*** $p < 0.001$ (extremely significant)

FIGURE 4.11   RATIOS OF T CELL SUBTYPES TO CD3+ T CELLS PRESENT IN THE LESION AND LESION-ADJACENT STROMA IN LOW-GRADE (LG) LESIONS COMPARED WITH HIGH-GRADE (HG) LESIONS. The dot in the center of each box represents the median value of the distribution; the borders of the box represent the upper and lower quartiles (25%-75%). Significant levels are indicated by asterisks:

* $p < 0.05$ (significant)
** $p < 0.01$ (very significant)
*** $p < 0.001$ (extremely significant)

4.2.4   T cell infiltrates in cervical carcinomas

With regard to the total T cell numbers the infiltration is even higher in cervical carcinoma samples in comparison to high-grade CIN for most of the different T cell phenotypes (mean cell numbers, ranges and standard deviations are shown in Table S9.1). Especially the stromal compartment showed an enhanced T cell infiltration where significant differences compared to the high-grade lesions could be found for the global T cell infiltration with CD3+ T lymphocytes ($p = 0.0414$), GranB+ T cells ($p = 0.0095$) and also Foxp3+ T cells ($p = 0.0243$). The higher total cell numbers were accompanied by

decreased epithelial to stromal ratio for GranB+ (p=0.0467) and Foxp3+ T lymphocytes (p=0.0464). For the other cell types (CD3+, CD8+ and CD3ζ+ T lymphocytes) no significant differences in the epithelial/stromal ratio could be observed (Table S13.x). Also most of the ratios calculated for all T cell subtypes to CD3+ cell counts as a measure for the proportion of distinct cell phenotypes among all T lymphocytes, were decreased in cervical carcinomas compared to high-grade CIN. The decrease was significant for the intraepithelial CD8/CD3 ratio (p=0.0090) and the stromal CD3ζ/CD3 ratio (p=0.0090), which represents the lowest CD3ζ/CD3 ratio of all stages. The only exception is the significantly higher GranB/CD3 ratio (p=0.0418) in cervical carcinoma samples compared to high-grade lesions.

In summary, cervical precancerous lesions displayed generally increasing T lymphocyte densities with worsening lesion grade from low-grade lesions to high-grade lesions and towards cancer. Thereby, T cell densities in the transforming infection stage of low-grade CIN were not yet different form non-transforming CIN1 lesions. Although the increase of immune cell densities could be observed for different T cell markers, the presence of regulatory T cells could be identified in all lesion stages and is more pronounced in the stroma than in the epithelium. Based on the data shown in Table S9.1 an increase from low-grade lesions (stromal mean cell density for both non-transforming and transforming low-grade lesions together: 10.8 cells/0.0625 mm^2) to CIN3 (mean 19.3 cells/0.0625 mm^2) could be observed (p=0.0076). The Foxp3+ T cell density was further increased in invasive cancer with a mean density of 42.1 cells/0.0625 mm^2 compared with high-grade lesions (p=0.0243). The ranges of densities were remarkable in all diseases stages with 0.0-20.0 cells/0.0625 mm^2 in low-grade lesions, 1.5-16.8 cells/0.0625 mm^2 in high-grade lesions and 3.3-97.8 cells/0.0625 mm^2 in cervical cancers.

4.3 Alterations of human leukocyte antigen expression in cervical intraepithelial neoplasia and cancers

As shown in section 4.2 there is a striking contradiction between high numbers of infiltrating lymphocytes in high-grade cervical dysplasia and carcinomas indicating that immune cells are attracted to the lesion site. However, these lesions obviously have progressed to finally become an established and morphologically visible high-grade lesion demonstrating that despite the presence of T cells in the microenvironment a certain number of already established high-grade lesions cannot be completely eradicated and will further progress to become invasive tumors. High T lymphocyte infiltration of both CD4+ and CD8+ T lymphocytes in association with cancer development has also been observed in other tumor entities (HAN et al., 2014; MATKOWSKI et al., 2009).

These observations might imply that tumor cells under the immunoselective pressure evolve strategies that provide protection from recognition and elimination by cytotoxic T cells (GARCIA-LORA et al., 2001). Indeed, as adaption to the host's immune system and in order to circumvent an immune attack tumor cells are able to modulate the immune response by changing their own characteristics. One of these changes represent the alteration of the expression and function of human leucocyte antigen (HLA) class I and class II on the surface of tumor cells. In comparison with the modification of the

tumor microenvironment by changes in the cytokine milieu and immune cell composition, is a much more immediate mechanism. In the context of HPV-associated diseases this might also be of importance: transforming cervical lesions and carcinomas constitutively express the viral oncoproteins E6 and E7 which could be degraded for antigen processing and subsequent presentation by HLA class I molecules and might be recognized by effector cells such as cytotoxic T lymphocytes. As outlined in chapter 1.4.2 alterations in antigen-presentation pathways might result in a less effective presentation of viral and tumor-associated antigens and prevents the tumor from being recognized by the host T cells.

HLA class I antigens are composed of a heavy chain (glycoprotein) which is encoded by genes within the HLA regions of chromosome 6p (HLA-A, -B, -C) and a light chain (β2m) encoded by a gene located on chromosome 15q. HLA class I antigens are normally expressed on all nucleated cells of the body. HLA class II antigens are also heterodimeric molecules composed of an alpha and a beta chain. This class of antigen-presenting molecules is usually expressed by professional antigen-presenting cells of the immune system. Tumors of different origins have been reported to show altered human leucocyte antigen expression which can be gradual and range from down-regulation to total loss of classical HLA class I antigens but also gradual induction of *de novo* expression of HLA class II antigens.

The project described in this chapter aims at the characterization of altered HLA class I antigen and HLA class II antigen expression profiles in cervical intraepithelial neoplasia and cancers to answer the question if these modifications might contribute to cervical carcinogenesis. Some reports on altered HLA class I expression are conflicting and it remains still unclear whether HLA class I antigens are completely lost during cervical carcinogenesis – suggesting a strong selection pressure for negative cell clones, or whether their expression is only reduced – suggesting functional impairment, but potentially enabling re-expression by drug intervention, vaccination or immune modulation.

Cervical lesions of different grade, CIN2 (n=9), CIN3 (n=13) and invasive squamous cell carcinoma (SCC) samples (n=19) were analyzed by immunohistochemical staining for HLA class I antigen heavy chains (HLA-A, HLA-B and HLA-C) and the light chain (beta-2-microglobuline, β2m) and also HLA class II antigens in order to find out if these molecules are differentially expressed in increasing histomorphological lesion grades.

4.3.1   Altered HLA class I antigen expression in cervical intraepithelial neoplasia and cervical carcinoma

For the characterization of HLA class I antigen expression a panel of antibodies was used as described previously (KLOOR et al., 2005) to determine the expression levels of the HLA class I heavy and light chains separately. The monoclonal antibodies HC-10 and HCA-2 recognize different epitopes of the HLA class I heavy chains: while HC-10 recognizes a determinant expressed on β2m-free HLA-A10, HLA-A28, HLA-A29, HLA-A30, HLA-A31, HLA-A32 and HLA-A33 heavy chains and on β2m-free

HLA-B and HLA-C heavy chains the monoclonal antibody HCA-2 binds to a determinant expressed on β2m-free HLA-A (excluding HLA-A24), HLA-B7301 and HLA-G heavy chains.

To determine the expression of the HLA class I light chain the monoclonal antibody L368 recognizing β2m was used.

Importantly, HLA class I complexes are denatured by formalin fixation during the tissue processing and dissociate into the heavy chain and the light chain. Therefore, it is not possible do detect intact and functionally active HLA class I complexes. Thus only a combination of antibodies can allow the distinction between free heavy chains or β2m molecules respectively and those assembled to HLA-class I heavy chains/β2m complexes transferred to and located on the cell surface. Membranous localization of HLA heavy chains (A/B/C) indicated intact HLA class I complexes transferred to the tumor cell surface. In contrast, altered expression or complete loss of membranous β2m staining and disturbances in membranous HLA class I heavy chain staining is a sign for defects in the antigen presentation pathway being either impaired or non-functional.

Lesions were classified as having normal, heterogeneous or negative HLA class I staining pattern based on criteria summarized in Table 4.3.

score	staining pattern	% cells positive within lesion/tumor
positive	strong, homogeneous overall expression	> 75%
heterogeneous	faint and patchy, weak overall expression	25-75%
negative	absent or restricted to single cells (immune cells or locally induced expression)	< 25%

TABLE 4.3   SCORING SYSTEM FOR THE EVALUATION OF HLA CLASS I AND II STAINING PATTERNS.

Examples of staining pattern are shown in Figure 4.12 for the HCA-2 antibody.
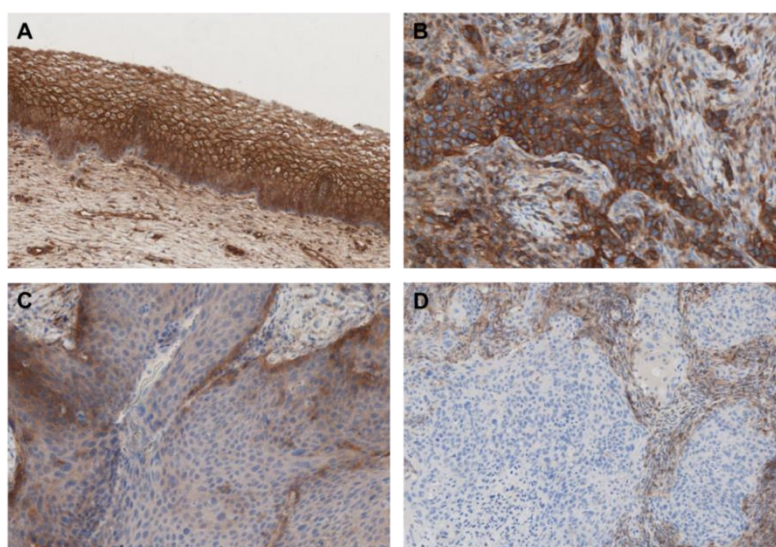
FIGURE 4.12   REPRESENTATIVE HCA-2 STAINING PATTERNS OBSERVED IN CIN AND CERVICAL CANCER SAMPLES (200x MAGNIFICATION). Shown are examples for A) positive staining (strong and membranous) in normal, non-dysplastic epithelium, B) positive staining of invasive SCC, C) heterogeneous expression pattern and D) invasive SCC with negative HCA-2 staining pattern.

Cytoplasmic and membranous staining of cells of the normal, non-dysplastic epithelium, precancerous lesions and tumors was recorded separately and are summarized in Table 4.4. Representative staining results for p16^{INKa} and all HLA class I antigen markers are shown in Figure 4.13.

	HLA class I heavy chain								HLA class I light chain			
	HC-10 cytoplasm		HC-10 membrane*		HCA-2 cytoplasm		HCA-2 membrane*		β2m cytoplasm		β2m membrane*	
non-neoplastic epithelium												
positive (%)	19	100.0%	19	100.0%	19	100.0%	15	78.9%	19	100.0%	19	100.0%
heterogeneous (%)	0	0.0%	0	0.0%	0	0.0%	4	21.1%	0	0.0%	0	0.0%
negative (%)	0	0.0%	0	0.0%	0	0.0%	0	0.0%	0	0.0%	0	0.0%
Samples analyzed	**19**		**19**		**19**		**19**		**19**		**19**	
CIN 2												
positive (%)	9	100.0%	9	100.0%	6	66.7%	1	11.1%	9	100.0%	9	100.0%
heterogeneous (%)	0	0.0%	0	0.0%	1	11.1%	3	33.3%	0	0.0%	0	0.0%
negative (%)	0	0.0%	0	0.0%	2	22.2%	5	55.6%	0	0.0%	0	0.0%
Samples analyzed	**9**		**9**		**9**		**9**		**9**		**9**	
CIN 3												
positive (%)	12	92.3%	9	69.2%	6	54.5%	2	18.2%	12	92.3%	8	61.5%
heterogeneous (%)	1	7.7%	3	23.1%	2	18.2%	3	27.3%	1	7.7%	4	30.8%
negative (%)	0	0.0%	1	7.7%	3	27.3%	6	54.5%	0	0.0%	1	7.7%
Samples analyzed	**13**		**13**		**11**		**11**		**13**		**13**	
invasive SCC												
positive (%)	16	84.2%	15	78.9%	8	47.1%	2	11.8%	16	84.2%	8	42.1%
heterogeneous (%)	2	10.5%	3	15.8%	4	23.5%	4	23.5%	3	15.8%	6	31.6%
negative (%)	1	5.3%	1	5.3%	5	29.4%	11	64.7%	0	0.0%	5	26.3%
Samples analyzed	**19**		**19**		**17**		**17**		**19**		**19**	

TABLE 4.4 HLA CLASS I ANTIGEN EXPRESSION IN CIN2, CIN3 AND INVASIVE SCC. Data for HC-10 and HCA-2 heavy chain antibodies and β2m are shown for the cytoplasmic and membranous separately.

Normal, non-dysplastic epithelium if present and analyzable on the same slide was characterized for HC-10, HCA-2 and β2m staining patterns. In total, n=19 regions could be found that were adjacent to CIN2 or CIN3 lesions. The normal epithelial regions showed positive staining in 100.0% of the cells and also a clear membranous staining for all three antibodies.

In cervical precancerous lesions and cancers a high frequency of HLA class I alterations could be observed.

All samples investigated for HLA class I antigen expression were p16^{INK4a}-positive. The staining results for HC-10 showed that all CIN2 samples displayed normal expression in both cytoplasm and membranous localization (100.0%). A heterogeneous membranous staining could be observed in 3 of 13 (23.1%) of CIN3 lesions and 3 out of 19 samples (15.8%) of invasive SCC. Lesions totally negative for membranous HC-10 staining were rare and represented 1of 13 (7.7%) of CIN3 and 1 of 19 (5.3%) of invasive SCC.

The HCA-2 staining demonstrated that heterogeneous or absent cytoplasmic staining occurred more frequently in comparison with HC-10 antibody staining. Positive HCA-2 cytoplasmic staining could only be observed in 6 of 9 (66.7%) of CIN2, in 6 of 11 (54.5%) of CIN3, and 8 of 17 (47.1%) of invasive SCC samples. Conversely, heterogeneous expression and total losses were frequent: regarding the membranous expression more than half of CIN2 (5 of 9, 55.6%) and CIN3 (6 of 11, 54.5%), and 11 of 17 (64.7%) of invasive SCC are negative for membranous HCA-2 staining.
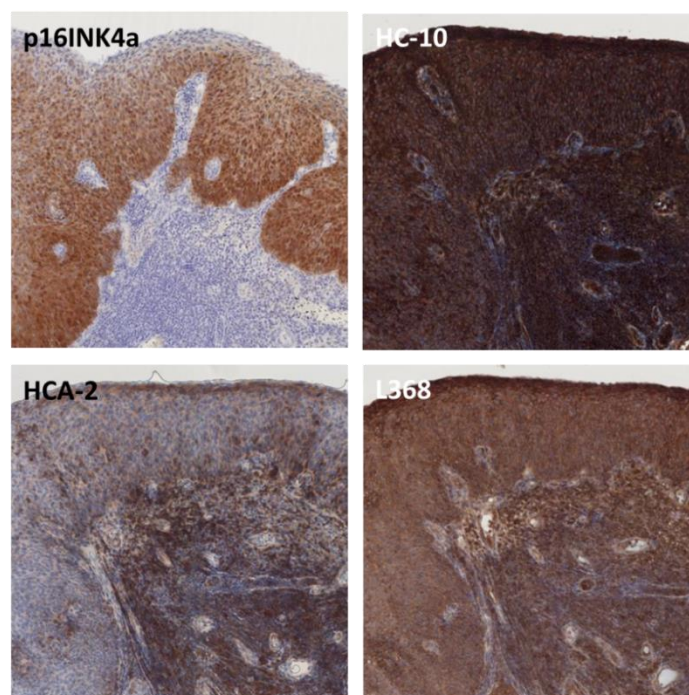
FIGURE 4.13   EXEMPLARY STAINING RESULTS FOR ALL MARKERS IN A CERVICAL CANCER SAMPLE (SCC) AT 200x MAGNIFICATION. Shown are the p16^{INK4a}-staining and the slides stained for all three HLA class I antigen markers (HC-10, HCA-2 and L368).

Regarding the staining for β2m the results demonstrated the vast majority of cervical precancers and cancers are positive for cytoplasmic β2m (100.0% of CIN2, 92.3% of CIN3 and 84.2% of invasive SCC). Heterogeneous expression is found in a small proportion of CIN3 and invasive SCC (7.7% and 15.8%) and none of the samples is negative for cytoplasmic β2m expression. Regarding the membranous expression of β2m all CIN2 samples displayed normal expression (100.0%) while CIN3 and invasive SCC to a certain extent display altered membrane staining. However, still 61.5% of CIN3 and 42.1% of invasive SCC are positive for membranous β2m.

The correlation analyses between expression intensities (negative, homogenous and positive) and stage of the disease showed that the HC-10 membranous staining was differently distributed between all precancerous lesions (CIN2 and CIN3) and invasive cancers (SCC) with $p < 0.0001$. CINs lesion more often showed a positive staining (in 13/22 samples) while in SCC more often a heterogeneous staining pattern could be observed (in 15/19 samples). Regarding the HCA-2 staining no differences between the two groups could be shown for the membranous staining, but the overall cytoplasmic expression was different between CIN and SCC: CIN lesions more frequently showed positive staining patterns (in 9 out of 20 CINs), while 9 of 17 SCC samples were negative for HCA-2 staining ($p = 0.0005$). For membranous β2m-expression a strong trend towards more positive staining pattern in CIN (17 of 22 samples) in comparison to SCC samples (8 of 19 samples) could be observed. In contrast, SCC samples showed a higher tendency to be negative for membranous β2m-expression (5 of 19 samples) compared with CIN samples (1 out of 22).

4.3.2   Human leucocyte antigen class II expression in cervical intraepithelial neoplasia and cervical cancer

HLA class II antigens are normally expressed on professional antigen-presenting cells (APCs), but have also been reported to be expressed by distinct solid tumors (ALTOMONTE et al., 2003; DENGJEL et al., 2006). The mechanisms involved in the expression of HLA class II antigens and their role in the interaction of the tumor cells with the host's immune system as well as the role of immunoselection in HLA class II antigen loss are largely unknown. To investigate the role of HLA class II antigen expression in the development of cervical intraepithelial neoplasia and progression towards cancer, cervical lesions were stained with a monoclonal antibody against HLA class II chains DR, -DQ, -DP (LGII-612.14).

The analysis was performed in the cohort used for the characterization of HLA class I antigen expression. With CIN2 already displaying strong HLA class II antigen *de novo* expression the question arose whether or not low-grade CIN (CIN1) also showed this expression pattern. To explicitly address this question the cohort was enlarged by an additional set of CIN1 samples (n=19) and a further subset of CIN2 samples (n=9). In parallel to the study of immune cell infiltrates in different infection stages of low-grade CIN lesions (chapter 4.x) the HLA class II expression pattern was correlated with the p16^{INK4a} status of these additionally included lesions.

The same categories of staining patterns were applied as for HLA class I antigen staining (Table 4.3). Examples of the different HLA class II antigen staining patterns are shown in Figure 4.14.
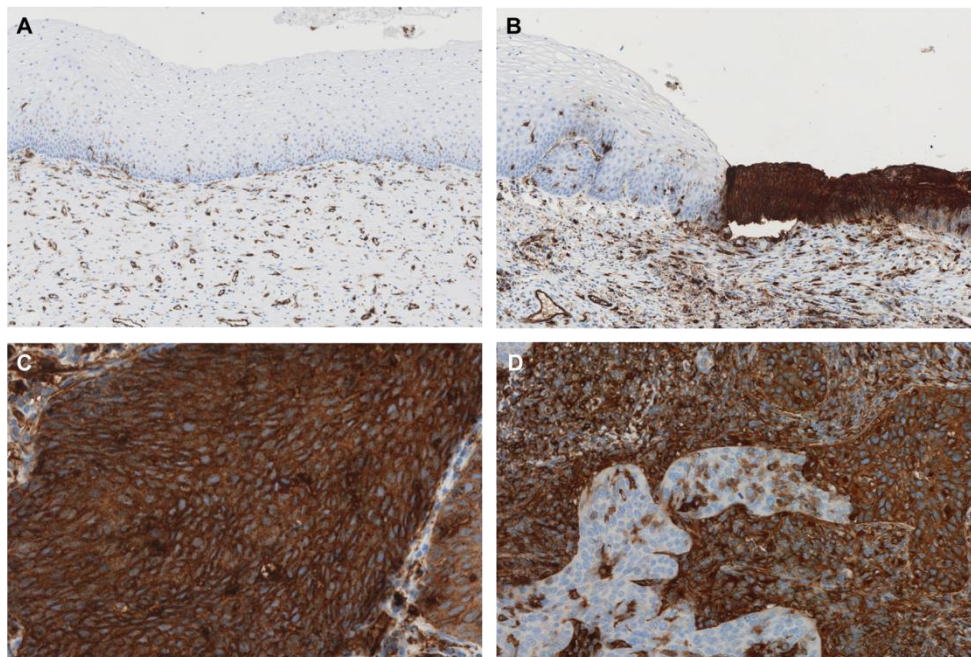
FIGURE 4.14   EXEMPLARY LGII.612-14 STAINING PATTERNS OBSERVED IN CIN AND CERVICAL CANCER SAMPLES. Shown are A) normal, non-dysplastic epithelium which is negative for HLA class II antigen expression B) the transition from adjacent normal epithelium to a CIN lesion with a strongly positive staining pattern, C) positive invasive SCC and D) heterogeneous staining pattern in invasive SCC with areas negative and positive for LGII.612-14 staining.

The results of HLA class II antigen expression were recorded separately for the cytoplasm and the membranous localization and are summarized in Table 4.5.

Again, if normal non-dysplastic epithelium adjacent to the lesions was present, it was also analyzed for HLA class II antigen expression (n=29). Positive staining was completely absent in the normal stratified cervical epithelium or restricted to single cells in the epithelium only. However, HLA class II antigen expression can frequently be detected in dysplastic epithelium as shown in Figure 4.14.

Interestingly, 15 of 18 investigated CIN2 samples showed cytoplasmic HLA class II antigen expression (heterogeneous or positive staining) in the lesion and only 3 of 18 (16.7%) were negative for staining with the LGII.612-14 antibody. Importantly, more than half of the CIN2 lesions (55.6%) (10 out of 18 cases) displayed strong and positive HLA class II antigen expression. This suggests that HLA class II antigen expression is a very common event during the initial steps of transforming HPV infection.

	HLA class II			
	LGII-612.14 cytoplasm		LGII-612.14 membrane*	
non-neoplastic epithelium				
positive (%)	0	0.0%	0	0.0%
heterogeneous (%)	0	0.0%	0	0.0%
negative (%)	29	100.0%	29	100.0%
Samples analyzed	**29**		**29**	
CIN 1				
positive (%)	6	31.6%	3	15.8%
heterogeneous (%)	4	21.1%	4	21.1%
negative (%)	9	47.3%	12	63.1%
Samples analyzed	**19**		**19**	
CIN 2				
positive (%)	10	55.6%	8	44.4%
heterogeneous (%)	5	27.8%	6	33.3%
negative (%)	3	16.6%	4	22.3%
Samples analyzed	**18**		**18**	
CIN 3				
positive (%)	7	53.8%	5	38.4%
heterogeneous (%)	4	30.8%	6	46.2%
negative (%)	2	15.4%	2	15.4%
Samples analyzed	**13**		**13**	
invasive SCC				
normal (%)	11	57.9%	10	52.6%
heterogeneous (%)	5	26.3%	6	31.6%
negative (%)	3	15.8%	3	15.8%
Samples analyzed	**19**		**19**	

TABLE 4.5 HLA CLASS II ANTIGEN EXPRESSION IN NORMAL EPITHELIUM, CIN1, CIN2, CIN3 LESIONS AND INVASIVE SCC. Data are shown for the cytoplasmic and membranous expression separately.

In CIN3 lesions 84.6% (11 out of 13 samples) of the lesions were found to be positive for HLA class II antigens with more than half of them (53.8%) being strongly stained and considered positive. The same trend could also be observed in invasive cancers. Here, a positive HLA class II staining pattern could be observed in 11 of 19 cases (57.9%).

The observation that the majority of CIN2 lesions displayed HLA class II antigen expression prompted the idea to characterize low-grade CIN1 lesions - included retrospectively - for the expression of HLA class II antigens in order more precisely determine the time point of the induction of its expression. Again, in a non-negligible proportion of samples (10 of 19, 52.7%) HLA class II expression could be observed. In comparison with high-grade lesions (CIN2/3) and cancers, however, the percentage of negative lesions was relatively high (47.35%).

As for the immune cell infiltrates (chapter 4.2) the low-grade lesions were stratified for their $p16^{INK4a}$-status representing thus non-transforming ($p16^{INK4a}$-negative) and transforming ($p16^{INK4a}$-positive) CIN1 in order to estimate a possible correlation of HLA class II with the biological infection stage.
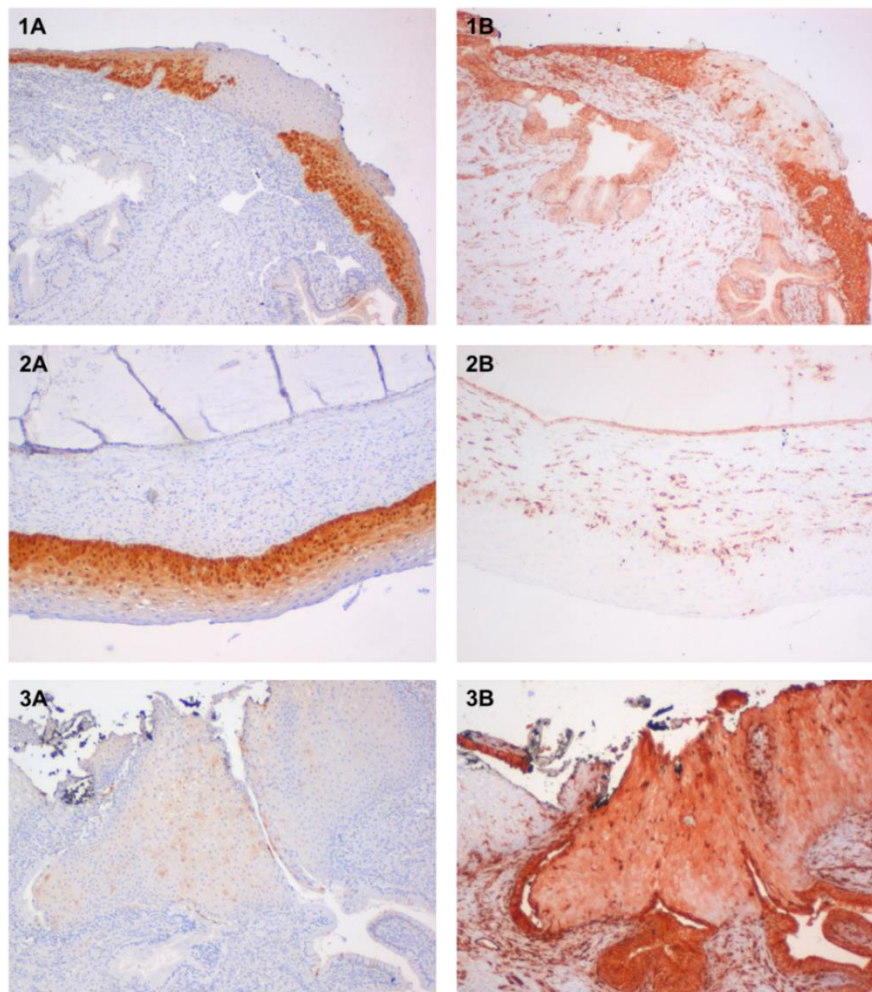
FIGURE 4.15   REPRESENTATIVE STAININGS FOR THE CORRELATION OF (A) $P16^{INK4A}$ EXPRESSION AND (B) HLA CLASS II ANTIGEN EXPRESSION IN LOW-GRADE CIN (CIN1). Shown are examples for 1) perfectly matching $p16^{INK4a}$-positive areas with HLA class II positive regions 2) a $p16^{INK4a}$-positive lesion that is HLA class II negative and C) a $p16^{INK4a}$-negative (focal $p16^{INK4a}$-expression) that is HLA class II positive.

Among CIN1 9 out of 19 (47.4%) were $p16^{INK4a}$-negative and 10 out of 19 (52.6%) were $p16^{INK4a}$-positive. A possible association between $p16^{INK4a}$ expression reflecting the infection stage and HLA class II antigen expression in CIN1 lesions could not be found when HLA class II antigen expression – cytoplasmic or membranous – and the $p16^{INK4a}$ expression status in low-grade lesions were correlated.

This result confirmed the observations made during the microscopic evaluation with regard to the occurrence of all possible combinations of p16^{INK4a} expression with HLA class II antigen presence or absence (Figure 4.15). The distribution HLA class II antigen expressing lesions among p16^{INK4a}-negative and p16^{INK4a}-positive CIN1 is shown in Table 4.6.

p16^{INK4a} status	LGII-612.14 negative	LGII-612.14 positive
p16^{INK4a}-negative	3/9 (33.3%)	6/10 (60.0%)
P16^{INK4a}-positive	6/9 (66.6%)	4/10 (40.0%)
p-value	p=0.245	

TABLE 4.6   DISTRIBUTION OF HLA CLASS II EXPRESSION IN p16^{INK4a}-NEGATIVE AND p16^{INK4a}-POSITIVE CIN1 LESIONS.

The distribution of HLA class II antigen expression was also correlated to the grade of the disease by comparing all precancerous lesions with the invasive cancer samples: no correlation could be observed between the membranous HLA class II antigen expression and the disease stage represented by all CIN lesions and invasive SCC samples (p=0.182). The comparison of single, unpooled CIN stages (CIN1, CIN2 and CIN3 separately) and SCC samples with each other revealed that membranous HLA class II antigen expression was significantly different lower in CIN1 lesions than all high-grade lesions (CIN2, CIN3) and cancers (p=0.019).

In order to find out if there was a correlation between HLA class II expression and the alterations of HLA class I antigen expression reported in the previous section (4.3.1) the samples that were initially included in the study (CIN2, CIN3 and invasive SCC) before enlargement by CIN1 and further CIN2 samples and for which both staining data sets were available, were investigated. A significant association between HLA class II and class I antigen expression was not observed. The presence and absence of HLA class II expression was correlated with the HC-10 staining pattern (p=0.996) and HCA-2 staining (p=0.532) and also β2m expression (p=0.361). A significant association between HLA class II and class I antigen expression was not observed.

While the normal, non-dysplastic epithelium was negative for HLA class II staining, a strong and uniform staining pattern was observed in glandular cells and the columnar epithelium of the transformation zone of the cervix uteri (Figure 4.15 3B).

4.4   Immune cell infiltrates under immuno-stimulatory treatment

It has been demonstrated that immune modulation by topical treatment with imiquimod, a TLR-agonist, might positively influence the local immune response and lead to regression of dysplastic lesions (TERLOU et al., 2010).

The efficacy of topical imiquimod treatment in patients with cervical intraepithelial neoplasia has been tested for the first time in the frame of a phase I (double-blind randomized, placebo-controlled) trial conducted in Austria (GRIMM et al., 2012). The treatment protocol and the clinical outcome of the patients analyzed in the here presented study are summarized in Figure 4.16.

The patients included in the Austrian trial represent an exceedingly precious cohort. Although the sample size is relatively small, the included biopsies represent a precious source of tissue of non-excised lesions that were treated with an immuno-modulatory agent and observed for 20 weeks. This cohort therefore provides highly important longitudinal information about the influence of immuno-modulatory agents on the immune cell composition and the clinical behavior of these lesions.
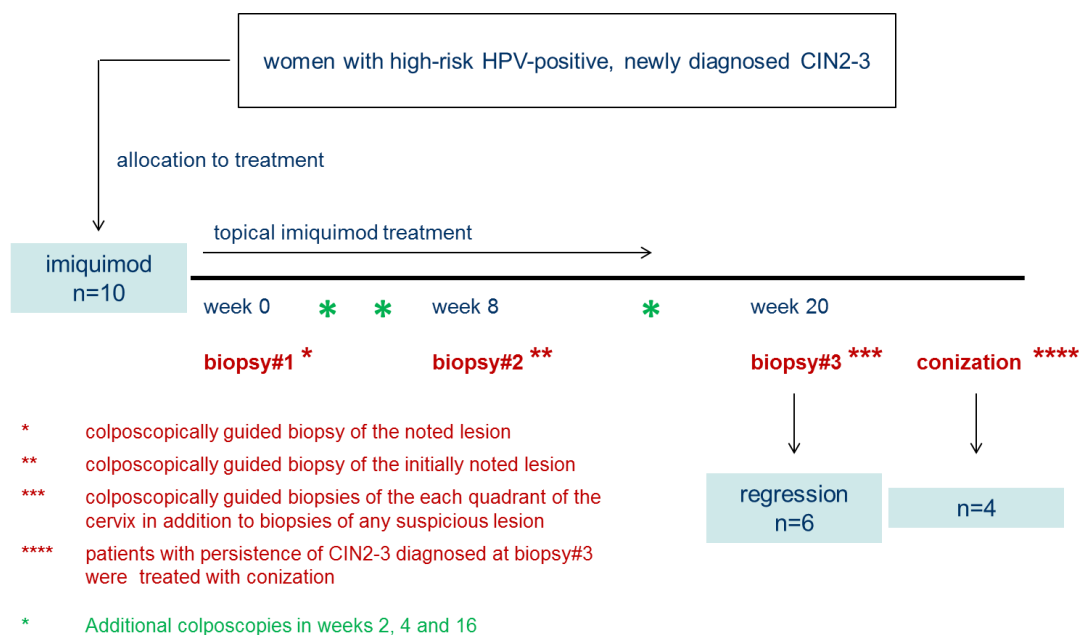
FIGURE 4.16   SCHEME OF THE AUSTRIAN IMIQUIMOD TRIAL WITH TIMING OF THE OBTAINED PUNCH BIOPSIES. Procedure is shown for the 10 patients of the imiquimod arm that were analyzed in the presented study.

4.4.1   Characterization of the study cohort

In a cooperation project with the Medical University of Vienna, Austria samples of the above described imiquimod trial could be obtained for immunological characterization. 10 patients with a CIN2/3 diagnosis that had received a 16-week imiquimod treatment were included in the analysis each providing cervical biopsies before (week 0), during (week 8) and after (week 20) treatment. Tissue sections of the biopsies were stained for $p16^{INK4a}$, CD3 and CD8. Image annotation and processing were performed based on the method described in section 4.1 and blinded to the patient ID and the clinical outcome. All patient related information at this stage of the analysis was subjected to pseudonymisation except the histomorphological classification (lesion grades) as the lesion grade that led to the diagnosis was needed for the definition of the region to be analyzed on the $p16^{INK4a}$ reference

slide as well as for the annotation of the slides stained with T cell markers. Once the immune cells were quantified the clinical parameters were uncovered: 6 of the patients had regressing disease (defined as CIN1 or less) and 4 of the patients had persistent disease or had even progressed (defined as CIN2 or CIN3). The characteristics of all 10 patients are listed in Table 4.7.

patient	week 0 (CIN grade)	week 8 (CIN grade)	week 20 (CIN grade)	clinical outcome
1	CIN2	(no CIN)	CIN3	progression
2	CIN2	CIN1	no CIN	regression
3	CIN3	CIN2	CIN1/no CIN	regression
4	CIN2	no CIN	CIN1/no CIN	regression
5	CIN2	n.a	CIN2	persistence
6	CIN2	n.a	CIN2	persistence
7	CIN2	CIN1	no CIN	regression
8	CIN 3	CIN3	CIN3	persistence
9	CIN2	no CIN	CIN1	regression
10	not available	no CIN	no CIN	regression

TABLE 4.7 OVERVIEW OF THE CHARACTERISITICS OF THE PATIENTS SELECTED FOR THIS APPROACH. All patients received a 16-week imiquimod treatment; n.a = not analyzable. Histologic CIN grades were recorded to evaluate the treatment efficacy for CIN2/3 patients which was defined as histologic regression of the initial high-grade lesions to histologically proven CIN1 or less (normal epithelium).

4.4.2   T cell infiltrates in non-responders and responders to imiquimod before treatment

Immune cell infiltrates, as CD3+ and CD8+ T cells, were quantified by application of the automated quantification method presented in chapter 4.1. The lesions were annotated as described previously on the basis of the p16^{INK4a} reference slide. The areas for all regions of interest as well as the T cell densities in these regions were calculated. Cell densities of both T cell phenotypes were compared between patients that had persistent or progressing disease and did not respond to the imiquimod therapy ("non-responders") and patients whose lesions had regressed during the treatment ("responders"). Densities for each phenotype separately as well as ratios of CD8+ T cells to all CD3+ cells in the different regions were compared in week 0 and week 20 biopsies.

Before treatment (week 0 biopsy) the infiltration with CD3+ T cells is very high in patients who did not respond to the imiquimod therapy (progressing/persistent lesions) compared with patients whose lesion had regressed after imiquimod therapy (Figure 4.17). The mean cell density of CD3+ T cells in the epithelium of non-responders is much higher (537.0 cells/mm^2) compared with responders (160.8 cells/mm^2). However, these differences are not statistically significant (p=0.190). This trend can also be observed in the stromal compartments where again non-responders had higher CD3+ T cell

numbers (1883.9 cell/mm^2) compared with non-responders (945.9 cells/mm^2) (p=0.190) (margin 500) (supplementary Figures S9.1 and S9.2 and supplementary Table S9.3).

Interestingly, with regard to CD8+ T cell infiltrating the lesion and the stroma the densities are higher in responders than in non-responders in week 0 before treatment is started. The mean cell densities for CD8+ T cells in the epithelium of non-responders is 82.1 cells/mm^2 compared with 113.8 cells/mm^2 in responders (p=0.730). The difference in the stromal compartment margin 100 is even more pronounced (394.2 vs. 973.3 cells/mm^2, p=0.286) (supplementary Figures S9.1 and S9.2). The same trend could also be observed for the more distant stromal compartments and also for the CD8/CD3 cell ratios in all regions of interest (supplementary Figures S9.1 and S9.2 and supplementary Table S9.4).
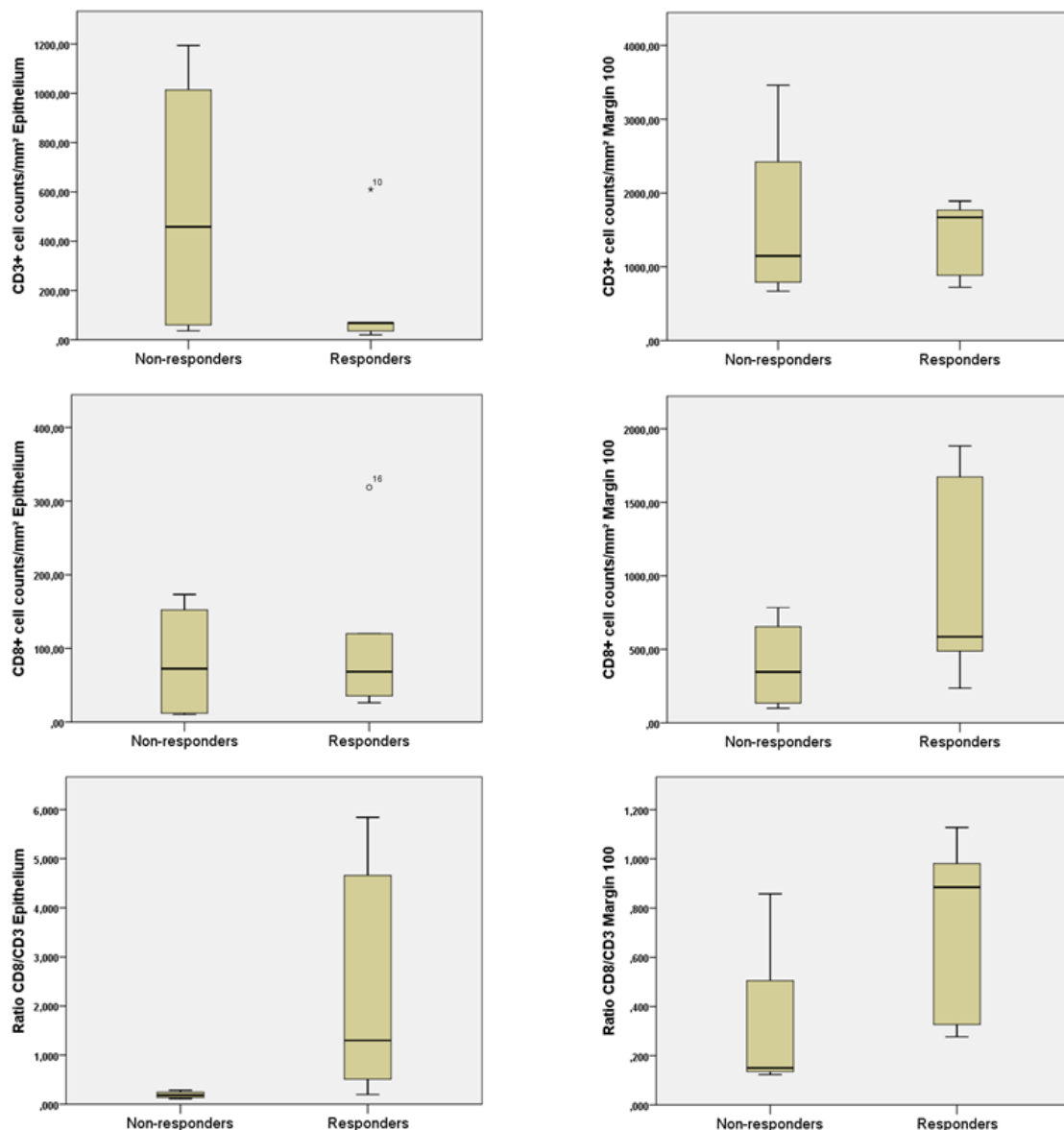
FIGURE 4.17   CD3+, CD8+ CELL COUNTS AND CD8/CD3 RATIO IN THE INITIAL BIOSPSY (WEEK 0) IN NON-RESPONDERS AND RESPONDERS. Results are shown as Box-Whisker-Plots for A) the epithelium and B) the first stromal compartment (margin 100). The line in the center of each box represents the median value of the distribution; the borders of the box represent the upper and lower quartiles (25-75%).

4.4.3 T cell infiltrates in non-responders and responders to imiquimod after treatment

In the biopsies taken 4 weeks after the treatment (week 20 biopsy) CD3+ T cell densities are comparably high in non-responders and in responders to imiquimod in the lesion and stromal compartment (Figure 4.18 and supplementary Figures S9.3 and S9.4). For example, in the epithelium the mean cell density is 287.8 cells/mm^2 in non-responders and 371.1 cells/mm^2 in responders (p=0.429) (supplementary Table 9.3).
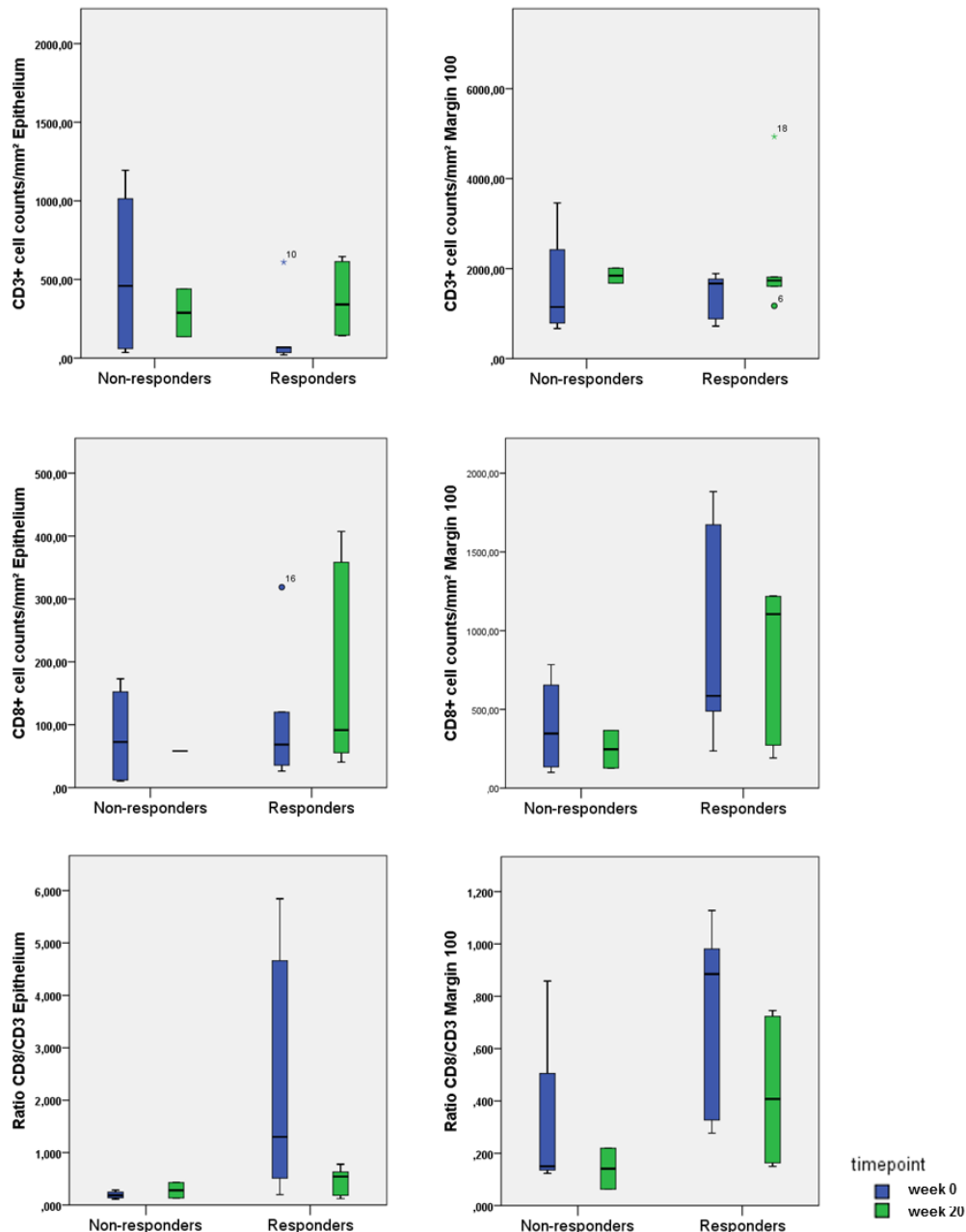
FIGURE 4.18 COMPARISON OF CD3+, CD8+ CELL COUNTS AND THE CD8/CD3 RATIO IN THE INITIAL BIOSPSY (WEEK 0) AND THE LAST BIOPSY (WEEK 20) IN NON-RESPONDERS AND RESPONDERS. Results are shown as box-whisker-plots for A) the epithelium and B) the first stromal compartment (margin 100). The line in the center of each box represents the median value of the distribution; the borders of the box represent the upper and lower quartiles (25-75%).

As the direct comparison between week 0 and week 20 shown in Figure 4.18 demonstrates the assimilation of responders and non-responders in terms of T cell densities is caused by an increased CD3+ T cells densities in responders compared to non-responders. This can be observed in the epithelium and the stroma of responders is also reflected by the comparison of the mean cell densities of week 0 and week 20 (see also supplementary Figures S9.6 and S9.7 and supplementary Table S9.3). With regard to CD8+ T cells the direct comparison of both time points (week 0 and week 20) for non-responders and responders revealed that CD8+ T cell densities also slightly increase over time in patients responding to the treatment but not in non-responders (Figure 4.18 and supplementary Figures S9.6 and S9.7). Non-responders in contrast show decreasing CD8+ T cell densities in week 20 compared with week 0 which results in a more pronounced difference between the groups at the end of the treatment. In week 20 the CD8 mean cell density in the epithelium of non-responders is 58.2 cells/mm^2 compared with 174.1 cells/mm^2 in responders (p=0.643).

To get a better insight in how the T cell infiltrates develop during the treatment in the two groups, the mean cell densities of every single patient at each time point is shown in a line chart and both groups (non-responders vs. responders) were directly compared (Figure 4.19). This contrasting juxtaposition revealed that the majority of the responders' infiltrate densities is located above the highest value of the non-responders' T cell densities in week 20. However, the groups are different in the middle of treatment were non-responders show an increase and responders a decrease in T cell densities. Interestingly, these differences are completely reversed in the last weeks of the treatment until week 20. T cell densities in non-responders show a massive decrease while those of responders continuously increase. The majority of responders therefore quit the treatment with clearly higher T cell densities compared with non-responders
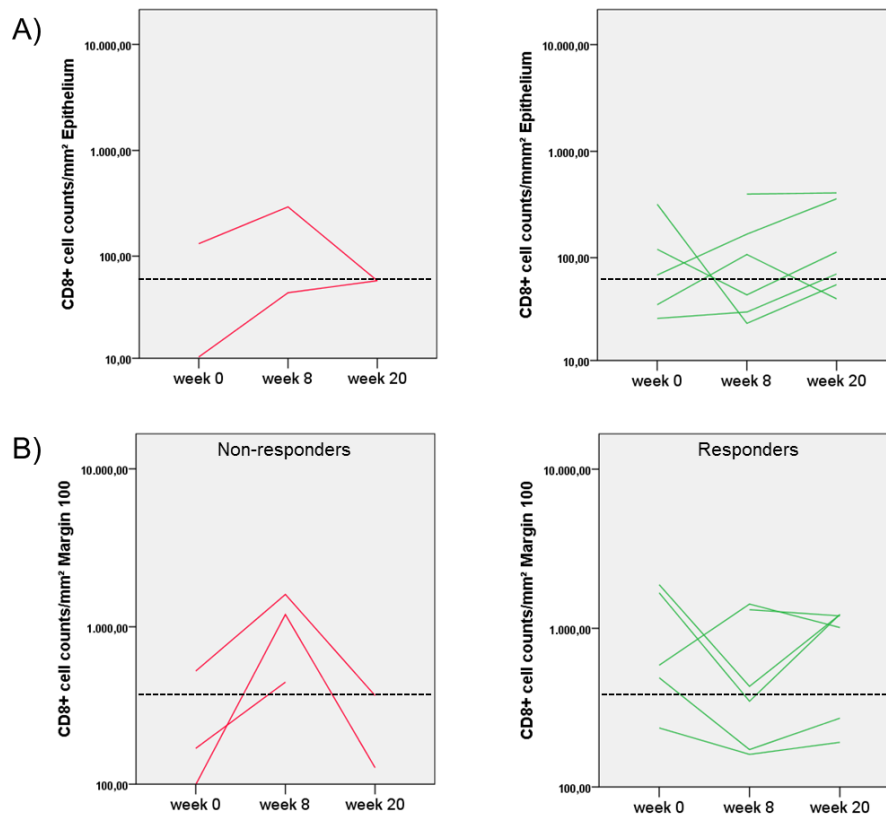
FIGURE 4.19 DEVELOPMENT OF CD8+ T CELL DENSITIES OVER TIME IN NON-RESPONDERS COMPARED WITH RESPONDERS. Results for non-responders (red) and responders (green) are shown as line chart for A) the epithelium and B) the first stromal compartment (margin 100). The dashed line represents the highest count of non-responders in week 20.

5. TREATMENT OPTIONS FOR HPV-ASSOCIATED PRECANCERS AND CANCERS

Despite important advances in the prevention of HPV infections and screening programs the world-wide incidence rates for cervical and other HPV-associated ano-genital precancerous lesions and cancers are not expected to decrease significantly within the next 15 to 20 years. On the contrary, the incidence is expected to increase in developing countries. The introduction of the prophylactic vaccines was demonstrated to reduce the risk for HPV infections for young girls. However the currently available vaccines provide protection against four HPV types of 14 considered to be potentially carcinogenic. Although protection might be provided by herd immunity, this effect requires a certain vaccination coverage and young women already infected with HPV do not necessarily benefit from subsequent vaccination and still might develop cervical cancer twenty years later. Screening programs based on Pap test in developed countries are well established, but getting women to attend the cervical cancer screening in developing countries remains a major concern. In the light of all these factors there is still a need for therapeutic intervention strategies. Different approaches are conceivable, many of them are based on therapeutic vaccines based on RNA, DNA, peptides or full-length proteins of diverse HPV-antigens.

In this part of the thesis, based on the insights that could be gained in the first part of this thesis, two different intervention strategies involving immune modulation of the cancer environment will be investigated. The first strategy aims at local application of a newly developed substance that might enhance the local immune response by induction of inflammatory processes. In a second approach the effect of regulatory T cell depletion on the efficiency of immune attack towards autologous tumor cells shall be investigated.

5.1   Effects of TLR agonist treatment on immune cells

It has been shown in the past that TLR-agonists act as immune modifiers that, locally applied, can positively influence the immune response and potentially reverse immune suppression. The substance imiquimod is a well characterized immune stimulatory agent that is approved for the treatment of condylomata accuminata, actinic keratosis and basal cell carcinoma, but is also tested in patients with vulvar intraepithelial neoplasia. Within the scope of this thesis the potency of a new, second-generation immune modifier was evaluated. The substance called TMX-202 was obtained from Telormedix SA, Bioggio, Switzerland and is a modified purine base derivative that is supposed to be even more potent than actually available immuno-stimulatory agents such as imiquimod.

TMX also is a TLR7 agonist and was tested *in vitro* by measuring the effects on PBMCs of healthy donors. It has been demonstrated in the past that TLR-9 agonist treatment increased the expression of the corresponding TLR-9 on B cells (BOURKE et al., 2003). It is conceivable that the new TLR agonist TMX also positively correlates with TLR expression on peripheral immune cells and thus further enhances the innate and adaptive immune response by a positive feedback loop between stimulation and activation of TLRs and their expression. To gain a better understanding of its mode of action and its potency to induce immune responses the effects of TMX-202 on TLR7 mRNA and protein levels were investigated (chapters 5.1.1 and 5.1.2).

The down-stream effect of TLR stimulation is the induction of inflammation that provokes the attraction of further immune cells to the treated site and thus stimulates both the innate and the adaptive immune response. To gain insight in the potency of the new TLR-agonist to induce inflammation the cytokine release was measured (chapter 5.1.3).

As a long term goal, the TLR-agonist should be included in a combinatory drug composed of TMX-202 and other immune modifiers that could be locally applied and thus is suitable for non-invasive anogenital lesions.

5.1.1 The effect of TLR7 agonist treatment on the TLR7 mRNA expression levels in PBMCs

To characterize the effects of the second-generation TLR7 agonist TMX on PBMCs a total number of 4 healthy donors were tested. Peripheral blood mononuclear cells were isolated from freshly drawn blood and cultured for 72 hours in the presence of imiquimod, TMX or the vector control DMSO (as described in 3.x). The expression of TLR7 was first measured on the transcript level by quantitative real-time PCR. Possible effects of the substances on mRNA levels were compared between the compounds. An additional negative control is represented by untreated cells that were frozen at day 0 and not subjected to *in vitro* culture. Furthermore, cells that were not treated with any substance but cultured under the same conditions as those that received the treatment were included in the analysis. For normalization purposes controls were included that were treated with the same amounts of DMSO that were added with substance (dissolved in DMSO) to TMX-treated cells. Each treatment experiment was normalized with the corresponding DMSO concentration in order to take into account the effect of DMSO.

The mRNA levels in PBMCs that were frozen on day 0 before treatment was started were similar to those of cultured, but untreated cells (data not shown). Therefore the values obtained for DMSO-treated cells were normalized against these untreated cells cultured under the same conditions. The DMSO controls were then used to normalize the corresponding values obtained for PBMCs treated with the immuno-modulatory agents by matching the DMSO concentrations used during stimulation.

In the first approach involving the first two donors, the effects of the new TLR7 agonist TMX-202 at a concentration of 10 µM was compared with imiquimod at a concentration of 30 µM. This concentration was reported previously in the context of immune cell *in vitro* vaccination approach (FAHEY et al., 2009) while the TMX-concentration was based on preliminary *in vitro* data communicated by Telormedix.

The results of the TLR7 quantitative real-time PCR for donors 1 and 2 (Figure 5.1) demonstrated that imiquimod in both donors induced higher mRNA levels compared to the DMSO control. Donor 1 displayed high fold changes of TLR7 mRNA after treatment with both of the substances, imiquimod and TMX-202, but mRNA expression was more up-regulated after TMX treatment. Donor 2 also showed increased TLR7 mRNA after imiquimod treatment expression, while TMX treatment did not show an effect on TLR7 mRNA levels. Here again, following imiquimod treatment higher fold-changes could be measured.
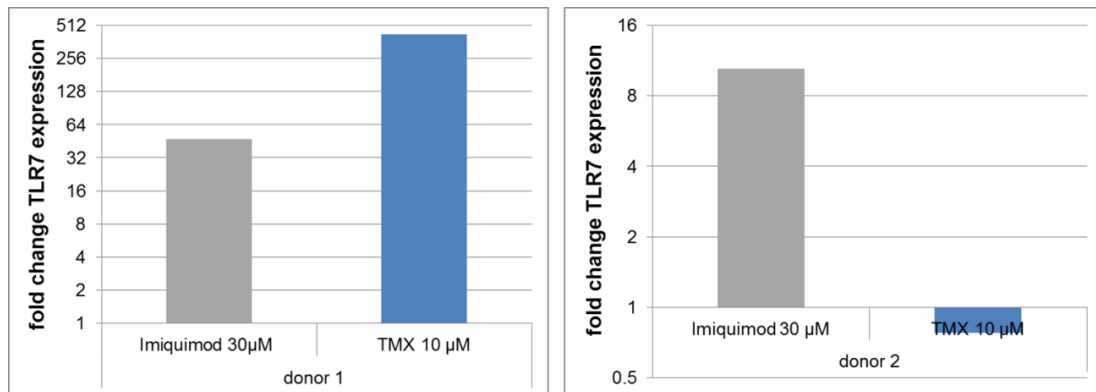
FIGURE 5.1   TLR7 mRNA EXPRESSION IN PBMCS TREATED WITH TMX AND IMIQUIMOD. Changes of mRNA levels in comparison to the DMSO control are displayed on the y-axis (fold-change). The experimental groups are displayed on the x-axis. The bars represent the results for the tested groups.

Two further donors were tested to compare the effects of TMX-treatment administered in different concentrations. The 10µM dosage from the first experiment was compared with a reduced TMX-202 concentration (1µM). Furthermore, another aspect was investigated in this second experiment, as not only the PBL fraction but also the adherent cell fraction representing mainly monocytes was analyzed separately. Thus, changes in TLR7 mRNA levels were measured under two different TMX-202 concentrations separately for monocytes and lymphocytes (PBLs) (Figure 5.2). Donor 3 displayed down-regulation of TLR7 mRNA expression in all cases except for the 1 µM concentration in the monocyte fraction. Donor 4 showed a general TMX-induced up-regulation of TLR7 mRNA expression levels compared with the corresponding DMSO controls. The 1µM dosage had a higher effect on mRNA levels than the 10µM in both of the cell types, monocytes and PBLs.
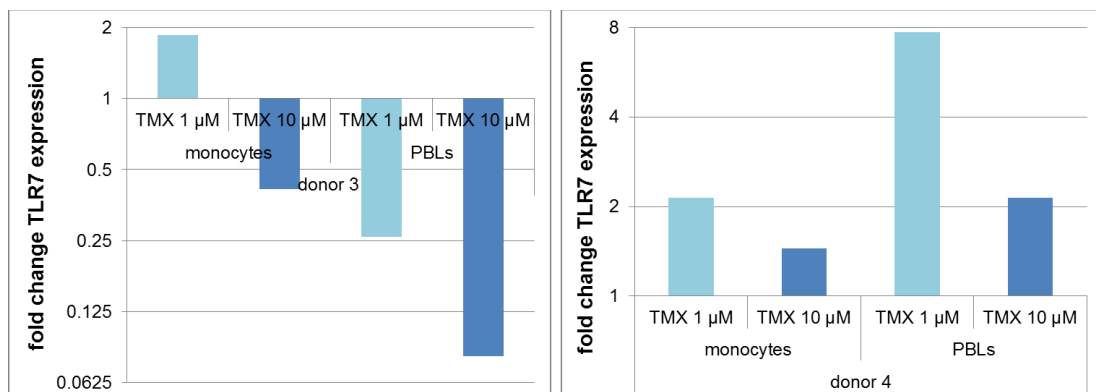
FIGURE 5.2   TLR7 mRNA EXPRESSION IN MONOCYTES AND LYMPHOCYTES (PBLs) TREATED WITH DIFFERENT TMX CONCENTRATIONS. Changes of mRNA levels in comparison to the DMSO control are displayed on the y-axis (fold-change). The experimental groups are displayed on the x-axis. The bars represent the results for the tested groups.

5.1.2   The effect of TLR7 agonist treatment on the TLR7 protein expression in PBMCs

A second fraction of the same PBMCs that were tested for TLR7 mRNA expression levels was subjected to TLR7 Western Blot in order to investigate the effect of TLR7 agonist treatment on the protein level. As a positive control for TLR7 expression a B cell lymphoma cell line (Raji) was included. Whole cell lysates of the same samples were tested, including the DMSO controls, the d0 uncultured PBMCs and PBMCs under treatment. As a loading control actin expression was investigated.

The results for donors 1 and 2 treated with imiquimod and TMX-202 are shown in Figure 5.3.

The baseline TLR7 expression in uncultured and immediately stored PBMCs (d0) was difficult to evaluate for both donors. No effects of any of the treatments (neither controls nor substances) could be observed in donor 1. Donor 2 showed comparable TLR7 protein levels for the DMSO controls and TMX, however, also less expression in imiquimod-treated cells.
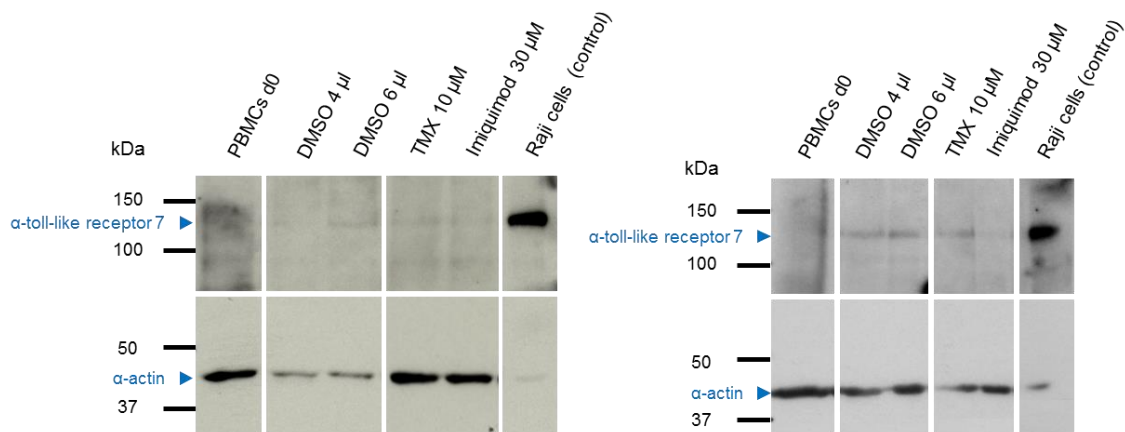
FIGURE 5.3   TLR7 PROTEIN EXPRESSION IN PBLs TREATED WITH TMX AND IMIQUIMOD. Shown are the results of the anti-TLR7 western blots of donor 1 (left) and donor 2 (right). TLR7 expression of treated PBMCs is compared with uncultured control PBMCs (PBMCs d0), DMSO controls and the TLR7 positive control (Raji cells).

The results for donors 3 and 4 treated with two different TMX concentrations (1µM and 10µM) are shown in Figure 5.4. Donor 3 showed slight baseline TLR7 expression and similar intensities of the protein bands for the DMSO control and 1µM TMX. A strong signal for 10µM TMX treated PBLs could be observed which might not be related to the treatment as a stronger signal can also be observed for actin. Although lacking baseline TLR7 expression in donor 4 could be explained by very protein concentration in the sample due to the lacking actin signal, the comparison between the highest DMSO control (4 µl) and the TMX-treated samples revealed an induction of TLR7 protein expression following treatment.
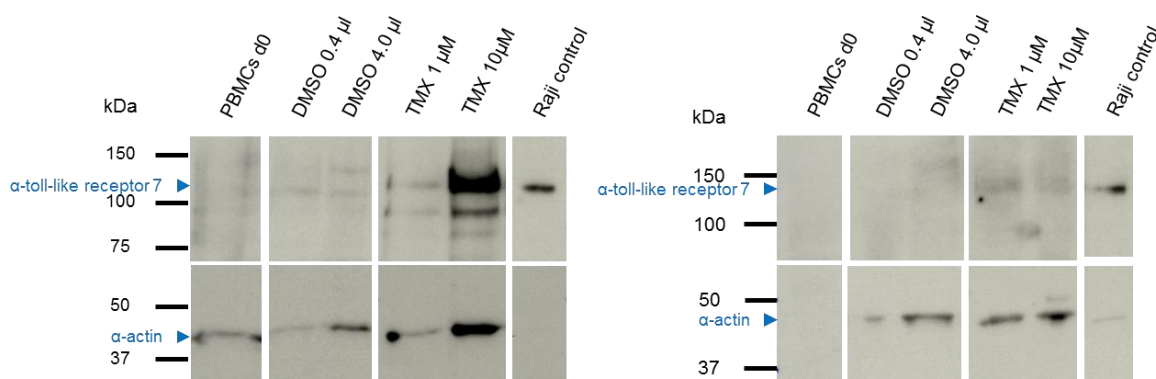
FIGURE 5.4   TLR7 PROTEIN EXPRESSION IN PBLs TREATED WITH TMX AND IMIQUIMOD. Shown are the
results of the anti-TLR7 western blots of donor 3 (left) and donor 4 (right). TLR7 expression of treated
PBMCs is compared with uncultured control PBMCs (PBMCs d0), DMSO controls and the TLR7
positive control (Raji cells).

In summary, the effects of different treatment approaches on the TLR7 expression on the protein level
that has been investigated in the PBMCs of 4 healthy individuals remained inconclusive. In most cases
no changes in protein expression could be observed – or could not definitively be related to the
treatment – and the observed protein expression was not concordant with changes in TLR7 mRNA
levels during treatment. The only exception is donor 4 who displayed higher protein levels for both
TMX concentrations compared to the DMSO controls. This is in concordance with the increase in
mRNA levels measured following treatment with TMX-202.

5.1.3   Release of the pro-inflammatory cytokine IL-6 of PBMCs upon treatment with TLR7 agonists

Following the investigation of mRNA and protein levels induced by TLR agonist treatment, another,
more functional readout to investigate the effects of TMX-202 treatment was chosen based on the
quantification of interleukin (IL)-6 released by immune cells. IL-6 is a potent inducer of inflammation
and therefore indicative for the initiation of innate and adaptive immune responses. The supernatants
from PBMCs cultures that were treated with imiquimod, TMX-202 and the controls were tested in IL-
6 ELISA.

Although the effects of TMX treatment on mRNA and protein expression in the four tested donors
remained inconclusive, it could be shown by ELISA that the IL-6 release was consistently induced by
TMX treatment (Figures 5.5 and 5.6). The IL-6 release of stimulated PBMCs into the cell culture
medium was significantly higher than under DMSO control treatment. Massive IL-6 release was
induced with 1μM TMX compared with the DMSO control in donors 3 and 4 (p=0.0036 and
p<0.0001), but further increased in dose-dependent manner with 10μM TMX compared with the 1μM
TMX treatment (p=0.0002 and p=0.0004) (Figure 5.6). The IL-6 concentrations released under
imiquimod treatment in donors 1 and 2 did not exceed the IL-6 release measured in the DMSO

controls or untreated cells (Figure 5.5). Interestingly, in one donor (donor 4) DMSO equally induced a slightly higher IL-6 release compared with the untreated control cells (p=0.0247).
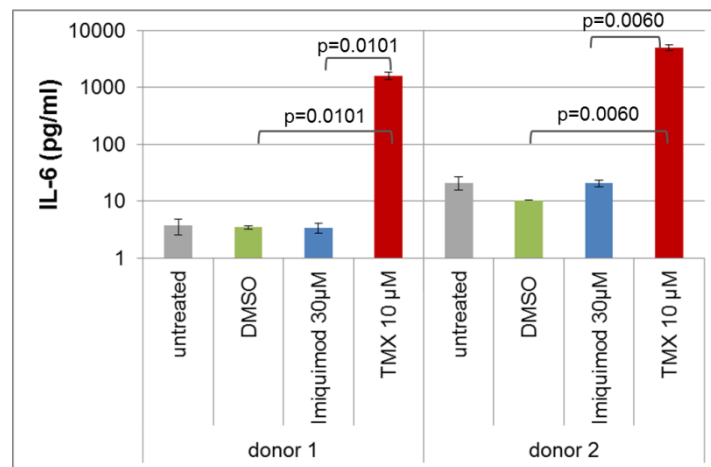
FIGURE 5.5   IL-6 SECRETION BY PBMCS TREATED WITH IMIQUIMOD AND TMX-202. The IL-6 concentration (pg/ml) is presented on the y-axis. The experimental groups for donors 1 and 2 are displayed on the x-axis. The colored bars represent the means for the tested groups, standard deviations are shown as black whiskers (comparison by unpaired t-test, p-values are indicated).
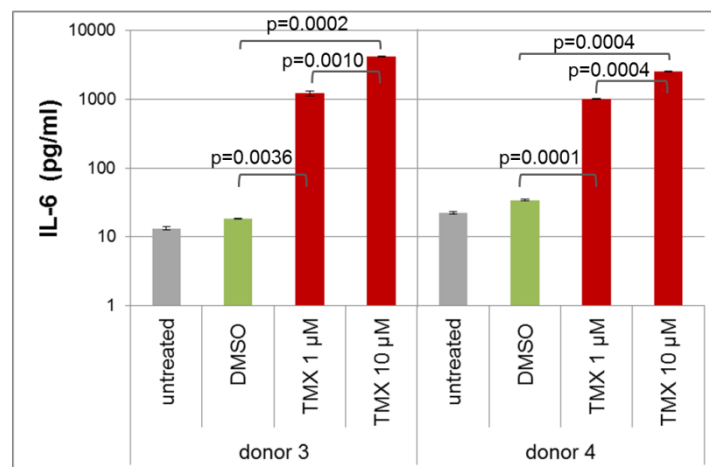
FIGURE 5.6   IL-6 SECRETION BY PBMCS TREATED WITH DIFFERENT TMX-202 CONCENTRATIONS. The IL-6 concentration (pg/ml) is presented on the y-axis. The experimental groups for donors 3 and 4 are displayed on the x-axis. The colored bars represent the means for the tested groups, standard deviations are shown as black whiskers (comparison by unpaired t-test, p-values are indicated).

5.2   Effects of TMX-202 treatment on the *in vitro* priming of naïve T lymphocytes with HPV-associated and host cell antigens and the generation of antigen-specific T cells

The potency of the new TLR agonist was investigated on a functional level in a large experiment based on the in vitro priming of naïve T cells with HPV-related antigens that were loaded on dendritic cells for antigen-presentation. This experimental setup allowed the effects of TMX-202 to be investigated for both of the arms, the innate and the adaptive immunity. The final read-out of the treatment, however, focused on the adaptive immune response as was evaluated by the potency of stimulated T cells to kill tumor cells. This was measured in a heterologous system based on PBMCs of a healthy HLA-A2 positive donor and CaSki cells. TMX-202 treatment was applied during the complete procedure starting with the generation of dendritic cells from monocytes and continued during the stimulation of T cells with the antigen-presenting cells until the end of the experiment. As potentially relevant antigens in HPV-associated cancers p16^{INK4a}, strongly overexpressed in HPV-associated tumors, and HPV16 L1, one of the most immunogenic HPV antigens, were chosen.

While for p16^{INK4a} a peptide was available that has been demonstrated in previous experiments to bind to HLA-A2 antigens, potential HPV16 L1 peptides had to be evaluated for their binding capacities to HLA molecules in a T2 cell based peptide binding assay.

5.2.1   Determination of L1 peptides bound to HLA class I antigens with high affinity for stimulation assays

In order to define out of a panel of predicted L1 peptides (for sequences see chapter 3.1.7, for predicted peptide panel see supplementary Table S9.8) those that have the highest binding affinity to HLA class I antigens and therefore being suitable for *in vitro* priming of T cells they were tested in peptide-binding assay based on T2 cells. The mean fluorescence intensities (MFIs) for each peptide were measured and compared with the negative and positive controls. As negative control served T2 cells incubated in absence of any peptide thus defining the baseline fluorescence intensity. To compare the effect of beta2-microglobuline (β2m) on the MFI the negative control was performed with and without β2m added to the culture. It could be shown that the addition of β2m to the cells, required for stabilizing the complex built of HLA class I antigens and peptide, did not increase the MFI in absence of any peptides (Figure 5.7). Peptides that were reported to have high binding affinities (L1_323) or were evaluated before in the context of other experiments (p16_R1 and viral MP) were included to obtain reference MFIs as positive controls. The values for all three positive controls (L1_323, p16_R1 and viral MP) were significantly higher than the negative control (Figure 5.7).

For the T cell *in vitro* priming the peptides with highest MFIs were chosen by applying the following inclusion criteria: Only peptides that fulfilled two distinct criteria, having significantly higher MFIs compared with the negative control and with a MFI at least as high as the positive control with the lowest MFI. The L1-peptides L1_2, L1_12 and L1-97 had MFIs that were significantly higher than the

negative control (all p<0.0001). Furthermore, the MFIs of the L1 peptides were significantly higher than the control peptide with the lowest MFI which was viral MP (Figure 5.7).
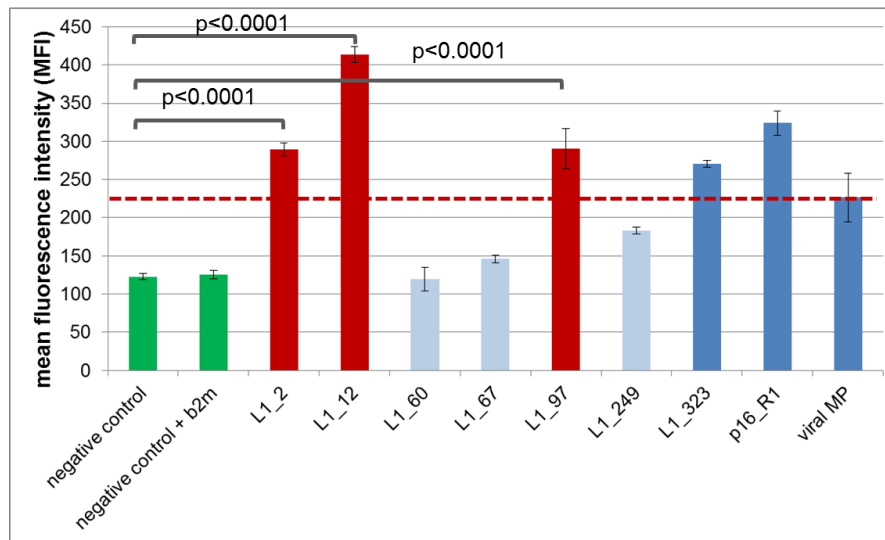
FIGURE 5.7   MEAN   FLUORESCENCE   INTENSITIES   (MFIs)   MEASURED   FOR   DIFFERENT   HPV16   L1 PEPTIDES IN A T2-CELL BASED PEPTIDE BINDING ASSAY.

The peptide binding assay was repeated once and the result obtained in the first assay could be confirmed. Again, the peptides L1_2, L2_12 and L1_97 were revealed to be the best binding ones and therefore chosen for subsequent T cell *in vitro* priming (supplementary Figure S9.8).

5.2.2   The effect of TMX treatment on dendritic cell maturation

The generation of antigen-specific T lymphocytes was based on an autologous system that involved antigen-presenting cells of the same healthy donor from whom also T cells were obtained. Being the most potent antigen-presenting cells, dendritic cells (DCs) were generated from the adherent PBMC fraction, the monocytes, under the influence of a basic cytokine cocktail including GM-CSF and IL-4. To test the potency of the immune modulatory agent TMX on the innate immune system, involving maturation of dendritic cells from monocytes, and also on the adaptive immunity in terms of interacting with T cells and priming them towards the chosen antigens, TMX was added to the dendritic cell culture. Following the standard protocols for dendritic cell generation from monocytes the cells require a "maturation cocktail" consisting of different pro-inflammatory cytokines including IL-1β, TNF-α, PGE-2 and IL-6. As TMX leads to IL-6 secretion of peripheral immune cells creating a strongly pro-inflammatory milieu as shown in section 5.1.3 one could hypothesize that TMX treatment also might have an influence on dendritic cell maturation and that the endogenous IL-6 production could replace the exogenously added cytokine cocktail. The effect of TMX on monocytes and generation of dendritic cells was evaluated by the cell counts obtained after dendritic cell culture, morphology of the growing cells and expression of co-stimulatory molecules CD80 and CD86 on dendritic cells which is a sign for DC maturation.

The cell counts of harvested monocytes and dendritic cells – although varying between different cycles of DC generation - demonstrate that the numbers of harvested cells depends on the treatment. Cell numbers were calculated as the percentage of full PBMCs that could be harvested after 6 days culture period. Obviously the number of monocytes that became adherent and thus were separated from the non-adherent lymphocytes varied from one generation cycle to another. However, out of the cells that initially became adherent, more cells could be obtained after TMX stimulation compared with DMSO controls. The difference was most pronounced after the second and third round of dendritic cell generation with a 1.8- and 2.1-fold increase in cell numbers (Figure 5.8).
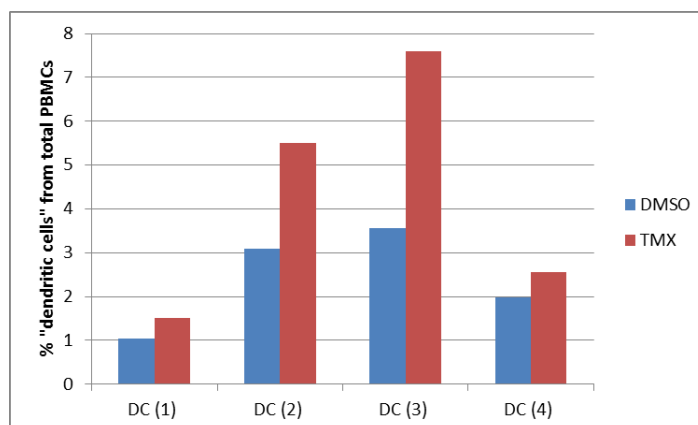
FIGURE 5.8   CELL NUMBERS OBTAINED DURING THE FOUR DENDRITIC CELL GENERATION CYCLES. The percentage of dendritic cells that could be harvested from total PBMCs subjected to adherence for monocyte isolation is displayed on the y-axis. The 4 cycles of DC generation are shown on the x-axis with the bars representing the different tested groups (DMSO and TMX).

Also, the morphology of monocyte culture is indicative for the maturation of dendritic cells: while newly adhered monocytes are regular and round, growing and maturing dendritic cells display the typical, longish and branched, dendrite-like morphology. The cultures that obtained TMX treatment in comparison with the DMSO controls showed faster, at an earlier time point, and to a higher extent cells with a dendrite-like morphology. The morphologic changes became obvious 48 hours after treatment with TMX had started and could be observed in more cells than in the culture containing DMSO treated cells. After 96 hours under TMX treatment the monocyte culture displayed clear morphologic signs of dendritic cells. Still, these cells were more frequent than in the DMSO-treated culture (Figure 5.9). These effects could be observed in all 4 successively established DC cultures, independently of the cell density and the rate of yield of monocytes from full PBMCs.
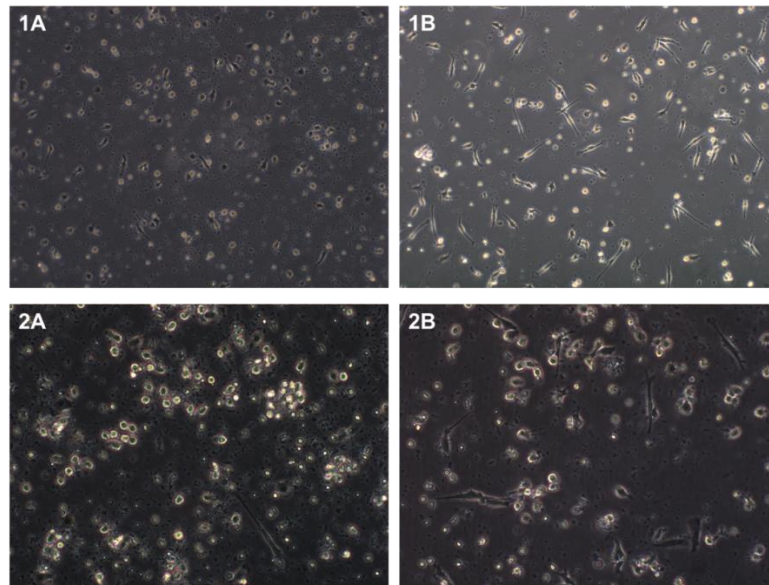
FIGURE 5.9   REPRESENTATIVE MICROSCOPIC IMAGES OF THE MORPHOLOGY OF DENDRITIC CELLS GENERATED FROM MONOCYTES UNDER THE INFLUENCE OF CONTROL SUBSTANCE DMSO (A) AND TMX (B). Shown are examples for 1) early dendritic cell culture (48h) at 20x magnification and 2) a later time point of dendritic cell generation (96h) at 40x magnification.

The expression of CD80 and CD86 is indicative for activated antigen-presenting cells – B cells and monocytes. They are co-stimulatory molecules that bind to CD28 and CTLA-4, which are the corresponding ligands on T cells. CD80 and CD86 together play an important role in T cell activation and priming towards distinct antigens. They are up-regulated during the activation of monocytes and maturation of dendritic cells (CD86 is a marker for early maturation, while CD80 is a marker for mature DC). While morphology and cell numbers were recorded for all DC cultures the expression of co-stimulatory molecules could only be investigated in one out of 4 DC cultures because there was not a decent amount of cells available in the other cycles. The cell numbers were limited and in most cases all available DC had to be used for the T cell stimulation to assure the ratio of 1:10 between antigen-presenting cells and T cells. FACS analysis of the available DCs revealed that culturing monocytes in presence of TMX in comparison with DMSO treatment leads to higher expression of CD80 (28.8% vs. 19.92%) and CD86 (41.95% vs. 28.8%). The results are shown in Figures 5.10 and 5.11.
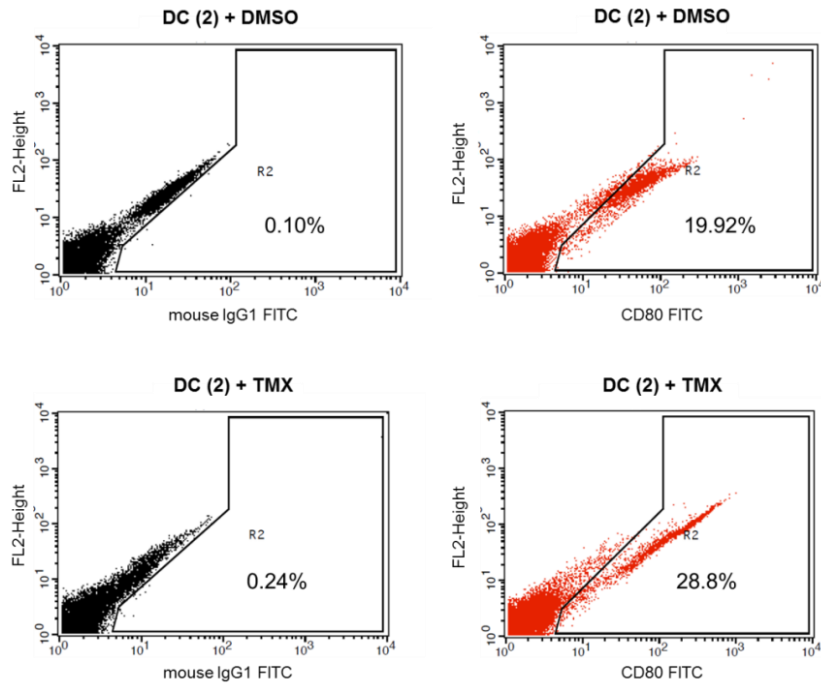
FIGURE 5.10   RESULTS OF THE FACS ANALYSIS FOR CD80 EXPRESSED ON DENDRITIC CELLS. The results are shown for DC generation under DMSO treatment (top) and TMX treatment (bottom). The fluorescence intensities for CD80 are given on the x-axis. Region borders (R2) were defined based on the isotype control with the FI for mouse IgG1 given on the x-axis. The percentage of cells that are CD80+ is given in R2.
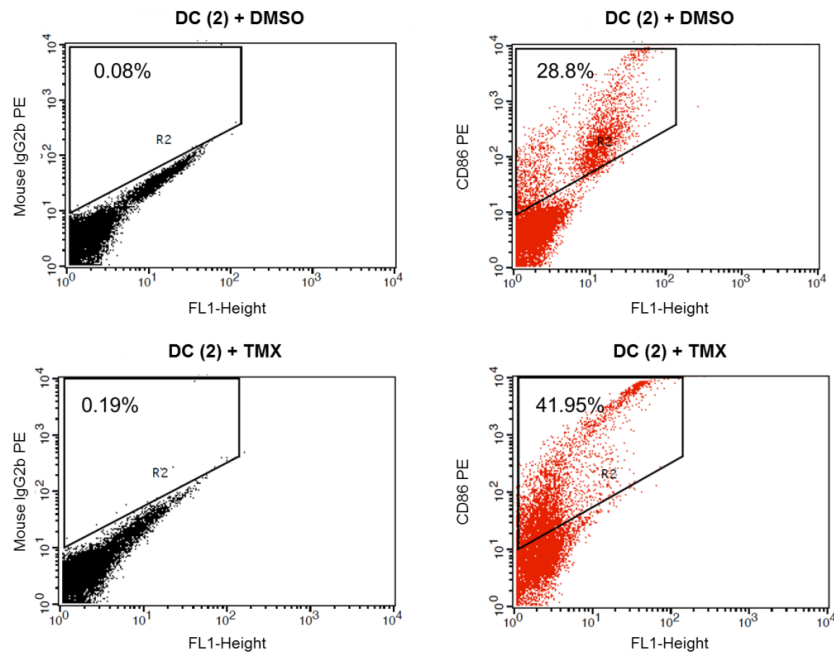
FIGURE 5.11   RESULTS OF THE FACS ANALYSIS FOR CD86 EXPRESSED ON DENDRITIC CELLS. The results are shown for DC generation under DMSO treatment (top) and TMX treatment (bottom). The fluorescence intensities for CD86 are given on the y-axis. Region borders (R2) were defined based on the isotype control with the FI for mouse IgG2b given on the y-axis. The percentage of cells that are CD86+ is given in R2.

5.2.3   The effect of TMX treatment on stimulation of naïve T cells with HPV-associated antigenic peptides

The priming of naïve T cells with peptide-loaded dendritic cells was carried out in 4 cycles over 24 days. Functional analyses during the stimulation period were not possible as T cell numbers were limited and all available cells were used for the final killing assay.

However, the appearance of the T cells in culture and their morphology was recorded. Also, after each stimulation cycle that has been completed, T cell numbers were determined upon harvesting and reseeding cells with newly generated dendritic cells. From the photos taken of the T cell cultures (Figure 5.12) it becomes obvious that, although the same T cell numbers were initially seeded, T cells under TMX developed differently from those treated with DMSO only. On day 10 of the stimulation T cells that were treated with DMSO were less dense compared with the TMX-treated T cells (Figure 5.12. 1A and 1B). Although they seemed to recover until day 21 they still appeared to be less close to each other and more scattered over the well than the T cell culture treated with TMX (Figure 5.12 2A and 2B).
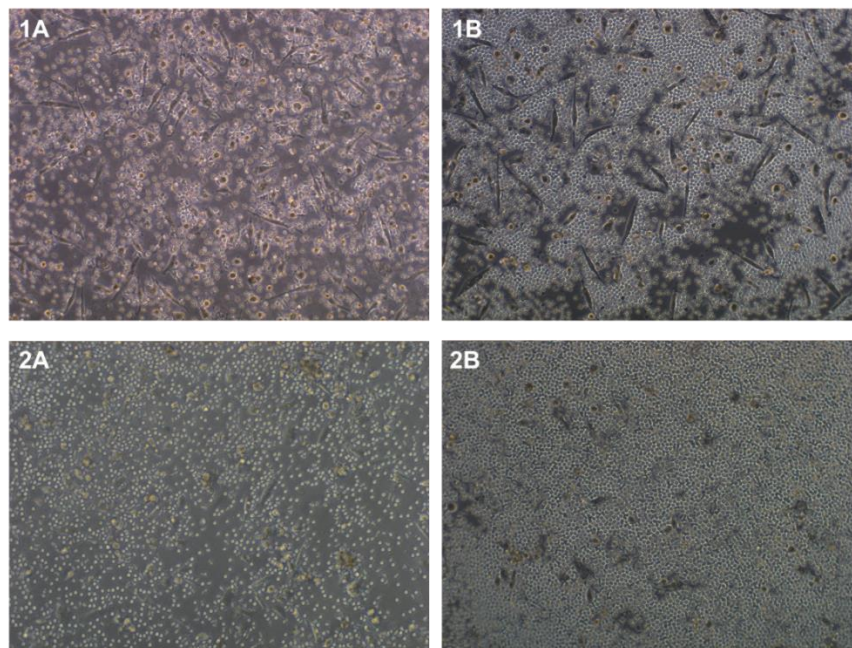
FIGURE 5.12   APPEARANCE OF T CELLS DURING STIMULATION WITH PEPTIDE-LOADED DENDRITIC CELLS UNDER THE INFLUENCE OF CONTROL SUBSTANCE DMSO (A) AND TMX (B). Shown are examples for 1) an earlier time point of T cell priming (day 10) and 2) a later time point of T cell stimulation (day 21) at 20x magnification.

The morphologic appearance of the T cell cultures was confirmed by the cell numbers recorded upon harvesting and re-stimulation. Figure 5.13 demonstrates the development of T cell numbers over time during the stimulation. While T cells stimulated under TMX treatment with TMX-generated DCs continuously grew until day 17, T cells numbers under DMSO conditions decreased until day 11. Nonetheless, they recovered until day 21 and finally both cultures were harvested with more than $3x10^6$ cells and thus globally showed a positive growing tendency.
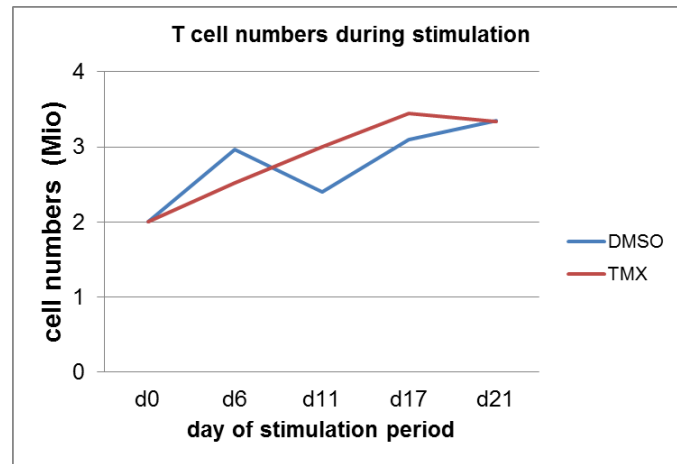
FIGURE 5.13   DEVELOPMENT OF T CELL NUMBERS DURING THE *IN VITRO* PRIMING. Shown are the cell numbers for T cells stimulated in presence of TMX and in presence of the control substance DMSO.

5.2.4   The effect of TMX treatment on the killing potency of stimulated T cells against CaSki cells

The final read-out of the T cell *in vitro* priming was the killing assay of CaSki cells in a heterologous tumor cell – immune cell system. To minimize the reactivity of T cells against tumor cells due to HLA mismatching, a PBMC donor expressing the HLA-A2 allele was chosen.

The reactivity of T cells stimulated with peptides against L1 and $p16^{INK4a}$ and cultured either under TMX or DMSO treatment was compared. Therefore they were co-incubated with tumor cells and the degranulation rate as measured by CD107a expression on the cell surface was evaluated.

First, the gate for T cells was defined by T cell cultured alone. Its suitability was also checked for T cells that were co-incubated with CaSki cells (Figure 5.14). Then two gates containing CD8+CD107a+ T cells (R2) and the total fraction of CD8+ cells irrespective of CD107a expression (R4) were defined. The percentage of cells that upon co-incubation with tumor cells expressed CD107a on their cell surface and that simultaneously expressed CD8 (cytotoxic T lymphocytes) were higher in the T cell culture that had undergone a treatment with TMX compared with the cells that were treated with DMSO (p=0.1353). In a second step the degranulation rate of CD8+ T cells measured upon co-incubation with CaSki cells was calculated by diving the fraction of CD8+/CD107+ T cells by total amount of CD8+ T cells measured in the corresponding well. The percentage of CD107a-expressing CTLs among all CD8+ T cells again tended to be higher in TMX-treated T cells (8.26%) compared with DMSO-treated T cell culture (6.75%) (p=0.2202) (Figure 5.15).

In conclusion, a slightly higher CD107a release could be obtained by TMX-treatment compared with untreated cells. This is true for CD8+CD107a+ T cells and the fraction of CD107a+ T cells among all CD8+ T cells (degranulation rate of CD8+ T cells).
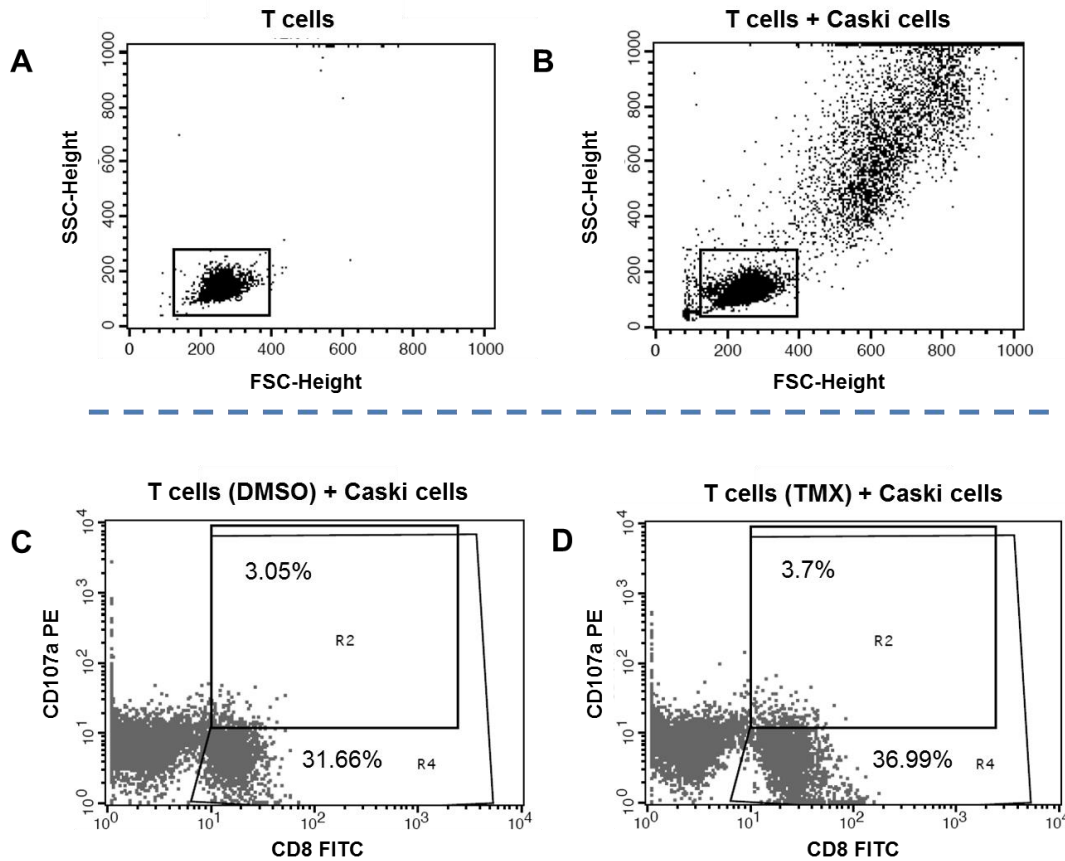
FIGURE 5.14   EXEMPLARY RESULTS OF THE FACS ANALYSIS FOR CD8 AND CD107A. The gating strategy in the FSC/SSC is shown for A) T cells and B) T cells with CaSki cells. One of the duplicates is shown for C) the co-incubation of T cells with CaSki cells under DMSO treatment and D) TMX treatment. The fluorescence intensities for CD8 (x-axis) and CD107a (y-axis) are given. Region borders were defined based on the isotype controls (not shown). The percentage of cells that are CD8+CD107a+ is given in R2 and the percentage of CD8+ cells in R4.
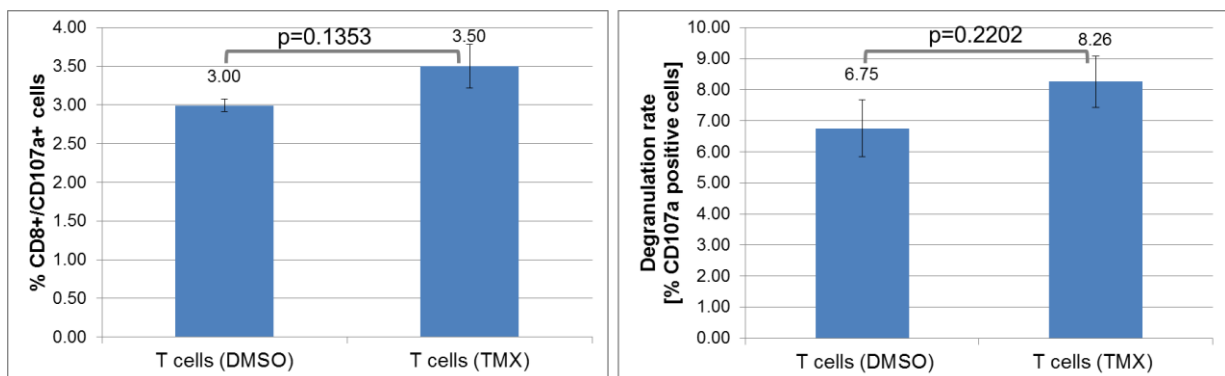
FIGURE 5.15   EVALUATION OF THE CD8+ T CELLS FOR THE DEGRANULATION MARKER CD107A AND DEGRANULATION RATE. The percentage of positive cells is presented on the y-axis. The experimental groups are displayed on the x-axis. The blue bars represent the results for the tested groups, standard deviations are shown as black whiskers (comparison by Student's t-test, p-values are indicated).

5.3   Establishment of an autologous system for the development and evaluation of therapeutic intervention strategies in HPV-associated diseases

The previous results (chapter 4.2) demonstrated that regulatory T cells might play a role in the carcinogenesis of cervical cancers and that immuno-modulatory treatment might reverse the immunosuppressive state of the host's immune system and lead to better killing of cervical cancer cells (CaSki) (chapter 5.2.4). Other strategies, such as cell-based approaches, might also be of importance in the battle against HPV-cancers and will be considered in this thesis. For the investigation of immunological questions autologous models based on tumor cells and immunocytes deriving from the same donor are of special interest as they provide advantages in terms of avoidance of cross-reactivity and cytotoxicity due to unmatched HLA allelic phenotypes. However, autologous HPV-associated tumor models for the cervix as well as for other sites are lacking. One major part of this thesis therefore was to establish a HPV-positive tumor cell line for these purposes. This was based on tumor samples of head and neck squamous cell carcinoma (HNSCC) patients that could be obtained from collaboration partners of the University Hospitals Giessen and Muenster. As cervical cancer and HPV-positive HNSCC have the same underlying mechanisms of tumorigenesis, HNSCC tumor might also function as a reliable model for HPV-related diseases.

In the course of this project, one HNSCC cell line from a HPV-positive patient could be established and used for further immunological studies.

5.3.1   The cell line HN038M: general features and patient's characteristics

In the course of this project tumors samples of 31 HPV-positive HNSCC patients, primary tumors together with or without the corresponding metastatic lymph nodes, were obtained. The tissue was prepared and cultured as described in section 3.2.4. After many attempts, one cell line out of these 31 primary cultures could successfully be established by explant culture. This cell line derives from a lymph node metastasis of a male patient who underwent his first surgery in March 2013.

The patient's and the tumor's characteristics as well as the clinical course of the disease are summarized in Table 5.1.

The tissue of the primary tumor and the metastasis was prepared as described in section 3.2.4. Following the enzymatic digestion of the tissue two tumor explant cultures were initiated, one containing the primary tumor cells and the other containing the metastatic cell material. Regular microscopic evaluation showed that the culture containing the primary tumor cells in contrast to the metastasis seven weeks after tumor preparation still did not contain adherent and growing tumor cell cluster and therefore was discarded.

Parameter	Description
Sex	male
Age	58 years at diagnosis (march 2013)
exposure to noxa	heavy smoker
primary tumor	
HPV-association	p16^{INK4a} status as determined before surgery: positive
localization	oropharyngeal cancer of the palatine/lingual tonsil
Size	resected mucosal tissue (7,5 x 5,5 x 1,5 cm^3), with a ulcerous area of about 2,1 x 1,5 cm^2 in the center of the tissue
cTNM staging	cT3, cN2b, cM0
pTNM staging	pT2, pN2b (14/18), L1, V0
metastatic LN	10 of 11 lymph nodes on the right side affected (level IIb) 4 of 7 lymph nodes on the right side affected (Level V)
grade of malignity	G2
	R0
ICD-O code	8070/3
further clinical course	recurrent disease, relapse within one year: detection of multiple metastases
beginning of January 2014	➤ second surgery: macroscopically recurrent disease could not be observed; removal of a lymph node conglomerate ➤ lymph node metastasis could be identified ➤ partially necrotic tissue, moderately differentiated (G2) ➤ squamous cell epithelium ➤ ICD-O-Code: 8070/6
end of January 2014	➤ third surgery with removal of further lymph nodes ➤ in 1/25 "metastasis of the known primary tumor" ➤ poorly differentiated (G3) ➤ ICD-O-Code: 8070/6

TABLE 5.1   OVERVIEW OF THE MAIN CHARACTERISITCS AND THE CLINICAL COURSE OF THE PATIENT FROM WHOM THE CELL LINE IS DERIVED.

The explant culture of the metastasis after 3 weeks has already shown macroscopically and microscopically detectable tumor cell clusters within the fibroblast layer (Figure 5.16 A). After the fibroblasts had undergone apoptosis, the tumor cell nests remained stably attached to the cell culture flask. However, they did not further expand across their initial "borders" determined by the outer cells and, although cells proliferated, only the minority of the newly generated cells adhered to the free space of the bottom of the flask (Figure 5.16 B). In this state the tumor cells remained stable over 11 months. The culture was subjected to repeated trypsinization in order to detach the cells from the bottom and allow them to adhere again but in a more homogeneously distributed pattern.

Finally, cell proliferation and adherence of newly generated cells to the flask could be stimulated by this treatment (Figure 5.16 C and D). The culture after 13 months became 90% confluent, could be split and analyzed by FACS staining and cytometry analysis in order to determine the content of epithelial cells (Figure 5.17).
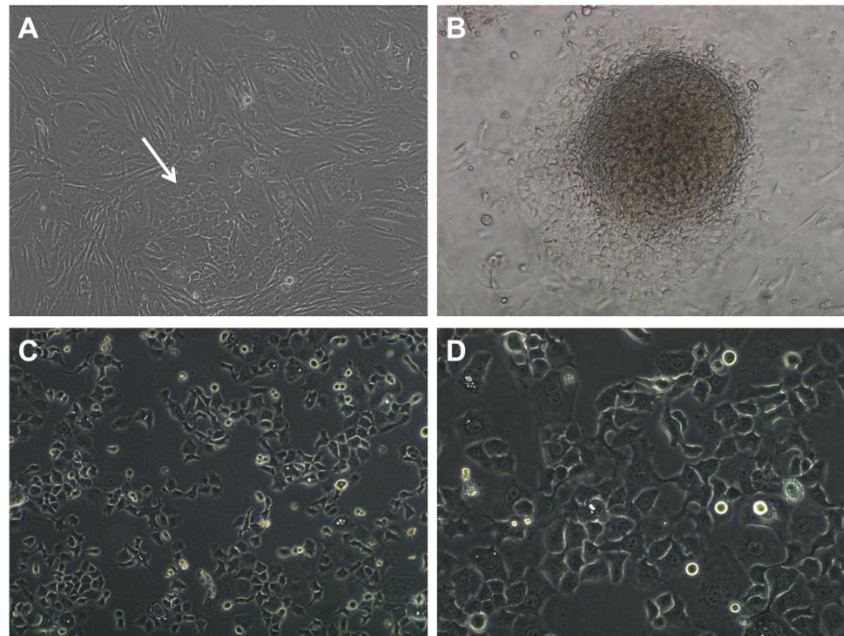
FIGURE 5.16   MORPHOLOGIC APPEARANCE OF THE CELL LINE HN038M. Shown are A) an initial tumor cell nest (arrow) embedded in fibroblasts (week3), B) expanded tumor cell nest (month 8) and C) tumor cells of the established cell line at 100x magnification and B) at200x magnification.

The analysis revealed that the culture contained ~ 99% of BerEP4+ cells, a marker for epithelial cells that have been stable for more than 13 months and still proliferate autonomously. The FACS results could be confirmed several times and the tumor cells were subjected to further characterization which is described in sections 5.3.2 to 5.3.4

To date the culture is stable, continuously growing and has until now undergone 43 passages.
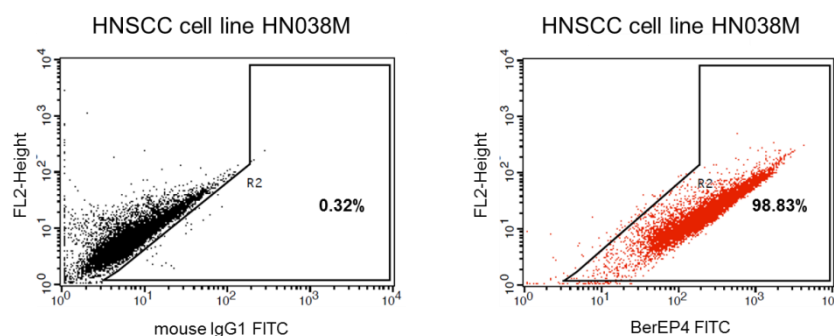
FIGURE 5.17   EXAMPLARY RESULTS OF THE FACS ANALYSIS FOR BEREP4 OF THE NEWLY GENERATED TUMOR CELL LINE. One of the replicates of tumor cells harvested at confluence (passage x) is shown. The fluorescence intensity (FI) for BerEP4 is given on the x-axis. Region borders (R2) were defined based on the isotype control with the FI for mouse IgG1 given on the x-axis. The percentage of cells that are BerEP4+ is given in R2.

5.3.2 Determination of the HPV-status and oncogene activity

To further characterize the established cell line and to validate the clinical finding in terms of HPV-association of the tumor, the formalin-fixed paraffin-embedded tissue of the metastasis was ordered to compare the characteristics of the tumor cell line with the archived tumor material. Therefore, tissue sections were stained for p16^{INK4a} to confirm the original diagnosis of the pathologist. The original FFPE material of the lymph node metastasis showed a strong and diffuse staining for p16^{INK4a} (Figure 5.18).
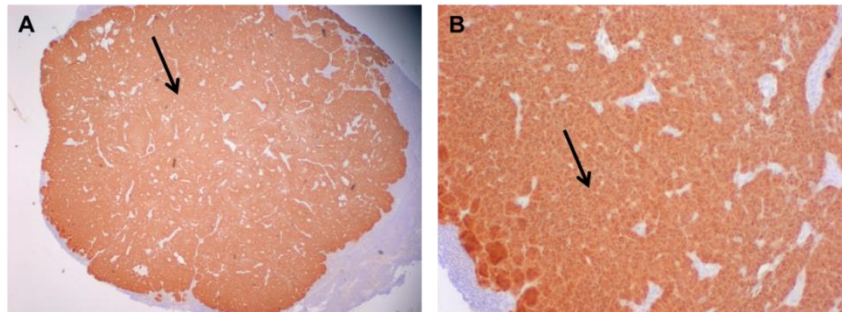
FIGURE 5.18 p16^{INK4a} IMMUNOHISTOCHEMISTRY OF FORMALIN-FIXED PARAFFIN-EMBEDDED METASTATIC TUMOR TISSUE OF THE PATIENT FROM WHOM THE CELL LINE IS DERIVED. Shown is A) on overview of the lymph node metastasis at 20x magnification and B) details at 40x magnification (p16^{INK4a}-positive tumor is marked by an arrow).

In order to assure that the cultured cells still have this feature equally and were not selected for p16^{INK4a}-negative cell clones, p16^{INK4a} cytology staining on cultured cells was performed. Therefore, tumor cells were harvested and spun down onto a microscopy glass slide. The p16^{INK4a} staining for cytological preparations revealed that virtually all cells contained in the sample strongly stained for p16^{INK4a} indicating viral oncogene activity (Figure 5.19 A,B).
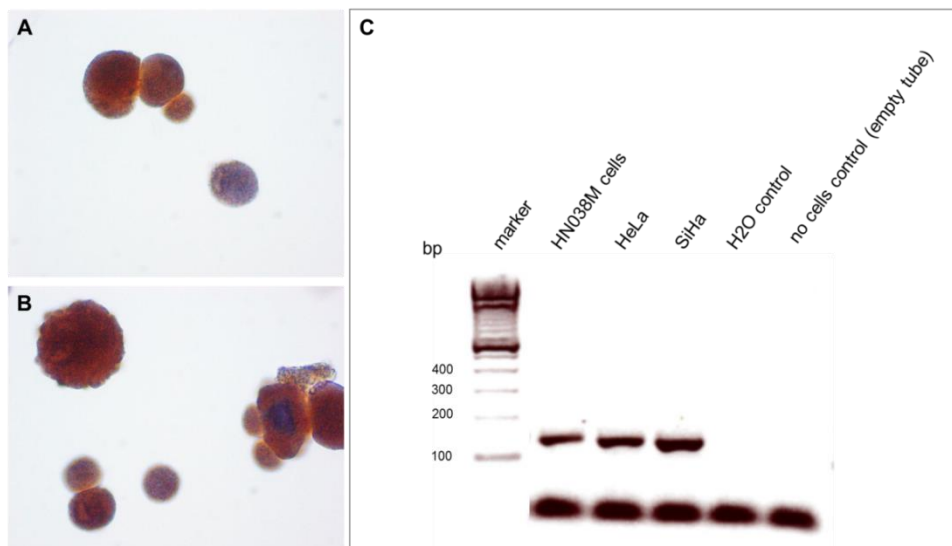
FIGURE 5.19 p16^{INK4a} CYTOLOGY OF THE HNSCC CELL LINE HN038M AND HPV DNA STATUS VISUALIZED BY GP5+/6+ LUMINEX PCR. A) and B) Staining of tumor cells of the HN038M cell line (passage 14) shows a clear p16^{INK4a}-staining (brown signal). C) Agarose gel following GP5+/6+ PCR shows amplification of HPV DNA in the HN038M tumor cells and in the positive controls (HeLa and SiHa) but not in the negative controls.

In order to proof the underlying HPV-infection in the cells and the oncogene activity the tumor cells were subjected to HPV-genotyping and viral oncoprotein expression of HPV16 E7.

The GP5+/6+ PCR demonstrated that HPV DNA was amplified (Figure 5.19 C) and the subsequent Luminex-based HPV genotyping revealed that the sample was positive for HPV16 DNA. The HPV status was also compared with the original FFPE tissue samples of the primary tumor and the metastases to validate these findings. HPV genotyping demonstrated that the archived tumor material also harbored HPV16 DNA (supplementary Table 9.9).

In order to examine whether p16^{INK4a} overexpression was linked to viral oncogene activity, the viral oncogene expression was investigated by western blot analysis for HPV16 E7 expression.

For the characterization of the protein expression the viral oncoprotein E7 was investigated. Samples of different subcultures that have undergone varying numbers of passages (7 and 16 passages) were analyzed for viral oncoprotein E7 expression and compared with each other. They were also compared with HPV16-positive SiHa cells which were used as positive control for HPV oncoprotein expression. As shown in Figure 5.20 the tumor cell line HN038M displayed a strong staining for the viral oncoprotein E7 (located at 17 kDa) at earlier passages as well as at a later time point when the tumor cell had undergone more passages.
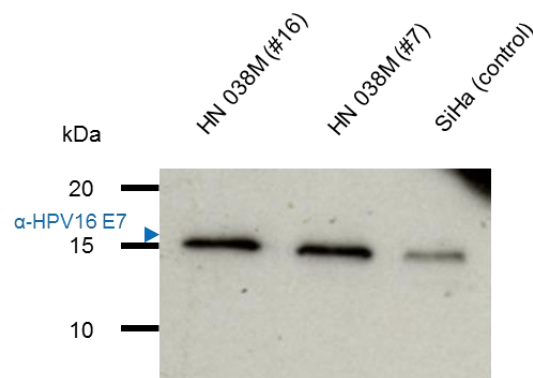
FIGURE 5.20   WESTERN BLOT ANALYSIS OF DIFFERENT FRACTIONS OF THE HNSCC CELL LINE HN038M FOR HPV16E7. Tumor cells of different passages (passage 16 and passage 7) were tested and compared with HPV16-positive cell line SiHa used as control.

The tumor cell line was further characterized for HLA class I antigen expression, which is an important factor for immunological studies. Expression of HLA class I antigens is the prerequisite for the recognition of cells by T cells and therefore required for by CD8+ T cells.

Tumor cells of the cell line HN038M were characterized for HLA class I expression by flow cytometry analysis. It could be demonstrated in two independent experiments that virtually all cells were positive for HLA class I antigens (Figure 5.21).
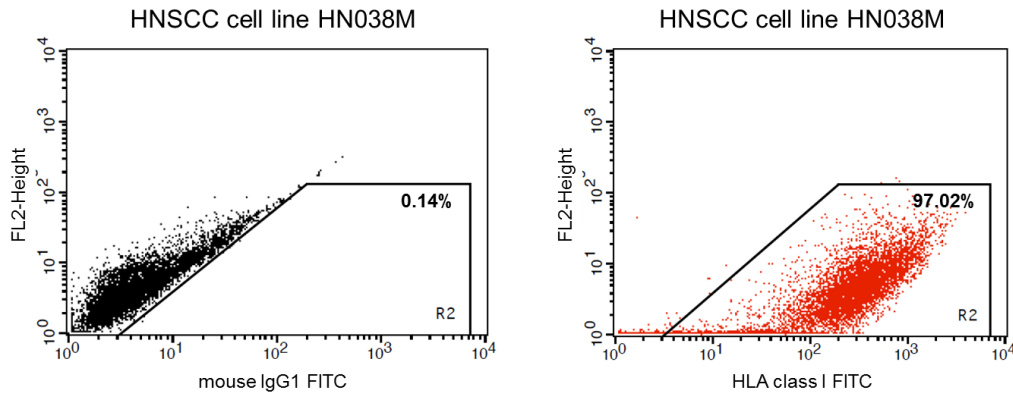
FIGURE 5.21   REPRESENTATIVE RESULTS OF THE FACS ANALYSIS FOR HLA CLASS I ANTIGENS OF THE NEWLY GENERATED TUMOR CELL LINE. One of the replicates of tumor cells harvested at confluence (passage x) is shown. The fluorescence intensity (FI) for HLA class I antigens is given on the x-axis. Region borders (R2) were defined based on the isotype control with the FI for mouse IgG1 given on the x-axis. The percentage of cells that are HLA class I positive is given in R2.

5.3.3   Cell line validation via short-tandem-repeat profiling

The detection of misidentification of standard cell lines and the increasing awareness of the danger for cross-contamination, the proof of authenticity of established and newly generated cell lines that are used in experiments has become indispensable. Short-tandem-repeat (STR) profiling is a DNA fingerprinting method based on the characterization of hypervariable DNA sequences, so called microsatellites, and recommended for cell line authentication. It allows the determination of a unique, cell-line specific profile based on 8 different STR loci. The comparison with database comprising all characterized and registered cell lines allows to authenticate the cell line and to exclude cross-contamination with other cell lines.

Cell line authentication was carried out by Multiplexion GmbH, Heidelberg. STR profiling and comparison with database revealed that the newly generated HNSCC cell line HN038M has a unique sequence, showing only 90% identity with already known cell lines (less than 96% identity is defined as a cell line being not identical with the compared "best hit" cell line). The search for the best hit among cell lines registered in the database identified the cell line UACC-257. This is a melanotic melanoma cell line of non-epithelial origin which is not in use in our laboratory. The established HNSCC cell line has not been present in database to date and shows a genotype code that is unique to this cell line and does not match to any of the cell lines contained in the database.

best database hit	identity	genotype code
UACC-257	90%	AATTAAAAAATTAAAAATAAAWA TTTTTTTAAWTWTATTTAATTATWT (W= uncertain signal)

TABLE 5.2   CHARACTERISITICS OF THE TUMOR CELL LINE HN038M.

All these characteristics revealed by cell line characterization exclude cross-contamination of the primary culture with additional cells from other cell line (established cell lines). In conclusion, the identity of the cell line was confirmed with a unique sequence being revealed for the sample. Furthermore, the characteristic genotype code, which represents a 48-letter code for 24 single nucleotide polymorphism (SNP) locations, was identified. The main characteristics are summarized in Table 5.2, for more detailed information provided by the company see also supplementary Figure 9.9. As the newly generated cell line is currently not present in the Multiplex Cell Authentication (MCA) database (CASTRO et al., 2013) and does not show identity with any other cell lines reported therein, the novelty could be proofed and cross-contamination was excluded.

5.4 Effect of regulatory T cell depletion on the cellular immune response against autologous tumor cells

The presence of regulatory T cells in low-grade lesions and their increasing frequencies in high-grade lesion and invasive cervical cancer (chapter 4.2) is a hint for the role they play in all steps of cervical carcinogenesis. Their contribution to tumor progression and metastasis and the resulting poor prognosis for patients has been, apart from cervical cancer, also been demonstrated in other tumor entities (reviewed in HALVORSEN et al., 2014). With the availability of the above described autologous model system that could successfully be established the idea was prompted to test the immunosuppressive effects of Tregs in vitro and measure the cell-mediated cytotoxicity in presence and absence of Tregs. Therefore, peripheral blood lymphocytes could be obtained from the patient who gave rise to the cell line that were subjected to Treg depletion and used for the killing assay.

5.4.1 T cell purity and Treg depletion

The efficiency of Treg depletion was monitored by flow cytometry analysis by comparing the total (undepleted) T cell fraction with the T cells following Treg depletion. The results are shown in Figure 5.22 and demonstrate that depletion of CD25+ T cells by magnetic labelling decreased the amount of CD4+CD25+ T cells from 1.93% in undepleted T cells to 0.75% in Treg depleted T cells.
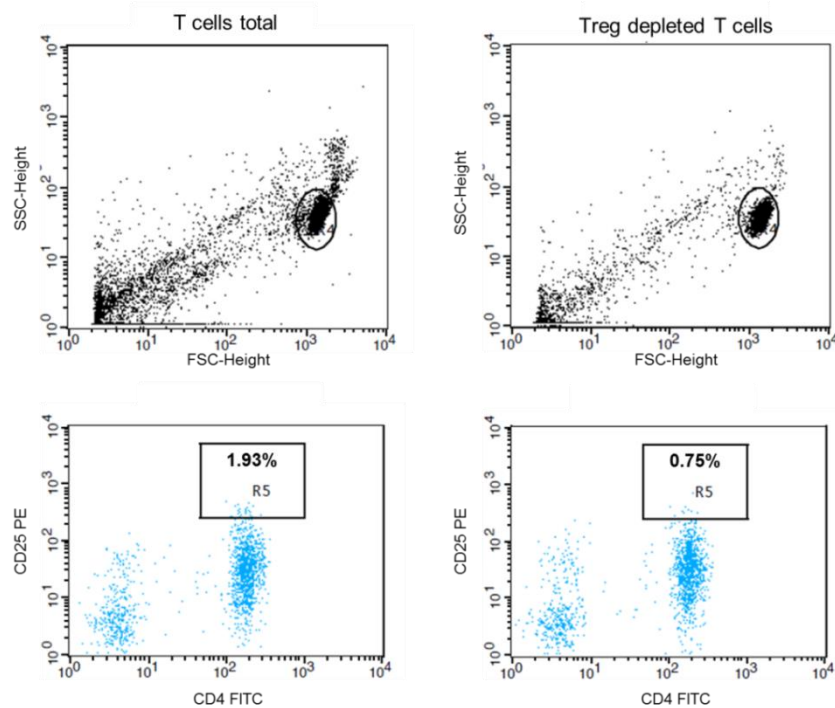
FIGURE 5.22   RESULTS OF THE FACS ANALYSIS OF CD4+CD25+ T CELLS CONTAINED IN THE T CELL FRACTIONS USED FOR CD107a DEGRANULATION ASSAY BEFORE AND AFTER MAGNETIC DEPLETION OF TREG CELLS. The gating strategy in the FSC/SSC is shown in the upper part of the figure and was applied for both T cell fractions. The frequencies of Tregs before (total T cells) and after Treg depletion are shown in lower part of the figure. The fluorescence intensities for CD4 (x-axis) and CD107a (y-axis) are displayed. The percentage of cells that are CD4+CD107a+ are given in R5.

5.4.2   Characterization of the effect of Treg depletion on the killing potency of autologous T cells against the tumor cell line HN038M

The cytotoxic effect of T cells against tumor cells that were either depleted from regulatory T cells or not was measured by CD107a expression on the cell surface as described in section 3.x. CD107a degranulation in T effector cells is induced upon recognition of and activation by tumor cells. As the Treg depletion via magnetic labelling (chapter 3.2.4) targets the CD4+ T cell population of T cells isolated from PBMCs the killing effect also was measured by analyzing the CD4+ T cell population. Although an additional staining for CD8+ T cells was not possible due to restricted cell numbers, the fraction of non-CD4+ T cells can be considered to reflect effects of CD8+ T cells. The gating was performed on T cells as shown in chapter 5.2 and the defined gate was then also checked for samples consisting of T cells co-incubated with tumor cells. T cells were analyzed by plotting CD107a expression against CD4 expression and defining a gate for CD107a+ cells among the CD4+ and non-CD4+ T cells respectively which represented two clearly distinguishable cell populations (Figure 5.23). The values for CD4+CD107a+ T cells were obtained by applying the same gates for all samples.
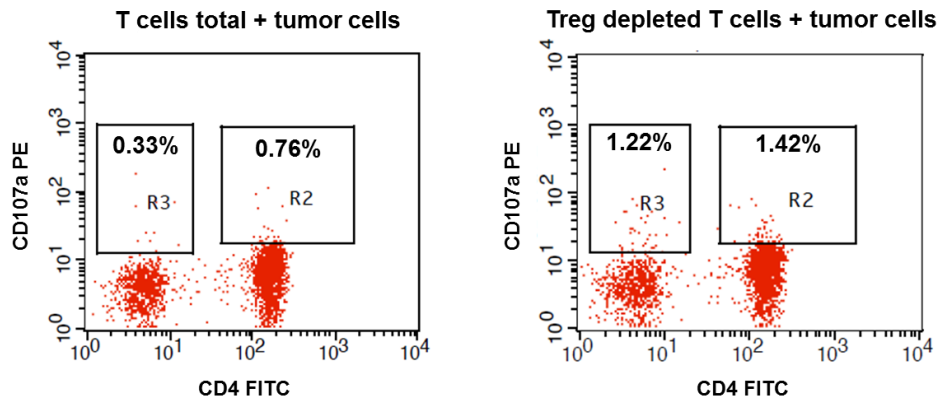
FIGURE 5.23   RESULTS OF THE FACS ANALYSIS FOR CD4 AND CD107A. One of the duplicates is shown for the
co-incubation of autologous tumor cells with total T cells (left) and Treg depleted T cells (right). The
fluorescence intensities for CD4 (x-axis) and CD107a (y-axis) are given. Region borders were defined
based on the isotype controls (not shown). The percentage of cells that are CD4+CD107a+ are given in
R2 and the percentage of CD4-CD107a+ cells in R3.

The results obtained from the comparison between Treg depleted and total T cells are shown in Figure
5.x. Treg depleted T cells compared with total non-depleted T cell fraction showed a slightly better
killing effect as measured by the percentage of CD107+ cells among the CD4+ T cells as defined by
region R2. Interestingly, this effect can also be observed in the non-CD4+ T cell fraction (R3).
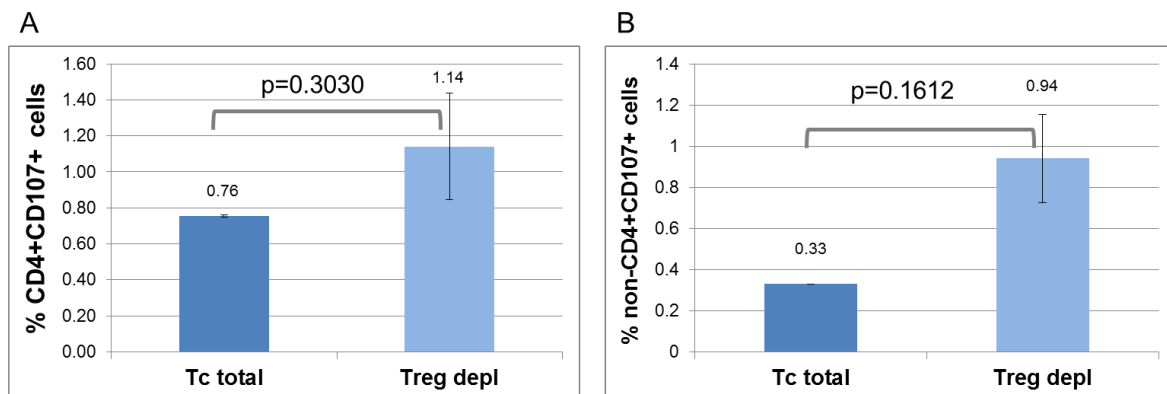
FIGURE 5.24   EVALUATION OF THE CD4+ AND NON-CD4+ T CELLS FOR THE DEGRANULATION MARKER
CD107A. The percentage of positive cells is presented on the y-axis. The experimental groups are
displayed on the x-axis. The blue bars represent the results for the tested groups, standard deviations are
shown as black whiskers (comparison by Student's t-test, p-values are indicated).

In summary, a higher degranulation rate could be observed in the CD4+ T cell fraction and also in the
non-CD4+ T cell population after Treg depletion. The effect was even more pronounced in the non-
CD4+ T cell fraction where the proportion of CD107a+ T cells following Treg depletion was 3 times
higher compared with the total T cell fraction.

5.4.3 The killing capacities of T cells co-incubated with autologous tumor cells can also be monitored in real-time

The effect of Treg depletion on tumor cell killing was monitored by a second experimental approach. Thereby changes in impedance caused by cytotoxic effects mediated by T cells against tumor cells were measured as explained in section 3.2.4. These effects are displayed as cell indices, a unit that reflects changes in size and morphology of the cells, grade of adherence of the cells to the plate as well as cell density (PEPER et al., 2014). The results obtained from this measurement are shown in Figure 5.x. While the ascending curves represent the growing phase of tumor cells during the first 96 hours (represented by the dotted line), the descending curves represent the co-incubation of tumor cells with the effector cells during the following 96 hours (continuous line). T cells were added following the adherence and growing of tumor cells, 96 hours after the experiment has been started (marked by an arrow).
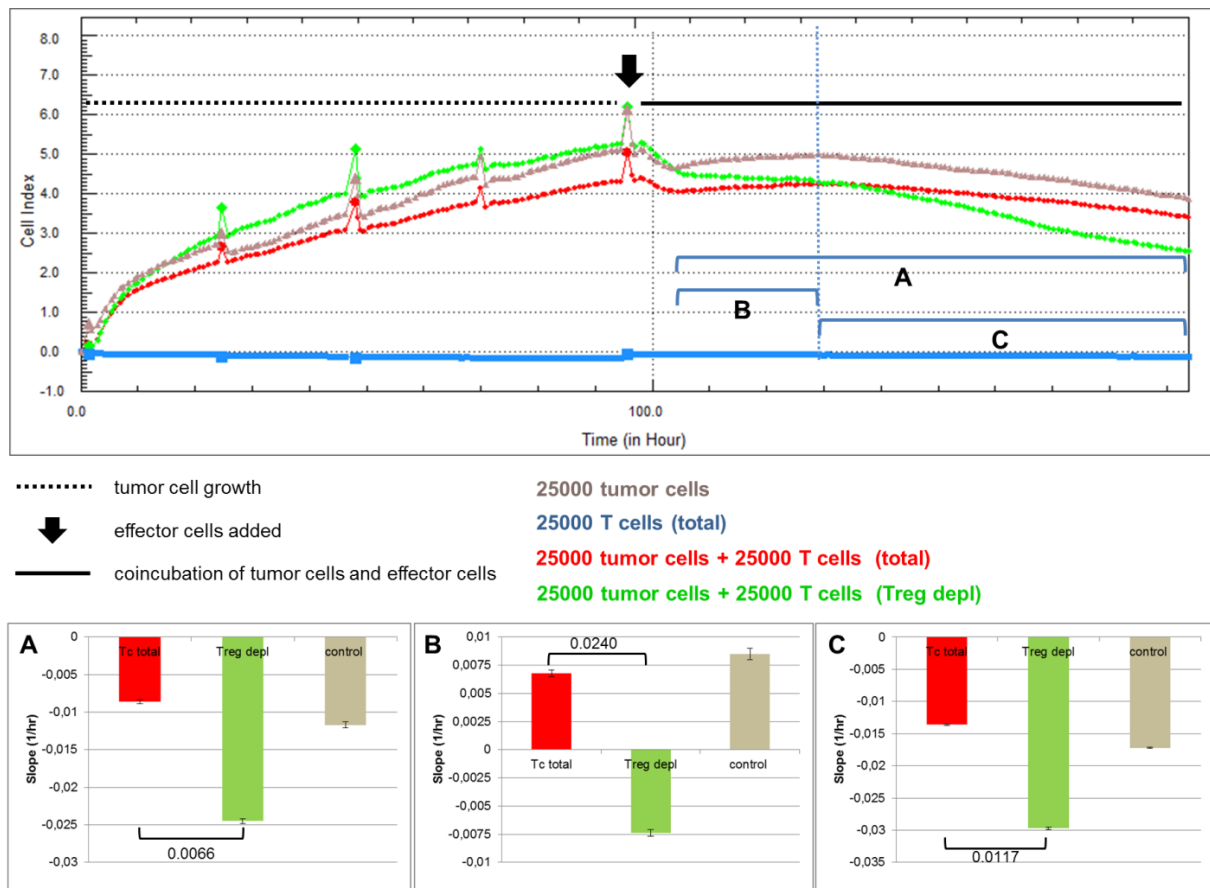
FIGURE 5.25   DYNAMIC REAL-TIME MONITORING OF T CELL-MEDIATED CYTOTOXICTY AGAINST AUTOLOGOUS TUMOR CELLS MEDIATED BY TOTAL T CELLS AND TREG DEPLETED T CELLS. The values recorded by the xCELLigence system are displayed as dimensionless cell indices. Controls (grey and blue) were also measured and compared with the co-cultures of tumor cells and T cells (green and red) (top). Slope values were defined in distinct phases of the killing marked by the brackets A, B and C and visualized as bar graphs (bottom).

The spikes interrupting the curve during the tumor cell growing phase can be explained by the daily removal of the plate from the analyzing unit for change of the media. A massive decrease of cell index values directly after addition of the T cells to the culture could be observed at t=96 hours. This coincides with the time point when T cells were added and thereby half of the tumor cell medium was replaced by lymphocyte medium. This decrease in some samples is followed by a recovery phase accompanied be a re-increase of the cell index (between t=96 hours and t=105 hours).

As depicted in Figure 5.25 the addition of non-adherent T cells to the wells did not have any effect on the impedance and the resulting cell index (blue control curve). Slight differences in the growing behavior of tumor cells during the first 96 hours is reflected by higher or lower cell index values of the tumor cell cultures that were then subjected to different treatments. At that time point the tumor cells subsequently co-incubated with the total T cell fraction had a higher cell index than tumor cells co-incubated with Treg depleted T cells (cell indices for different time points are summarized in Table 5.3).

Time point (hours after start of experiment)	description	T cell total cell index	Treg depleted cell index	p-value
96:00	after tumor cell growing phase	4.34	5.23	0.0569
105:00	after media change and recovering	4.02	4.47	0.2544
132:00	crossing point of both curves	4.21	4.21	0.9273
192:00	end of experiment	3.38	2.38	0.0619

TABLE 5.3   CELL INDICES FOR TUMOR CELLS CO-INCUBATED WITH TOTAL T CELLS AND TREG DEPLETED T CELLS. The values recorded by the xCELLigence system are displayed for different time points beginning after tumor cell adherence and proliferation.

The starting point for measuring the real effect of T cells on tumor cells was set to 105 hours after start of the experiment which represent the end of the recovery phase. Here, the indices for the Treg depletion experiment were still higher than for the total T cell experiment. These differences in the cell indices underscore even more the effects that the different T cell fractions had on the tumor cells which will be explained below.

During the following 96 hours of co-incubation of total T cells with tumor cells the curve showed a slight overall decrease its course is comparable with the grey control curve (tumor cells without T cells). The tumor cell culture that later on was treated with the Treg depleted T cells had reached a higher cell index after 96 hours growing. After change of the media the cells did not show a recovering phase but from that time point on a constantly decreasing curve which, although initially higher, crossed the curve of the tumor cells treated with total T cells at approximately 132 hours. At the end of the measurement the cell index of this curve was far lower (2.38) than that of tumor cells treated with total T cells (3.38) (p=0.0619).

The trends of the curves can be better characterized by determining the slope (in 1/h) over the complete co-incubation period (starting from the recovering phase, phase A) and also in single sections (B, C) (Figure 5.25). The analysis of the overall slope demonstrated that the values for total T cells and Treg depleted T cells are negative, but the values for the "Treg depleted" curve show a greater descending slope. The analysis of the slope in the first killing phase (B) demonstrated, that the

slope was positive for the total T cell curve (+0.0068) while the Treg curve was decreasing (-0.0074). In the last section (C) from the crossing point until the end of the experiment (132 hours - 192 hours) both curves displayed negative slopes, the slope for the Treg curve (-0.0297) however is twice the value of the total T cell curve (-0.0136). The graphical visualization of the slope values calculated for the different cultures and the control also demonstrated that the curve for total T cells (red) is similar to the control curve (grey) and that the curve for Treg depletion (green) behaves completely different. The slope values explain the differences observed for the cell indices for the both co-cultures, with the Treg curve starting at a higher cell index and finally falling below the total T cell curve.

In summary, the real-time measurement of the T cell mediated cytotoxicity against autologous tumor cells demonstrated that Treg depletion enhances the killing of tumor cells and thus confirms the results obtained in the first experiment by CD107a degranulation assay.

6. DISCUSSION AND CONCLUSION

6.1   Overview of the results obtained during the thesis

The central goals of this thesis were to generate a deeper understanding of the immune status of patients with HPV-associated precancerous lesions and cancers and evaluate possible intervention strategies to enhance anti-tumoral immune responses.

In the first part (chapter 4) immune markers that might contribute to tumor immune evasion were investigated on the immune cell side and on the tumor cell side. It could be shown that immune infiltrates in cervical lesions are denser in high-grade lesions compared to low-grade lesions. This was observed for different immune cell markers (CD3, CD8, GranB, Foxp3 and CD3ζ) and does not point to a clear immune activation or suppression (chapter 4.2). Invasive cervical cancer, however, was characterized by a further significant increase in Foxp3+ regulatory T cells accompanied by significantly decreased CD8/CD3 and CD3/CD3ζ ratios which might be a hint for the immunosuppressive state of patients with invasive disease. Although the changes between different infection and histomorphological stages in precancers were not significant large variances in T cells densities in all histomorphological CIN grades could be observed, for example for Tregs and also CD8+ T cells. This might indicate that more or less infiltration with distinct T cell subtypes - effector T cells or immune suppressive T cells - is associated with progression or regression of the lesions. To also gain a deeper insight in the immunological modification on the tumor side contributing to immune evasion mechanisms the expression of HLA antigens was investigated within this thesis (chapter 4.3). Alterations in terms of HLA class I antigen losses and down-regulation, especially of HLA class I heavy chain A, and HLA class II *de novo* expression in precancerous lesions and cancers were common. The selective down-regulation of HLA class I antigens could represent another effective immune evasion mechanism. Interestingly, it could be demonstrated in a longitudinal setting (chapter 4.4) that immune infiltrates in CIN can be influenced by local immune modulatory drug treatment based on imiquimod and that a response to the immune stimulatory treatment with imiquimod is associated with increasing immune cell densities of CD3+ and CD8+ T cells. The major methodological approach of this first part (chapter 4.1) was the establishment of automated cell detection and quantification platform for immune cell infiltrates in cervical precancerous lesions. This tool allows high-throughput screening of larger cohorts on the search for immunological prognostic markers and also for monitoring of treatment strategies.

Based on the findings obtained from the immunological characterization of CIN lesions and cervical carcinoma samples in the first part therapeutic strategies could be deduced for the second part of this work (chapter 5). The approach based on immuno-modulatory drug treatment was pursued in this chapter and also depletion of regulatory T lymphocytes was evaluated in different experimental settings. Immune modulation by TLR-agonist treatment was further investigated by comparing two

different compounds: the approved substance imiquimod and a new purine base derivative called TMX-202 were tested for efficiency regarding immune stimulation (chapter 5.1). It was demonstrated that TMX-202 in comparison to imiquimod induces massive IL-6 secretion. In an *in vitro* priming experiment of naïve T cells it was also shown that this substance can stimulate the adaptive immune response and enhance the killing of CaSki cells. One aim of the second part was also to establish a HPV-positive HNSCC tumor cell line as an autologous model for HPV-associated cancers (chapter 5.2). Autologous systems are of special interest for immunological studies involving tumor cell killing as alloreactivity of immune cells against an incompletely HLA-matched tumor cell lines can be a problem. This model was used to test another strategy aiming at the circumvention of possible immune suppressive effects mediated by regulatory T cells (chapter 5.3). The killing effects of T cells after Treg depletion and without Treg depletion against the autologous tumor cell line were compared and found to be enhanced with Treg depleted T cells in two independent experimental approaches.
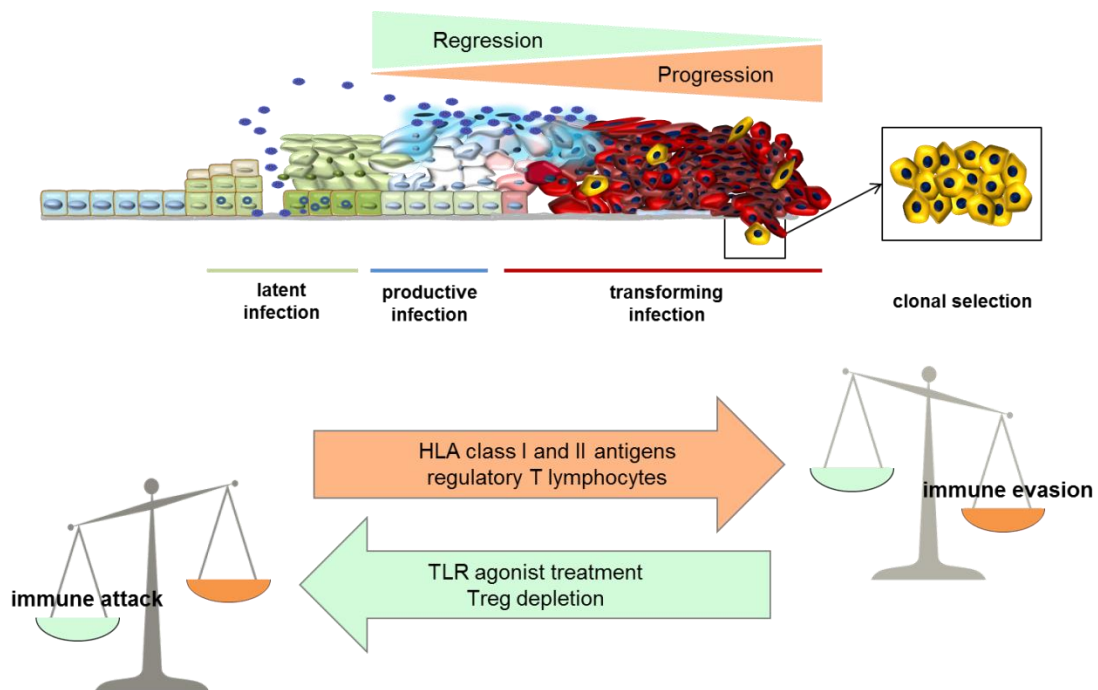
FIGURE 6.1 THE HPV-RELATED CANCER PROGRESSION MODEL INTERPRETED IN THE CONTEXT OF THE RESULTS OBTAINED IN THE COURSE OF THIS THESIS.

6.2 An automated cell quantification tool allows the analysis of the immune cell contexture of cervical precancerous lesions in high-throughput approaches

The tumor micromilieu is thought to be highly important for a better understanding of the factors that influence tumor development and progression. Parameters of interest are the immune cell composition in term of densities and different phenotypes of immune cells entering the tumor area but also features inherent to these cells such as production of enzymes or cytokines that might be released in the tumor environment. The importance of the "immune cell contexture" in primary tumors of different sites and their metastases has frequently been reported and it has been demonstrated that the quality of this tumor micromilieu impacts the clinical outcome of the patients (reviewed in FRIDMAN et al., 2011; FRIDMAN et al., 2012; FRIDMAN et al., 2014).

The idea to search for biomarkers that might be relevant for prognosis and for the prediction of the patient's clinical outcome is widespread in the field of oncology and tumor biology and not restricted to any tumor entity (LLOYD et al., 2010) (GALON et al., 2006). On the hunt for suitable prognostic cancer biomarkers whole slide imaging and automated quantification tools are the approaches that scientists currently strive for. The impact of this methodological approach is reflected by the number of up-to-date publications related to this topic (IRSHAD et al., 2014) and the multitude of reviews that address not only general aspects of digitalized pathology and the state-of-the-art of this relatively new field but also the challenges for imaging informatics and the needs of pathologists (KOTHARI et al., 2013; TAYLOR, 2014; WEBSTER and DUNSTAN, 2014).

The characterization and definition of prognostic biomarkers is also highly important in the screening of cervical intraepithelial neoplasia (CIN). They are frequently detected especially in young women, but they often remain without any clinical consequence due to a high regression rate. Virtually all women diagnosed with a high-grade CIN are surgically treated resulting in over-treatment. To solve this problem reliable biomarkers are necessary for prognosis and risk-adapted treatment strategies.

The first step in the direction of virtual microscopy of cervical precancers was done with the establishment of a platform used for the scanning and evaluation of cervical cytology slides (GRABE et al., 2010). At that time an algorithm was developed that allows the automated detection of $p16^{INK4a}$ stained cells and reliable discrimination from unstained cells.

In the context of immune cell characterization aiming at identification of potentially immune suppressive or cell-mediated cytotoxic mechanisms that could represent progression and regression markers the developed tool for automated cell detection and quantification is highly important. It is a prerequisite for defining immunological markers indicative for the clinical course of cervical intraepithelial neoplasia. One major aim of the presented thesis was the development of such a platform for the quantification of immune cell infiltrates in cervical precancerous lesions.

As outlined in chapter 4.1 this aim could be achieved in a cooperation project with the TIGA Center, Heidelberg. Continuous feedback given between computer scientists, pathologists and immunologist allowed the method to be brought to perfection. The use of available server structures for data storage allowed all cooperation partners involved in the project to have access to the whole slide scans. The establishment of the method was based on CIN samples stained for CD3 and CD8 and involved continued control of the cell detection rate and manual comparison of computed cell signals with the

brown DAB staining signals of digitalized slides. Several rounds of improvement including adaption of annotation tools and defining the threshold for signal recognition also for weaker stains were undergone until the algorithm finally was applied to the patient samples.

The established system has several advantages in comparison with existing manual approaches in the investigation of immunological approaches. (1) It offers high reproducibility as the procedure is based on standardized immunohistochemical staining protocols and application of a defined cell detection and quantification algorithm. (2) It represents an objective way for cell quantification and assures reliable discrimination of positively stained cells from negative cells. Especially the precise demarcation of the basal membrane allows immune cells in this region exactly to be determined: this is very challenging during manual quantification and requires the utmost concentration of the investigator as high immune cell densities can be found in this region. (3) Manual quantification methods mostly are restricted to smaller areas. This novel method which is based on whole-slide-images of the affected tissue allows the comprehensive assessment of not only the tumor or lesion itself but also of the surrounding tissue, the whole microenvironment which seems to largely impact the course of the disease. (4) It offers time-effectiveness and allows high-throughput screening of large cohorts which could be analyzed for a variety of different (immunological) markers.
The advantages of the automated system over manual counting of positively stained cells under the microscope in terms of objectivity reproducibility of the results are widely recognized (FUCHS et al., 2008). Nonetheless, the established platform shall be applied to larger sample sets in the near future to validate the method. Thereby, the intra-observer variability by comparison of repeated manual counting and automated quantification shall be evaluated as well as the inter-observer variability by comparison of manually and automatically quantified immune cell counts of different investigators.

In the long run the technological basis of this study shall be further developed, the parameters to be analyzed shall be expanded and the underlying algorithms have then to be adapted to these needs. Many other markers could be interesting and as their diversity is high and the sample material limited immune-fluorescence allowing double staining appears as an interesting option. Additionally, further immune-cell related information, such as definition of T cell clusters, that frequently are observed in the tumor microenvironment (EDWARDS et al., 1995; HALAMA et al., 2009), might be of interest. Therefore the coordinates of each cell have to be offset against the positions of the surrounding cells to evaluate how many cells are in direct contact with each other and how far they are located from the epithelium.
The actually available operations shall also be extended and one major aim is rendering the annotation of the lesions easier and faster. Currently the exact annotation of the lesion has to be performed manually by drawing the exact borders at the basal and superficial cell layers. The improvement could be achieved by including a previously described algorithm that allows the automated separation of stromal and tumor tissue based on a DAPI staining of the nuclei (LAHRMANN et al., 2011). This algorithm could be adapted to CIN lesions allowing the automated annotation of the basal membrane. This procedure would then require only an approximate demarcation of the abnormal epithelium to initiate the annotation, the basal membrane, however, would then be automatically detected in this region and the ROIs would be calculated as described in chapter 4.1.2. This method would be even more time efficient and exact.

Another challenge of the project and a step towards even more automation regarding the annotating step of the process is the usage of registration methods (MOLES LOPEZ et al., 2014). By elaborating this method, the lesion regions would have to be defined only once on the p16^{INK4a} reference slide, either manually or automatically, which would then be used as template to automatically transfer the annotated region to all other stained and digitalized slides by pattern recognition. The p16^{INK4a} staining could be reliably used for the detection of transformed high-grade lesions, as it is a surrogate for oncogene overexpression and in these cases displays as strong and diffuse staining pattern. A few slides, however, do not express p16^{INK4a} and still would have to be annotated manually. Nevertheless, image registration could reduce the workload as an annotated p16^{INK4a} stained slide could be used as a reference template for several other consecutive stained slides.

Also the morphological appearance could be used and integrated in the computational detection of the lesion as CIN lesions are graded according to the degree of morphologically atypical epithelial cells. While in CIN1 the basal third of the epithelium is affected, CIN2 is defined as showing abnormalities until the middle third and in CIN3 atypical cells can also be found in superficial third of the epithelium. For p16^{INK4a}-negative low-grade lesion that have not yet entered the transforming infection stage a combination of information gained from the morphological appearance and an epithelial marker would be conceivable to identify the p16^{INK4a}-negative lesions (KEENAN et al., 2000; WANG et al., 2007). An algorithm could be developed that recognizes the lesion by computational analysis of the cellular morphology and p16^{INK4a} positivity in parallel and by specifically distinguishing the lesion from the background and also the stromal tissue. This would allow an objective and standardized definition of the intraepithelial neoplasia and thus the corresponding p16^{INK4a} reference slide could be used as template for the automated annotation of the following serial slides stained with different immune markers.

In conclusion, this methodological approach is in accordance with the actual needs of the classical pathology and the contemporary trend towards whole slide imaging that replaces visual inspection and evaluation of glass slides under the microscope and allows for high-throughput analyses. Automated quantification platforms allow the classical pathological discipline to be transferred in to the world of digitalization. The establishment of such a system for CIN lesions was a necessary step to make up leeway and close the gap to the achievements already made for other tumor entities (GALON et al., 2006; KUNZ et al., 2014; LLOYD et al., 2010). This new approach facilitates sharing of sample material between pathologists and scientists as it did also in the here described cooperation project and might improve the reproducibility not only in terms of pathological diagnosis (BUENO et al., 2014) but especially in the scientific investigation of biomarkers predicting the clinical course of CIN lesions. The established method allows the immune cell contexture in the whole affected area to be taken into account and immune cells to be quantified in a standardized and objective way and therefore is highly relevant for the prediction of biomarkers and as guidance for immunotherapy.

6.3 Immune cell densities and composition are different in high-grade lesions and cancers compared with low-grade lesions

A non-negligible proportion of morphologically defined low-grade CIN1 overexpresses p16^{INK4a} (TSOUMPOU et al., 2009) indicating that within these lesions there is to a certain extent already viral oncogene overexpression constituting the initial transforming event. Only a small fraction of these early transforming infections stages, however, progresses towards higher stages (CIN2/CIN3) (WANG et al., 2004). The study presented herein addressed the question whether density and phenotype of infiltrating immune cells are different in low-grade CIN that have already entered the transforming stage (p16^{INK4a}-positive) and those that are still in the permissive stage (p16^{INK4a}-negative) and thus correlates with the early induction of transformation in low-grade lesions or whether this shift rather is associated with established and morphologically advanced high-grade dysplasia that may have accumulated chromosomal instability. To answer these questions, different T cell phenotypes in CIN were quantified in a cross-sectional study cohort and analyzed in relation to the p16^{INK4a}-expression of the lesions. In addition to well characterized immune cell markers (CD3, CD8, Granzyme B and Foxp3) also CD3 ζ-chain was included as here data for CIN are scarcer.

T cell infiltrates were compared between non-transforming and transforming infection stages in low-grade CIN (chapter 4.2.2). The analysis revealed that p16^{INK4a}-positivity in a substantial proportion of low-grade CIN (CIN1) representing the early transforming infection stages, was not associated with significant changes in densities of different T cell phenotypes infiltrating the lesion-adjacent stroma and the lesion. T cell densities in these p16^{INK4a}-positive low-grade CIN were similar to those in p16^{INK4a}-negative low-grade CIN demonstrating that the onset of p16^{INK4a} expression which represents the beginning of the transforming infection state was demonstrated is not associated with changes in T cells densities or in the composition of the infiltrate.

Changes obviously occur at a later time point after transforming processes have been initiated: in later CIN stages (CIN2/3) compared to low-grade CIN the T cell infiltrate densities fundamentally changed irrespective of the T cell phenotype (chapter 4.2.3). The finding of increased T cell density in high-grade lesions – observed for all investigated T cell subtypes in both compartments (except epithelial T$_{reg}$ cells) - is in accordance with other studies describing also denser infiltration and altered immune cell composition in increasing clinicopathologic CIN stages (BONTKES et al., 1997; JAAFAR et al., 2009; MONNIER-BENOIT et al., 2006).

Additionally, the higher absolute T cell infiltration in high-grade CIN compared to low-grade lesion was accompanied by lesion/stroma ratios tending to be decreased for all T cell subtypes except for GranB which was slightly increased. This demonstrates that despite dense infiltration with immune cells attracted to the adjacent stromal compartment the recruitment of T cells into the lesion, where T cell effectors should do their job and eliminate transformed cells, is hampered in high-grade lesions. This effect may - in combination with immunological tolerance – favor progression and the outgrowth of the lesion although dense immune cell infiltrates are present at the lesion site.

Invasive cervical carcinomas were compared with high-grade CIN (chapter 4.2.3) and showed a further increase in total T cell numbers. Significantly higher densities were observed for CD3+, GranB+ and Foxp3+ T cells. This is also in agreement with several other studies reporting on higher

densities of CD4+ T lymphocytes (ADURTHI et al., 2008; LODDENKEMPER et al., 2009), CD8+ T cells (ADURTHI et al., 2008; EDWARDS et al., 1995; LODDENKEMPER et al., 2009) and also Foxp3+ regulatory T lymphocytes (ADURTHI et al., 2008; HOU et al., 2012; WU et al., 2011).

One explanation for the denser T cell infiltration in high-grade CIN and cancer could be the increased antigenicity due to the permanent viral oncogene expression as proposed by Loddenkemper et al. (LODDENKEMPER et al., 2009) or the potential expression of tumor-associated cellular antigens.

It has been described in literature that genomic alterations are induced following viral oncogene overexpression initiating transformation of the host cells and that the accumulation of distinct secondary alterations is driving the progression of a lesion (DUENSING and MUNGER, 2004). However, studies based on comparative genomic hybridization revealed that these genomic alterations are rare in low-grade lesions irrespective of their $p16^{INK4a}$-status (THOMAS et al., 2013). The results obtained from the presented study show that despite $p16^{INK4a}$-positivity indicating viral E6 and E7 overexpression, transforming low-grade CIN are not yet characterized by marked immune cell infiltrate changes, which only occur – as well as the accumulation of genomic alterations (chromosomal alterations) - in later high-grade stages of CIN.

Interestingly, the lesion/stroma ratio for GranB+ activated CTLs and also the epithelial CD8+/CD3+ ratio were significantly decreased in invasive cancer samples, a finding confirmed by other studies speculating on the ineffectiveness of effector T lymphocyte responses despite a strong infiltration due to immunoregulation mechanisms provoking further T cell recruitment to the lesion/tumor while disease progression is unhampered at the same time (ADURTHI et al., 2008; EDWARDS et al., 1995; LODDENKEMPER et al., 2009; MONNIER-BENOIT et al., 2006). Immune suppression mechanisms seem to be more important in high-grade lesions where all sorts of immune cells are attracted to a greater extent. In cervical cancer the highest Treg density could be found, which was constantly increasing with disease severity. The presence of regulatory T cells, however, could also be observed in low-grade lesions. This finding together with the fact that they show large variances in each of the diagnostic categories point to the role they could play in disease progression and clinical outcome of the patients. Also one might speculate that the observed increase of total CD3+ T cell infiltration correlates with an increased proportion of other types of immune regulating, inhibiting cells. This would have to be tested with other markers. With only one immune regulation T cell type, represented by T_{reg} cells, investigated in this study, the exact mode of action of immune control mechanisms enabling HPV-transformed cells to evade the immune system and allow disease progression, remains still to be identified in prospective studies. A comprehensive overview will be given in chapter 6.4 where different immune regulation mechanisms as possible markers for future studies will be discussed. Also strategies adapted by the tumor cells themselves might be involved in the circumvention of host immune responses and enable the cells to further grow out to high-grade lesions and invasive cancers. One of these mechanisms is the alteration of the antigen-presentation capacity (chapter 4.3) which prevents potential HPV-associated antigens to be presented to immune cells. This could hamper the activation of cytotoxic T lymphocytes – that as demonstrated in the course of this analysis are frequently are present in the tumor environment – and thus favor disease progression.

T cell infiltration of CIN lesions and the adjacent stromal compartment is highly heterogeneous with regard to the T cell densities and also phenotypes and was shown to increase with histomorphological lesion grades. The correlation of T cell infiltrates with the $p16^{INK4a}$ status and thereby with biologically defined progression steps of precancerous lesions, which was done for the first time in this study,

demonstrated that there are no differences in the T cell numbers between p16^{INK4a}-negative and p16^{INK4a}-positive low-grade CIN. Only in later, morphologically more advanced high-grade CIN (p16^{INK4a}-positive CIN2/3) remarkable alterations of T cell densities could be found. This is in agreement with the idea of the local selection and outgrowth of more advanced abnormal subclones that have acquired genomic alterations and the influence that these aberrations have on the local immune milieu during progression of established lesions.

The above described heterogeneous T cell densities within the same histomorphological category were reported previously for example for T$_{reg}$ cells by Adhurti et al. who argue that this T cell phenotype varies over time and is dependent of persisting HPV infections (ADURTHI et al., 2008). It has been demonstrated that also a proportion of established high-grade CIN (CIN2/3) regress spontaneously (MUNK et al., 2007) and one could speculate that the dynamics of progression and regression correlates with the variation in T cell densities and that this could be a valuable progression marker especially for high-grade lesions that all are p16^{INK4a}-positive for which reason p16^{INK4a} alone cannot predict progression. The density and phenotype of infiltrating immune cells could be a source of predictors for the natural course of CIN and the clinical outcome as it has been described for various other cancer types (CUNHA et al., 2012; DAVIDSSON et al., 2013; GALON et al., 2006; KIM et al., 2013). Single longitudinal studies reported on higher GranB-expressing cytotoxic T cells in regressing CIN (TRIMBLE et al., 2010; WOO et al., 2008) and this might also be true for other T cell types in both outcome groups.

With the samples deriving from the Austrian imiquimod trial described in section 4.4 and based on automated high-throughput screening methods as described previously (chapters 4.1 and 6.2) these analyses can be transferred to a prospective study of high clinical relevance. T cell densities and phenotypes there can be investigated in relation to the clinical outcome and the correlation with regression or progression of the lesions is likely to contribute to a better understanding of the here discussed heterogeneity in T cell densities. This might allow the definition of the "immune evasion phenotype" – an immunological phenotype associated with immune evasion. Once this combination of immune characteristics is defined it could also be used as a clinically relevant immune cell marker panel to estimate the progression risk of patients.

6.4 HLA class I and class II antigen expression is altered in cervical intraepithelial neoplasia and cancers

Alterations of HLA class I antigens on tumor cells have been reported in different tumor entities and are believed to play – in addition to the variation in T cell infiltrate densities – an important role in the battle of the host's immune system against cancer cells. Modulation of the antigen presentation capacities of the tumor cells is an elaborated mechanism by which tumor cells adopt to the host's immune system to possibly evade an immune attack (CHANG and FERRONE, 2007). HLA class I antigen expression is reported to be associated with the clinical outcome of the patients in different cancers such as HNSCC (MEISSNER et al., 2005), rectal cancer (REIMERS et al., 2014) and melanoma (HICKLIN et al., 1998). For cervical cancer patients a negative correlation between absent HLA class I heavy chain expression and a poor clinical outcome (MEHTA et al., 2008) has been

shown which is explained by presence or absence of recruitment of distinct T cell phenotypes to the tumor (JORDANOVA et al., 2008). The vast majority of these analyses have been performed in cancer patients while the role of HLA class I and class II antigen modulation in earlier stages of cervical carcinogenesis is less well characterized. Also studies involving both components of HLA class I complexes, the heavy chain and the light chain, together with HLA class II antigen expression have been lacking. To close these gap CIN and cervical cancer samples (n=40) were analyzed for HLA class I and HLA class II antigen expression (chapter 4.3).

With regard to HLA class I antigen expression, the analyses performed during this thesis demonstrated that normal, non-dysplastic epithelium adjacent to the lesions showed strong, homogenous and membranous expression for HLA class I heavy chains and β2m in all observed regions. In contrast, CIN and invasive cancers are characterized by a high frequency of alterations in HLA class I antigen expression.

Importantly, the observed losses of HLA class I expression in the majority of the analyzed samples do not represent total HLA class I loss, but often affect only parts of the lesion/tumor defined as heterogeneous expression pattern. About 40 % of lesions (45.0% of CIN and 35.3% of cancers) still retain the expression of HLA class I heavy chain A of the cell surface. With regard to cytoplasmic expression the percentage of lesions that express HLA class I heavy chain A is about 75% (80.0% of CIN and 70.6% of cancers).

Alterations of HLA class I heavy chain expression is more frequently were observed of for the staining with HCA-2 representing HLA class I heavy chain A epitopes while staining results for HC-10 (heavy chains B and C) and β2m less frequently showed alterations.

Possible mechanisms explaining the higher frequencies of losses observed with the HCA-2 antibody mainly recognizing HLA-A heavy chains could be discussed as following: One potential explanation might be that in these cervical lesions a selective loss of the HLA-A locus occurs more frequently as compared with the HLA-B and HLA-C loci which visualized by the HC-10 antibody (reviewed in SELIGER et al., 2002). Selective loss of HLA class I allospecificities in malignant cells has also been reported in melanoma (PASCHEN et al., 2003), renal cell carcinoma (LUBOLDT et al., 1996) and colorectal cancer (KLOOR et al., 2005). This alteration potentially reflects immune selection caused by the massive immune infiltrates entering the tumor microenvironment (chapter 4.2) and might be involved in down-regulated presentation of tumor-associated antigens. Additionally, tumor antigens with a higher antigenic potential might be bound by HLA heavy chain A compared with the other classical heavy chains of the HLA class I complex. Selective loss or down-regulation of HLA-A could then be considered as an adaption of the tumor cells under the immune selective pressure of the host's immune system (CHANG et al., 2003). It is known from other tumor types that the presence or absence of distinct HLA haplotypes, not only HLA class I but also class II antigens, contribute to a higher susceptibility for cancer (RAZMKHAH and GHADERI, 2013), and it is conceivable that this is also true for the development of cervical and other HPV-associated cancers.

Concerning the observed HC-10 staining pattern (less frequent alterations), a definitive conclusion concerning HLA-B and HLA-C heavy chains in this context cannot be drawn for different reasons. First of all, the antibody has overlapping specificity for HLA-B and HLA-C heavy chains and also for

some HLA-A epitopes. If one of the antigens is down-regulated, the presence of the other heavy chain subtype would still result in a positive staining signal (STAM et al., 1986).

Furthermore, other underlying mechanisms such as defects in the antigen-processing in the cytosol and endoplasmatic reticulum might also be involved resulting in disturbed antigen loading and transport to the cell membrane. This could be caused by loss of transporter-associated with antigen processing (TAP) (BANDOH et al., 2010) or tapasin (HAN et al., 2008) which are involved in the transport of antigenic peptides into the endoplasmatic reticulum and loading on HLA class I molecules.

Total loss of HLA class I antigens is causally linked to complete loss of β2m expression due to structural defects of one of the β2m locus on chromosome 15. In this case, HLA class I heavy chains cannot any longer be trafficked by the endoplasmatic reticulum and golgi apparatus to be finally expressed on the cell membrane (reviewed in SELIGER et al., 2002). Cytoplasmic β2m expression is retained in 100% of CIN2 samples and heterogeneous expression of β2m expression could only be observed in the minority of CIN3 and cancer samples. None of the samples were negative for cytoplasmic β2m expression. This implies that loss of β2m is not the major mechanism of immune evasion contributing to the cervical carcinogenesis. This is in contrast to other tumor types such as melanoma or microsatellite unstable colorectal cancers where the β2m wild-type allele is lost (PASCHEN et al., 2003; TIKIDZHIEVA et al., 2012).

The fact that expression in most of the regions is retained argues against a total functional disruption.

Selective loss or down-regulation could be mediated by the interaction of HPV with the expression of HLA class I molecules. It has been shown that HPV16 E7 induces HLA class I down-regulation (BOTTLEY et al., 2008) as well as HPV16 E5 (CAMPO et al., 2010). This might represent a mechanism developed by the virus to circumvent immune attack of virally infected cells by preventing antigen-presentation of viral antigen and thus to establish the infection and promote the completion of the viral life cycle (ASHRAFI et al., 2005).

Once the underlying mechanisms are clear, the re-induction of full HLA class I antigen expression by therapeutic intervention (LANZA et al., 1995) may be a goal and naturally occurring immune responses might then be successfully eradicate the lesion. In addition, treatment strategies based on vaccines or other immune enhancing therapeutics can probably restore or further enhance the immune attack against tumor cells.

The method based of immunohistochemical analyses of HLA class I complexes certainly has limitations. The formalin fixation process of the tumor samples leads to dissociation of assembled complexes into free heavy chains and β2m. In contrast to fresh, unfixed tissue material or cells, where functional HLA class I complexes can be detected for example with the W6/32 antibody recognizing assembled HLA-A/B/C complexes, on paraffin-embedded tissue the heavy and light chains have to be stained separately by distinct antibodies as described previously (KLOOR et al., 2005). This is the reason why this approach does not allow functional conclusions to be drawn from the analysis. Although membranous expression of the components are considered to be a surrogate for the potential antigen-presentation capacity by HLA I antigen complexes, this method is remains of limited accuracy. However, the observed higher frequency of HLA-A losses are not thought to be caused by deficient antibody specificity as the antibodies used in this study are well characterized and widely

accepted for use in immunohistochemical analyses of HLA class I expression patterns (SERNEE et al., 1998 and STAM et al., 1986).

HLA class II antigen expression can be detected in different solid tumors of non-lymphoid origin (ALTOMONTE et al., 2003) and also cervical precancerous stages and cancers were found to be positive for HLA class II molecules (CHIL et al., 2003; GLEW et al., 1992). The biological function in the context of antigen-presentation and activation of effector T cells still remains unclear. The investigation of HLA class II antigen expression was therefore included in the characterization of antigen-presentation mechanisms with the aim to unravel a possible correlation with the classical antigen-presentation pathway mediated by HLA class I antigens.

The staining with the monoclonal antibody LG-612.14 for HLA class II chains DP, DQ and DR demonstrated that the majority of CIN2 and CIN3 lesions are positive for HLA class II antigens. Around 80% of them displayed membranous HLA class II antigen staining. Similarly, cervical carcinoma samples also are positive for membranous HLA class II molecules in around 85% of all cases.
This is a strikingly high percentage of precancerous lesions and invasive cancers compared with other solid tumors of different origins that are reported to express HLA class in tumor cells. Among these are melanoma, gastric, colorectal and breast cancer which to a lesser extent show HLA class II antigen expression, 50-60% of melanoma for example (reviewed in ALTOMONTE et al., 2003).

These observations raise the question of the biological significance and the functional relevance in terms of antigen-presentation. In consideration of the fact that around 85% of CIN2, CIN3 and invasive cancers express HLA class II with 38.4% to 52.6% being scored "positive" and showing membranous expression on virtually all tumor cells, this might probably not contribute to efficacious antigen-presentation directly mediated by tumor cells and a stimulation of anti-tumoral immune responses.
Although it has been shown in the past that tumors – under inflammatory processes - might present peptides via the HLA class II antigen complex to CD4+ T cells and that these can mediate cytotoxicity leading to tumor rejection (DENGJEL et al., 2006; EKKIRALA et al., 2014) the sole binding and presentation of peptides does not necessarily lead to the induction of a cell-mediated immune response. This also requires the presence of co-stimulatory molecules, such as CD28, and their absence rather induces antigen-specific immune tolerance mechanisms favoring disease progression (BAL et al., 1990; GASPARI et al., 1988; HARDING et al., 1992).
With the results seen in this light one might speculate whether HLA class II antigen-negative low-grade lesions therefore represent those that are more likely to regress as they would not – as described in this scenario – induce immune suppression. This question however can only be addressed in a study providing information about the functional role of HLA class II antigen expression for example by correlating it with different immune cell phenotypes present in these lesions and with the clinical outcome of the patients which requires a longitudinal setting such as the Austrian Imiquimod trial.

By interpreting the alterations in HLA class I and class II alterations as adaptions of the tumor cells under the immunoselective pressure of the host's anti-tumoral immune responses, the roles of HLA

class I and II in enabling CD8+ T lymphocytes and NK cells to recognize, bind and kill tumor cells have also to be taken into consideration. The frequently observed HLA class I down-regulation or complete loss in tumors was early associated with impaired CD8+ CTL-mediated anti-tumoral responses (reviewed in GARRIDO et al., 1997). The absence of HLA class I molecules on the tumor cell however is associated with the induction of NK-cell mediated killing (BOTTINO et al., 2004). From the developing tumor's point of view this would be a weak immune evasion mechanism. It was demonstrated that HLA class II molecules expressed on tumor cells protect them from being attacked and lysed by NK cells (JIANG et al., 1996). Expression of HLA class II antigens might therefore also be considered as – secondary – evolutionary development allowing tumor progression. The combined alterations, HLA class I down-regulation and HLA class II expression on tumor cells could therefore represent mechanisms that play together to circumvent cell-mediated cytotoxicity.

HLA class II expression could be caused by HPV infections and interference of the virus the host cell's antigen-presentation machinery. Such a correlation, however, could not be demonstrated (GLEW et al., 1992). One could speculate that a so far unknown event that is related to the transformation processes in high-grade lesions be associated with HLA class II antigen expression. The observed staining pattern in precancerous lesions could also represent the phenotypical heritage of the initially infected keratinocytes that did not resolve the HPV infection and further grew out to precancerous lesions. This hypothesis is supported by the observed peculiar staining pattern of columnar epithelium in the squamocolumnar junction in combination with the absence of HLA class II expression in normal squamous epithelium. It has recently been shown that a distinct cell population present in the squamocolumnar junction zone is susceptible to HPV infections and furthermore is characterized by a distinct protein expression profile (HERFS et al., 2012). It is conceivable that HLA class II expression is another characteristic of these highly metaplastic cells. If the assumption holds true that the vast majority of cervical lesions originate in this region and develop by clonal expansion of distinct cells, the strong HLA class II expression could be explained by the maintenance of this phenotype in outgrowing lesions. This was hypothesized earlier in a study also observing high expression in the metaplastic epithelium and strong expression in cervical precancerous lesions and cancers (CHIL et al., 2003). This phenomenon then would rather be explainable by cell-intrinsic characteristics than an adaption caused by interaction of the viral infection with the host cell's antigen-presentation machinery. Interestingly, only half of the CIN1 were positive for HLA class II antigen staining and this did not correlate with $p16^{INK4a}$ expression representing the transforming infection stage. Considering the high frequencies of HLA class II expression in later stages, one could speculate that low-grade lesions positive for HLA class II antigen expression are more likely to progress which could not addressed in this study but requires a longitudinal approach.

6.5   The density and composition of immune cell infiltrates can be influenced by immuno-modulatory drugs

Several studies have demonstrated that the composition of immune infiltrates and the behavior of immune cells such as migration can be influenced by immune modifying agents such as imiquimod (HACKSTEIN et al., 2012; HUANG et al., 2009b; SUZUKI et al., 2000). Imiquimod is TLR7/8 agonist and its potential to enhance the patient's immune response prompted physicians to initiate a multitude of trials in order to investigate is efficacy in off-label indications such HPV-associated vulvar intraepithelial neoplasia (WESTERMANN et al., 2013) (VAN SETERS et al., 2002) (VAN SETERS et al., 2008). Although imiquimod is known to cause local and systemic side effects, it appears to be a promising alternative to surgical standard treatment. In particular, in women affected by multifocal VIN imiquimod treatment can replace cold knife excision as a first intervention option (FREGA et al., 2013). Also in CIN patients there is a non-negligible need for conservative treatment strategies as the surgical standard treatment, LEEP conization, is supposed to affect the outcome of subsequent pregnancies and provoke pre-term birth (ARBYN et al., 2008; SIMOENS et al., 2012).

The Austrian imiquimod trial was the first randomized, placebo-controlled trial performed to test the efficacy of topical imiquimod treatment in patients with high-grade CIN (GRIMM et al., 2012). Three biopsies per patient were taken over 20 weeks during the treatment and after the completion of the treatment protocol and the clinical outcome of each patient was defined based on the last biopsy taken. These tissue specimens allow the investigation of changes in immune cells densities under treatment with a TLR7/8 agonist and might give insights in how the immune modifier acts and which immune cell composition is associated with a clinical response to the treatment. Of this unique patient cohort cervical biopsies of 10 patients could be obtained who received imiquimod therapy over 16 weeks. Albeit numerically restricted, these samples represent very valuable patient material allowing address questions that have never been investigated before.

The tissue specimens that could be obtained of this trial were characterized by p16^{INK4a} staining and then analyzed based on the method described in chapter 4.1 for total T cell infiltration represented by CD3+ cells and cytotoxic lymphocytes represented by CD8+ T cells. The obtained data were comparatively evaluated as immune infiltrates in non-responders and responders to the imiquimod treatment (described in chapter 4.4). In a first approach the question was addressed whether CD3 and CD8 T cells in initial CIN2/3 biopsies are different between lesions that subsequently regressed (responders to imiquimod) and those that persisted or even progressed (non-responders). Interestingly, in non-responders a higher initial infiltration with CD3+ T cells was observed compared with responders. The fact that these patients do not respond to the imiquimod treatment might be an evidence for the presence of cell types others than effector cells present in the lesion microenvironment. Although only one single T cell subtype was investigated (represented by CD8+ T cells) and a definitive conclusion cannot be drawn from these results, the preliminary results allow the speculation that the difference between non-responders and responders lies in a higher densities of T cells phenotypes eventually responsible for immune regulation such as Treg cells. The higher absolute T cell densities represented by CD3+ T cells could possibly be explained by a higher fraction of these

"unfavorable" cell types which are absent in responders and thus having a lower CD3+ T cell infiltration. Responders were characterized by lower total CD3 T cell infiltration. They had, however, higher total CD8+ T cell densities and CD8/CD3 T cell ration compared with non-responders. The higher proportion of cytotoxic T cells in responders before treatment might constitute a better initial situation probably leading to an enhanced response to imiquimod.

Additionally, the cohort is predestined to answer the question whether the immune cell densities and composition are different between non-responders and responders at the end of the imiquimod treatment. It allows also the analysis of possible changes of the local immune cell composition that occur during the treatment and their effect on the clinical response of the patients. The total T cell infiltration with CD3+ T cells in responders after treatment compared with the initial biopsy indicated that imiquimod locally applied to the cervix attracted immune cells to the lesion site. Responders also showed a further increased infiltration with CD8+ T cells that could not be observed in non-responders. The densities after treatment exceeded the CD8+ cell counts of the initial biopsies taken before the treatment was started. However, the CD8/CD3 ratios were not higher after treatment compared with the initial CD8/CD3 ratio in the biopsies taken before treatment, which might indicate that together with CD8+ cytotoxic T cells also other T cell subtypes must have been attracted to the lesion site in a proportional way representing a non-negligible proportion of T cells. This might be an explanation why the CD8/CD3 ratio is not influenced to the extent one would expect from the absolute CD8+ cell counts. In non-responders the total T cell infiltration represented by CD3+ T cells was not different at the end of the treatment compared with the initial biopsies. Interestingly, non-responders after treatment compared with week 0 showed a further decreased CTL infiltration regarding the absolute cell counts leading also to even lower CD8/CD3 ratios than before the treatment. The exact composition of the initially dense CD3+ T cell infiltrate in non-responders, aside from the characterization of CD8+ T cell densities, remains largely unclear and warrants further investigation of immune cell phenotypes possibly responsible for the unfavorable immune cell composition that might be associated with treatment resistance. On the other hand, it is also worthwhile to characterize in more detail T cell subtypes others than CTLs in responders and the underlying mechanisms contributing to a clinical response to imiquimod.

It has been demonstrated before that generally low immune cell densities in the tumor environment are associated with a poorer prognosis in cervical cancer (NEDERGAARD et al., 2007), especially low CD8+ T cell counts in combination with high regulatory T cells infiltration correlates with poor prognosis (SHAH et al., 2011). A major aim of cancer immunotherapy therefore is to enhance the anti-tumoral immune responses and to attract immune cells to the lesion site. It has been shown in the past that imiquimod treatment in patients with vulvar intraepithelial neoplasia contributes to the normalization of immune cell counts, for example by maturation of immature Langerhans cells, and thus induces histological regression of the lesions (TERLOU et al., 2010). Changes in immune cell counts are conceivable to be also the underlying reason for regression of the proportion of CIN patients that had responded to imiquimod therapy. It appears to be obvious that the enhanced CD8+ T cell infiltration into the lesion might contribute to the better outcome of these patients as it has been reported before (DE VOS VAN STEENWIJK et al., 2013; PIERSMA et al., 2007) and that imiquimod also in cervical intraepithelial neoplasia might be able to expand pre-existing CD8+ T cell response (TODD et al., 2004).

As discussed above (chapter 1.3.3), p16^{INK4a} is a reliable marker routinely used in clinical practice and specifically highlighting the stage of infection as it is a surrogate that indicates the presence of HPV oncogene activity and induction of transformation of the cell (VON KNEBEL DOEBERITZ et al., 2012). Its overexpression, however, only proofs the presence of HPV transformed cells and does not indicate if the lesion will progress into high-grade CIN and cancer or regress, which happens in a non-negligible proportion of all cases (SCHIFFMAN and WENTZENSEN, 2010). Until now the prediction of possible regression and progression therefore has remained an unsolved diagnostic problem and consequently in the clinical practice all high-grade CINs are routinely treated by surgical intervention irrespective of the individual risk for progression. The characterization of distinct immune cell phenotypes and the combination of different immune markers to define a biomarker tool appears as an interesting option for the prediction of the progression risk. Although the here presented analysis was based on a small sample size of only 10 patients and differences were not yet significant the data argue for a consistently differential T cell distribution in non-responders compared with responders.

The both markers analyzed so far representing the total T cell infiltration as measured by CD3+ T cells and possible cytotoxic responses as indicated by CD8+ T cells already provided interesting insights in their potential prognostic role (as measured by responsiveness to imiquimod treatment). However, other immunological markers might be of interest to gain more insight in the mode of action of imiquimod and to identify further prognostically relevant mechanisms. In the past, imiquimod has been reported in the context of Langerhans cell migration (SUZUKI et al., 2000) and recruitment of CD8+ T cells via the integrin CD49a (SOONG et al., 2014). It induces furthermore the expression of cytokines and chemokines, such as CXCR3, IFN-γ and reduces IL-10 and TGF-β expression (HUANG et al., 2009b; SOONG et al., 2014; WENZEL et al., 2005). Interestingly, imiquimod also seems to turn myeloid and plasmacytoid dendritic cells into effector cells by inducing them to express perforin, Granzyme B and TRAIL (STARY et al., 2007). These markers only represent a restricted selection of possible markers that could be analyzed to determine the effects of TLR7/8 agonist treatment and to characterize the typical immune cell phenotypes of regressing or progression lesions. Also markers that represent immune evasion mechanisms would have to be taken into consideration to characterize the "immune evasion phenotype". Markers that might contribute to progression of lesions or mediate resistance to immuno-modulatory treatments are discussed in more detail in the following section 6.6.

The samples obtained from the Austrian imiquimod trial demonstrate how important longitudinal information is for the understanding of immune cell densities and phenotypes influencing the course of the disease. As the trial included also a placebo-controlled patient group the natural course of CIN without therapeutic intervention (Figure 6.2), T cell infiltrates can be associated with progressions of treated and untreated patients also a T cell infiltration profile important for spontaneous regression (under placebo) might be identified. By its longitudinal setting and the placebo controlled patient group the Austrian trial is a precious study cohort to better understand immune cell composition in regressing and progressing CIN lesions in the placebo group or in the imiquimod group. This allows also the determination of immune cell compositions associated with spontaneous regression or susceptibility to imiquimod therapy. On the long run this cohort could be the clue for a better understanding of the factors that influence progression and regression and might be decisive for the definition of immune markers for a more risk adapted treatment of patients. Thus, not all patients with

high-grade lesions might have to undergo classical surgical treatment but could alternatively be tightly monitored and wait for spontaneous regression or non-surgically be treated with an immune modulator.
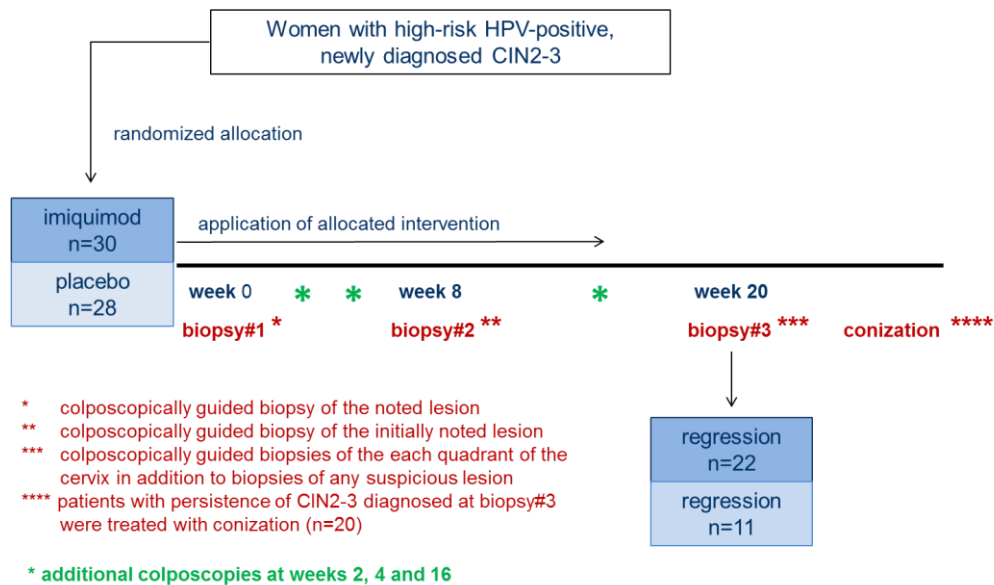
FIGURE 6.2 OVERVIEW OF THE TREATMENT SCHEDULE OF THE AUSTRIAN IMIQUIMOD TRIAL AND OUTCOME OF THE PATIENTS. The setup of this trial does not only allow to compare effects of imiquimod treatment in responders and non-responders but also to define T cell phenotypes associated spontaneous regression (placebo group) or disease progression (under treatment or placebo).

With preliminary results (chapter 4.4) obtained in the here described characterization of CD3+ and CD8+ T cell infiltrates clinical impact of this study begins to show even though only few samples and only two T cell markers were investigated so far. Despite the relatively small sample size differences in immune cell densities could be observed when the patients were stratified for clinical outcome. Furthermore, it could be demonstrated that the local therapy of cervical intraepithelial neoplasia with the immuno-modulatory drug imiquimod can influence the T cell infiltration in terms of density and composition. Significant differences remain to be shown in a larger setting where all patients of both treatment arms, in total 59 patients, shall be included.

As discussed formerly (section 6.1) the densities and phenotypes of tissue infiltrating immune cells is investigated in various cancer types to define prognostic markers. Furthermore, the characterization of the immune cell contexture (FRIDMAN et al., 2014) is indispensable for the mechanistic understanding of cancer immunotherapy playing a more and more important role in clinical praxis. The whole-slide-imaging and quantification platform implemented in CIN histopathology (chapter 4.1) will be used to characterize the patient cohort of the imiquimod trial. The developed method will allow quantifying in a standardized way the immune cell composition of the complete microenvironment and provides a highly information-rich profile which can be used for the definition of a prognostic biomarker tool.

6.6   The search for the prognostic markers characterizing the immune evasion phenotype has to be continued

The characterization of immune infiltrates in cervical intraepithelial neoplasia (chapter 4.2) has demonstrated that despite a generally higher infiltration with different T cell phenotypes in high-grade CIN, these lesions have progressed to a certain extent and may further progress into invasive cancer (SCHIFFMAN and WENTZENSEN, 2010). In addition to the presence of T_{reg} cells in the cancer environment, decreasing CD3ζ-expression possibly leading to a lack in T cell activation and changed ratios of effector cells (decreased CD8/CD3 ratio) that were observed in the CIN studies, other markers still may be of interest and contribute to progression (Table 6.1). This chapter discusses possible markers and reviews mechanisms described also in other than HPV-related diseases that could be considered in the further analyses of the Austrian imiquimod cohort (chapter 6.5) in order to define the immune profile that characterizes the immune evasion phenotype of progressing CIN.

Of course, not all immune cell phenotypes, receptors and ligands or cytokines represent markers exclusively associated with immune suppression and evasion. The majority of the here listed mechanism are originally associated with cytotoxic immune response (Table 6.x). However, their altered expression, down-regulation or changes in their ratios to other markers or cell phenotypes harbor potential immune inhibiting effects.

The following list does not claim to be complete but rather is a try to summarize the most important players in immune evasion that exert the effect on different levels. The different aspects were classified in different categories in dependence on whether immune cell phenotypes or rather signaling molecules or receptor and ligands are involved.

Evasion mechanism	Effect	References
A) immune cell phenotypes		
CD4+CD25+Foxp3+ T_{reg} cells	promote progression of primary tumors, possibly also involved in promoting metastasis	(HALVORSEN et al., 2014)
CD4+CD69+CD25- T_{reg} cells	express CD122 and membrane-bound TGF-β1 by which they mediate immune escape and tumor progression	(HAN et al., 2009)
reversal of the CD4/CD8 T cell ratio	Together with presence of Treg cells has a negative impact on clinical outcome	(SHAH et al., 2011)
immature dendritic cells	convert anergic T cells into immune suppressive Treg cells	(PLETINCKX et al., 2014)
loss of co-stimulatory molecules CD27 and CD28 on T cells	Senescent T cell phenotype induced by tumor cells; leads to suppression of responder T cells proliferation and promotes tumor progression	(MONTES et al., 2008)
γδ-T17 cells	accumulation of myeloid-derived suppressor cells	(WU et al., 2014)
myeloid derived suppressor cells (MDSCs)	suppression of T-cell and NK cell function	reviewed in (DIAZ-MONTERO et al., 2014)

lack of Langerhans cells	impaired antigen-presentation in the epithelium	(FAUSCH et al., 2002)
CCR8(+) inflammatory myeloid cells (monocytes and granulocytes)	CCL1 secreted by tumors binds CCR8 → tumor-induced inflammation → immune evasion	(ERUSLANOV et al., 2013)
B) cytokine and chemokine microenvironment		
TGF-β	immunosuppressive cytokine that hampers the Th1 response	(PALOMARES et al., 2014)
IL-10	immunosuppressive cytokine that hampers the Th1 response	(SYRJANEN et al., 2009)
IL-13	immunosuppressive cytokine that hampers the Th1 response	(DEEPAK et al., 2010)
chemokine CXCL12 and chemokine receptor CXCR4	promote tumor growth, invasion, metastasis and therapeutic resistance	reviewed in (CHATTERJEE et al., 2014)
C) endothelial factors, T cell homing and migration		
decreased mucosal addressin cell adhesion molecule (MAdCAM) expression	decreased CD8+ T cell access to cervical tissue	(TRIMBLE et al., 2010)
vascular cell adhesion molecule-1 (VCAM-1)	expression by tumor cells promotes T cell migration away from the tumor	(WU, 2007)
E-cadherin down-regulation	associated with decreased numbers of Langerhans cells in the epithelial and viral immune evasion	(LEONG et al., 2010)
D) antigen processing and presentation in tumor cells		
HLA class I antigen down-regulation	promotes escape of tumor cells from recognition and destruction by HLA class I-restricted, antigen-specific cytotoxic T lymphocytes	reviewed in (CHANG et al., 2003)
increased non-classical HLA class I antigen (HLA-G) expression	impairs the cell-mediated anti-tumoral immune response	(RODRIGUEZ et al., 2012)
dysregulation of transporter associated with antigen processing (TAP)	Disturbed antigen loading on HLA class I heavy chains resulting in impaired antigen presentation	(BANDOH et al., 2010)
E) altered immune cell ligand/receptor expression		
up-regulation of CD94/NKG2A	inhibitory NK receptors	(SHEU et al., 2005)
MHC class I chain-related molecule A (MICA) down-regulation	CTL and NK cell ligand, impaired effector cell activation	(LU et al., 2011)
abnormal CTLA-4 expression and dysregulation	down-regulation of T cell proliferation and effector function	(MAO et al., 2010)
PD-L1 expression in tumors	binding to PD-1 on TILs leads to impaired T cell functions through suppression of T cell receptor signaling	(MAINE et al., 2014), reviewed in (MCDERMOTT and ATKINS, 2013)
Fas and FasL expression on	Changes in Fas expression promotes tumor growth	(ABRAMS, 2005)

tumor cells	by reduced apoptosis sensitivity, FasL expression on tumor cells mediates killing of T cells entering the tumor	
F) other mechanisms		
micro-RNAs (miRNA-155)	reduced levels of miRNA-155 results in decreased numbers of CD8+ effector T cells	(DUDDA et al., 2013)
IDO, TDO expression in tumor cells	catalyzes immunosuppressive kynurenine leading to cell cycle arrest and functional anergy of effector cells, T_{reg} differentiation and activation	reviewed in (MUNN and MELLOR, 2013; PLATTEN et al., 2012)
matrix-metalloproteinase (MMP-1, MMP-2 and MMP-9) expression	NK cell dysfunction; down-regulation of IL-2 receptor a (IL-2Ra) expression on activated tumor-infiltrating lymphocytes	(PENG et al., 2014) (SHEU et al., 2001)
increased inducible nitric oxide synthase (iNOS) expression, high levels of nitric oxide (NO)	nitric oxide acts as signaling molecule and promotes cancer formation, progressions and metastasis	(CHENG et al., 2014)
microparticles (subtype of extracellular vesicles containing nucleic acids and proteins)	involved in immune evasion, angiogenesis, tumor invasion and metastasis	(VOLOSHIN et al., 2014)
expression of sialic acids on tumor cells	promote immune evasion via interaction with the inhibitory receptor Siglec	(BULL et al., 2014)
TLR4 expression on tumor cells	TLR stimulation induces synthesis of IL-6, iNOS and other factors, mediates resistance of tumor cells to CTL attack and promotes immune evasion	(HUANG et al., 2005)

TABLE 6.1   POTENTIAL MARKERS FOR THE DEFINITION OF THE "IMMUNE EVASION PHENOTYPE". A combination of markers that contribute to immune evasion in HPV-related precancerous stages and cancers could be used as a diagnostic biomarker tool.

The immunohistochemical analyses of cervical precancerous and cancerous lesions performed in the first part of this work gave hints of immunosuppressive and immune evasion mechanisms that might play a role in the progression of HPV-associated diseases. The presence of Tregs in these lesions, varying from low densities to high infiltration within one diagnostic category and increased in cancers compared to precancerous stages as well as varying densities of effector T cell phenotypes in the lesions implies that these variations might contribute to either the progression or regression of the lesions. Furthermore, this indicates that the quality of the immune infiltrates might correlate with the clinical outcome and could be the basis for defining prognostic markers. To better understand which combination of markers is the most relevant for prediction of progression or regression. Here again the longitudinal nature of the Austrian imiquimod trial is extremely valuable as it allows to decipher distinct immunological constitutions associated with progression of high-grade lesions – in untreated patients and under the influence of imiquimod. In combination with the automated cell quantification method allowing high-throughput screening of larger patient cohorts and a broad variety of different immune markers the identification of a prognostically relevant biomarker tool usable for treatment decision appears as a realistic goal.

The positive effect of immuno-modulatory drugs on the density and composition of the T cell infiltrate could be demonstrated for imiquimod for CD3+ and CD8+ T lymphocytes (chapter 4.4).

In the second part of this thesis different intervention strategies were investigated in more detail in immune and tumor cell based *in vitro* assays. Here, immuno-modulatory agents (chapter 5.1) and also manipulations directly on the cellular levels in terms of Treg depletion (chapter 5.3) were analyzed to explore the potential of different immunological treatment strategies.

6.7 A new immune modulatory drug, TMX-202, shows promising effects the priming of naïve T cells to HPV-associated antigens

Immune modulation has been shown to be one mechanism that potentially leads to tumor eradication by enhancing the host's immune responses against abnormal cells. Aldara, the 5% imiquimod cream formulation, is an immuno-modulatory TLR7/8 ligand-based substance approved for the treatment of warts, actinic keratosis and basal squamous carcinoma (chapter 1.x). Because of lacking conservative treatment options it is also given as an off-label drug to patients with anal and vulvar intraepithelial lesions and melanoma in situ (DAVID et al., 2011) and investigated in a multitude of trials to prove its efficacy in these off-label indications. Its efficacy could also be demonstrated in the first randomized, controlled trial enrolling high-grade CIN patients (GRIMM et al., 2012). Although imiquimod is considered to be safe, it causes local and systemic adverse effects which require the treatment protocol to be interrupted (chapter 1.5.3). Considering the potent immuno-modulatory capacity of imiquimod by induction of a strong cytokine release and a Th1-dominant anti-tumor immune response and the non-deniable need for such an immune stimulating treatment it is worthwhile to consider alternate drugs for TLR activation.

In cooperation with a company specialized in immuno-modulatory drugs, Telormedix S.A., which provided a new substance for initial tests, the potency of TMX-202 a purine-like TLR7 agonist bioconjugated to a phospholipid (Figure 1.11) agonist could be tested in different experiments (CRAIN et al., 2013). Within the presented thesis, its immuno-stimulatory effects were tested *in vitro* in the HPV-setting as it could be an interesting substance for a combinatorial drug approach that increases the immune response to papillomaviruses. The results obtained in these experiments contributed to a patent application.

It has been shown in the past that the TLR expression levels in B cells can be up-regulated by both activation of the antigen-receptor or stimulation of the TLR itself by treatment with a TLR-ligand (BOURKE et al., 2003). This finding implies that external stimuli simulating infection could regulate the expression levels of TLRs by a positive feedback loop. Therefore, possible regulatory mechanisms on the expression levels of TLRs were also tested under the influence of imiquimod and the new TLR-ligand TMX-202 and measured on the transcript and protein level. The PBMCs of four healthy donors were treated, two of them with imiquimod and TMX-202 to compare the effects of the approved and the newly developed drug and two of them were treated with different TMX-202 concentrations.

Donor 1 showed high changes in TLR7 mRNA expression which have to be interpreted with caution, as RNA concentrations following isolation were low. These low mRNA levels might have resulted in low Ct values and high-fold changes when visualized in a log2 scale. Also the effects of imiquimod on the PBLs of the first two donors were contradictory as donor 2 displayed higher changes in TLR7 mRNA expression following imiquimod treatment while donor 1 responded to TMX-202 treatment with mRNA up-regulation. Whether this is a specific effect of imiquimod or rather induced by potential side effects that could be caused by the imidazoquinoline cannot be deduced from only donors tested. Also the results obtained for donors 3 and 4 were inconsistent with donor 3 showing no effect or even decreasing mRNA expression levels and donor 4 increasing TLRL7 mRNA expression. On the protein level for donors 1 to 3 no effect of any of the treatments could be observed. The PBMCs of donor 4, however, displayed increased TLR7 protein expression following treatment with TMX. In summary, only donor 4 showed a convincing influence of TMX-202 on both mRNA and protein levels that were consistently up-regulated after treatment and under both applied concentrations of 1µM and 10µM. The fact that natural infections lead to up-regulation of the corresponding TLRs *in vivo* accompanied by an enhanced cytokine release in a time dependent manner (HUANG et al., 2009a; KAUR et al., 2014) might be a reason for the responsiveness of donor 4. A previous infection might have induced immune cell activation and thus enhanced their responsiveness. Secondary stimulation with a TLR-ligand might faster and to a higher extent than in the PBMCs of the other donors have up-regulated TLR7 expression on mRNA and protein level. The immune cells might still have been in an activated state and thus shown a greater reaction to the external stimulation.

However, most importantly the down-stream effect of TLR agonist treatment which is considered to be the release of pro-inflammatory cytokines stimulating both innate and adaptive immunity (STANLEY, 2002). The pro-inflammatory cytokine plays a pivotal role in linking both arms of the immune system and mediates the transitions from inflammatory processes to the acquired immune response (reviewed in JONES, 2005). The pro-inflammatory processes after imiquimod and TMX-202 treatment were therefore measured by IL-6 ELISA using the supernatants deriving from PBMC stimulation and were compared between the different treatment groups. It could be shown that imiquimod induced significantly higher IL-6 levels compared with the controls. TMX treatment, however, further increased the IL-6 release (by approximately two powers of ten) which was extremely significant compared with controls. These results confirmed data published for dose-dependent IL-6 release measured in whole blood following TMX-202 treatment (CRAIN et al., 2013). In addition, it could be shown that the substance has a strong potential for the induction of a pro-inflammatory cytokine milieu and this is not dependent on the TLR7 mRNA or protein expression levels but rather dose-dependent.

With these insights gained in the mechanisms how TMX-202 could link the innate with the adaptive immune response its potential to probably enhance T cell responses against HPV-associated antigens were tested additionally in an in vitro approach. This experiment is based on the priming of naïve T cells with HPV-associated antigens loaded on dendritic cells in order generate antigen-specific T cells by bringing them repeatedly in contact with antigens presented by professional APCs. Therefore a well-established protocol used in our department was used (KAUFMANN et al., 2001).

One of the peptides used in this experimental approach were p16^{INK4a}, a host cell protein which by its specific overexpression in HPV-transformed lesions and all HPV-induced cancers is a potential target protein for secondary vaccination approaches. In contrast to the viral proteins it is not HPV-type specific. The second antigen is the major capsid protein L1 of HPV16 which is known to be a strongly antigenic protein on which the prophylactic vaccines are based. The antigenicity of p16^{INK4a} as well as of HPV16 L1 were demonstrated in our phase I/IIa p16^{INK4a} vaccination clinical trial and by a therapeutic vaccine based on chimeric virus-like particles consisting of a L1p16^{INK4a} fusion protein (FAULSTICH, 2014). Both studies demonstrated that p16^{INK4a}-specific and L1-specific cellular immune responses can be developed following vaccination.

For p16^{INK4a} the peptide sequence used in the clinical trial was used. For L1 a series of 9-mer and 10-mer HLA-A2 restricted peptides were predicted and chosen as described in section 3.x and were tested in a peptide-binding assay. One L1 sequence that was reported to induce L1-specific T cells following *in vitro* priming was included as positive control (KAUFMANN et al., 2001), together with an influenza matrix protein sequence, to evaluate the binding capacities to HLA antigens in the peptide binding assay. The p16^{INK4a} peptide used in the clinical trial also was considered to have a high binding affinity and therefore was considered to be a control peptide for the newly synthesized L1 9-mer peptides.

Of the tested L1 peptides three (L1_2, L_12 and L1_97; sequences in chapter 3.x) were demonstrated to meet criteria defined to identify the best binding antigens: they had a significantly higher MFI reflecting the binding capacity as compared with the background control and furthermore had a higher MFI compared with the lowest "positive" control.

The effects of TMX-202 stimulation during T cell priming were compared with DMSO as vector control and investigate on different levels: on the one hand dendritic cells were characterized in more detail and on the other hand T lymphocytes were evaluated by their potency to kill tumor cells as measured by CD107a degranulation rates.

The experiment was based on an autologous but HLA-A2 matched cell system involving CaSki cells as targets and T lymphocytes obtained from a HLA-A2 positive healthy donor as described formerly (RESSING et al., 1996).

The effect of TMX-202 treatment during maturation of dendritic cell from monocytes was generally monitored by changes in the morphology and also cell numbers. In comparison to DMSO treated control cells monocytes under the influence of the immuno-modulatory drug earlier and to a larger extent showed a changing morphology from regularly shaped and round adherent monocytes, the plasmacytoid morphology, to the dendrite-like morphology with branched cell appendices (SOUMELIS and LIU, 2006). The better effect of TMX-202 treatment in comparison to the DMSO control could also be demonstrated by higher cell numbers obtained from the original fraction of PBMCs used for adherence of monocytes. Under TMX-202 influence consistently higher cell numbers could be harvested demonstrating the higher rate of surviving and maturing cells under immuno-modulatory drug treatment. Furthermore, it could be demonstrated that TMX-202 treated dendritic cells extent expressed the co-stimulatory molecules CD80 and CD86 to higher extent compared with the DMSO treated cells. CD80 and CD86 become expressed during maturation of dendritic cells and are functionally relevant for T cell activation (DILIOGLOU et al., 2003). These results imply that dendritic cells generated from monocytes and treated with a basic mixture of GM-CSF and IL-4 become functionally mature under the treatment with TMX-202. This is in accordance with recently

published data also demonstrating that TLR-ligands can induce dendritic cell maturation (DEIFL et al., 2014) (MASSA and SELIGER, 2013). This further indicates that the standard protocol based on GM-CSF and IL-4 supplemented with a cytokine cocktail consisting of IL-1β, TNF-α, PGE-2 and IL-6 for the final maturation of dendritic cells (COLIC et al., 2004) might be substituted by one single agent, the immune modifier TMX-202, which by inducing high levels of IL-6 can also lead to functional maturation of dendritic cells.

With regard to the TMX-202 mediated effects on T cells during the repeated stimulations with peptide-loaded dendritic cells the only parameters that could be investigated were the T cell morphology and viability as estimated by microscopic inspection and T cell numbers representing T cell proliferation as counted before each re-stimulation. As described in section 5.x at day x of the in vitro priming the T cells numbers in the DMSO experiment decreased, which was also reflected by less dense T cell culture upon visual inspection, while the TMX-treated T lymphocytes showed a continuously increasing growth curve. However, DMSO-treated T cells recovered over time until the end of the experiment and reached almost the number of the T cells under TMX treatment. This could be interpreted as a first hint for the efficacy of the immuno-modulatory drug to promote adaptive T cell responses either indirectly by stimulation with dendritic cells matured under TMX-treatment or by direct effects of the immuno-modulatory treatment on T cell differentiation and proliferation.

The final readout of the 22 days lasting stimulation experiment was the measurement of T cell mediated killing of CaSki cells as indicated by CD107a released upon co-incubation of the effector cells with the target cells. Recognition of tumor cells induces cytolytic vesicles in effector T cells to localize to the membrane and to release lytic enzymes by fusion with the outer cell membrane and thereby CD107a contained in the inner membrane of the vesicles is transferred to the cell surface. The killing rates of T cells stimulated under DMSO treatment were compared with the killing potential of the T cell culture that were treated with the new immune modulator TMX-202. It could be demonstrated that T cells cultured in presence of TMX-202 led to better killing rates as represented by a higher fraction of CD107a-expressing CD8+ T cells. The treatment seems to promote a better stimulation of T lymphocytes and induction of antigen-specificity. It is conceivable that this is either related to more potent antigen-presentation mechanisms mediated by dendritic cells matured with TMX-202 substituting the classical pro-inflammatory cytokine mix (DEIFL et al., 2014), or caused directly by TMX-202 affecting T cell proliferation and differentiation into effector T cells (JIN et al., 2012).

Although the killing rates are not significantly different between the DMSO and the TMX-202 T cell experiment and the fractions of CD107a-expressing T cells killings were relative small, one should consider that the frequencies of naïve CD8+ T cells in the peripheral blood in general is very low. They represent only approximately 2.5% of all leukocytes contained in the peripheral blood (CHEVALLIER et al., 2013).

It cannot completely ruled out that alloreactivity of the T lymphocytes against the heterologous tumor cell line also contributed to the killing effect, but the differences in the killing effects of the two T cell cultures (DMSO and TMX-202) still remain obvious. Spontaneous, non-antigen-specific reactivity of T cells in the presence of CaSki cells was not included in the experimental setup as all T cells were

stimulated with the mixture of possible antigens and this approach was solely focused on the effects that an immune modulator could contribute to such an *in vitro* "vaccination" of naïve T cells.

To minimize the risk for alloreactivity of T cells against tumor cells, albeit matched for the HLA-A allele (HLA-A2), killing assays preferably should be carried out in an autologous cell system as it was established in the course of this thesis (chapter 5.2). Unfortunately, at the time point when the here discussed experiment was carried out the tumor cell line was not yet established.

6.8 The generation of a HPV-associated head and neck squamous cell carcinoma cell line for immunological studies based on an autologous system

Although a restricted number of HPV-positive head and neck squamous cell carcinoma cell lines are available and sporadically new HPV16-positive cell lines deriving form head and neck cancers are published (TANG et al., 2012) they might not be optimal for certain immunological studies. The establishment of an autologous system that provides a HPV-positive cancer cell line and at the same time - preferentially freshly isolated - immune cells of the same patients is invaluable. In our department this goal could be achieved for a colorectal cancer cell line in the past but a model until now was still lacking for HPV-associated cancers. Therefore the establishment of a HPV-positive cell line deriving from a HNSCC patient can be considered the major methodological approach of the second part of this thesis. Once a tumor cell culture was continuously growing and had undergone several passages without losing its adherence and proliferation capacities, which could be observed in 1 out of 31 tumor explant cultures, it was subjected to further analyses to proof its association with HPV infection. The metastatic tumor cell line HN038M was stable for 11 months, showed continued proliferation and contained nearly 100% tumor cells after 13 months and 2 passages. The portion of epithelial cells contained in the culture was determined using BerEP4 antibody directed against the epithelial cell adhesion molecule (EpCAM) by which cells of epithelial origin can be stained specifically (BREZICKA, 2005) as the antibody does not bind to fibroblasts which are of mesodermal origin. This demonstrates that the underlying tumor preparation protocol established during this work (section 3.4.2) successfully eradicates contaminating fibroblast over time by sequential trypsinization and the maintenance of tumor cells keeping their proliferating potential.

Importantly, only a fraction of about 20% of all HNSCC tumors is contributable to HPV (GILLISON et al., 2000). The primary tumor from which the metastasis derived that could be established as cell line was an oropharyngeal cancer located in the area of the palatine/lingual tonsil where most of the typical HPV-associated oropharyngeal cancers occur. Nonetheless, the cell line had to be characterized for clear signs of HPV presence and contribution of the virus to the tumorigenesis. These results were also compared with the analysis performed in the cooperating clinic. Such investigations allowed the non-HPV induced cancers clearly to be distinguished from those who are caused by underlying HPV infection and transformation caused by viral oncoproteins E6 and E7 that interfere with the host cell pathways.

The staining of cultured tumor cells for p16^{INK4a} revealed a strongly positive staining pattern for the cells harvested from the culture of HN038M. As p16^{INK4a} is a surrogate for viral oncogene

overexpression in transforming infection (chapter 1.3.3), this result indicates the underlying HPV-infection and transforming processes induced by the virus – more specifically by the activity of the viral oncogene E7 – in the cell line HN038M (VON KNEBEL DOEBERITZ et al., 2012). However, as p16^{INK4a} in the head and neck occasionally is expressed without any relation to HPV (PRIGGE et al., 2014) the sample was further subjected to HPV genotyping and viral oncogene expression was analyzed by western blot analysis.

The GP5+/6+ primer-based PCR for amplification of HPV DNA clearly revealed amplified DNA located between the 100bp and 200bp marker bands for the tumor cell samples and the positive controls. It could be shown by Luminex-based HPV genotyping (SCHMITT et al., 2006) that the tumor cells of the HN038M cell line harbor HPV16 DNA (SCHMITT et al., 2006). These results were compared with the characteristics of the tissue material that was directly formalin-fixed and paraffin-embedded following surgery. The paraffin-embedded tissue was stained for p16^{INK4a} by immunohistochemistry and it could be demonstrated that the conserved material of the metastasis equally shows a strong and diffuse staining pattern of p16^{INK4a}-positive cells.

Furthermore, HPV genotyping was also performed with DNA obtained from the original formalin-fixed tissue samples it was demonstrated that both primary tumor and metastasis of this patient also are positive for HPV16.

To rule out the possibility of an underlying permissive HPV infection that would not contribute to the transformation of the tumor cells but rather represent a secondary effect, the cell lines was tested for HPV16 E7 oncogene expression. Western blot analysis of samples collected at different time points representing an earlier and a later passage, revealed that the cell line strongly expresses the E7 oncoprotein; with the same total amount of protein loaded on the gel, the cell line expresses even higher E7 levels as the SiHa control. It can therefore be concluded that in this cell line HPV16 infection and oncoprotein activity was the driving mechanisms for carcinogenesis (MCLAUGHLIN-DRUBIN and MUNGER, 2009).

In the context of the planned immunological experiments involving killing of tumor cell by autologous immune cells, HLA class I antigen expression was an important characteristic of this cells line to be determined. HLA class I antigen expression and other antigen-processing components are frequently reported to be altered in HNSCC and might represent a major mechanism that contributes to immune evasion and thus tumor progression and metastasis (BANDOH et al., 2010; TANG et al., 2009) (MANDIC et al., 2004; NÄSMAN et al., 2013; PRIME et al., 1987). Flow cytometry analysis of the tumor cell line HN038M for HLA class I expression was performed with a monoclonal antibody (clone W6/32) detects functional HLA class I antigens expressed on the cell surface by recognizing heavy chains A, B and C. The analysis demonstrated that virtually all tumor cells expressed HLA class I molecules on their cell surface (97.02 %). In conclusion, there were no concerns to use this cell in subsequent immunological studies investigating the potential effect of regulatory T cells on the killing efficiency of effector T cells. The high HLA class I expression was considered to be the prerequisite for tumor cells to be theoretically recognized, bound and killed by cytotoxic T lymphocytes.

Finally, the cell line was characterized by short tandem repeat (STR) profiling to exclude cross-contamination by established and frequently used cell lines. The awareness of the rising frequency of falsely identified cell lines and cross-contamination of cultures by standard cell lines, led the American Type Culture Collection (ATCC) Standards Development organization workgroup to initiate a

consensus standard on the authentication of cell lines based on STR profiling which should be applied to standardize the procedure of cell line characterization and to assure the reliability of published results (BARALLON et al., 2010; CONNEXIN et al., 2010). The STR profiling allows cell lines to be identified on the individual level, to compare them with and distinguish them from cell lines contained in the database (NIMS et al., 2010). The STR profiling, carried out by Multiplexion GmBH, Heidelberg, showed that the new cell line HN038M is not identic with any of the cell lines contained in the database which is defined as less than 96% identity with the best fitting comparison sequence. Therefore, cross-contamination with other cell lines frequently used in the same laboratory room, such as the HPV-associated cell lines CaSki, HeLa, SiHa and the colorectal cancer cell line HCT116, can be excluded and the originality of the new HNSCC is demonstrated.

With the tumor preparation and treatment protocol adapted to head and neck squamous cell carcinoma, the sampling of HPV+ tumors preparation and establishment of cultures will be continued in order to establish further autologous HPV-associated cell lines in the future. Enlarging the numbers of HPV-associated tumor cell lines of patients that are alive is a valuable enrichment for the scientific community and would allow performing - as long as patient does well - further immunological studies based on autologous tumor and immune cells.

With the cell line in hands a cell-based immuno-modulatory intervention strategy was tested by applying depletion of regulatory T lymphocytes from the T cell fraction and evaluating their killing potential against autologous tumor cells in comparison to undepleted T cells.

6.9 Regulatory T cells seem to have an inhibitory effect on anti-tumoral immune responses against autologous tumor cells of a HPV-positive HNSCC patient

The contribution of regulatory T lymphocytes to cancer progression is one non-negligible mechanism frequently discussed and considered as a major concern. The presence of dense Treg infiltrates are reported in different tumor entities and their frequent occurrence in cancers is causally linked to tumor development at different sites of the body (KIM et al., 2013; MICHEL et al., 2008; SHAH et al., 2011; WOLF et al., 2003). Regulatory T cells are thought to hamper different kinds of therapeutic vaccination approaches or other strategies elaborated to induce T cell mediated anti-tumoral responses – not only in the HPV-setting. In the context of cancer immunotherapy Treg depletion therefore plays a crucial role (reviewed in CURIEL, 2007 and NISHIKAWA and SAKAGUCHI, 2014). Results from the here described study (chapter 4.2) and also published data demonstrate that regulatory T lymphocytes play a non-negligible role in HPV-associated cervical cancers and the precursor lesions (LODDENKEMPER et al., 2009; MOLLING et al., 2007; VISSER et al., 2007; WU et al., 2011).

The regulatory T cell phenotype characterized as CD4+CD25+Foxp3+ T cells has been shown to contribute to suppression of cytotoxic responses and in vitro Treg depletion is reported to T cell mediated immune responses (CHEN et al., 2012). The effect of Treg depletion, however, is rarely investigated in the setting of HPV-related diseases (CHUANG et al., 2009; TUVE et al., 2007) and mainly demonstrated in mouse models. Only one study could be found investigating Treg depletion in

the context of nasopharyngeal carcinoma – without, however, considering possible underlying HPV infections (FOGG et al., 2013). Data concerning the role of Tregs in HPV-associated OSCC and the impact of Treg depletion is scarce.

The established HPV16-positive tumor cell line deriving from an OSCC patient was used for an initial experiment which aimed at the investigation of the potential immunosuppressive effect mediated by regulatory T lymphocytes. The killing potential of PBMCs isolated from the blood of the OSCC patients against the autologous tumor cell line HN038M was measured in two different experimental approaches and was based on the comparison between Treg depleted T cells and the total (undepleted) T cell fraction. This last chapter thus completes the circle with regard to the immunohistochemical analyses performed in the first part of this work. Although it could not be demonstrated that regulatory T cells contribute to progression of precancerous lesions - because of the cross-sectional nature of the study -, the enormous variances in different diagnostic CIN grades might imply a functional role in tumor development.

In a broad general approach - without considering possible underlying mechanisms - the effect of Treg depletion was measured by the impedance-based Roche Xcelligence System. The assay principle is explained in detail in section 3.2.4 and is based on impedance measurement reflecting changes in cell density, adherence and morphology. These changes for example can be caused by manipulations such as drug treatment inducing apoptosis. The convincing argument in favor of this system is the possibility to monitor the effects of treatments on tumor cells in real-time and in a label-free manner. It has been demonstrated to be applicable for monitoring vaccine-based cytotoxicity on tumor cells (PHAM et al., 2014), T cell mediated killing (PEPER et al., 2014) and also was compared with ^{51}Cr-release assay (measuring the release of ^{51}Cr from labelled target cells upon cytolysis) to demonstrate that the impedance-based assay can detect changes in the levels of antigen-specific cytotoxic T cells with increased sensitivity compared with the standard chromium release assay (ERSKINE et al., 2012). It therefore represents an attractive alternative assay to established experiments as exposure to gamma radiation or other labelling reagents can be avoided, high reproducibility can be obtained and fewer cells are required for the experimental setup.

For the above describe experiment the cell index values were measured during the growing phase and the killing phase of tumor cells and for Treg depleted T cells and the total T cell fraction. The cell index calculated for the T cell control wells demonstrated that the addition of effector cells to the adherent tumor cells did not affect the impedance. Therefore the impedance curves for the co-incubated T cells and tumor cells can be considered to represent the true killing effect on tumor cells without requiring further normalization for T cell impedance. It could be shown that the T cells after Treg depletion induces a stronger decrease in cell index values and also in the slopes calculated for the cell index curves compared with the total T cell fraction (Figure 5.25). Decreasing cell indices can be interpreted as being caused by tumor cell lysis and T cell mediated cytotoxicity. The differences between Treg depleted T cells and the total T cell fraction are significant over the total killing period and also in the two defined sub-phases representing the first and second killing phase.

To take into account the effects mediated by T cells with or without previous Treg depletion more specifically, CD107a degranulation assay was performed to gain information about the cytotoxic potential of the effector cells. This assay was first described in 2003 as a "novel technique to enumerate antigen-specific CD8+ T cells using a marker expressed on the cell surface following

activation induced degranulation, a necessary precursor of cytolysis" (BETTS et al., 2003). Although the here described experiment was performed in an antigen-independent manner it has been demonstrated that CD8+ T cells expressing CD107a are involved in antigen-specific cytotoxicity (BETTS et al., 2003) and that such assays allows the identification and analysis of tumor-reactive T cells *in vitro* (RUBIO et al., 2003).

The performed CD107a degranulation assay showed that among T cells stained for CD4 and CD107a those subjected to Treg depletion showed a higher fraction expression CD107a compared with T cells that were not depleted from regulatory T cells. It has been reported that CD4+ T cells also can cytotoxic potential and contribute to elimination of tumor cells (reviewed in MARSHALL and SWAIN, 2011 and APPAY, 2004). This same trend could also been seen in the fraction of non-CD4+ T lymphocytes. This opens the question of the nature of the phenotype of the T cells contained in this population. Based on the assay principle for T cell isolation (chapter 3.2.4) which selects for CD3+ T cells the presence of natural killer cells (CD3-negative) in the isolated T cell fraction can be ruled out. Furthermore, the presence of HLA class I antigens on the tumor cells has been demonstrated and it is unlikely that NK cells, if present, would have any killing effect against HLA class I antigen expressing tumor cells (MORETTA et al., 1996). It can therefore be assumed that the non-CD4+T cell population is composed of a fraction of CD8+ CTLs and also natural killer T cells (NKT cells) which in contrast to NK cells express CD3.

The percentage of CD107-expressing cells in both fractions, non-CD4+ and CD4+ T cells, are relatively low. It has been demonstrated in different settings that the frequencies of antigen-specific T cells are relatively low, and one can speculate that antigen-specific T cells circulating in the blood are even less frequent than tumor-infiltrating lymphocytes at the tumor site (reported frequencies range from 0.01% to 0.4% for CD8+ T cells) (HE et al., 1999; POLLACK et al., 2014). For HPV-associated antigens, due to effective immune evasion mechanisms the frequencies for antigens specific T cells might even be lower as reported for low levels of E7-specific precursor T cells (1 of 3947 T cells) in the blood (HOFFMANN et al., 2006). However, although changes remain low with regard to the absolute CD107+ T cell frequencies, the killing rate is 3 times higher after Treg depletion in the non-CD4+ T cell fraction and such changes might have tremendous effects in vivo in respect to the low frequencies of potential antigen-specific T cells.

In conclusion, both assays by addressing different parameters, the changes in impedance caused lysed tumor cells and the CD107a expression on the cell surface of T cells, demonstrated that Treg depletion enhances the killing efficiency of the remaining T cell fraction and that Treg mediated suppression might play a role in the investigated OSCC tumor probably having participated in disease progression. This finding might also be an explanation for disease recurrence after surgical treatment in this patient although HPV-associated HNSCC in general have a better prognosis and clinical outcome. Depletion of regulatory T cells might therefore be an important treatment option to be considered for HPV-associated diseases in general and in OSCC in particular where data so far have been lacking and allows the circumvention of immunosuppressive effects.

Intervention strategies in this context for example might be based on drugs that specifically target Tregs (FOGG et al., 2013). Recently also therapeutic approaches involving chemotherapeutic agents for control and reversal of the immunosuppressive effects mediated by regulatory T lymphocytes

might be applicable in anti-cancer therapy (reviewed in ALIZADEH and LARMONIER, 2014; D'ARENA et al., 2011; OHKURA et al., 2011).

A combined therapy is conceivable involving immune stimulating agents such as TLR ligands and drugs combatting immune suppression, in the same way as today classical chemotherapeutic agents are combined such as cytostatic and cytotoxic drugs or combinations of antibody-based anti-cancer treatments. Probably here again, the combination of different strategies might be more effective than one single therapy alone by addressing the variability of mechanisms developed by HPV-associated diseases to circumvent the host's immune attack

Importantly, the single treatment strategies described in this thesis show a tendency to contribute to a reduced tumor growth. The combination of these strategies, however, is conceivable to improve and potentiate the effects obtained with each of these strategies alone.

6.10   Future prospects

The initial immunohistochemical analysis of immune cell infiltrated in cervical intraepithelial neoplasia and cancers demonstrated that changes of immune cell infiltrate are not associated with the onset of transforming infections in histomorphological low-grade lesions. The observed T cell densities are not yet different compared with non-transforming low-grade lesions. However, as lesions of the same histomorphological grade with different biological and clinical behavior are pooled within one diagnostic group - an approach which could not be avoided due to nature of most of the available patient cohorts - the T cells infiltrate data cannot be related to the clinical outcome of the patients. Interestingly, broad ranges of immune cell densities could be observed for distinct T cell subtypes, e.g. regulatory T cells and CD8+ cytotoxic T lymphocytes indicating that samples are characterized by a large heterogeneity. This might reflect samples of patients with either progressing or regressing disease. Only patients samples stratified for the clinical behavior of the lesions could unravel the impact of distinct immune cell phenotypes on disease outcome. The changes in immune cell densities and the phenotypic composition have to be in a prospective setting in order to gain a better understanding of how these changes are related with the clinical outcome of the patients.

These aspects could perfectly be addressed in the patient cohort of the Austrian imiquimod trial. In the course of the 20 weeks treatment and observation protocol three biopsies per patient were sampled. The effect of a topical immuno-modulatory drug, imiquimod, was tested in a randomized, placebo-controlled setting and the efficiency of the treatment was determined by comparing the imiquimod-treated arm with the placebo-group. The small number of patient samples that could be obtained for the first analyses of T cell infiltrates in imiquimod treated patients represents extremely precious material and served as a basis for the first analyses of immune infiltrates in imiquimod-treated lesions. The first step was taken towards a deeper understanding of the immunophenotypic reversal mediated by immune modifiers such as TLR-ligands. However, if access will be gained to the placebo-treated patient samples, the natural course of untreated high-grade CIN lesions over time can be monitored and immune cell infiltrate data correlated with the course of the disease, e.g. progression or regression. The analysis of these samples is therefore considered to help answering the questions that could not be addressed in the cross-sectional study. T cell phenotypes that contribute to spontaneous regression

without previous therapeutic intervention can be investigated, as well as distinct immune phenotypes that rather are associated with disease persistence or progression. Also the analyses that have been initiated with the patients of the imiquimod treatment arm will be expanded to enlarge the sample size and validate the results obtained so far.

In this context further immune markers might be relevant and should be included to enlarge the immune phenotypic characterization. Based on the list shown in section 6.6 the best marker combinations can be defined after having been evaluated in preliminary immunohistochemical analyses as it was done for some of the most important T cell markers in the first cross-sectional approach. It has to be demonstrated that the chosen markers are reliable predictors of the biological behavior of the disease and the clinical outcome of the patients. The final biomarker set might also be a combination of immune cell and tumor cell markers as long as they alone and even more in combination are predictive for the clinical course of the disease.

On the long run this precious cohort will allow to define an "immune score", a biomarker-based tool that could be applicable in the clinical routine to predict the risk for progression of CIN lesions and also the chance to respond to non-surgical interventions such as topical treatment with TLR agonists. This tool might help to make individualized and risk-adapted treatment decisions, minimize over-treatment of a clinically heterogeneous disease and permit at least a distinct proportion of young women to obtain conservative treatment.

HLA class I and class II antigens is a potential component of this novel "immune score". However, with the results obtained so far, their biological relevance and their contribution to immune evasion or effective anti-tumoral immune responses is still not clear. Their impact on the quality of the immune response that might be initiated has to be elucidated by additional analyses. In a first approach T cell densities and also different T cell phenotypes infiltrating the tumor microenvironment should be correlated with the expression pattern of antigen-presenting molecules in the lesions. The best, clinically most relevant approach again would be a longitudinal one allowing the correlation with the patients' outcome to reveal the role of these alterations in the context of immune evasion or either immune attack of the host. First analyses demonstrated that HLA class II expression indeed seems to impact immune densities in terms of CD3+ and CD8+ T cells. Thereby, a higher proportion of cells expressing HLA class II antigens as well as a higher fraction of cells showing membranous expression were associated with a trend towards denser T cell infiltrates (data not shown).

All these investigations that finally should lead to the definition of an "immune score" for use in the diagnosis and prognosis will be based on the newly developed automated quantification method described in this thesis. It represents a highly standardized and objective method to quantify immune cells as the results of cell counting are not biased by subjective criteria defined by the investigator. Especially for the development of a clinically relevant immune cell based biomarker tool, the reliability of the results has to be demonstrated and they need to be validated in a larger sample cohort. Here, the established quantification platform is the method of choice as it allows high-throughput screening of large cohorts.

.
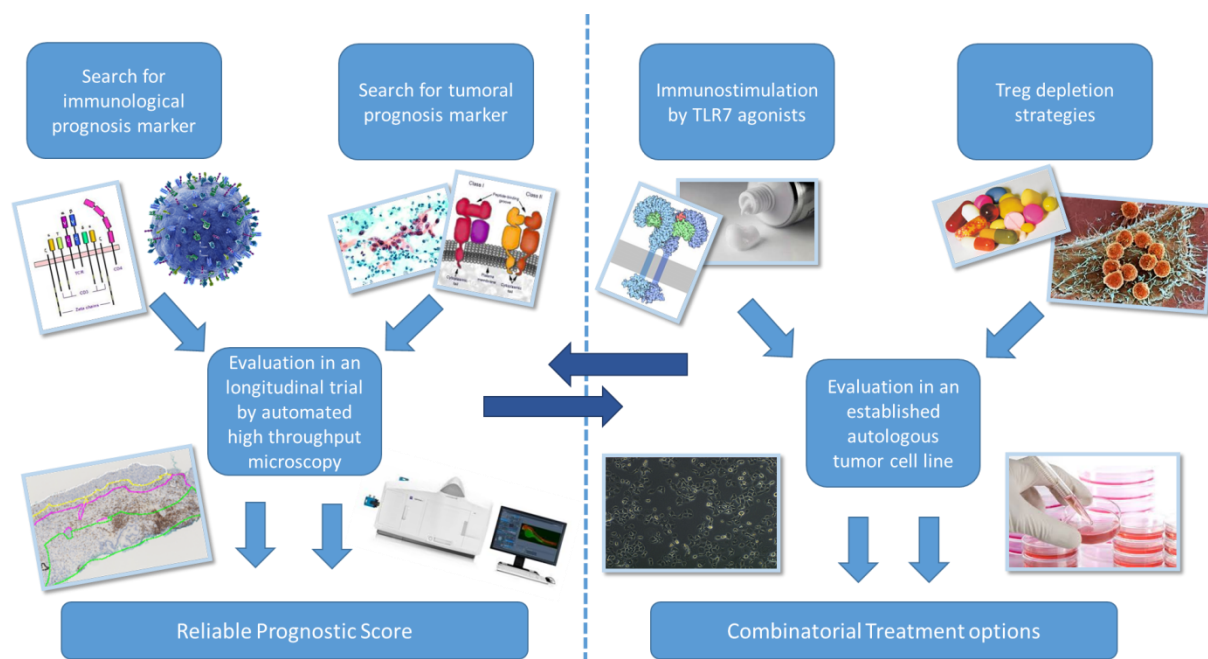
FIGURE 6.3   GRAPHICAL OVERVIEW OF THE POSSIBILITIES TO COMBINE THE RESULTS AND ESTABLISHED METHODS IN THE FUTURE IN ORDER TO DEVELOP NEW DIAGNOSTIC TOOLS AND TREATMENT STRATEGIES. #

The Austrian imiquimod trial together with the multitude of imiquimod trials performed in vulvar intraepithelial neoplasia (VIN) patients demonstrated the clinical efficacy of TLR-agonist based treatment that aims at immune modulation of the lesion microenvironment. The promising results obtained in this study make TLR-agonist treatment a strategy to be pursued. However, in consideration of the known side effects of imiquimod further immuno-modulatory treatment strategies were evaluated in the second part of the thesis. A second generation TLR-agonist, TMX-202, was tested in the in vitro priming of naïve T cells to p16^{INK4a} and HPV16 L1 peptides.

REFERENCES FOR IMAGES USED IN FIGURE 6.x

http://emedicine.medscape.com/article/2086864-overview (30.11.2014)

http://de.wikipedia.org/wiki/CD3-Rezeptor (30.11.2014)

http://www.mskcc.org/blog/cancer-immunotherapy-named-science-magazine-breakthrough-year (30.11.2014)

http://www.zejournal.info/infos-insolites/1-articles-infos-insolites/1944-il-braque-une-pharmacie-avec-un-tube-de-creme-de-beaute (30.11.2014)

http://www.duden.de/rechtschreibung/Tablette (30.11.2014)

http://www.mikroelektronik.fraunhofer.de/de/presse-und-medien/vue-nachrichten/article/zeiss-setzt-bei-lichtblattmikroskop-auf-technologie-des-fraunhofer-ipms.html (30.11.2014)

http://www.rcsb.org/pdb/101/motm.do?momID=143 (30.11.2014)

http://www.biooncology.com/therapeutic-targets/cd79b (30.11.2014)

http://www.soc.ucsb.edu/sexinfo/article/cervical-cancer (30.11.2014)

http://www.genengnews.com/insight-and-intelligenceand153/cancer-cell-line-identity-crisis/73502226/ (30.11.2014)

It could be shown that the substance has effects on dendritic cells maturation and T cell proliferation and also contributes to a slightly increased killing potential of T cells in the context of HPV-associated diseases. These first results warrant further studies to better characterize the potential of the new TLR-agonist. The planning of a vaccination experiment based on p16^{INK4a}L1 chimeric virus-like particles in a mouse model is under way. Here, TMX can be evaluated as a potential adjuvant. It is well conceivable that the cellular immune responses against L1 and p16^{INK4a} in mice vaccinated with the chimeric VLPs are potentiated by using TMX as an adjuvant, as effects were observed on both levels, the innate immunity and also adaptive immune responses

With the oral squamous cell carcinoma cell line generated in the course of this thesis a valuable autologous model was established which can serve as basis for further immunological studies. For example the effect of TMX-202 treatment could now be validated in an autologous system to allay concerns regarding the alloreactivity between immune cells and an allogeneic tumor cell line. It represents a perfect model for the generation of antigen-specific T cells by *in vitro* priming with the auto-antigen p16^{INK4a} and viral antigens such as L1 and to test the killing potential of T cells against autologous tumor cells. The patient recruitment will be continued to obtain further tumor tissue samples for the generation of more cell lines. These are necessary to validate the results obtained from one single patient and to evaluate whether or not the findings are representative for HPV-associated diseases and the conclusions that were drawn can be generalized

Although the results look promising, the effect of regulatory T cell depletion demonstrated in the autologous cell line HN038M will have to be tested in further cell lines to validate the results obtained in one patient. A combination strategy consisting of Treg depletion along with immuno-modulatory drug treatment would be highly interesting as the better killing effect observed after Treg depletion could further be enhanced if anti-tumoral response of the remaining cell fraction would be "enhanced" by TLR-ligand treatment. The experiment demonstrated how important strategies aiming at Treg depletion might be for the improvement of cancer immunotherapy approaches.

This treatment strategy in general could be further refined by using drugs specifically targeting Tregs in order to deplete them from the total T cell fraction. A multitude of new and already established drugs are actually discussed to selectively eliminate the immunosuppressive effected mediated by regulatory T lymphocytes. Among these cyclophosphamide (Cytoxan) (CAMISASCHI et al., 2013), denileukin diftitox (TELANG et al., 2011) and ipilimumab (HODI et al., 2010) represent interesting therapeutic   drugs.

7. REFERENCES

ABRAMS, S.I. (2005). Positive and negative consequences of Fas/Fas ligand interactions in the antitumor response. Front Biosci *10*, 809-821.

ADURTHI, S., KRISHNA, S., MUKHERJEE, G., BAFNA, U.D., DEVI, U., and JAYSHREE, R.S. (2008). Regulatory T cells in a spectrum of HPV-induced cervical lesions: cervicitis, cervical intraepithelial neoplasia and squamous cell carcinoma. Am J Reprod Immunol *60*, 55-65.

ADURTHI, S., MUKHERJEE, G., KRISHNAMURTHY, H., SUDHIR, K., BAFNA, U.D., UMADEVI, K.*, et al.* (2012). Functional tumor infiltrating TH1 and TH2 effectors in large early-stage cervical cancer are suppressed by regulatory T cells. Int J Gynecol Cancer *22*, 1130-1137.

AKIRA, S., and TAKEDA, K. (2004). Toll-like receptor signalling. Nat Rev Immunol *4*, 499-511.

ALBERS, A.E., and KAUFMANN, A.M. (2009). Therapeutic human papillomavirus vaccination. Public health genomics *12*, 331-342.

ALIZADEH, D., and LARMONIER, N. (2014). Chemotherapeutic targeting of cancer-induced immunosuppressive cells. Cancer Res *74*, 2663-2668.

ALTOMONTE, M., FONSATTI, E., VISINTIN, A., and MAIO, M. (2003). Targeted therapy of solid malignancies via HLA class II antigens: a new biotherapeutic approach? Oncogene *22*, 6564-6569.

AMADOR-MOLINA, A., HERNANDEZ-VALENCIA, J.F., LAMOYI, E., CONTRERAS-PAREDES, A., and LIZANO, M. (2013). Role of innate immunity against human papillomavirus (HPV) infections and effect of adjuvants in promoting specific immune response. Viruses *5*, 2624-2642.

ANTINORE, M.J., BIRRER, M.J., PATEL, D., NADER, L., and MCCANCE, D.J. (1996). The human papillomavirus type 16 E7 gene product interacts with and trans-activates the AP1 family of transcription factors. EMBO J *15*, 1950-1960.

APPAY, V. (2004). The physiological role of cytotoxic CD4(+) T-cells: the holy grail? Clin Exp Immunol *138*, 10-13.

ARBYN, M., KYRGIOU, M., SIMOENS, C., RAIFU, A.O., KOLIOPOULOS, G., MARTIN-HIRSCH, P.*, et al.* (2008). Perinatal mortality and other severe adverse pregnancy outcomes associated with treatment of cervical intraepithelial neoplasia: meta-analysis. BMJ *337*, a1284.

ASHRAFI, G.H., HAGHSHENAS, M.R., MARCHETTI, B., O'BRIEN, P.M., and CAMPO, M.S. (2005). E5 protein of human papillomavirus type 16 selectively downregulates surface HLA class I. Int J Cancer *113*, 276-283.

BAIS, A.G., BECKMANN, I., LINDEMANS, J., EWING, P.C., MEIJER, C.J., SNIJDERS, P.J.*, et al.* (2005). A shift to a peripheral Th2-type cytokine pattern during the carcinogenesis of cervical cancer becomes manifest in CIN III lesions. J Clin Pathol *58*, 1096-1100.

BAL, V., MCINDOE, A., DENTON, G., HUDSON, D., LOMBARDI, G., LAMB, J.*, et al.* (1990). Antigen presentation by keratinocytes induces tolerance in human T cells. Eur J Immunol *20*, 1893-1897.

BANDOH, N., OGINO, T., KATAYAMA, A., TAKAHARA, M., KATADA, A., HAYASHI, T.*, et al.* (2010). HLA class I antigen and transporter associated with antigen processing downregulation in metastatic lesions of head and neck squamous cell carcinoma as a marker of poor prognosis. Oncol Rep *23*, 933-939.

BARALLON, R., BAUER, S.R., BUTLER, J., CAPES-DAVIS, A., DIRKS, W.G., ELMORE, E.*, et al.* (2010). Recommendation of short tandem repeat profiling for authenticating human cell lines, stem cells, and tissues. In Vitro Cell Dev Biol Anim *46*, 727-732.

BASLER, C.F., and GARCIA-SASTRE, A. (2002). Viruses and the type I interferon antiviral system: induction and evasion. Int Rev Immunol *21*, 305-337.

BECKMAN, R.A., and LOEB, L.A. (2005). Negative clonal selection in tumor evolution. Genetics *171*, 2123-2131.

BERGERON, C., RONCO, G., REUSCHENBACH, M., WENTZENSEN, N., ARBYN, M., STOLER, M.*, et al.* (2014). The clinical impact of using p16 immunochemistry in cervical histopathology and cytology: An update of recent developments. Int J Cancer *doi: 10.1002/ijc.28900. [Epub ahead of print]*.

BERNARD, H.U. (2005). The clinical importance of the nomenclature, evolution and taxonomy of human papillomaviruses. J Clin Virol *32 Suppl 1*, S1-6.

BETTS, M.R., BRENCHLEY, J.M., PRICE, D.A., DE ROSA, S.C., DOUEK, D.C., ROEDERER, M.*, et al.* (2003). Sensitive and viable identification of antigen-specific CD8+ T cells by a flow cytometric assay for degranulation. J Immunol Methods *281*, 65-78.

BEUCHER, S. (1992). The watershed transformation applied to image segmentation. Scanning Microsc Int *6*, 299–314.

BIGNOLD, L.P. (2002). The mutator phenotype theory can explain the complex morphology and behaviour of cancers. Cell Mol Life Sci *59*, 950-958.

BIGNOLD, L.P. (2003). The mutator phenotype theory of carcinogenesis and the complex histopathology of tumours: support for the theory from the independent occurrence of nuclear abnormality, loss of specialisation and invasiveness among occasional neoplastic lesions. Cell Mol Life Sci *60*, 883-891.

BONTKES, H.J., DE GRUIJL, T.D., WALBOOMERS, J.M., VAN DEN MUYSENBERG, A.J., GUNTHER, A.W., SCHEPER, R.J.*, et al.* (1997). Assessment of cytotoxic T-lymphocyte phenotype using the specific markers granzyme B and TIA-1 in cervical neoplastic lesions. Br J Cancer *76*, 1353-1360.

BOSCOLO-RIZZO, P., DEL MISTRO, A., BUSSU, F., LUPATO, V., BABOCI, L., ALMADORI, G.*, et al.* (2013). New insights into human papillomavirus-associated head and neck squamous cell carcinoma. Acta Otorhinolaryngol Ital *33*, 77-87.

BOTTINO, C., MORETTA, L., PENDE, D., VITALE, M., and MORETTA, A. (2004). Learning how to discriminate between friends and enemies, a lesson from Natural Killer cells. Mol Immunol *41*, 569-575.

BOTTLEY, G., WATHERSTON, O.G., HIEW, Y.L., NORRILD, B., COOK, G.P., and BLAIR, G.E. (2008). High-risk human papillomavirus E7 expression reduces cell-surface MHC class I molecules and increases susceptibility to natural killer cells. Oncogene *27*, 1794-1799.

BOURKE, E., BOSISIO, D., GOLAY, J., POLENTARUTTI, N., and MANTOVANI, A. (2003). The toll-like receptor repertoire of human B lymphocytes: inducible and selective expression of TLR9 and TLR10 in normal and transformed cells. Blood *102*, 956-963.

BREZICKA, T. (2005). Expression of epithelial-cell adhesion molecule (Ep-CAM) in small cell lung cancer as defined by monoclonal antibodies 17-1A and BerEP4. Acta Oncol *44*, 723-727.

BRINKMAN, J.A., HUGHES, S.H., STONE, P., CAFFREY, A.S., MUDERSPACH, L.I., ROMAN, L.D.*, et al.* (2007). Therapeutic vaccination for HPV induced cervical cancers. Dis Markers *23*, 337-352.

BUCK, C.B., DAY, P.M., and TRUS, B.L. (2013). The papillomavirus major capsid protein L1. Virology *445*, 169-174.

BUENO, G., DENIZ, O., FERNANDEZ-CARROBLES MDEL, M., VALLEZ, N., and SALIDO, J. (2014). An automated system for whole microscopic image acquisition and analysis. Microsc Res Tech *77*, 697-713.

BULL, C., DEN BROK, M.H., and ADEMA, G.J. (2014). Sweet escape: Sialic acids in tumor immune evasion. Biochim Biophys Acta.

BURD, E.M. (2003). Human papillomavirus and cervical cancer. Clin Microbiol Rev *16*, 1-17.

CAMISASCHI, C., FILIPAZZI, P., TAZZARI, M., CASATI, C., BERETTA, V., PILLA, L.*, et al.* (2013). Effects of cyclophosphamide and IL-2 on regulatory CD4+ T cell frequency and function in melanoma patients vaccinated with HLA-class I peptides: impact on the antigen-specific T cell response. Cancer Immunol Immunother *62*, 897-908.

CAMPO, M.S., GRAHAM, S.V., CORTESE, M.S., ASHRAFI, G.H., ARAIBI, E.H., DORNAN, E.S.*, et al.* (2010). HPV-16 E5 down-regulates expression of surface HLA class I and reduces recognition by CD8 T cells. Virology *407*, 137-142.

CASTRO, F., DIRKS, W.G., FAHNRICH, S., HOTZ-WAGENBLATT, A., PAWLITA, M., and SCHMITT, M. (2013). High-throughput SNP-based authentication of human cell lines. Int J Cancer *132*, 308-314.

CHAIWONGKOT, A., VINOKUROVA, S., PIENTONG, C., EKALAKSANANAN, T., KONGYINGYOES, B., KLEEBKAOW, P.*, et al.* (2013). Differential methylation of E2 binding sites in episomal and integrated HPV 16 genomes in preinvasive and invasive cervical lesions. International journal of cancer Journal international du cancer *132*, 2087-2094.

CHAN, M., HAYASHI, T., KUY, C.S., GRAY, C.S., WU, C.C., CORR, M.*, et al.* (2009). Synthesis and immunological characterization of toll-like receptor 7 agonistic conjugates. Bioconjug Chem *20*, 1194-1200.

CHAN, P.K., LIU, S.J., CHEUNG, J.L., CHEUNG, T.H., YEO, W., CHONG, P.*, et al.* (2011). T-cell response to human papillomavirus type 52 L1, E6, and E7 peptides in women with transient infection, cervical intraepithelial neoplasia, and invasive cancer. J Med Virol *83*, 1023-1030.

CHANG, C.-C., CAMPOLI, M., and FERRONE, S. (2003). HLA class I defects in malignant lesions: What have we learned? The Keio Journal of Medicine *52*, 220-229.

CHANG, C.-C., and FERRONE, S. (2007). Immune selective pressure and HLA class I antigen defects in malignant lesions. Cancer immunology, immunotherapy : CII *56*, 227-236.

CHATTERJEE, A., PULIDO, H.A., KOUL, S., BELENO, N., PERILLA, A., POSSO, H.*, et al.* (2001). Mapping the sites of putative tumor suppressor genes at 6p25 and 6p21.3 in cervical carcinoma: occurrence of allelic deletions in precancerous lesions. Cancer Res *61*, 2119-2123.

CHATTERJEE, S., BEHNAM AZAD, B., and NIMMAGADDA, S. (2014). The intricate role of CXCR4 in cancer. Adv Cancer Res *124*, 31-82.

CHATURVEDI, A.K., ANDERSON, W.F., LORTET-TIEULENT, J., CURADO, M.P., FERLAY, J., FRANCESCHI, S.*, et al.* (2013). Worldwide trends in incidence rates for oral cavity and oropharyngeal cancers. J Clin Oncol *31*, 4550-4559.

CHATURVEDI, A.K., ENGELS, E.A., PFEIFFER, R.M., HERNANDEZ, B.Y., XIAO, W., KIM, E.*, et al.* (2011). Human papillomavirus and rising oropharyngeal cancer incidence in the United States. J Clin Oncol *29*, 4294-4301.

CHEN, Y.L., CHANG, M.C., CHEN, C.A., LIN, H.W., CHENG, W.F., and CHIEN, C.L. (2012). Depletion of regulatory T lymphocytes reverses the imbalance between pro- and anti-tumor immunities via enhancing antigen-specific T cell immune responses. PLoS ONE *7*, e47190.

CHENG, H., WANG, L., MOLLICA, M., RE, A.T., WU, S., and ZUO, L. (2014). Nitric oxide in cancer metastasis. Cancer Lett *353*, 1-7.

CHEVALLIER, P., ROBILLARD, N., ILLIAQUER, M., ESBELIN, J., MOHTY, M., BODIN-BRESSOLLETTE, C.*, et al.* (2013). Characterization of various blood and graft sources: a prospective series. Transfusion (Paris) *53*, 2020-2026.

CHIL, A., SIKORSKI, M., BOBEK, M., JAKIEL, G., and MARCINKIEWICZ, J. (2003). Alterations in the expression of selected MHC antigens in premalignant lesions and squamous carcinomas of the uterine cervix. Acta Obstet Gynecol Scand *82*, 1146-1152.

CHOW, L.T., BROKER, T.R., and STEINBERG, B.M. (2010). The natural history of human papillomavirus infections of the mucosal epithelia. APMIS *118*, 422-449.

CHUANG, C.M., HOORY, T., MONIE, A., WU, A., WANG, M.C., and HUNG, C.F. (2009). Enhancing therapeutic HPV DNA vaccine potency through depletion of CD4+CD25+ T regulatory cells. Vaccine *27*, 684-689.

COLIC, M., MOJSILOVIC, S., PAVLOVIC, B., VUCICEVIC, D., MAJSTOROVIC, I., BUFAN, B.*, et al.* (2004). Comparison of two different protocols for the induction of maturation of human dendritic cells in vitro. Vojnosanit Pregl *61*, 471-478.

CONGER, K.L., LIU, J.S., KUO, S.R., CHOW, L.T., and WANG, T.S. (1999). Human papillomavirus DNA replication. Interactions between the viral E1 protein and two subunits of human dna polymerase alpha/primase. J Biol Chem *274*, 2696-2705.

CONNEXIN, J.S., CONNEXIN, P.D., and CONNEXIN, A.L. (2010). Cell line misidentification: the beginning of the end. Nat Rev Cancer *10*, 441-448.

CRAIN, B., YAO, S., KEOPHILAONE, V., PROMESSI, V., KANG, M., BARBERIS, A.*, et al.* (2013). Inhibition of keratinocyte proliferation by phospholipid-conjugates of a TLR7 ligand in a Myc-induced hyperplastic actinic keratosis model in the absence of systemic side effects. Eur J Dermatol *23*, 618-628.

CUNHA, L.L., MORARI, E.C., GUIHEN, A.C., RAZOLLI, D., GERHARD, R., NONOGAKI, S.*, et al.* (2012). Infiltration of a mixture of immune cells may be related to good prognosis in patients with differentiated thyroid carcinoma. Clin Endocrinol (Oxf) *77*, 918-925.

CURIEL, T.J. (2007). Tregs and rethinking cancer immunotherapy. J Clin Investig *117*, 1167-1174.

D'ARENA, G., DEAGLIO, S., LAURENTI, L., DE MARTINO, L., DE FEO, V., FUSCO, B.M.*, et al.* (2011). Targeting regulatory T cells for anticancer therapy. Mini Rev Med Chem *11*, 480-485.

DARRAGH, T.M., COLGAN, T.J., THOMAS COX, J., HELLER, D.S., HENRY, M.R., LUFF, R.D.*, et al.* (2013). The Lower Anogenital Squamous Terminology Standardization project for HPV-associated lesions: background and consensus recommendations from the College of American Pathologists and the American Society for Colposcopy and Cervical Pathology. Int J Gynecol Pathol *32*, 76-115.

DAVID, C.V., NGUYEN, H., and GOLDENBERG, G. (2011). Imiquimod: a review of off-label clinical applications. J Drugs Dermatol *10*, 1300-1306.

DAVIDSSON, S., OHLSON, A.L., ANDERSSON, S.O., FALL, K., MEISNER, A., FIORENTINO, M.*, et al.* (2013). CD4 helper T cells, CD8 cytotoxic T cells, and FOXP3(+) regulatory T cells with respect to lethal prostate cancer. Mod Pathol *26*, 448-455.

DE GIORGI, V., SALVINI, C., CHIARUGI, A., PAGLIERANI, M., MAIO, V., NICOLETTI, P.*, et al.* (2009). In vivo characterization of the inflammatory infiltrate and apoptotic status in imiquimod-treated basal cell carcinoma. Int J Dermatol *48*, 312-321.

DE MARTEL, C., FERLAY, J., FRANCESCHI, S., VIGNAT, J., BRAY, F., FORMAN, D.*, et al.* (2012). Global burden of cancers attributable to infections in 2008: a review and synthetic analysis. Lancet Oncol *13*, 607-615.

DE VILLIERS, E.M., FAUQUET, C., BROKER, T.R., BERNARD, H.U., and ZUR HAUSEN, H. (2004). Classification of papillomaviruses. Virology *324*, 17-27.

DE VOS VAN STEENWIJK, P.J., HEUSINKVELD, M., RAMWADHDOEBE, T.H., LOWIK, M.J., VAN DER HULST, J.M., GOEDEMANS, R.*, et al.* (2010). An unexpectedly large polyclonal repertoire of HPV-specific T cells is poised for action in patients with cervical cancer. Cancer Res *70*, 2707-2717.

DE VOS VAN STEENWIJK, P.J., PIERSMA, S.J., WELTERS, M.J., VAN DER HULST, J.M., FLEUREN, G., HELLEBREKERS, B.W.*, et al.* (2008). Surgery followed by persistence of high-grade squamous intraepithelial lesions is associated with the induction of a dysfunctional HPV16-specific T-cell response. Clin Cancer Res *14*, 7188-7195.

DE VOS VAN STEENWIJK, P.J., RAMWADHDOEBE, T.H., GOEDEMANS, R., DOORDUIJN, E.M., VAN HAM, J.J., GORTER, A.*, et al.* (2013). Tumor-infiltrating CD14-positive myeloid cells and CD8-positive T-cells prolong survival in patients with cervical carcinoma. Int J Cancer *133*, 2884-2894.

DEEPAK, P., KUMAR, S., JR., KISHORE, D., and ACHARYA, A. (2010). IL-13 from Th2-type cells suppresses induction of antigen-specific Th1 immunity in a T-cell lymphoma. Int Immunol *22*, 53-63.

DEIFL, S., KITZMULLER, C., STEINBERGER, P., HIMLY, M., JAHN-SCHMID, B., FISCHER, G.F.*, et al.* (2014). Differential activation of dendritic cells by toll-like receptors causes diverse differentiation of naive CD4(+) T cells from allergic patients. Allergy *69*, 1602-1609.

DENGJEL, J., NASTKE, M.D., GOUTTEFANGEAS, C., GITSIOUDIS, G., SCHOOR, O., ALTENBEREND, F.*, et al.* (2006). Unexpected abundance of HLA class II presented peptides in primary renal cell carcinomas. Clin Cancer Res *12*, 4163-4170.

DENNY, L.A., FRANCESCHI, S., DE SANJOSE, S., HEARD, I., MOSCICKI, A.B., and PALEFSKY, J. (2012). Human papillomavirus, human immunodeficiency virus and immunosuppression. Vaccine *30 Suppl 5*, F168-174.

DHARMAPURI, S., AURISICCHIO, L., NEUNER, P., VERDIRAME, M., CILIBERTO, G., and LA MONICA, N. (2009). An oral TLR7 agonist is a potent adjuvant of DNA vaccination in transgenic mouse tumor models. Cancer Gene Ther *16*, 462-472.

DIAZ-MONTERO, C.M., FINKE, J., and MONTERO, A.J. (2014). Myeloid-derived suppressor cells in cancer: therapeutic, predictive, and prognostic implications. Semin Oncol *41*, 174-184.

DIEBOLD, S.S., KAISHO, T., HEMMI, H., AKIRA, S., and REIS E SOUSA, C. (2004). Innate antiviral responses by means of TLR7-mediated recognition of single-stranded RNA. Science *303*, 1529-1531.

DILIOGLOU, S., CRUSE, J.M., and LEWIS, R.E. (2003). Function of CD80 and CD86 on monocyte- and stem cell-derived dendritic cells. Exp Mol Pathol *75*, 217-227.

DOEBERITZ, M., and VINOKUROVA, S. (2009a). Host factors in HPV-related carcinogenesis: cellular mechanisms controlling HPV infections. Arch Med Res *40*, 435-442.

DOEBERITZ, M.K., and VINOKUROVA, S. (2009b). Host factors in HPV-related carcinogenesis: cellular mechanisms controlling HPV infections. Arch Med Res *40*, 435-442.

DOORBAR, J. (2005). The papillomavirus life cycle. J Clin Virol *32 Suppl 1*, S7-15.

DOORBAR, J. (2006). Molecular biology of human papillomavirus infection and cervical cancer. Clin Sci (Lond) *110*, 525-541.

DOORBAR, J. (2013). The E4 protein; structure, function and patterns of expression. Virology *445*, 80-98.

DUDDA, J.C., SALAUN, B., JI, Y., PALMER, D.C., MONNOT, G.C., MERCK, E.*, et al.* (2013). MicroRNA-155 is required for effector CD8+ T cell responses to virus infection and cancer. Immunity *38*, 742-753.

DUENSING, S., and MUNGER, K. (2002). The human papillomavirus type 16 E6 and E7 oncoproteins independently induce numerical and structural chromosome instability. Cancer Res *62*, 7075-7082.

DUENSING, S., and MUNGER, K. (2004). Mechanisms of genomic instability in human cancer: insights from studies with human papillomavirus oncoproteins. Int J Cancer *109*, 157-162.

DUESBERG, P., MANDRIOLI, D., MCCORMACK, A., and NICHOLSON, J.M. (2011). Is carcinogenesis a form of speciation? Cell Cycle *10*, 2100-2114.

DUNNE, E.F., UNGER, E.R., STERNBERG, M., MCQUILLAN, G., SWAN, D.C., PATEL, S.S.*, et al.* (2007). Prevalence of HPV infection among females in the United States. JAMA *297*, 813-819.

DWORACKI, G., MEIDENBAUER, N., KUSS, I., HOFFMANN, T.K., GOODING, W., LOTZE, M., *et al.* (2001). Decreased zeta chain expression and apoptosis in CD3+ peripheral blood T lymphocytes of patients with melanoma. Clin Cancer Res *7*, 947s-957s.

EDWARDS, R.P., KUYKENDALL, K., CROWLEY-NOWICK, P., PARTRIDGE, E.E., SHINGLETON, H.M., and MESTECKY, J. (1995). T lymphocytes infiltrating advanced grades of cervical neoplasia. CD8-positive cells are recruited to invasion. Cancer *76*, 1411-1415.

EKKIRALA, C.R., CAPPELLO, P., ACCOLLA, R.S., GIOVARELLI, M., ROMERO, I., GARRIDO, C., *et al.* (2014). Class II Transactivator-Induced MHC Class II Expression in Pancreatic Cancer Cells Leads to Tumor Rejection and a Specific Antitumor Memory Response. Pancreas *43*, 1066-1072.

ERSKINE, C.L., HENLE, A.M., and KNUTSON, K.L. (2012). Determining optimal cytotoxic activity of human Her2neu specific CD8 T cells by comparing the Cr51 release assay to the xCELLigence system. J Vis Exp, e3683.

ERUSLANOV, E., STOFFS, T., KIM, W.J., DAURKIN, I., GILBERT, S.M., SU, L.M., *et al.* (2013). Expansion of CCR8(+) inflammatory myeloid cells in cancer patients with urothelial and renal carcinomas. Clin Cancer Res *19*, 1670-1680.

FAHEY, L.M., RAFF, A.B., DA SILVA, D.M., and KAST, W.M. (2009). Reversal of human papillomavirus-specific T cell immune suppression through TLR agonist treatment of Langerhans cells exposed to human papillomavirus type 16. Journal of immunology (Baltimore, Md : 1950) *182*, 2919-2928.

FAULSTICH, F. (2014). Generation and evaluation of chimeric particles consisting of HPV16 L1 and p16^{INK4a} for second generation HPV vaccines. Dissertation.

FAUSCH, S.C., DA SILVA, D.M., RUDOLF, M.P., and KAST, W.M. (2002). Human Papillomavirus Virus-Like Particles Do Not Activate Langerhans Cells: A Possible Immune Escape Mechanism Used by Human Papillomaviruses. The Journal of Immunology *169*, 3242-3249.

FAUSCH, S.C., FAHEY, L.M., DA SILVA, D.M., and KAST, W.M. (2005). Human Papillomavirus Can Escape Immune Recognition through Langerhans Cell Phosphoinositide 3-Kinase Activation. The Journal of Immunology *174*, 7172-7178.

FELLER, L., WOOD, N.H., KHAMMISSA, R.A., CHIKTE, U.M., MEYEROV, R., and LEMMER, J. (2010). HPV modulation of host immune responses. SADJ *65*, 266-268.

FERLAY, J., SHIN, H.R., BRAY, F., FORMAN, D., MATHERS, C., and PARKIN, D.M. (2010). Estimates of worldwide burden of cancer in 2008: GLOBOCAN 2008. Int J Cancer *127*, 2893-2917.

FOGG, M., MURPHY, J.R., LORCH, J., POSNER, M., and WANG, F. (2013). Therapeutic targeting of regulatory T cells enhances tumor-specific CD8+ T cell responses in Epstein-Barr virus associated nasopharyngeal carcinoma. Virology *441*, 107-113.

FREGA, A., SESTI, F., SOPRACORDEVOLE, F., BIAMONTI, A., SCIRPA, P., MILAZZO, G.N., *et al.* (2013). Imiquimod 5% cream versus cold knife excision for treatment of VIN 2/3: a five-year follow-up. Eur Rev Med Pharmacol Sci *17*, 936-940.

FRIDMAN, W.H., GALON, J., PAGÈS, F., TARTOUR, E., SAUTÈS-FRIDMAN, C., and KROEMER, G. (2011). Prognostic and predictive impact of intra- and peritumoral immune infiltrates. Cancer Res *71*, 5601-5605.

FRIDMAN, W.H., PAGES, F., SAUTES-FRIDMAN, C., and GALON, J. (2012). The immune contexture in human tumours: impact on clinical outcome. Nat Rev Cancer *12*, 298-306.

FRIDMAN, W.H., REMARK, R., GOC, J., GIRALDO, N.A., BECHT, E., HAMMOND, S.A.*, et al.* (2014). The immune microenvironment: a major player in human cancers. Int Arch Allergy Immunol *164*, 13-26.

FUCHS, T.J., WILD, P.J., MOCH, H., and BUHMANN, J.M. (2008). Computational pathology analysis of tissue microarrays predicts survival of renal clear cell carcinoma patients. Medical image computing and computer-assisted intervention : MICCAI International Conference on Medical Image Computing and Computer-Assisted Intervention *11*, 1-8.

FUENTES-GONZALEZ, A.M., CONTRERAS-PAREDES, A., MANZO-MERINO, J., and LIZANO, M. (2013). The modulation of apoptosis by oncogenic viruses. Virol J *10*, 182.

GALON, J., COSTES, A., SANCHEZ-CABO, F., KIRILOVSKY, A., MLECNIK, B., LAGORCE-PAGES, C.*, et al.* (2006). Type, density, and location of immune cells within human colorectal tumors predict clinical outcome. Science *313*, 1960-1964.

GANGULY, N., and PARIHAR, S.P. (2009). Human papillomavirus E6 and E7 oncoproteins as risk factors for tumorigenesis. J Biosci *34*, 113-123.

GARCIA-CHACON, R., VELASCO-RAMIREZ, S.F., FLORES-ROMO, L., and DANERI-NAVARRO, A. (2009). Immunobiology of HPV Infection. Arch Med Res *40*, 443-448.

GARCIA-LORA, A., ALGARRA, I., GAFORIO, J.J., RUIZ-CABELLO, F., and GARRIDO, F. (2001). Immunoselection by T lymphocytes generates repeated MHC class I-deficient metastatic tumor variants. Int J Cancer *91*, 109-119.

GARRIDO, F., RUIZ-CABELLO, F., CABRERA, T., PÉREZ-VILLAR, J.J., LÓPEZ-BOTET, M., DUGGAN-KEEN, M.*, et al.* (1997). Implications for immunosurveillance of altered HLA class I phenotypes in human tumours. Immunol Today *18*, 89-95.

GASPARI, A., TYRING, S.K., and ROSEN, T. (2009). Beyond a decade of 5% imiquimod topical therapy. J Drugs Dermatol *8*, 467-474.

GASPARI, A.A., JENKINS, M.K., and KATZ, S.I. (1988). Class II MHC-bearing keratinocytes induce antigen-specific unresponsiveness in hapten-specific Th1 clones. J Immunol *141*, 2216-2220.

GASPARINI, R., and PANATTO, D. (2009). Cervical cancer: from Hippocrates through Rigoni-Stern to zur Hausen. Vaccine *27 Suppl 1*, A4-5.

GEORGOPOULOS, N.T., PROFFITT, J.L., and BLAIR, G.E. (2000). Transcriptional regulation of the major histocompatibility complex (MHC) class I heavy chain, TAP1 and LMP2 genes by the human papillomavirus (HPV) type 6b, 16 and 18 E7 oncoproteins. Oncogene *19*, 4930-4935.

GIBB, R.K., and MARTENS, M.G. (2011). The impact of liquid-based cytology in decreasing the incidence of cervical cancer. Rev Obstet Gynecol *4*, S2-S11.

GILLISON, M.L., CASTELLSAGUE, X., CHATURVEDI, A., GOODMAN, M.T., SNIJDERS, P., TOMMASINO, M.*, et al.* (2014). Eurogin Roadmap: comparative epidemiology of HPV infection and associated cancers of the head and neck and cervix. Int J Cancer *134*, 497-507.

GILLISON, M.L., KOCH, W.M., CAPONE, R.B., SPAFFORD, M., WESTRA, W.H., WU, L.*, et al.* (2000). Evidence for a causal association between human papillomavirus and a subset of head and neck cancers. J Natl Cancer Inst *92*, 709-720.

GLEW, S.S., DUGGAN-KEEN, M., CABRERA, T., and STERN, P.L. (1992). HLA class II antigen expression in human papillomavirus-associated cervical cancer. Cancer Res *52*, 4009-4016.

GONZALES, R.W., RE; EDDINS, SL (2009). Digital Image Processing using Matlab. (Tennessee: Gatesmark Publishing).

GRABE, N., LAHRMANN, B., POMMERENCKE, T., VON KNEBEL DOEBERITZ, M., REUSCHENBACH, M., and WENTZENSEN, N. (2010). A virtual microscopy system to scan, evaluate and archive biomarker enhanced cervical cytology slides. Cell Oncol *32*, 109-119.

GRIMM, C., POLTERAUER, S., NATTER, C., RAHHAL, J., HEFLER, L., TEMPFER, C.B.*, et al.* (2012). Treatment of cervical intraepithelial neoplasia with topical imiquimod: a randomized controlled trial. Obstet Gynecol *120*, 152-159.

GUL, N., GANESAN, R., and LUESLEY, D.M. (2004). Characterizing T-cell response in low-grade and high-grade vulval intraepithelial neoplasia, study of CD3, CD4 and CD8 expressions. Gynecol Oncol *94*, 48-53.

HACKSTEIN, H., HAGEL, N., KNOCHE, A., KRANZ, S., LOHMEYER, J., VON WULFFEN, W.*, et al.* (2012). Skin TLR7 triggering promotes accumulation of respiratory dendritic cells and natural killer cells. PLoS ONE *7*, e43320.

HALAMA, N., ZOERNIG, I., SPILLE, A., WESTPHAL, K., SCHIRMACHER, P., JAEGER, D.*, et al.* (2009). Estimation of immune cell densities in immune cell conglomerates: an approach for high-throughput quantification. PLoS ONE *4*, e7847.

HALVORSEN, E.C., MAHMOUD, S.M., and BENNEWITH, K.L. (2014). Emerging roles of regulatory T cells in tumour progression and metastasis. Cancer Metastasis Rev.

HAMID, N.A., BROWN, C., and GASTON, K. (2009). The regulation of cell proliferation by the papillomavirus early proteins. Cell Mol Life Sci *66*, 1700-1717.

HAN, L.Y., FLETCHER, M.S., URBAUER, D.L., MUELLER, P., LANDEN, C.N., KAMAT, A.A.*, et al.* (2008). HLA class I antigen processing machinery component expression and intratumoral T-Cell infiltrate as independent prognostic markers in ovarian carcinoma. Clinical cancer research : an official journal of the American Association for Cancer Research *14*, 3372-3379.

HAN, S., ZHANG, C., LI, Q., DONG, J., LIU, Y., HUANG, Y.*, et al.* (2014). Tumour-infiltrating CD4(+) and CD8(+) lymphocytes as predictors of clinical outcome in glioma. Br J Cancer *110*, 2560-2568.

HAN, Y., GUO, Q., ZHANG, M., CHEN, Z., and CAO, X. (2009). CD69+ CD4+ CD25- T cells, a new subset of regulatory T cells, suppress T cell proliferation through membrane-bound TGF-beta 1. J Immunol *182*, 111-120.

HARDING, F.A., MCARTHUR, J.G., GROSS, J.A., RAULET, D.H., and ALLISON, J.P. (1992). CD28-mediated signalling co-stimulates murine T cells and prevents induction of anergy in T-cell clones. Nature *356*, 607-609.

HARWOOD, C.A., SURENTHERAN, T., SASIENI, P., PROBY, C.M., BORDEA, C., LEIGH, I.M*., et al.* (2004). Increased risk of skin cancer associated with the presence of epidermodysplasia verruciformis human papillomavirus types in normal skin. Br J Dermatol *150*, 949-957.

HE, X.S., REHERMANN, B., LOPEZ-LABRADOR, F.X., BOISVERT, J., CHEUNG, R., MUMM, J*., et al.* (1999). Quantitative analysis of hepatitis C virus-specific CD8(+) T cells in peripheral blood and liver using peptide-MHC tetramers. Proc Natl Acad Sci U S A *96*, 5692-5697.

HEINE, H., and LIEN, E. (2003). Toll-like receptors and their function in innate and adaptive immunity. Int Arch Allergy Immunol *130*, 180-192.

HEMMI, H., KAISHO, T., TAKEUCHI, O., SATO, S., SANJO, H., HOSHINO, K*., et al.* (2002). Small anti-viral compounds activate immune cells via the TLR7 MyD88-dependent signaling pathway. Nat Immunol *3*, 196-200.

HERFS, M., YAMAMOTO, Y., LAURY, A., WANG, X., NUCCI, M.R., MCLAUGHLIN-DRUBIN, M.E*., et al.* (2012). A discrete population of squamocolumnar junction cells implicated in the pathogenesis of cervical cancer. Proceedings of the National Academy of Sciences *109*, 10516-10521.

HICKLIN, D.J., WANG, Z., ARIENTI, F., RIVOLTINI, L., PARMIANI, G., and FERRONE, S. (1998). beta2-Microglobulin mutations, HLA class I antigen loss, and tumor progression in melanoma. J Clin Investig *101*, 2720-2729.

HODI, F.S., O'DAY, S.J., MCDERMOTT, D.F., WEBER, R.W., SOSMAN, J.A., HAANEN, J.B*., et al.* (2010). Improved survival with ipilimumab in patients with metastatic melanoma. N Engl J Med *363*, 711-723.

HOFFMANN, T.K., ARSOV, C., SCHIRLAU, K., BAS, M., FRIEBE-HOFFMANN, U., KLUSSMANN, J.P*., et al.* (2006). T cells specific for HPV16 E7 epitopes in patients with squamous cell carcinoma of the oropharynx. Int J Cancer *118*, 1984-1991.

HOLLDACK, J. (2014). Toll-like receptors as therapeutic targets for cancer. Drug Discov Today *19*, 379-382.

HOPMAN, A.H., THEELEN, W., HOMMELBERG, P.P., KAMPS, M.A., HERRINGTON, C.S., MORRISON, L.E*., et al.* (2006). Genomic integration of oncogenic HPV and gain of the human telomerase gene TERC at 3q26 are strongly associated events in the progression of uterine cervical dysplasia to invasive cancer. J Pathol *210*, 412-419.

HORN, J., DAMM, O., KRETZSCHMAR, M.E., DELERE, Y., WICHMANN, O., KAUFMANN, A.M*., et al.* (2013). Estimating the long-term effects of HPV vaccination in Germany. Vaccine *31*, 2372-2380.

HOU, F., LI, Z., MA, D., ZHANG, W., ZHANG, Y., ZHANG, T*., et al.* (2012). Distribution of Th17 cells and Foxp3-expressing T cells in tumor-infiltrating lymphocytes in patients with uterine cervical cancer. Clin Chim Acta *413*, 1848-1854.

HUANG, B., ZHAO, J., LI, H., HE, K.-L., CHEN, Y., MAYER, L*., et al.* (2005). Toll-Like Receptors on Tumor Cells Facilitate Evasion of Immune Surveillance. Cancer Res *65*, 5009-5014.

HUANG, S., WEI, W., and YUN, Y. (2009a). Upregulation of TLR7 and TLR3 gene expression in the lung of respiratory syncytial virus infected mice. Wei Sheng Wu Xue Bao *49*, 239-245.

HUANG, S.J., HIJNEN, D., MURPHY, G.F., KUPPER, T.S., CALARESE, A.W., MOLLET, I.G.*, et al.* (2009b). Imiquimod enhances IFN-gamma production and effector function of T cells infiltrating human squamous cell carcinomas of the skin. J Investig Dermatol *129*, 2676-2685.

HUH, K., ZHOU, X., HAYAKAWA, H., CHO, J.Y., LIBERMANN, T.A., JIN, J.*, et al.* (2007). Human papillomavirus type 16 E7 oncoprotein associates with the cullin 2 ubiquitin ligase complex, which contributes to degradation of the retinoblastoma tumor suppressor. J Virol *81*, 9737-9747.

IRSHAD, H., VEILLARD, A., ROUX, L., and RACOCEANU, D. (2014). Methods for nuclei detection, segmentation, and classification in digital histopathology: a review-current status and future potential. IEEE reviews in biomedical engineering *7*, 97-114.

JAAFAR, F., RIGHI, E., LINDSTROM, V., LINTON, C., NOHADANI, M., VAN NOORDEN, S.*, et al.* (2009). Correlation of CXCL12 expression and FoxP3+ cell infiltration with human papillomavirus infection and clinicopathological progression of cervical cancer. Am J Pathol *175*, 1525-1535.

JANEWAY, C.A., JR., and MEDZHITOV, R. (2002). Innate immune recognition. Annu Rev Immunol *20*, 197-216.

JIANG, Y.Z., COURIEL, D., MAVROUDIS, D.A., LEWALLE, P., MALKOVSKA, V., HENSEL, N.F.*, et al.* (1996). Interaction of natural killer cells with MHC class II: reversal of HLA-DR1-mediated protection of K562 transfectant from natural killer cell-mediated cytolysis by brefeldin-A. Immunology *87*, 481-486.

JIN, B., SUN, T., YU, X.H., YANG, Y.X., and YEO, A.E. (2012). The effects of TLR activation on T-cell development and differentiation. Clin Dev Immunol *2012*, 836485.

JONES, E.E., and WELLS, S.I. (2006). Cervical cancer and human papillomaviruses: inactivation of retinoblastoma and other tumor suppressor pathways. Curr Mol Med *6*, 795-808.

JONES, S.A. (2005). Directing transition from innate to acquired immunity: defining a role for IL-6. J Immunol *175*, 3463-3468.

JORDANOVA, E.S., GORTER, A., AYACHI, O., PRINS, F., DURRANT, L.G., KENTER, G.G.*, et al.* (2008). Human leukocyte antigen class I, MHC class I chain-related molecule A, and CD8+/regulatory T-cell ratio: which variable determines survival of cervical cancer patients? Clinical cancer research : an official journal of the American Association for Cancer Research *14*, 2028-2035.

JUNG, C., and KIM, C. (2010). Segmenting clustered nuclei using H-minima transform-based marker extraction and contour parameterization. IEEE Trans Biomed Eng *57*, 2600-2604.

KAJITANI, N., SATSUKA, A., KAWATE, A., and SAKAI, H. (2012). Productive Lifecycle of Human Papillomaviruses that Depends Upon Squamous Epithelial Differentiation. Frontiers in microbiology *3*, 152.

KANODIA, S., DA SILVA, D.M., and KAST, W.M. (2008). Recent advances in strategies for immunotherapy of human papillomavirus-induced lesions. International journal of cancer Journal international du cancer *122*, 247-259.

KANODIA, S., FAHEY, L.M., and KAST, W.M. (2007). Mechanisms used by human papillomaviruses to escape the host immune response. Curr Cancer Drug Targets *7*, 79-89.

KAUFMANN, M., NIELAND, J., SCHINZ, M., NONN, M., GABELSBERGER, J., MEISSNER, H.*, et al.* (2001). HPV16 L1E7 chimeric virus-like particles induce specific HLA-restricted T cells in humans after in vitro vaccination. International journal of cancer Journal international du cancer *92*, 285-293.

KAUR, R., CASEY, J., and PICHICHERO, M. (2014). Cytokine, chemokine, and toll-like receptor expression in middle ear fluids of children with acute otitis media. Laryngoscope.

KAWANA, K., ADACHI, K., KOJIMA, S., KOZUMA, S., and FUJII, T. (2012). Therapeutic Human Papillomavirus (HPV) Vaccines: A Novel Approach. The open virology journal *6*, 264-269.

KAWANA, K., YASUGI, T., and TAKETANI, Y. (2009). Human papillomavirus vaccines: current issues & future. Indian J Med Res *130*, 341-347.

KEENAN, S.J., DIAMOND, J., MCCLUGGAGE, W.G., BHARUCHA, H., THOMPSON, D., BARTELS, P.H.*, et al.* (2000). An automated machine vision system for the histological grading of cervical intraepithelial neoplasia (CIN). J Pathol *192*, 351-362.

KERSEMAEKERS, A.M., VAN DE VIJVER, M.J., KENTER, G.G., and FLEUREN, G.J. (1999). Genetic alterations during the progression of squamous cell carcinomas of the uterine cervix. Genes Chromosomes Cancer *26*, 346-354.

KIM, S.T., JEONG, H., WOO, O.H., SEO, J.H., KIM, A., LEE, E.S.*, et al.* (2013). Tumor-infiltrating lymphocytes, tumor characteristics, and recurrence in patients with early breast cancer. Am J Clin Oncol *36*, 224-231.

KLAES, R., FRIEDRICH, T., SPITKOVSKY, D., RIDDER, R., RUDY, W., PETRY, U.*, et al.* (2001). Overexpression of p16(^{INK4A}) as a specific marker for dysplastic and neoplastic epithelial cells of the cervix uteri. Int J Cancer *92*, 276-284.

KLOOR, M., BECKER, C., BENNER, A., WOERNER, S.M., GEBERT, J., FERRONE, S.*, et al.* (2005). Immunoselective pressure and human leukocyte antigen class I antigen machinery defects in microsatellite unstable colorectal cancers. Cancer Res *65*, 6418-6424.

KORZENIEWSKI, N., SPARDY, N., DUENSING, A., and DUENSING, S. (2011). Genomic instability and cancer: lessons learned from human papillomaviruses. Cancer Lett *305*, 113-122.

KOTHARI, S., PHAN, J.H., STOKES, T.H., and WANG, M.D. (2013). Pathology imaging informatics for quantitative analysis of whole-slide images. J Am Med Inform Assoc *20*, 1099-1108.

KUNZ, P., FELLENBERG, J., MOSKOVSZKY, L., SAPI, Z., KRENACS, T., POESCHL, J.*, et al.* (2014). Osteosarcoma microenvironment: whole-slide imaging and optimized antigen detection overcome major limitations in immunohistochemical quantification. PLoS ONE *9*, e90727.

KURIMOTO, A., OGINO, T., ICHII, S., ISOBE, Y., TOBE, M., OGITA, H.*, et al.* (2004). Synthesis and evaluation of 2-substituted 8-hydroxyadenines as potent interferon inducers with improved oral bioavailabilities. Bioorg Med Chem *12*, 1091-1099.

KUSS, I., SAITO, T., JOHNSON, J.T., and WHITESIDE, T.L. (1999). Clinical significance of decreased zeta chain expression in peripheral blood lymphocytes of patients with head and neck cancer. Clin Cancer Res *5*, 329-334.

LAHRMANN, B., HALAMA, N., SINN, H.P., SCHIRMACHER, P., JAEGER, D., and GRABE, N. (2011). Automatic tumor-stroma separation in fluorescence TMAs enables the quantitative high-throughput analysis of multiple cancer biomarkers. PLoS ONE *6*, e28048.

LANZA, L., PEIRANO, L., BOSCO, O., CONTINI, P., FILACI, G., SETTI, M.*, et al.* (1995). Interferons up-regulate with different potency HLA class I antigen expression in M14 human melanoma cell line. Possible interaction with glucocorticoid hormones. Cancer Immunol Immunother *41*, 23-28.

LAURSON, J., KHAN, S., CHUNG, R., CROSS, K., and RAJ, K. (2010). Epigenetic repression of E-cadherin by human papillomavirus 16 E7 protein. Carcinogenesis *31*, 918-926.

LEONG, C.M., DOORBAR, J., NINDL, I., YOON, H.S., and HIBMA, M.H. (2010). Deregulation of E-cadherin by human papillomavirus is not confined to high-risk, cancer-causing types. Br J Dermatol *163*, 1253-1263.

LIGGETT, W.H., JR., and SIDRANSKY, D. (1998). Role of the p16 tumor suppressor gene in cancer. J Clin Oncol *16*, 1197-1206.

LLOYD, M.C., ALLAM-NANDYALA, P., PUROHIT, C.N., BURKE, N., COPPOLA, D., and BUI, M.M. (2010). Using image analysis as a tool for assessment of prognostic and predictive biomarkers for breast cancer: How reliable is it? Journal of pathology informatics *1*, 29.

LODDENKEMPER, C., HOFFMANN, C., STANKE, J., NAGORSEN, D., BARON, U., OLEK, S.*, et al.* (2009). Regulatory (FOXP3+) T cells as target for immune therapy of cervical intraepithelial neoplasia and cervical cancer. Cancer Sci *100*, 1112-1117.

LONGWORTH, M.S., WILSON, R., and LAIMINS, L.A. (2005). HPV31 E7 facilitates replication by activating E2F2 transcription through its interaction with HDACs. EMBO J *24*, 1821-1830.

LU, J., AGGARWAL, R., KANJI, S., DAS, M., JOSEPH, M., POMPILI, V.*, et al.* (2011). Human ovarian tumor cells escape gammadelta T cell recognition partly by down regulating surface expression of MICA and limiting cell cycle related molecules. PLoS ONE *6*, e23348.

LUBOLDT, H.J., KUBENS, B.S., RUBBEN, H., and GROSSE-WILDE, H. (1996). Selective loss of human leukocyte antigen class I allele expression in advanced renal cell carcinoma. Cancer Res *56*, 826-830.

MAINE, C.J., AZIZ, N.H., CHATTERJEE, J., HAYFORD, C., BREWIG, N., WHILDING, L.*, et al.* (2014). Programmed death ligand-1 over-expression correlates with malignancy and contributes to immune regulation in ovarian cancer. Cancer Immunol Immunother *63*, 215-224.

MANDIC, R., LIEDER, A., SADOWSKI, M., PELDSZUS, R., and WERNER, J.A. (2004). Comparison of surface HLA class I levels in squamous cell carcinoma cell lines of the head and neck. Anticancer Res *24*, 973-979.

MAO, H., ZHANG, L., YANG, Y., ZUO, W., BI, Y., GAO, W.*, et al.* (2010). New insights of CTLA-4 into its biological function in breast cancer. Curr Cancer Drug Targets *10*, 728-736.

MARSHALL, N.B., and SWAIN, S.L. (2011). Cytotoxic CD4 T cells in antiviral immunity. J Biomed Biotechnol *2011*, 954602.

MARTIN, C.M., and O'LEARY, J.J. (2011). Histology of cervical intraepithelial neoplasia and the role of biomarkers. Best Pract Res Clin Obstet Gynaecol *25*, 605-615.

MASSA, C., and SELIGER, B. (2013). Fast dendritic cells stimulated with alternative maturation mixtures induce polyfunctional and long-lasting activation of innate and adaptive effector cells with tumor-killing capabilities. J Immunol *190*, 3328-3337.

MATKOWSKI, R., GISTEREK, I., HALON, A., LACKO, A., SZEWCZYK, K., STASZEK, U.*, et al.* (2009). The prognostic role of tumor-infiltrating CD4 and CD8 T lymphocytes in breast cancer. Anticancer Res *29*, 2445-2451.

MATSUI, S., AHLERS, J.D., VORTMEYER, A.O., TERABE, M., TSUKUI, T., CARBONE, D.P.*, et al.* (1999). A model for CD8+ CTL tumor immunosurveillance and regulation of tumor escape by CD4 T cells through an effect on quality of CTL. J Immunol *163*, 184-193.

MCBRIDE, A.A. (2013). The papillomavirus E2 proteins. Virology *445*, 57-79.

MCCREDIE, M.R., SHARPLES, K.J., PAUL, C., BARANYAI, J., MEDLEY, G., JONES, R.W.*, et al.* (2008). Natural history of cervical neoplasia and risk of invasive cancer in women with cervical intraepithelial neoplasia 3: a retrospective cohort study. Lancet Oncol *9*, 425-434.

MCDERMOTT, D.F., and ATKINS, M.B. (2013). PD-1 as a potential target in cancer therapy. Cancer medicine *2*, 662-673.

MCLAUGHLIN-DRUBIN, M.E., CRUM, C.P., and MÜNGER, K. (2011). Human papillomavirus E7 oncoprotein induces KDM6A and KDM6B histone demethylase expression and causes epigenetic reprogramming. Proc Natl Acad Sci U S A *108*, 2130-2135.

MCLAUGHLIN-DRUBIN, M.E., and MUNGER, K. (2009). The human papillomavirus E7 oncoprotein. Virology *384*, 335-344.

MCLAUGHLIN-DRUBIN, M.E., and MUNGER, K. (2013). Biochemical and functional interactions of human papillomavirus proteins with polycomb group proteins. Viruses *5*, 1231-1249.

MCLAUGHLIN-DRUBIN, M.E., PARK, D., and MUNGER, K. (2013). Tumor suppressor p16^{INK4A} is necessary for survival of cervical carcinoma cell lines. Proc Natl Acad Sci U S A *110*, 16175-16180.

MEDZHITOV, R. (2007). Recognition of microorganisms and activation of the immune response. Nature *449*, 819-826.

MEHTA, A.M., JORDANOVA, E.S., KENTER, G.G., FERRONE, S., and FLEUREN, G.J. (2008). Association of antigen processing machinery and HLA class I defects with clinicopathological outcome in cervical carcinoma. Cancer Immunol Immunother *57*, 197-206.

MEISSNER, M., REICHERT, T.E., KUNKEL, M., FERRONE, S., and SELIGER, B. (2005). Defects in the Human Leukocyte Antigen Class I Antigen Processing Machinery in Head and Neck Squamous Cell Carcinoma : Association with Clinical Outcome Association with Clinical Outcome. 2552-2560.

MELSHEIMER, P., VINOKUROVA, S., WENTZENSEN, N., BASTERT, G., and VON KNEBEL DOEBERITZ, M. (2004). DNA aneuploidy and integration of human papillomavirus type 16 e6/e7 oncogenes in intraepithelial neoplasia and invasive squamous cell carcinoma of the cervix uteri. Clin Cancer Res *10*, 3059-3063.

MICHEL, S., BENNER, A., TARIVERDIAN, M., WENTZENSEN, N., HOEFLER, P., POMMERENCKE, T.*, et al.* (2008). High density of FOXP3-positive T cells infiltrating colorectal cancers with microsatellite instability. Br J Cancer *99*, 1867-1873.

MIGHTY, K.K., and LAIMINS, L.A. (2014). The role of human papillomaviruses in oncogenesis. Recent Results Cancer Res *193*, 135-148.

MOGENSEN, T.H. (2009). Pathogen recognition and inflammatory signaling in innate immune defenses. Clin Microbiol Rev *22*, 240-273, Table of Contents.

MOLES LOPEZ, X., BARBOT, P., VAN EYCKE, Y.R., VERSET, L., TREPANT, A.L., LARBANOIX, L.*, et al.* (2014). Registration of whole immunohistochemical slide images: an efficient way to characterize biomarker colocalization. J Am Med Inform Assoc.

MOLHO-PESSACH, V., and LOTEM, M. (2007). Viral carcinogenesis in skin cancer. Curr Probl Dermatol *35*, 39-51.

MOLLING, J.W., DE GRUIJL, T.D., GLIM, J., MORENO, M., ROZENDAAL, L., MEIJER, C.J.L.M.*, et al.* (2007). CD4(+)CD25hi regulatory T-cell frequency correlates with persistence of human papillomavirus type 16 and T helper cell responses in patients with cervical intraepithelial neoplasia. International journal of cancer Journal international du cancer *121*, 1749-1755.

MONNIER-BENOIT, S., MAUNY, F., RIETHMULLER, D., GUERRINI, J.S., CAPILNA, M., FELIX, S.*, et al.* (2006). Immunohistochemical analysis of CD4+ and CD8+ T-cell subsets in high risk human papillomavirus-associated pre-malignant and malignant lesions of the uterine cervix. Gynecol Oncol *102*, 22-31.

MONTES, C.L., CHAPOVAL, A.I., NELSON, J., ORHUE, V., ZHANG, X., SCHULZE, D.H.*, et al.* (2008). Tumor-induced senescent T cells with suppressor function: a potential form of tumor immune evasion. Cancer Res *68*, 870-879.

MORETTA, A., BOTTINO, C., VITALE, M., PENDE, D., BIASSONI, R., MINGARI, M.C.*, et al.* (1996). Receptors for HLA class-I molecules in human natural killer cells. Annu Rev Immunol *14*, 619-648.

MUNK, A.C., KRUSE, A.J., VAN DIERMEN, B., JANSSEN, E.A., SKALAND, I., GUDLAUGSSON, E.*, et al.* (2007). Cervical intraepithelial neoplasia grade 3 lesions can regress. APMIS *115*, 1409-1414.

MUNN, D.H., and MELLOR, A.L. (2013). Indoleamine 2,3 dioxygenase and metabolic control of immune responses. Trends Immunol *34*, 137-143.

NAKAGOMI, H., PETERSSON, M., MAGNUSSON, I., JUHLIN, C., MATSUDA, M., MELLSTEDT, H.*, et al.* (1993). Decreased expression of the signal-transducing zeta chains in tumor-infiltrating T-cells and NK cells of patients with colorectal carcinoma. Cancer Res *53*, 5610-5612.

NAKAMURA, T., SHIMA, T., SAEKI, A., HIDAKA, T., NAKASHIMA, A., TAKIKAWA, O.*, et al.* (2007). Expression of indoleamine 2, 3-dioxygenase and the recruitment of Foxp3-expressing regulatory T cells in the development and progression of uterine cervical cancer. Cancer Sci *98*, 874-881.

NÄSMAN, A., ANDERSSON, E., NORDFORS, C., GRÜN, N., JOHANSSON, H., MUNCK-WIKLAND, E.*, et al.* (2013). MHC class I expression in HPV positive and negative tonsillar squamous cell carcinoma in correlation to clinical outcome. International journal of cancer Journal international du cancer *132*, 72-81.

NATALE, C., GIANNINI, T., LUCCHESE, A., and KANDUC, D. (2000). Computer-assisted analysis of molecular mimicry between human papillomavirus 16 E7 oncoprotein and human protein sequences. Immunol Cell Biol *78*, 580-585.

NEDERGAARD, B.S., LADEKARL, M., THOMSEN, H.F., NYENGAARD, J.R., and NIELSEN, K. (2007). Low density of CD3+, CD4+ and CD8+ cells is associated with increased risk of relapse in squamous cell cervical cancer. Br J Cancer *97*, 1135-1138.

NGUYEN, H.P., RAMIREZ-FORT, M.K., and RADY, P.L. (2014). The biology of human papillomaviruses. Curr Probl Dermatol *45*, 19-32.

NIMS, R.W., SYKES, G., COTTRILL, K., IKONOMI, P., and ELMORE, E. (2010). Short tandem repeat profiling: part of an overall strategy for reducing the frequency of cell misidentification. In Vitro Cell Dev Biol Anim *46*, 811-819.

NISHIKAWA, H., and SAKAGUCHI, S. (2014). Regulatory T cells in cancer immunotherapy. Curr Opin Immunol *27*, 1-7.

NOYA, F., CHIEN, W.M., BROKER, T.R., and CHOW, L.T. (2001). p21cip1 Degradation in differentiated keratinocytes is abrogated by costabilization with cyclin E induced by human papillomavirus E7. J Virol *75*, 6121-6134.

OH, J.M., KIM, S.H., CHO, E.A., SONG, Y.S., KIM, W.H., and JUHNN, Y.S. (2010). Human papillomavirus type 16 E5 protein inhibits hydrogen-peroxide-induced apoptosis by stimulating ubiquitin-proteasome-mediated degradation of Bax in human cervical cancer cells. Carcinogenesis *31*, 402-410.

OHKURA, N., HAMAGUCHI, M., and SAKAGUCHI, S. (2011). FOXP3+ regulatory T cells: control of FOXP3 expression by pharmacological agents. Trends Pharmacol Sci *32*, 158-166.

OLDSTONE, M.B. (1998). Molecular mimicry and immune-mediated diseases. FASEB J *12*, 1255-1265.

OSTOR, A.G. (1993). Natural history of cervical intraepithelial neoplasia: a critical review. Int J Gynecol Pathol *12*, 186-192.

OTSU, N. (1979). A threshold selection method from grey level histograms. IEEE Trans Syst Man Cybern *9*, 62–66.

PALEFSKY, J. (2009). Human papillomavirus-related disease in people with HIV. Curr Opin HIV AIDS *4*, 52-56.

PALOMARES, O., MARTIN-FONTECHA, M., LAUENER, R., TRAIDL-HOFFMANN, C., CAVKAYTAR, O., AKDIS, M.*, et al.* (2014). Regulatory T cells and immune regulation of allergic diseases: roles of IL-10 and TGF-beta. Genes Immun.

PARKER, K.C., BEDNAREK, M.A., and COLIGAN, J.E. (1994). Scheme for ranking potential HLA-A2 binding peptides based on independent binding of individual peptide side-chains. J Immunol *152*, 163-175.

PARKIN, D.M., and BRAY, F. (2006). Chapter 2: The burden of HPV-related cancers. Vaccine *24 Suppl 3*, S3/11-25.

PASCHEN, A., MENDEZ, R.M., JIMENEZ, P., SUCKER, A., RUIZ-CABELLO, F., SONG, M.*, et al.* (2003). Complete loss of HLA class I antigen expression on melanoma cells: a result of successive mutational events. Int J Cancer *103*, 759-767.

PASSMORE, J.A., BURCH, V.C., SHEPHARD, E.G., MARAIS, D.J., ALLAN, B., KAY, P.*, et al.* (2002). Single-cell cytokine analysis allows detection of cervical T-cell responses against human papillomavirus type 16 L1 in women infected with genital HPV. J Med Virol *67*, 234-240.

PATEL, S., and CHIPLUNKAR, S. (2009). Host immune responses to cervical cancer. Curr Opin Obstet Gynecol *21*, 54-59.

PENG, Y.P., ZHANG, J.J., LIANG, W.B., TU, M., LU, Z.P., WEI, J.S.*, et al.* (2014). Elevation of MMP-9 and IDO induced by pancreatic cancer cells mediates natural killer cell dysfunction. BMC Cancer *14*, 738.

PEPER, J.K., SCHUSTER, H., LOFFLER, M.W., SCHMID-HORCH, B., RAMMENSEE, H.G., and STEVANOVIC, S. (2014). An impedance-based cytotoxicity assay for real-time and label-free assessment of T-cell-mediated killing of adherent cells. J Immunol Methods *405*, 192-198.

PETER, M., STRANSKY, N., COUTURIER, J., HUPE, P., BARILLOT, E., DE CREMOUX, P*., et al.* (2010). Frequent genomic structural alterations at HPV insertion sites in cervical carcinoma. J Pathol *221*, 320-330.

PETT, M.R., ALAZAWI, W.O., ROBERTS, I., DOWEN, S., SMITH, D.I., STANLEY, M.A*., et al.* (2004). Acquisition of high-level chromosomal instability is associated with integration of human papillomavirus type 16 in cervical keratinocytes. Cancer Res *64*, 1359-1368.

PHAM, P.V., NGUYEN, N.T., NGUYEN, H.M., KHUAT, L.T., LE, P.M., PHAM, V.Q*., et al.* (2014). A simple in vitro method for evaluating dendritic cell-based vaccinations. OncoTargets and therapy *7*, 1455-1464.

PIERSMA, S.J., JORDANOVA, E.S., VAN POELGEEST, M.I., KWAPPENBERG, K.M., VAN DER HULST, J.M., DRIJFHOUT, J.W*., et al.* (2007). High number of intraepithelial CD8+ tumor-infiltrating lymphocytes is associated with the absence of lymph node metastases in patients with large early-stage cervical cancer. Cancer Res *67*, 354-361.

PLATTEN, M., WICK, W., and VAN DEN EYNDE, B.J. (2012). Tryptophan Catabolism in Cancer: Beyond IDO and Tryptophan Depletion. Cancer Res *72*, 5435-5440.

PLETINCKX, K., VAETH, M., SCHNEIDER, T., BEYERSDORF, N., HUNIG, T., BERBERICH-SIEBELT, F*., et al.* (2014). Immature dendritic cells convert anergic non-regulatory T cells into Foxp3 IL-10 regulatory T cells by engaging CD28 and CTLA-4. Eur J Immunol.

POLLACK, S.M., JONES, R.L., FARRAR, E.A., LAI, I.P., LEE, S.M., CAO, J*., et al.* (2014). Tetramer guided, cell sorter assisted production of clinical grade autologous NY-ESO-1 specific CD8(+) T cells. Journal for immunotherapy of cancer *2*, 36.

PRIGGE, E.S., TOTH, C., DYCKHOFF, G., WAGNER, S., MULLER, F., WITTEKINDT, C*., et al.* (2014). p16 /Ki-67 co-expression specifically identifies transformed cells in the head and neck region. Int J Cancer.

PRIME, S.S., PITIGALA-ARACHCHI, A., CRANE, I.J., ROSSER, T.J., and SCULLY, C. (1987). The expression of cell surface MHC class I heavy and light chain molecules in pre-malignant and malignant lesions of the oral mucosa. Histopathology *11*, 81-91.

RAMMENSEE, H., BACHMANN, J., EMMERICH, N.P., BACHOR, O.A., and STEVANOVIC, S. (1999). SYFPEITHI: database for MHC ligands and peptide motifs. Immunogenetics *50*, 213-219.

RAZMKHAH, M., and GHADERI, A. (2013). HLA Class I Allele Frequencies in Southern Iranian Women with Breast Cancer. Iranian journal of basic medical sciences *16*, 140-143.

REIMERS, M.S., ENGELS, C.C., PUTTER, H., MORREAU, H., LIEFERS, G.J., VAN DE VELDE, C.J*., et al.* (2014). Prognostic value of HLA class I, HLA-E, HLA-G and Tregs in rectal cancer: a retrospective cohort study. BMC Cancer *14*, 486.

RESSING, M.E., VAN DRIEL, W.J., CELIS, E., SETTE, A., BRANDT, M.P., HARTMAN, M*., et al.* (1996). Occasional memory cytotoxic T-cell responses of patients with human papillomavirus type 16-positive cervical lesions against a human leukocyte antigen-A *0201-restricted E7-encoded epitope. Cancer Res *56*, 582-588.

REUSCHENBACH, M., TRAN, T., FAULSTICH, F., HARTSCHUH, W., VINOKUROVA, S., KLOOR, M., *et al.* (2011). High-risk human papillomavirus in non-melanoma skin lesions from renal allograft recipients and immunocompetent patients. Br J Cancer *104*, 1334-1341.

RICHART, R.M. (1973). Cervical intraepithelial neoplasia. Pathol Annu *8*, 301-328.

ROCCO, J.W., and SIDRANSKY, D. (2001). p16(MTS-1/CDKN2/^{INK4a}) in cancer progression. Exp Cell Res *264*, 42-55.

RODRIGUEZ, J.A., GALEANO, L., PALACIOS, D.M., GOMEZ, C., SERRANO, M.L., BRAVO, M.M., *et al.* (2012). Altered HLA class I and HLA-G expression is associated with IL-10 expression in patients with cervical cancer. Pathobiology *79*, 72-83.

ROJO, M.G., GARCIA, G.B., MATEOS, C.P., GARCIA, J.G., and VICENTE, M.C. (2006). Critical comparison of 31 commercially available digital slide systems in pathology. International journal of surgical pathology *14*, 285-305.

RUBIO, V., STUGE, T.B., SINGH, N., BETTS, M.R., WEBER, J.S., ROEDERER, M., *et al.* (2003). Ex vivo identification, isolation and analysis of tumor-cytolytic T cells. Nat Med *9*, 1377-1382.

RUIFROK, A.C., and JOHNSTON, D.A. (2001). Quantification of histochemical staining by color deconvolution. Anal Quant Cytol Histol *23*, 291-299.

SCHAPIRO, F., SPARKOWSKI, J., ADDUCI, A., SUPRYNOWICZ, F., SCHLEGEL, R., and GRINSTEIN, S. (2000). Golgi alkalinization by the papillomavirus E5 oncoprotein. J Cell Biol *148*, 305-315.

SCHIFFMAN, M., CASTLE, P.E., JERONIMO, J., RODRIGUEZ, A.C., and WACHOLDER, S. (2007). Human papillomavirus and cervical cancer. Lancet *370*, 890-907.

SCHIFFMAN, M., and WENTZENSEN, N. (2010). From human papillomavirus to cervical cancer. Obstet Gynecol *116*, 177-185.

SCHMITT, M., BRAVO, I.G., SNIJDERS, P.J., GISSMANN, L., PAWLITA, M., and WATERBOER, T. (2006). Bead-based multiplex genotyping of human papillomaviruses. J Clin Microbiol *44*, 504-512.

SELIGER, B., CABRERA, T., GARRIDO, F., and FERRONE, S. (2002). HLA class I antigen abnormalities and immune escape by malignant cells. Semin Cancer Biol *12*, 3-13.

SERNEE, M.F., PLOEGH, H.L., and SCHUST, D.J. (1998). Why certain antibodies cross-react with HLA-A and HLA-G: epitope mapping of two common MHC class I reagents. Mol Immunol *35*, 177-188.

SHAH, W., YAN, X., JING, L., ZHOU, Y., CHEN, H., and WANG, Y. (2011). A reversed CD4/CD8 ratio of tumor-infiltrating lymphocytes and a high percentage of CD4(+)FOXP3(+) regulatory T cells are significantly associated with clinical outcome in squamous cell carcinoma of the cervix. Cell Mol Immunol *8*, 59-66.

SHEPHERD, P.S., ROWE, A.J., CRIDLAND, J.C., COLETART, T., WILSON, P., and LUXTON, J.C. (1996). Proliferative T cell responses to human papillomavirus type 16 L1 peptides in patients with cervical dysplasia. The Journal of general virology *77 (Pt 4)*, 593-602.

SHEU, B.-C., CHIOU, S.-H., LIN, H.-H., CHOW, S.-N., HUANG, S.-C., HO, H.-N., *et al.* (2005). Up-regulation of Inhibitory Natural Killer Receptors CD94/NKG2A with Suppressed Intracellular Perforin Expression of Tumor-Infiltrating CD8+ T Lymphocytes in Human Cervical Carcinoma. Cancer Res *65*, 2921-2929.

SHEU, B.-C., HSU, S.-M., HO, H.-N., LIEN, H.-C., HUANG, S.-C., and LIN, R.-H. (2001). A Novel Role of Metalloproteinase in Cancer-mediated Immunosuppression. Cancer Res *61*, 237-242.

SILVA, C.S., MICHELIN, M.A., ETCHEBEHERE, R.M., ADAD, S.J., and MURTA, E.F. (2010). Local lymphocytes and nitric oxide synthase in the uterine cervical stroma of patients with grade III cervical intraepithelial neoplasia. Clinics (Sao Paulo) *65*, 575-581.

SIMOENS, C., GOFFIN, F., SIMON, P., BARLOW, P., ANTOINE, J., FOIDART, J.M.*, et al.* (2012). Adverse obstetrical outcomes after treatment of precancerous cervical lesions: a Belgian multicentre study. BJOG *119*, 1247-1255.

SMOLA, S. (2014). Human papillomaviruses and skin cancer. Adv Exp Med Biol *810*, 192-207.

SNIJDERS, P.J., STEENBERGEN, R.D., HEIDEMAN, D.A., and MEIJER, C.J. (2006). HPV-mediated cervical carcinogenesis: concepts and clinical implications. J Pathol *208*, 152-164.

SOONG, R.S., SONG, L., TRIEU, J., KNOFF, J., HE, L., TSAI, Y.C.*, et al.* (2014). Toll-like Receptor Agonist Imiquimod Facilitates Antigen-Specific CD8+ T-cell Accumulation in the Genital Tract Leading to Tumor Control through IFNgamma. Clin Cancer Res *20*, 5456-5467.

SOUMELIS, V., and LIU, Y.J. (2006). From plasmacytoid to dendritic cell: morphological and functional switches during plasmacytoid pre-dendritic cell differentiation. Eur J Immunol *36*, 2286-2292.

STAM, N.J., SPITS, H., and PLOEGH, H.L. (1986). Monoclonal antibodies raised against denatured HLA-B locus heavy chains permit biochemical characterization of certain HLA-C locus products. J Immunol *137*, 2299-2306.

STANLEY, M. (2006). Immune responses to human papillomavirus. Vaccine *24 Suppl 1*, S16-22.

STANLEY, M. (2008). Immunobiology of HPV and HPV vaccines. Gynecol Oncol *109*, S15-21.

STANLEY, M. (2012a). Epithelial Cell Responses to Infection with Human Papillomavirus. Clin Microbiol Rev *25*, 215-222.

STANLEY, M. (2012b). Perspective: Vaccinate boys too. Nature *488*, S10.

STANLEY, M.A. (2002). Imiquimod and the imidazoquinolones: mechanism of action and therapeutic potential. Clin Exp Dermatol *27*, 571-577.

STARY, G., BANGERT, C., TAUBER, M., STROHAL, R., KOPP, T., and STINGL, G. (2007). Tumoricidal activity of TLR7/8-activated inflammatory dendritic cells. J Exp Med *204*, 1441-1451.

STEBEN, M., and GARLAND, S.M. (2014). Genital warts. Best Pract Res Clin Obstet Gynaecol.

STEVENSON, M.M., and RILEY, E.M. (2004). Innate immunity to malaria. Nat Rev Immunol *4*, 169-180.

SUZUKI, H., WANG, B., SHIVJI, G.M., TOTO, P., AMERIO, P., TOMAI, M.A.*, et al.* (2000). Imiquimod, a topical immune response modifier, induces migration of Langerhans cells. J Investig Dermatol *114*, 135-141.

SYRJANEN, S., NAUD, P., SARIAN, L., DERCHAIN, S., ROTELI-MARTINS, C., LONGATTO-FILHO, A.*, et al.* (2009). Immunosuppressive cytokine Interleukin-10 (IL-10) is up-regulated in high-grade CIN but not associated with high-risk human papillomavirus (HPV) at baseline, outcomes of HR-HPV infections or incident CIN in the LAMS cohort. Virchows Arch *455*, 505-515.

TANG, A.L., HAUFF, S.J., OWEN, J.H., GRAHAM, M.P., CZERWINSKI, M.J., PARK, J.J., *et al.* (2012). UM-SCC-104: a new human papillomavirus-16-positive cancer stem cell-containing head and neck squamous cell carcinoma cell line. Head Neck *34*, 1480-1491.

TANG, Q., ZHANG, J., QI, B., SHEN, C., and XIE, W. (2009). Downregulation of HLA class I molecules in primary oral squamous cell carcinomas and cell lines. Arch Med Res *40*, 256-263.

TAYLOR, C.R. (2014). Issues in using whole slide imaging for diagnostic pathology: "routine" stains, immunohistochemistry and predictive markers. Biotech Histochem *89*, 419-423.

TELANG, S., RASKU, M.A., CLEM, A.L., CARTER, K., KLARER, A.C., BADGER, W.R., *et al.* (2011). Phase II trial of the regulatory T cell-depleting agent, denileukin diftitox, in patients with unresectable stage IV melanoma. BMC Cancer *11*, 515.

TERLOU, A., VAN SETERS, M., KLEINJAN, A., HEIJMANS-ANTONISSEN, C., SANTEGOETS, L.A.M., BECKMANN, I., *et al.* (2010). Imiquimod-induced clearance of HPV is associated with normalization of immune cell counts in usual type vulvar intraepithelial neoplasia. International journal of cancer Journal international du cancer *127*, 2831-2840.

THOMAS, L.K., BERMEJO, J.L., VINOKUROVA, S., JENSEN, K., BIERKENS, M., STEENBERGEN, R., *et al.* (2013). Chromosomal gains and losses in human papillomavirus-associated neoplasia of the lower genital tract - A systematic review and meta-analysis. Eur J Cancer.

TIKIDZHIEVA, A., BENNER, A., MICHEL, S., FORMENTINI, A., LINK, K.H., DIPPOLD, W., *et al.* (2012). Microsatellite instability and Beta2-Microglobulin mutations as prognostic markers in colon cancer: results of the FOGT-4 trial. Br J Cancer *106*, 1239-1245.

TODD, R.W., STEELE, J.C., ETHERINGTON, I., and LUESLEY, D.M. (2004). Detection of CD8+ T cell responses to human papillomavirus type 16 antigens in women using imiquimod as a treatment for high-grade vulval intraepithelial neoplasia. Gynecol Oncol *92*, 167-174.

TRIMBLE, C.L., CLARK, R.A., THOBURN, C., HANSON, N.C., TASSELLO, J., FROSINA, D., *et al.* (2010). Human Papillomavirus 16-Associated Cervical Intraepithelial Neoplasia in Humans Excludes CD8 T Cells from Dysplastic Epithelium. The Journal of Immunology *185*, 7107-7114.

TSOUMPOU, I., ARBYN, M., KYRGIOU, M., WENTZENSEN, N., KOLIOPOULOS, G., MARTIN-HIRSCH, P., *et al.* (2009). p16(^{INK4a}) immunostaining in cytological and histological specimens from the uterine cervix: a systematic review and meta-analysis. Cancer Treat Rev *35*, 210-220.

TUVE, S., CHEN, B.M., LIU, Y., CHENG, T.L., TOURE, P., SOW, P.S., *et al.* (2007). Combination of tumor site-located CTL-associated antigen-4 blockade and systemic regulatory T-cell depletion induces tumor-destructive immune responses. Cancer Res *67*, 5929-5939.

VAN SETERS, M., FONS, G., and VAN BEURDEN, M. (2002). Imiquimod in the treatment of multifocal vulvar intraepithelial neoplasia 2/3. Results of a pilot study. J Reprod Med *47*, 701-705.

VAN SETERS, M., VAN BEURDEN, M., TEN KATE, F.J., BECKMANN, I., EWING, P.C., EIJKEMANS, M.J., *et al.* (2008). Treatment of vulvar intraepithelial neoplasia with topical imiquimod. N Engl J Med *358*, 1465-1473.

VERNON, S.D., UNGER, E.R., MILLER, D.L., LEE, D.R., and REEVES, W.C. (1997). Association of human papillomavirus type 16 integration in the E2 gene with poor disease-free survival from cervical cancer. Int J Cancer *74*, 50-56.

VISSER, J., NIJMAN, H.W., HOOGENBOOM, B.N., JAGER, P., VAN BAARLE, D., SCHUURING, E., *et al.* (2007). Frequencies and role of regulatory T cells in patients with (pre)malignant cervical neoplasia. Clin Exp Immunol *150*, 199-209.

VOLOSHIN, T., FREMDER, E., and SHAKED, Y. (2014). Small But Mighty: Microparticles as Mediators of Tumor Progression. Cancer Microenviron.

VON KNEBEL DOEBERITZ, M. (2002). New markers for cervical dysplasia to visualise the genomic chaos created by aberrant oncogenic papillomavirus infections. Eur J Cancer *38*, 2229-2242.

VON KNEBEL DOEBERITZ, M., REUSCHENBACH, M., SCHMIDT, D., and BERGERON, C. (2012). Biomarkers for cervical cancer screening: the role of p16(^{INK4a}) to highlight transforming HPV infections. Expert Rev Proteomics *9*, 149-163.

WANG, S.S., TRUNK, M., SCHIFFMAN, M., HERRERO, R., SHERMAN, M.E., BURK, R.D.*, et al.* (2004). Validation of p16^{INK4a} as a marker of oncogenic human papillomavirus infection in cervical biopsies from a population-based cohort in Costa Rica. Cancer Epidemiol Biomarkers Prev *13*, 1355-1360.

WANG, Y., CROOKES, D., DIAMOND, J., HAMILTON, P., and TURNER, R. (2007). Segmentation of squamous epithelium from ultra-large cervical histological virtual slides. Conf Proc IEEE Eng Med Biol Soc *2007*, 775-778.

WEBSTER, J.D., and DUNSTAN, R.W. (2014). Whole-slide imaging and automated image analysis: considerations and opportunities in the practice of pathology. Vet Pathol *51*, 211-223.

WENTZENSEN, N., VINOKUROVA, S., and VON KNEBEL DOEBERITZ, M. (2004). Systematic review of genomic integration sites of human papillomavirus genomes in epithelial dysplasia and invasive cancer of the female lower genital tract. Cancer Res *64*, 3878-3884.

WENZEL, J., UERLICH, M., HALLER, O., BIEBER, T., and TUETING, T. (2005). Enhanced type I interferon signaling and recruitment of chemokine receptor CXCR3-expressing lymphocytes into the skin following treatment with the TLR7-agonist imiquimod. J Cutan Pathol *32*, 257-262.

WESTERMANN, C., FISCHER, A., and CLAD, A. (2013). Treatment of vulvar intraepithelial neoplasia with topical 5% imiquimod cream. Int J Gynaecol Obstet *120*, 266-270.

WESTRA, W.H. (2012). The morphologic profile of HPV-related head and neck squamous carcinoma: implications for diagnosis, prognosis, and clinical management. Head and neck pathology *6 Suppl 1*, S48-54.

WHITESIDE, T.L. (2004). Down-regulation of zeta-chain expression in T cells: a biomarker of prognosis in cancer? Cancer Immunol Immunother *53*, 865-878.

WISE-DRAPER, T.M., and WELLS, S.I. (2008). Papillomavirus E6 and E7 proteins and their cellular targets. Front Biosci *13*, 1003-1017.

WOLF, A.M., WOLF, D., STEURER, M., GASTL, G., GUNSILIUS, E., and GRUBECK-LOEBENSTEIN, B. (2003). Increase of regulatory T cells in the peripheral blood of cancer patients. Clin Cancer Res *9*, 606-612.

WOO, Y.L., STERLING, J., DAMAY, I., COLEMAN, N., CRAWFORD, R., VAN DER BURG, S.H.*, et al.* (2008). Characterising the local immune responses in cervical intraepithelial neoplasia: a cross-sectional and longitudinal analysis. BJOG *115*, 1616-1621; discussion 1621-1612.

WU, M.Y., KUO, T.Y., and HO, H.N. (2011). Tumor-infiltrating lymphocytes contain a higher proportion of FOXP3(+) T lymphocytes in cervical cancer. J Formos Med Assoc *110*, 580-586.

WU, P., WU, D., NI, C., YE, J., CHEN, W., HU, G*., et al.* (2014). γδT17 Cells Promote the Accumulation and Expansion of Myeloid-Derived Suppressor Cells in Human Colorectal Cancer. Immunity *40*, 785-800.

WU, T.C. (2007). The role of vascular cell adhesion molecule-1 in tumor immune evasion. Cancer Res *67*, 6003-6006.

YIM, E.K., and PARK, J.S. (2005). The role of HPV E6 and E7 oncoproteins in HPV-associated cervical carcinogenesis. Cancer research and treatment : official journal of Korean Cancer Association *37*, 319-324.

ZEHBE, I., PILCH, H., TOMMASINO, M., and MÄURER, M. (2002). Reduced T-cell receptor (TCR) zeta chain expression in cervical cancer. *8*, 2-11.

ZHAO, K.N., and CHEN, J. (2011). Codon usage roles in human papillomavirus. Rev Med Virol *21*, 397-411.

ZHENG, Z.M., and BAKER, C.C. (2006). Papillomavirus genome structure, expression, and post-transcriptional regulation. Front Biosci *11*, 2286-2302.

ZHOU, Q., ZHU, K., and CHENG, H. (2013). Toll-like receptors in human papillomavirus infection. Arch Immunol Ther Exp *61*, 203-215.

ZUR HAUSEN, H. (2011). Infections causing cancer (Weinheim: WILEYl-VCH).

ZUR HAUSEN, H., GISSMANN, L., STEINER, W., DIPPOLD, W., and DREGER, I. (1975). Human papilloma viruses and cancer. Bibl Haematol, 569-571.

ZUR HAUSEN, J., SCHULTE-HOLTHAUSEN, H., WOLF, H., DORRIES, K., and EGGER, H. (1974). Attempts to detect virus-specific DNA in human tumors. II. Nucleic acid hybridizations with complementary RNA of human herpes group viruses. Int J Cancer *13*, 657-664.

8. PUBLICATIONS, PRESENTATIONS AND POSTERS

Publications

VINOKUROVA S, VON KNEBEL DOEBERITZ M, SAUER M, REUSCHENBACH M. Compounds and Methods for increasing the Immune Response to Papillomavirus. Patent UH12178EP AD/NH *(submitted 12.2.2014)*.

SAUER, M., SCHÄFER, K., SINN, P., SCHMIDT, D., KLOOR, M., NELIUS, N., SOHN, C., EICHBAUM, M., VON KNEBEL DOEBERITZ, M., REUSCHENBACH, M. Immune cell infiltration in relation to p16^{INK4a} expression in cervical intraepithelial neoplasia. *Submitted*.

SAUER, M., REUSCHENBACH, M., WENTZENSEN, N., FERRONE, S., LAHRMANN, B., GRABE, N., SCHMIDT, D., VON KNEBEL DOEBERITZ, M., KLOOR, M. HLA class II antigen expression in cervical intraepithelial neoplasia and invasive cancer. *Manuscript in preparation.*

Presentations and Posters

Sauer M, Hampl M, Nehls N, Schlotfeldt I, Wentzensen N, Sinn P, von Knebel Doeberitz M, Reuschenbach M. **Local and systemic immune parameters in CIN and VIN patients**
27th *International Papillomavirus Conference, Berlin, Germany, 2011 (Poster).*

Sauer M, Hampl M, Schaefer K, Schlotfeldt I, Wentzensen N, Sinn P, von Knebel Doeberitz M, Reuschenbach M. **Characterization of the local immune response in cervical and vulvar intraepithelial lesions.** *EUROGIN, Prague, Czech Republic, 2012 (Oral presentation).*

Sauer M, Schaefer K, Schlotfeldt I, Wentzensen N, Sinn P, Schmidt D, von Knebel Doeberitz M, Reuschenbach M. **Immune cell infiltration in HPV-induced carcinogenesis.** *CIMT, Mayence, Germany, 2013 (Poster).*

Sauer M, Schaefer K, Schlotfeldt I, Wentzensen N, Sinn P, Schmidt D, von Knebel Doeberitz M, Reuschenbach M. **Immune cell infiltration in HPV-induced carcinogenesis.** *Tumorimmunology meets Oncology (TIMO IX), Halle (Saale), Germany (Oral presentation).*

Sauer M, Schaefer K, Schlotfeldt I, Wentzensen N, Sinn P, Schmidt D, Nelius N, von Knebel Doeberitz M, Reuschenbach M. **Immune cell infiltration in relation to p16^{INK4a} expression in cervical intraepithelial neoplasia and cancer.** *EUROGIN, Florence, Italy. 2013 (Oral presentation).*

Sauer M, Reuschenbach M, Wentzensen N, Ferrone S, Lahrmann B, Grabe N, Schmidt D, von Knebel Doeberitz M, Kloor M. **HLA class II antigen expression in cervical intraepithelial neoplasia and invasive cancer**. 29th *International Papillomavirus Conference, Seattle, USA, 2014 (Poster)*

9. SUPPLEMENTARY MATERIAL

9.1   Supplementary Figures
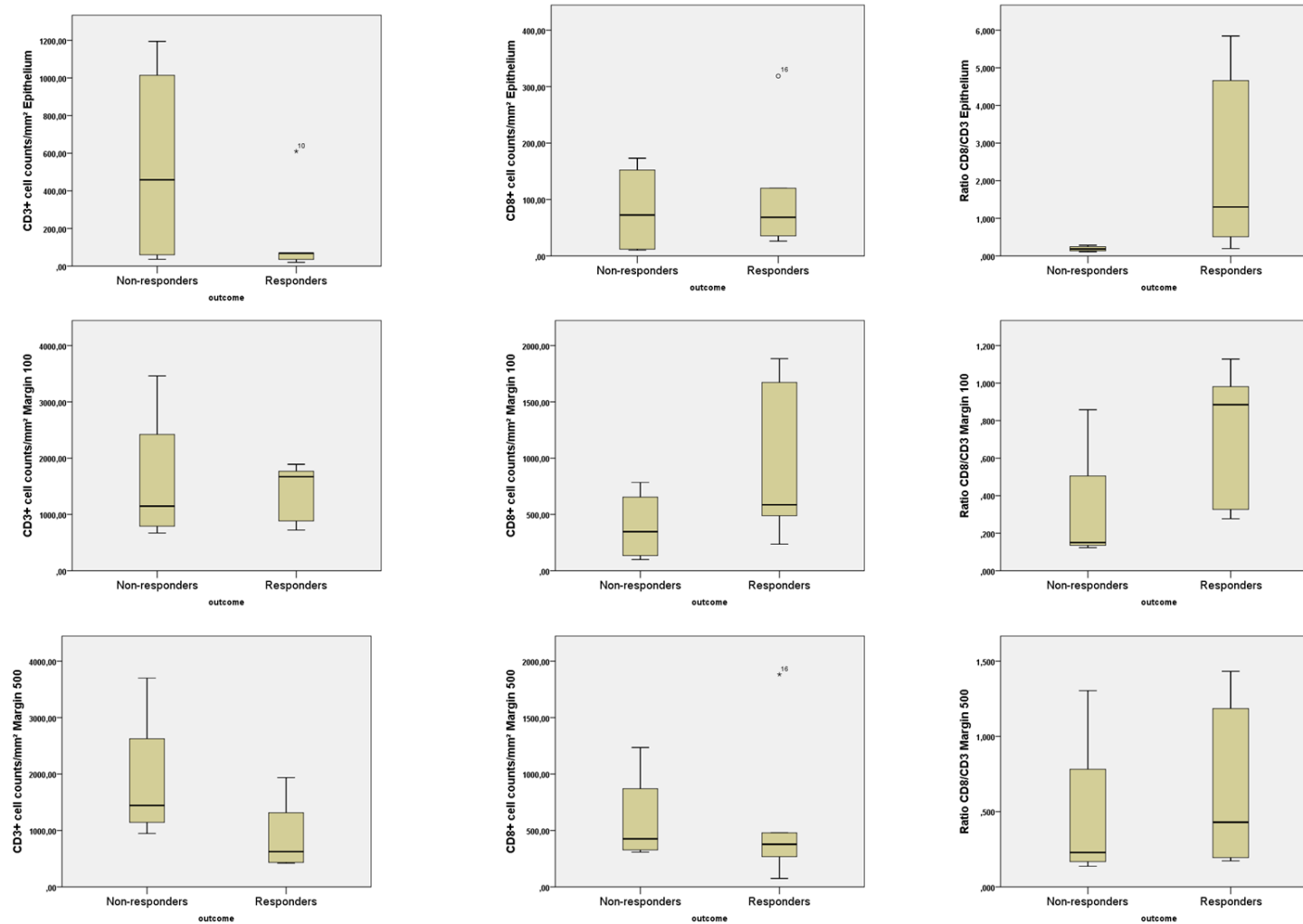
FIGURE S9.1   Distribution of CD3+ and CD8+ T cell counts/mm² and the Ratio CD8/CD3 in the epithelium and stromal compartments in non-responders compared with responders in week 0 (before treatment). The line in the center of each box represents the median value of the distribution; the borders of the box represent the upper and lower quartiles (25%-75%).
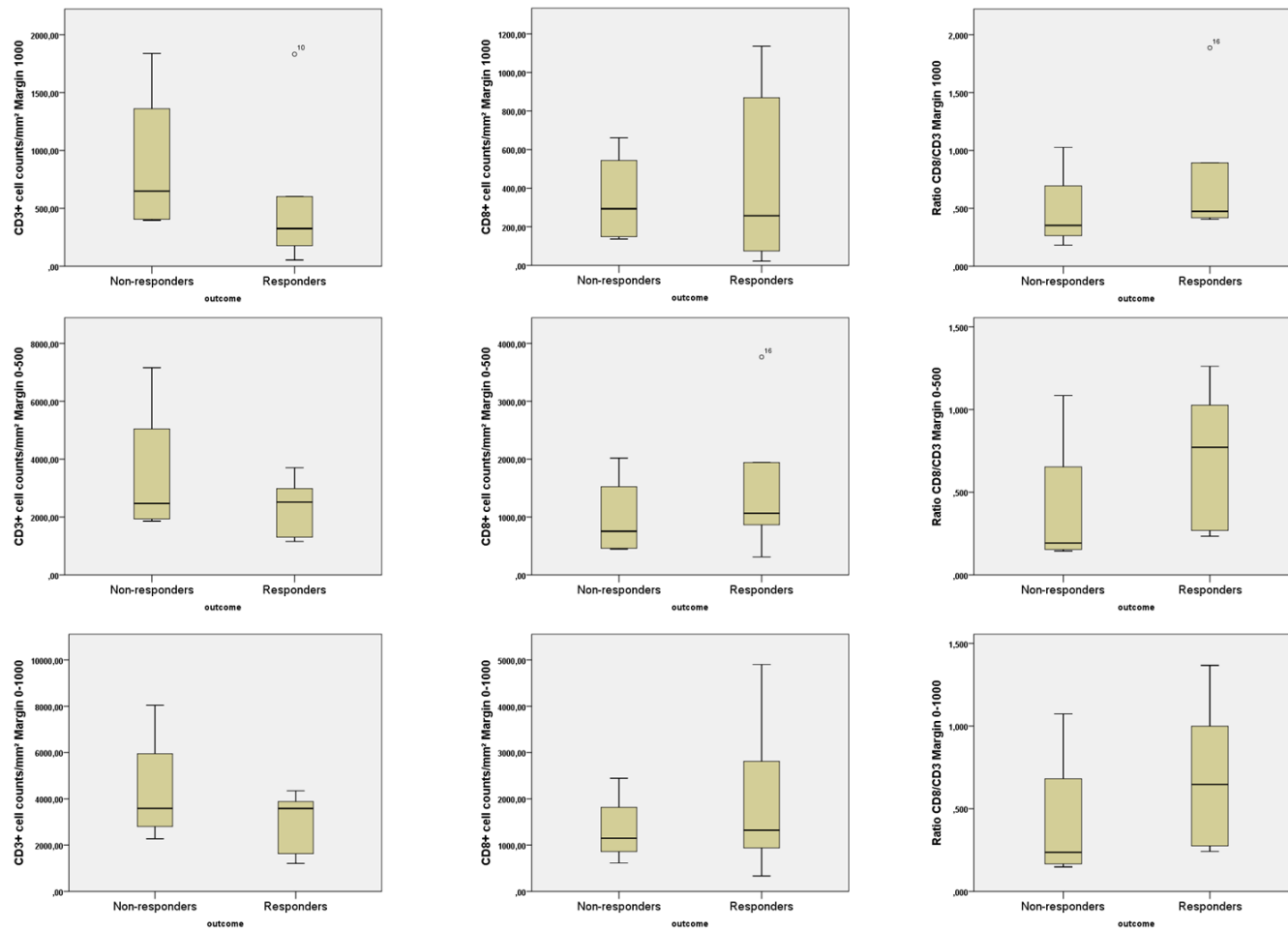
FIGURE S9.2 Distribution of CD3+ and CD8+ T cell counts/mm² and the Ratio CD8/CD3 in the stromal compartments in non-responders compared with responders in week 0 (before treatment). The line in the center of each box represents the median value of the distribution; the borders of the box represent the upper and lower quartiles (25%-75%).

FIGURE S9.x Distribution of CD3+ and CD8+ T cell counts/mm² and the Ratio CD8/CD3 in the stromal compartments in non-responders compared with responders in week 20 (after treatment). The line in the center of each box represents the median value of the distribution; the borders of the box represent the upper and lower quartiles (25%-75%).

FIGURE S9.x   Distribution of CD3+ and CD8+ T cell counts/mm² and the Ratio CD8/CD3 in the stromal compartments in non-responders compared with responders in week 20 (after treatment). The line in the center of each box represents the median value of the distribution; the borders of the box represent the upper and lower quartiles (25%-75%).

FIGURE S9.5   Distribution of ratios for epithelial to stromal cell counts non-responders compared with responders in week 20 (after treatment). The line in the center of each box represents the median value of the distribution; the borders of the box represent the upper and lower quartiles (25%-75%).
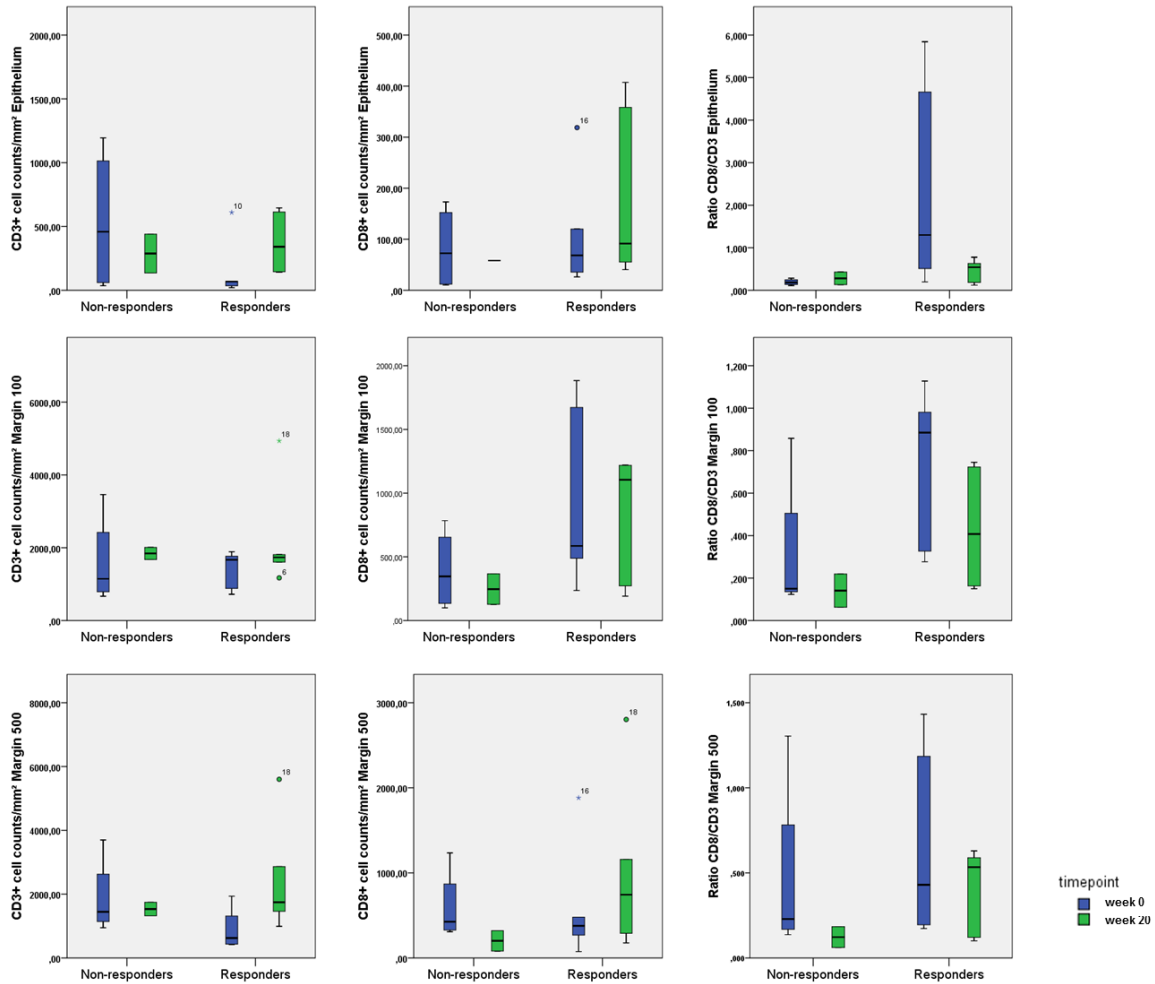
FIGURE S9.6 Distribution of CD3+ and CD8+ T cell counts/mm² and the Ratio CD8/CD3 in the epithelial and stromal compartments in non-responders compared with responders. Data for week 0 (before treatment) and week 20 (after treatment) are shown next to each other. The line in the center of each box represents the median value of the distribution; the borders of the box represent the upper and lower quartiles (25%-75%).
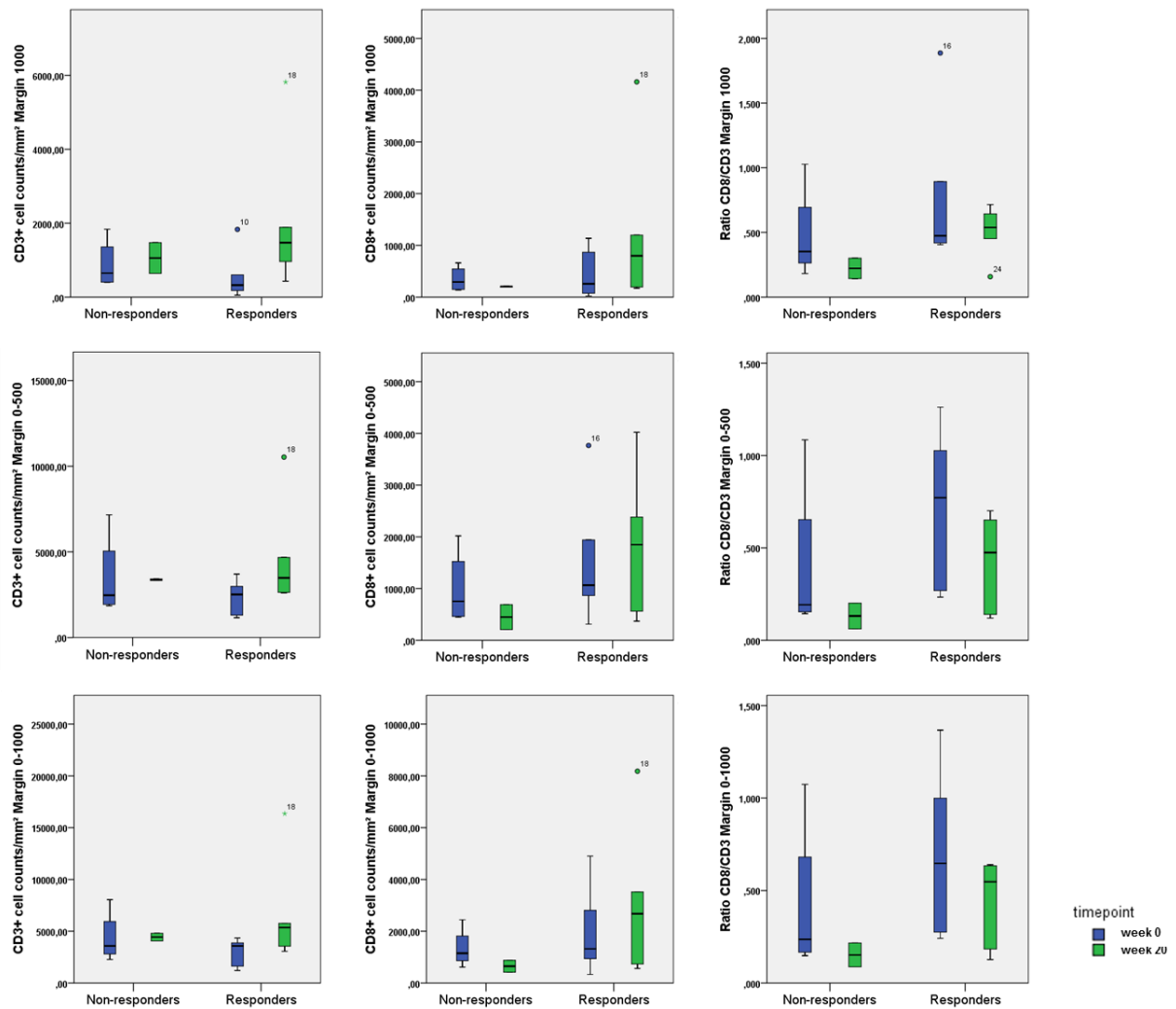
FIGURE S9.7   Distribution of CD3+ and CD8+ T cell counts/mm² and the Ratio CD8/CD3 in the stromal compartments in non-responders compared with responders. Data for week 0 (before treatment) and week 20 (after treatment) are shown next to each other. The line in the center of each box represents the median value of the distribution; the borders of the box represent the upper and lower quartiles (25%-75%).
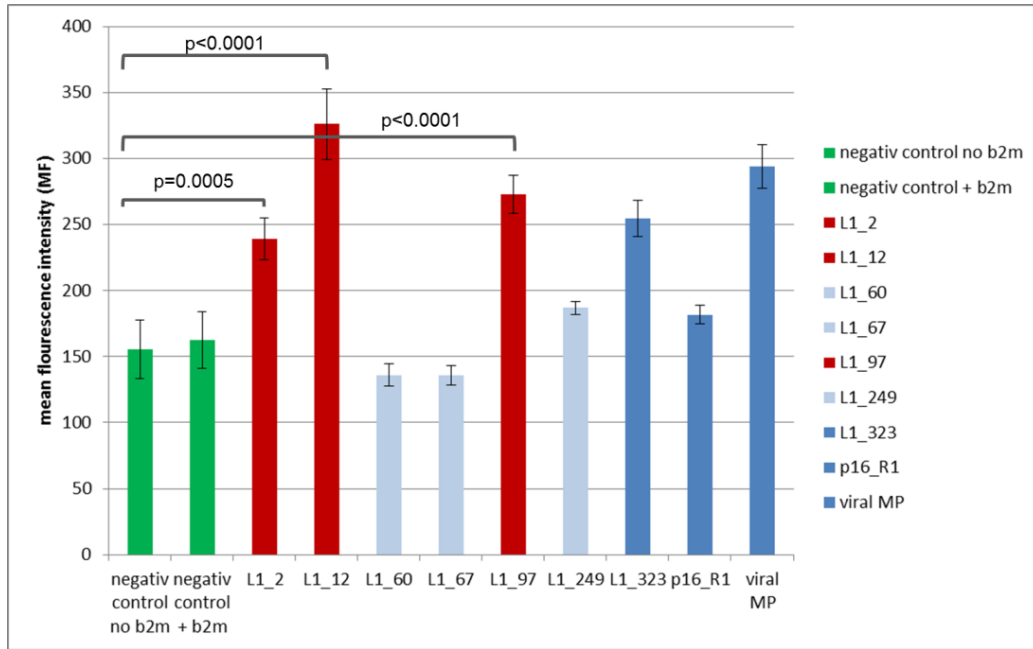
FIGURE S9.8 Peptide binding assay – repetition and validation of the results obtained in the first assay.

MULTIPLEXION

DKFZ

Magnus von Knebel Doeberitz

Clinical Cooperation Unit Applied Tumor Biology G105

Im Neuenheimer Feld 224

69120

CEO: Dr. Markus Schmitt
Brühl 33
88090 Immenstaad
Fon: (+49) 7545 7759044
Fax: (+49) 6221 424932
E-Mail: info@multiplexion.de
www.multiplexion.com

Human Cell Line Authentication Report

Report ID	769		Order ID	847
Report Date	28.06.2014		Order Date	23.06.2014
			Purchase No.	

Dear Magnus von Knebel Doeberitz,

Many thanks for your order. The Multiplex human Cell line Authentication Test (MCA) was performed as described at www.multiplexion.de. Please find below the results.
Best regards,
Dr. Markus Schmitt

Information from Customer				Results			Summary			
Sample ID	Sample Name	Cell line name	If other: exact name	DNA quality	Best Hit with DataBase	Identity (%)	Present in Database?	Cross-Contamin-ation?	Identity confirmed?	Genotype Code
1428	other	HN010		ok	NCH421K	83	no	no	unique sequence	TTTTTAAATAAAAATATWTATNNTT TTAATTAAATATTTAATTATAA
1429	other	HN014		ok	COLO-206F	90	no	no	unique sequence	ATTTATAATTATAATTATATAAWTTT ATAAAAAAWTATTTAATTAAAA
1430	other	HN038M		ok	UACC-257	90	no	no	unique sequence	AATTAAAAAATTAAAAATAAAWATT TTTTTAAWTWTATTTAATTATWT

Legend:

DNA quality:	ok, good DNA quality detected; invalid, DNA was absent or degraded or from non-human species
Identity (%)	Identity of submitted cell line to best hit of data base, identical: 96% and above, not indentical: <96%
Present in database?	indicates whether submitted cell line is included in MCA data base. If your cell line is not included, than no identity confirmation can be made.
Cross-contamination?	indicates whether detected cell line is cross-contaminated by additional cells from another human cell line, the contaminating cell line cannot be specifically identified
Identity confirmed?	"identity confirmed", indicates whether identity was confirmed by MCA (96% and above); "identity not confirmed", submitted cell line is present in data base, but the genotype code is different than expected; "unique sequence", cell line is not present in data base and shows a genotype code that is not related to any cell line included in the data base; "false, match with known cell line", cell line is not present in data base but shows a genotype code that is identical to a cell line included in the data base
Genotype Code	48-letter code for 24 SNP locations; W, uncertain signal; N, no call

FIGURE S9.9   Human Cell Line Authentication Report for the HNSCC cell line HN038.

9.1 Supplementary Tables

		intraepithelial				stromal				intraepithelial/stromal			
		mean	range	SD	p-value	mean	range	SD	p-value	mean	range	SD	p-value
CD3	Low-grade CIN				* p=0.1438				* p=0.2035				* p=0.6498
	p16- CIN1	17.6	7.3-37.3	9.92		56.3	15.8-136.8	43.30		0.46	0.07-1.04	0.330	
	p16+ CIN1	13.3	1.3-45.3	12.14		32.6	11.5-84.8	19.39		0.41	0.07-0.89	0.249	
	High-grade CIN				** p=0.0273				** p<0.0001				** p=0.0799
	CIN2	22.3	8.3-43.0	9.98		73.0	18.0-125.0	33.28		0.42	0.13-1.33	0.371	
	CIN3	25.2	4.3-99.3	25.52		110.1	33.5-260.5	63.10		0.26	0.06-0.64	0.212	
	Invasive disease				*** p=0.2968				*** p=0.0414				*** p=0.9244
	CxCa	43.8	2.0-161.1	42.72		140.5	34.3-336.0	77.58		0.41	0.02-1.52	0.403	
CD8	Low-grade CIN				* p=0.0864				* p=0.7856				* p=0.2012
	p16- CIN1	8.5	0.0-23.0	6.72		17.6	1.8-39.5	13.89		0.72	0.00-1.90	0.655	
	p16+ CIN1	4.8	0.3-20.0	5.22		14.4	3.0-27.3	8.57		0.42	0.01-1.14	0.351	
	High-grade CIN				** p=0.0012				** p<0.0001				** p=0.4774
	CIN2	14.8	3.7-32.3	9.68		37.0	7.8-56.8	16.90		0.59	0.14-1.85	0.642	
	CIN3	14.1	3.3-39.7	11.10		38.0	11.5-73.5	19.34		0.39	0.11-0.67	0.204	
	Invasive disease				*** p=0.8802				*** p=0.2045				*** p=0.3929
	CxCa	15.7	0.7-37.9	12.55		58.3	9.8-149.3	42.72		0.36	0.02-0.92	0.294	
GranB	Low-grade CIN				* p=0.9039				* p=0.5262				* p=0.9523
	p16- CIN1	0.5	0.0-1.7	0.67		0.9	0.0-3.5	1.21		0.68	0.00-1.67	0.689	
	p16+ CIN1	0.5	0.0-4.7	1.29		0.5	0.0-2.3	0.70		0.46	0.00-1.33	0.582	
	High-grade CIN				** p=0.0028				** p=0.0014				** p=0.1838
	CIN2	1.1	0.0-5.3	1.66		0.8	0.0-2.5	1.01		0.88	0.00-1.70	0.715	
	CIN3	2.2	0.0-8.3	2.29		2.7	0.8-12.3	2.75		0.73	0.00-1.93	0.542	
	Invasive disease				*** p=0.9193				*** p=0.0095				*** p=0.0467
	CxCa	1.5	0.0-5.3	1.63		5.7	0.0-20.0	5.98		0.40	0.00-1.67	0.427	
Foxp3	Low-grade CIN				* p=0.5375				* p=0.6444				* p=0.7237
	p16- CIN1	3.4	0.3-9.7	3.72		17.4	0.0-46.0	17.13		0.25	0.04-0.67	0.200	
	p16+ CIN1	2.2	0.0-9.0	2.49		7.6	1.5-16.8	5.58		0.32	0.00-1.33	0.355	
	High-grade CIN				** p=0.2558				** p=0.0076				** p=0.2136
	CIN2	5.8	2.0-17.0	4.05		21.7	6.0-37.8	12.29		0.39	0.07-1.06	0.343	
	CIN3	2.1	0.0-5.7	1.82		19.3	1.5-45.3	13.11		0.16	0.00-0.71	0.198	
	Invasive disease				*** p=0.5933				*** p=0.0243				*** p=0.0464
	CxCa	4.9	0.0-36.0	8.80		42.1	3.3-97.8	31.20		0.17	0.00-1.58	0.384	
CD3ζ	Low-grade CIN				* p=0.1910				* p=0.2282				* p=0.3897
	p16- CIN1	25.2	3.7-107.0	32.30		38.6	5.0-83.5	23.96		0.64	0.14-1.98	0.542	
	p16+ CIN1	10.4	3.7-31.0	7.42		26.5	8.5-49.0	13.97		0.42	0.14-0.73	0.203	
	High-grade CIN				** p=0.0286				** p=0.0022				** p=0.0672
	CIN2	15.6	8.3-22.7	5.22		56.5	16.0-81.8	21.94		0.37	0.14-1.38	0.383	
	CIN3	16.3	5.3-38.9	9.00		58.6	13.5-141.5	37.57		0.38	0.12-1.21	0.281	
	Invasive disease				*** p=0.7623				*** p=0.6801				*** p=0.6801
	CxCa	17.0	2.0-45.3	13.09		60.8	14.0-115.0	34.58		0.39	0.04-1.31	0.363	

TABLE S9.1   Mean cell numbers, ranges and standard deviations (SD) for all T cell phenotypes in correlation with the lesion grades and p16[INK4a] expression status: intraepithelial and stromal cell numbers (per 0.0625mm²) and ratio lesion/lesion-adjacent stroma.

(1) p-values (comparison p16[INK4a]-negative and p16[INK4a]-positive low-grade CIN)

(2) p-values (comparison low-grade CIN vs. high-grade CIN)

(3) p-values (comparison high-grade CIN vs. invasive disease)

		intraepithelial				stromal			
		mean	range	SD	p-value	mean	range	SD	p-value
CD8/CD3	Low-grade CIN				* p=0.1347				* p=0.1861
	p16- CIN1	0.48	0.00-1.00	0.265		0.31	0.09-0.52	0.139	
	p16+ CIN1	0.39	0.01-0.87	0.215		0.43	0.26-0.70	0.159	
	High-grade CIN				** p=0.0258				** p=0.1314
	CIN2	0.70	0.216-1.906	0.464		0.53	0.275-1.018	0.226	
	CIN3	0.79	0.11-1.94	0.532		0.41	0.13-0.77	0.183	
	Invasive disease				*** p=0.0090				*** p=0.2000
	CxCa	0.52	0.04-1.69	0.479		0.40	0.18-0.82	0.186	
GranB/CD3	Low-grade CIN				* p=0.9039				* p=0.8950
	p16- CIN1	0.04	0.00-0.11	0.049		0.02	0.00-0.05	0.020	
	p16+ CIN1	0.03	0.00-0.20	0.066		0.01	0.00-0.06	0.021	
	High-grade CIN				** p=0.0041				** p=0.0508
	CIN2	0.09	0.00-0.64	0.197		0.01	0.00-0.04	0.017	
	CIN3	0.19	0.00-0.77	0.230		0.03	0.00-0.14	0.038	
	Invasive disease				*** p=0.3762				*** p=0.0418
	CxCa	0.09	0.00-0.53	0.153		0.04	0.00-0.18	0.044	
Foxp3/CD3	Low-grade CIN				* p=0.8403				* p=0.6498
	p16- CIN1	0.20	0.03-0.68	0.237		0.26	0.00-0.54	0.164	
	p16+ CIN1	0.20	0.00-0.67	0.197		0.23	0.07-0.46	0.117	
	High-grade CIN				** p=0.7690				** p=0.8833
	CIN2	0.26	0.06-0.40	0.100		0.32	0.20-0.55	0.102	
	CIN3	0.18	0.00-1.31	0.301		0.22	0.02-0.54	0.138	
	Invasive disease				*** p=0.2318				*** p=0.5747
	CxCa	0.18	0.00-0.87	0.266		0.28	0.08-0.60	0.149	
CD3ζ/CD3	Low-grade CIN				* p=0.8576				* p=0.8980
	p16- CIN1	1.10	0.35-1.97	0.658		0.79	0.26-1.49	0.434	
	p16+ CIN1	0.99	0.32-1.75	0.459		0.88	0.49-1.60	0.340	
	High-grade CIN				** p=0.5522				** p=0.0700
	CIN2	0.80	0.53-1.00	0.174		0.82	0.60-1.27	0.206	
	CIN3	0.96	0.14-1.77	0.458		0.59	0.10-1.23	0.260	
	Invasive disease				*** p=0.1171				*** p=0.0090
	CxCa	0.67	0.23-1.88	0.525		0.47	0.16-0.80	0.176	

TABLE S9.2   Means, ranges and standard deviations (SD) for the ratios calculated between different T cell phenotypes and CD3+ T cells in correlation with the lesion grades and p16[INK4a] expression status (means per 0.0625mm²).

(1) p-values (comparison p16[INK4a]-negative and p16[INK4a]-positive low-grade CIN)

(2) p-values (comparison low-grade CIN vs. high-grade CIN)

(3) p-values (comparison high-grade CIN vs. invasive disease)

			progressing/persistent CIN2/3				regressing CIN2/3				
			mean	min	max	STD	mean	min	max	STD	p=
CD3	Epithel	V1	537,0	36,2	1194,3	570,45	160,8	20,2	610,1	252,08	0.190
		V4	751,3	114,5	1388,1	900,61	427,6	56,4	1846,7	698,63	1.000
		V7	287,8	135,8	439,8	215,02	371,1	140,4	645,6	231,96	0.429
	M100	V1	1606,1	669,7	3460,0	1270,71	1386,8	722,5	1890,1	541,14	0.905
		V4	4593,7	1960,1	6790,1	2444,51	1978,2	483,2	6193,9	2176,92	0.167
		V7	1843,5	1675,7	2011,2	237,26	2166,2	1172,4	4934,5	1375,77	1.000
	M500	V1	1883,9	946,7	3699,8	1236,12	945,9	420,9	1936,5	663,05	0.190
		V4	4565,1	2230,5	5750,2	2021,84	3079,7	237,7	7985,2	2800,21	0.381
		V7	1532,7	1320,3	1745,2	300,47	2401,4	991,4	5600,2	1689,64	0.643
	M1000	V1	883,0	396,2	1838,1	675,40	597,9	53,0	1831,8	719,44	0.286
		V4	3308,3	1907,0	5408,2	1852,21	2159,1	173,9	6842,0	2478,56	0.381
		V7	1056,9	639,0	1474,7	590,91	2008,0	432,1	5818,5	1948,59	0.643
	M0-500	V1	3490,1	1860,3	7159,8	2491,96	2332,6	1155,8	3703,6	1092,75	0.730
		V4	9158,8	4190,7	12540,3	4395,14	5057,9	734,3	14179,1	4926,73	0.381
		V7	3376,2	3331,5	3420,9	63,21	4567,6	2598,7	10534,6	3021,80	1.000
	M0-1000	V1	4373,0	2275,1	8042,6	2532,27	2930,6	1208,8	4346,4	1413,45	0.730
		V4	12467,1	6097,6	16153,7	5538,95	7217,0	908,2	21021,0	7240,28	0.381
		V7	4433,0	4059,9	4806,2	527,70	6575,6	3066,1	16353,1	4913,47	0.643

TABLE S9.3 Mean cell numbers, minima, maxima (per mm²) and standard deviations for CD3+ cell counts in progressing/persistent and regressing CIN2/3. The results are shown separately for the epithelium and all stromal compartments and all time points from week 0 over week 8 until week 20.

			progressing/persistent CIN2/3				regressing CIN2/3				
			mean	min	max	STD	mean	min	max	STD	p=
CD8	Epithelium	w 0	82,1	10,3	173,1	82,76	113,8	26,3	318,7	120,26	0,730
		w 8	169,0	44,6	293,3	175,84	128,2	23,5	397,0	142,67	0,643
		w 20	58,2	58,1	58,2	0,08	174,1	40,6	407,3	164,20	0,643
CD8	M100	w 0	394,2	99,2	784,0	319,65	973,3	236,1	1883,2	749,23	0,286
		w 8	1082,1	446,1	1603,0	586,98	640,6	160,7	1421,2	572,09	0,262
		w 20	246,9	127,4	366,4	169,03	852,2	191,5	1222,2	487,61	0,286
CD8	M500	w 0	598,8	308,8	1234,5	432,27	616,5	75,0	1882,3	723,28	0,730
		w 8	947,4	377,7	1276,5	495,33	964,1	144,4	1815,8	635,94	1,000
		w 20	201,3	80,8	321,8	170,38	985,8	176,9	2802,9	960,89	0,286
CD8	M1000	w 0	346,2	136,9	661,3	247,53	471,6	21,5	1136,3	501,54	1,000
		w 8	694,9	422,1	861,4	238,14	691,8	173,2	1712,1	630,56	0,714
		w 20	201,9	192,5	211,2	13,17	1220,1	171,4	4159,6	1508,64	0,429
CD8	M0-500	w 0	993,0	445,8	2018,5	734,29	1589,8	311,1	3765,5	1350,08	0,730
		w 8	2029,4	823,8	2790,9	1056,11	1604,7	316,8	3125,7	1173,83	1,000
		w 20	448,2	208,2	688,2	339,42	1838,0	368,4	4021,3	1330,51	0,286
CD8	M0-1000	w 0	1339,2	614,9	2444,4	779,36	2061,4	332,5	4901,8	1831,64	0,730
		w 8	2724,4	1625,1	3335,0	953,97	2296,4	490,0	4837,8	1791,11	0,548
		w 20	650,0	419,3	880,7	326,24	3058,1	563,5	8181,0	2781,83	0,286

TABLE S9.4   Mean cell numbers, minima, maxima (per mm²) and standard deviations for CD3+ cell counts in progressing/persistent and regressing CIN2/3. The results are shown separately for the epithelium and all stromal compartments and all time points from week 0 over week 8 until week 20.

			progressing/persistent CIN2/3				regressing CIN2/3				
			mean	min	max	STD	mean	min	max	STD	p=
CD3	Epithelium/M100	w 0	0,34	0,05	0,91	0,403	0,09	0,03	0,32	0,128	0,063
		w 8	0,13	0,06	0,20	0,103	0,20	0,06	0,44	0,148	0,857
		w 20	0,15	0,08	0,22	0,098	0,19	0,09	0,40	0,140	0,643
CD3	Epithelium/M500	w 0	0,32	0,03	0,88	0,396	0,24	0,04	0,98	0,411	1,000
		w 8	0,15	0,05	0,24	0,134	0,23	0,03	0,92	0,348	1,000
		w 20	0,21	0,08	0,33	0,180	0,23	0,07	0,65	0,243	1,000
CD3	Epithelium/M1000	w 0	0,90	0,02	2,01	0,946	0,27	0,11	0,39	0,143	0,730
		w 8	0,30	0,06	0,53	0,334	0,31	0,07	1,26	0,469	0,857
		w 20	0,26	0,21	0,30	0,061	0,28	0,08	0,67	0,221	1,000
CD3	Epithelium/M0-500	w 0	0,17	0,02	0,45	0,200	0,07	0,02	0,24	0,099	0,413
		w 8	0,07	0,03	0,11	0,059	0,09	0,02	0,30	0,107	1,000
		w 20	0,09	0,04	0,13	0,065	0,10	0,04	0,25	0,091	0,643
CD3	Epithelium/M0-1000	w 0	0,14	0,01	0,37	0,165	0,04	0,02	0,14	0,054	0,413
		w 8	0,06	0,02	0,09	0,052	0,07	0,02	0,24	0,088	1,000
		w 20	0,06	0,03	0,09	0,042	0,07	0,03	0,18	0,063	1,000

TABLE S9.5 Ratios for epithelial to stromal cells counts (means, minima, maxima and standard deviations) for CD3+ cell in progressing/persistent and regressing CIN2/3. The results for each stromal compartment are given and are shown separately for all time points from week 0 over week 8 until week 20.

			progressing/persistent CIN2/3				regressing CIN2/3				
			mean	min	max	STD	mean	min	max	STD	p=
CD8	Epithelium/M100	w 0	0,16	0,08	0,25	0,084	0,11	0,07	0,17	0,040	0,413
		w 8	0,11	0,04	0,18	0,103	0,24	0,05	0,62	0,207	0,429
		w 20	0,31	0,16	0,46	0,211	0,22	0,05	0,37	0,145	0,429
CD8	Epithelium/M500	w 0	0,12	0,03	0,26	0,106	0,24	0,09	0,45	0,154	0,286
		w 8	0,14	0,04	0,25	0,150	0,20	0,03	0,74	0,274	1,000
		w 20	0,45	0,18	0,72	0,382	0,29	0,02	0,65	0,241	0,429
CD8	Epithelium/M1000	w 0	0,33	0,02	0,82	0,363	0,47	0,14	1,22	0,438	0,556
		w 8	0,37	0,05	0,70	0,455	0,21	0,09	0,62	0,207	1,000
		w 20	0,29	0,28	0,30	0,018	0,32	0,01	0,89	0,309	1,000
CD8	Epithelium/M0-500	w 0	0,07	0,02	0,13	0,050	0,07	0,04	0,09	0,019	1,000
		w 8	0,06	0,02	0,11	0,062	0,12	0,03	0,34	0,116	0,429
		w 20	0,18	0,08	0,28	0,139	0,12	0,01	0,22	0,089	0,429
CD8	Epithelium/M0-1000	w 0	0,05	0,01	0,11	0,046	0,05	0,04	0,08	0,017	0,905
		w 8	0,05	0,01	0,09	0,055	0,09	0,02	0,22	0,081	0,643
		w 20	0,10	0,07	0,14	0,052	0,09	0,01	0,18	0,065	0,643

TABLE S9.6 Ratios for epithelial to stromal cells counts (means, minima, maxima and standard deviations) for CD8+ cell in progressing/persistent and regressing CIN2/3. The results are shown separately for the epithelium and all stromal compartments and all time points from week 0 over week 8 until week 20.

			progressing/persistent CIN2/3				regressing CIN2/3				
			mean	min	max	STD	mean	min	max	STD	p=
CD8/CD3	Epithelium	w 0	0,19	0,11	0,29	0,074	2,50	0,20	5,84	2,576	0,063
		w 8	0,30	0,21	0,39	0,127	0,46	0,20	0,79	0,256	0,643
		w 20	0,28	0,13	0,43	0,209	0,47	0,12	0,78	0,260	0,429
CD8/CD3	M100	w 0	0,32	0,12	0,86	0,359	0,72	0,28	1,13	0,391	0,063
		w 8	0,31	0,09	0,61	0,269	0,39	0,21	0,77	0,210	0,714
		w 20	0,14	0,06	0,22	0,110	0,43	0,15	0,75	0,278	0,286
CD8/CD3	M500	w 0	0,47	0,14	1,30	0,555	0,68	0,17	1,43	0,586	0,730
		w 8	0,28	0,07	0,57	0,261	0,44	0,12	0,62	0,219	0,262
		w 20	0,12	0,06	0,18	0,087	0,42	0,10	0,63	0,241	0,286
CD8/CD3	M1000	w 0	0,48	0,18	1,03	0,374	0,82	0,41	1,89	0,632	0,190
		w 8	0,25	0,15	0,45	0,172	0,46	0,25	1,00	0,283	0,262
		w 20	0,22	0,14	0,30	0,112	0,51	0,16	0,72	0,198	0,143
CD8/CD3	M0-500	w 0	0,40	0,14	1,09	0,404	0,71	0,23	1,26	0,456	0,190
		w 8	0,30	0,08	0,59	0,297	0,42	0,15	0,68	0,201	0,714
		w 20	0,13	0,06	0,20	0,132	0,43	0,12	0,70	0,254	0,286
CD8/CD3	M0-1000	w 0	0,42	0,15	1,07	0,438	0,71	0,24	1,37	0,481	0,413
		w 8	0,29	0,10	0,55	0,232	0,40	0,16	0,58	0,170	0,548
		w 20	0,15	0,09	0,22	0,092	0,45	0,13	0,64	0,232	0,286

TABLE S9.7   Ratios for CD8 to CD3 cell counts (means, minima, maxima and standard deviations) in progressing/persistent and regressing CIN2/3. The results for the epithelium and all stromal compartments and all time points from week 0 over week 8 until week 20 are shown.

x-mer	SYFPEITHI				BIMAS			
	Rank	Start position	aa-sequence	score	rank	Start position	aa-sequence	score
9-mer	1	60	ILVPKVSGL	30	1	67	GLQYRVFRI	139.17
	2	97	RLVWACVGV	23	2	249	YLRREQMFV	133.74
10-mer	1	12	YLPPVPVSKV	30	2	12	YLPPVPVSKV	735.86
	2	2	SLWLPSEATV	27	1	2	SLWLPSEATV	577.28

TABLE S9.8   Results of HLA-A2 epitope prediction for HPV16 L1. Two different databases, SYFPEITHI and BIMAS, were used for HLA epitope prediction in order to obtain L1 peptide sequences as potential antigens to be used for *in vitro* priming of T cells. The two peptides with the highest score of each database and for 9-mer and 10-mer peptides respectively were chosen for peptide synthesis. Because of total concordance between the two databased with regard to the results obtained for 10-mer peptides, in total 6 potentially antigenic L1 peptides were synthesized. In addition, the L1 peptide with the starting position 323 which is known from literature was synthesized as positive control.

Program	Luminex 100 IS
Build	2.3
Date	5/13/201 11:52:44 AM
SN	LX10000266007
TemplateName	Optiplex HPV Genotyping Kit
TemplateDescription	Beadmix-Zusammensetzung entspr der Progen-Beschichtung
SampleVolume	50 uL
DDGate	7000 to 20000
SampleTimeout	70 sec
DataType:	Mean Fluorescence Intensity

Sample	HPV06-R02	HPV11-R03	HPV16-R10	HPV18-R11	HPV26-R12	HPV31-R13	HPV33-R14	HPV35-R15	HPV39-R23	HPV42-R24	HPV43-R25	HPV44-R27	HPV45-R28	HPV51-R29	HPV52-R40	HPV53-R41	HPV56-R42	HPV58-R43	HPV59-R45	HPV66-R46	HPV68-R48	HPV70-R49	HPV73-R66	HPV82-R67	HPV β-globin-R64	HPVHYB1-R70	Total Events
HN038 M tumor cells	14.5	1	2627.5	0	1	0	3	2	3	1	2	1	1	1	2	1	2	1	1	2	2	1	4	3	17	4	2272
FFPE metastasis	8	0	2590	1	1	1	1	1	5	1	1	0	1	1	1.5	3	1	1	2	1	1	2	4	2	8.5	4	1095
FFPE primary tumor	10	2	1299	3	3	0	1	2	6	1.5	1	2	0	2	1	2.5	1	4	3.5	3	1	4	4	4	31	4	1570
HeLa positive control	16	0	87	415	0	1	1	1	3	1	1	1	4	1	1	2	1	1	2	2	1	2	4	4	62	4	2246
Caski positive control	17	0	3007	0	1	0	3	1	4	1	1	1	1	1	2	1.5	1	1	2	1	2	4	3	3	10	3	2621
H₂O control	17	0	1	1	1	1	1	1	5	1	1	0	1	1	2	2	1	2	2	1	2	1	3	3.5	8	3.5	2442
no tissue/cells (empty tube)	19	0	0	0	1	0	0	1.5	4	1	1	1	1	1	2	2	2	2	1	2	2	2	4	2	9	3	2483
hybridization control	17	1	1	0.5	0	0	0	2	4	2	1	1	1	1	3	2	1	1	2	2	2	1.5	3	3.5	8	775.5	2449

TABLE S9.9 HPV Genotyping results for the tumor cell line HN038M and the corresponding archived (FFPE) tissue of the corresponding lymph node metastasis and primary tumor. Results are displayed as mean intensity values (MFIs) for the samples and controls and for all tested HPV-types. Samples or controls positive for the corresponding HPV types are marked in blue, also the hybridization control is highlighted in blue.